https://doi.org/10.15388/vu.thesis.439
https://orcid.org/0000-0002-3008-9603

VILNIUS UNIVERSITY

Greta Leonavičienė

Complex single-cell analysis using hydrogel microcapsules

DOCTORAL DISSERTATION

Natural Sciences,
Biochemistry (N 004)

VILNIUS 2023

This dissertation was written between 2017 and 2021 in Vilnius University Life Sciences Center Institute of Biotechnology.
The research was supported by the Research Council of Lithuania under Grant No. 01.2.2-LMT-K-718-04-0002. The PhD candidate received a scholarship from the EU structural funds.

Academic supervisor – **Prof. Dr. Linas Mažutis** (Vilnius University, Natural Sciences, Biochemistry – N 004).

This doctoral dissertation will be defended in a public meeting of the Dissertation Defence Panel:

Chairman – **Prof. Dr. Kęstutis Sužiedėlis** (Vilnius University, Natural Sciences, Biochemistry – N 004);

Members:
Prof. Dr. Skirmantas Kriaučionis (Oxford University, Natural Sciences, Biochemistry – N 004);
Assoc. Prof. Dr. Aušra Sasnauskienė (Vilnius University, Natural Sciences, Biochemistry – N 004);
Dr. Remigijus Skirgaila (Thermo Fisher Scientific Baltics, Natural Sciences, Biochemistry – N 004);
Dr. Mindaugas Zaremba (Vilnius University, Natural Sciences, Biochemistry – N 004).

The dissertation shall be defended at a public meeting of the Dissertation Defense Panel at 14:00 (hour)/ on 24th February 2023 in R-401 auditorium of the Life Sciences Center (Vilnius University). Address: Saulėtekio av. 7, LT-10257 Vilnius, Lithuania.

The text of this dissertation can be accessed at the library of Vilnius, as well as on the website of Vilnius University: www.vu.lt/lt/naujienos/ivykiu-kalendorius

https://doi.org/10.15388/vu.thesis.439
https://orcid.org/0000-0002-3008-9603

VILNIAUS UNIVERSITETAS

Greta Leonavičienė

Kompleksinė pavienių ląstelių analizė panaudojant hidrogelines mikrokapsules

DAKTARO DISERTACIJA

Gamtos mokslai,
Biochemija (N 004)

VILNIUS 2023

Disertacija rengta 2017-2021 metais Vilniaus universiteto Gyvybės mokslų centro Biotechnologijos institute.
Mokslinius tyrimus rėmė Lietuvos mokslo taryba (LMT), sutarties Nr. 01.2.2-LMT-K-718-04-0002. Doktorantūros stipendija buvo finansuojama ES struktūrinių fondų lėšomis.

Mokslinis vadovas – **Prof. dr. Linas Mažutis** (Vilniaus universitetas, gamtos mokslai, biochemija – N 004).

Gynimo taryba:

Pirmininkas – **Prof. dr. Kęstutis Sužiedėlis** (Vilniaus universitetas, gamtos mokslai, biochemija – N 004).

Nariai:
Prof. dr. Skirmantas Kriaučionis (Oksfordo universitetas, gamtos mokslai, biochemija – N 004);
Doc. dr. Aušra Sasnauskienė (Vilniaus universitetas, gamtos mokslai, biochemija – N 004);
Dr. Remigijus Skirgaila (Thermo Fisher Scientific Baltics, gamtos mokslai, biochemija – N 004);
Dr. Mindaugas Zaremba (Vilniaus universitetas, gamtos mokslai, biochemija – N 004).

Disertacija ginama viešame Gynimo tarybos posėdyje 2023 m. vasario mėn. 24 d. 14 val. Gyvybės mokslų centre (Vilniaus universitetas) R-401 auditorijoje. Adresas: Saulėtekio al. 7, LT- 10257 Vilnius, Lietuva.

Disertaciją galima peržiūrėti Vilniaus universiteto bibliotekose ir VU interneto svetainėje adresu: https://www.vu.lt/naujienos/ivykiu-kalendorius

CONTENTS

ABBREVIATIONS 8

INTRODUCTION 11

1. LITERATURE REVIEW 15

1.1. SINGLE-CELL ANALYSIS USING DROPLET-BASED MICROFLUIDICS 15
1.1.1. The concept of single-cell analysis 15
1.1.2. Main technologies for single-cell isolation 16
1.1.3. The main principles of droplet-based microfluidics 19
1.1.4. Applications of droplet-based microfluidics to single-cell-omics 21
1.1.5. Multi-step reactions in water-in-oil droplets 26
1.2. HYDROGEL BEADS FOR SINGLE-CELL ISOLATION AND ANALYSIS 29
1.2.1. Hydrogel bead production 29
1.2.2. Nucleic acid processing in hydrogel beads 32
1.2.3. Cell cultivation in hydrogel beads 34
1.2.4. Challenges related to hydrogel bead-based systems 37
1.3. HYDROGEL MICROCAPSULES FOR SINGLE-CELL ISOLATION AND ANALYSIS 38
1.3.1. Microcapsule production and application 38
1.3.2. The concept of aqueous two-phase systems 41
1.3.3. ATPS-related microfluidic platforms 44
1.3.4. ATPS-based hydrogel microcapsules 44

2. MATERIALS AND METHODS 47

2.1. PEGDA MICROCAPSULE GENERATION AND APPLICATION 47
2.1.1. Fabrication and use of microfluidic devices 47
2.1.2. Aqueous two-phase system preparation 47
2.1.3. Microbial cell preparation 48
2.1.4. PEGDA microcapsule generation and cross-linking 49
2.1.5. Single E. coli genome amplification 50
2.1.6. Single-genome amplification from gram-positive bacteria 50
2.1.7. Microcapsule-based PCR 52
2.1.8. Scanning electron microscopy 52
2.1.9. Imaging of processed bacteria 52
2.1.10. PEGDA microcapsule dissolution and DNA extraction 53
2.1.11. E. coli culture in microcapsules and droplets 53
2.1.12. Imaging of encapsulated bacteria 53
2.1.13. Data analysis 54
2.2. GMA MICROCAPSULE GENERATION AND APPLICATION 54
2.2.1. Fabrication and use of microfluidic devices 54
2.2.2. Polymer solution preparation 55
2.2.3. Microcapsule generation and cross-linking 55
2.2.4. Preparation of cells 55
2.2.5. Preparation of PBMCs 56
2.2.6. Cell encapsulation 56
2.2.7. Cell fixation in ethanol 56

2.2.8. Cell lysis 57
2.2.9. Genomic DNA depletion 57
2.2.10. Reverse transcription 57
2.2.11. Multiplex PCR 58
2.2.12. Post-RT-PCR microcapsule staining 58
2.2.13. Fluorescence microscopy analysis 59
2.2.14. Flow cytometry 59
2.2.15. RT-qPCR 59
2.2.16. Double-stranded DNA retention in microcapsules 60
2.2.17. RNA leakage among microcapsules 61
2.2.18. Time-lapse of microcapsule decomposition 61
2.2.19. Mammalian cell culture in microcapsules 62
2.2.20. Data analysis 62
2.3. SINGLE-CELL RNA SEQUENCING 64
2.3.1. Fabrication and use of microfluidic devices 64
2.3.2. Preparation of mammalian cells 64
2.3.3. Preparation of bacterial cells 65
2.3.4. Bacteria lysis and gDNA depletion 65
2.3.5. RNA polyadenylation 66
2.3.6. Barcoding hydrogel bead preparation 66
2.3.7. Reverse transcription mix preparation 66
2.3.8. RNA barcoding 67
2.3.9. Reverse transcription 68
2.3.10. cDNA purification and amplification 68
2.3.11. Library fragmentation and adapter ligation 68
2.3.12. Final library amplification and indexing 69
2.3.13. Sequencing and data analysis 69

3. RESULTS AND DISCUSSION 70

3.1. MICROCAPSULES COMPRISING PEGDA-BASED SHELL 70
3.1.1. Development strategy of PEGDA microcapsules 70
3.1.2. PEGDA microcapsule generation 71
3.1.3. Single Escherichia coli genome amplification 73
3.1.4. Gram-positive bacteria lysis and SGA efficiency 76
3.1.5. Single-cell PCR 78
3.1.6. Bacteria culture and phenotypic analysis 79
3.1.7. Mammalian cell isolation in PEGDA microcapsules 82
3.2. MICROCAPSULES COMPRISING GMA-BASED SHELL 83
3.2.1. GMA microcapsule generation and their stability assessment 83
3.2.2. Mammalian cell and nucleic acid retention 86
3.2.3. High-throughput nucleic acid analysis in individual cells 89
3.2.4. Cell type identification based on digital RT-PCR readout 90
3.2.5. Post-RT-PCR microcapsule analysis by flow cytometry 92
3.2.6. Discrimination of true-positive and false-positive events 94
3.2.7. Leukemia cell discrimination from PBMCs 98
3.3. SINGLE-CELL RNA SEQUENCING 101

3.3.1. The strategy used to capture single-cell transcriptomes 101
3.3.2. Analysis of mammalian cell transcriptomes 102
3.3.3. Analysis of bacterial cell transcriptomes 104
3.4. DISCUSSION 107
CONCLUSIONS 112
LIST OF PUBLICATIONS AND PERSONAL CONTRIBUTIONS 113
LIST OF PATENT APPLICATIONS AND PERSONAL CONTRIBUTIONS 114
ACKNOWLEDGMENTS 115
SANTRAUKA 116
TRUMPOS ŽINIOS APIE DISERTANTĘ 163
BIBLIOGRAPHY 164
SUPPLEMENTARY MATERIAL 183
NOTES 187

ABBREVIATIONS

ABS	aqueous biphasic system
ACTB	beta (β)-actin,
ATPS	aqueous two-phase system
B2M	beta-2-microglobulin
BCR-ABL	breakpoint cluster region and Abelson proto-oncogene
BCs	barcodes
BHBs	barcoding hydrogel beads
BSA	bovine serum albumin
cDNA	copy DNA
ColA	collagenase A
Ct	cycle threshold
Cy5	cyanine 5
DAPI	4′,6-diamidino-2-phenylindole
DMEM	Dulbecco's Modified Eagle medium
DPBS	Dulbecco′s phosphate buffered saline
DTT	dithiothreitol
ECM	extracellular matrix
EDTA	ethylenediaminetetraacetic acid
FACS	fluorescence-activated cell sorting
FITC	fluorescein isothiocyanate
gDNA	genomic DNA
GMA	gelatin methacrylate
HBSS	Hanks’balanced salt solution
ICO-seq	isogenic colony sequencing
IMDM	Iscove's Modified Dulbecco's medium
inDrops	indexing droplets
IPTG	isopropyl β-D-1-thiogalactopyranoside
K-562	myelogenous leukemia cell line
KDE	kernel density estimation

LAP	lithium phenyl-2,4,6-trimethylbenzoylphosphinate
LB	luria broth
LED	light-emitting diode
MDA	multiple displacement amplification
mRNA	messenger RNA
NB4	promyelocytic leukemia cell line
NIH-3T3	mouse embryonic fibroblasts
NPV	negative predictive value
OD600	optical density at a wavelength of 600 nm
PBMC	peripheral blood mononuclear cells
PCR	polymerase chain reaction
PDMS	poly(dimethylsiloxane)
PEG	polyethylene glycol
PEGDA	polyethylene glycol diacrylate
PHB	polyhydroxybutyrate
PML-RARα	promyelocytic leukemia-retinoic acid receptor alpha
PPV	positive predictive value
PTFE	polytetrafluoroethylene
PTPRC	protein tyrosine phosphatase receptor type C
RFP	red fluorescent protein
RFU	relative fluorescence units
RPM	revolutions per minute
RPMI	Roswell Park Memorial Institute medium
rRNA	ribosomal RNA
RT	reverse transription, reverse transcriptase
RT-qPCR	quantitative reverse transcription-PCR
RTX	reverse transcription xenopolymerase
SAG	single amplified genome
scRNA-seq	single-cell RNA sequencing
scRT-PCR	single-cell reverse transcription-PCR

SDS	sodium dodecyl sulphate
SGA	single-genome amplification
SSC	saline-sodium citrate
TAE	Tris-acetate-EDTA
TBP	TATA-box binding protein
TSO	template switching oligo
TXRED	texas red
UMAP	uniform manifold approximation and projection
UMI	unique molecular identifier
W/O	water-in-oil
WGA	whole-genome amplification
YAP	Yes-associated protein 1

INTRODUCTION

Biological systems are intrinsically heterogeneous. Deciphering this heterogeneity is important for the comprehensive characterization of cell-to-cell differences and for a better understanding of individual cell properties and functions (1). However, unbiased analyte characterization may require separately sampling thousands of cells, which only becomes practical if high-throughput analytical methods are employed (2-5).

Droplet microfluidics is one of the most appealing technologies for ultra-high-throughput assays at a scale of ~10^6 reactions per one run (6-9). Individual cells or biomolecules can be isolated in pico- to nano-liter volume range droplets and processed using various molecular biology techniques. Among the most noticeable applications to date are antibody repertoire analysis (10-12), different screening assays (13-16), directed protein evolution (17,18), digital PCR (19), and single-cell sequencing (8,20,21).

Despite the high impact of droplet-based microfluidics on life sciences, the technology is not without limitations. Many standard molecular biology methods are built on multi-step sample processing in order to initiate, modify, or terminate a reaction. Usually, they are performed separately to ensure that the individual steps do not interfere with each other and that conditions are optimal. For example, the amplification and analysis of genetic material require performing cell lysis, a step that might be inhibitory or incompatible with subsequent enzymatic step(s) if performed in a single reaction mix. Complex and sequential operations are difficult to adapt to droplet format, mainly because the content of droplets cannot be easily changed once droplets are formed. Implementing multi-step reactions, in some cases, is possible using complex fluidic operations such as droplet reinjection (22-24), fusion (22-25), picoinjection (26,27), and splitting (28). However, these operations are challenging to realize in standard molecular biology laboratories as they require specific expertise in microfluidics.

A simplified alternative for performing multi-step reactions on individual cells is based on hydrogel bead approaches. The key feature relies on cell trapping into hydrogel microspheres (beads) so that several experimental steps could be performed using a pipette and laboratory tubes while cells and their nucleic acids are kept entangled within the hydrogel mesh. There are two main applications of hydrogel beads: single-cell cultivation (29-31) and nucleic acid purification by applying harsh lysis and several washing steps before subjecting a sample to the amplification step (32,33). The latter is especially relevant for microbial samples, where droplet technology is particularly disadvantaged due to the required harsh lysis (32). Unfortunately, most

hydrogel bead-based methods also suffer from a few main shortages. First, during hydrogel bead generation and gelation, a significant fraction of encapsulated cells is typically lost as cells tend to partition to the water-oil interface (34-37). Secondly, the uniform porosity of the entire hydrogel presents a trade-off between the efficiency of enzymatic reactions and the retention of encapsulated molecules. As a result, many published reports rely on hydrogel bead re-encapsulation in W/O droplets to perform the final analysis steps (32,38). Therefore, considering the features provided by W/O droplets and hydrogel beads, there was an evident need for a new technique that would allow conducting complex molecular biology reactions more reliably and practically.

The work reported in this thesis reveals the development and use of a new type of microcompartments (microcapsules), the distinguishing feature of which is a liquid core surrounded by a thin hydrogel shell. Combining the advantages offered by droplet microfluidics, hydrogels, and aqueous two-phase systems (ATPSs), the highly uniform microcapsules carrying cells or biomolecules can be generated at ultra-high throughput rates. The hydrogel shell acts as a semi-permeable membrane retaining encapsulated cells and large molecules while allowing smaller molecules (such as proteins and oligonucleotides) to diffuse through passively. As a result of this permeability, multi-step workflows can be performed by immersing the microcapsules in an appropriate reaction buffer using a regular laboratory pipette and tubes. Although several approaches for generating microcapsules have been reported (33,39-43), none of them are well-suited for multi-step molecular biology assays that rely on nucleic acid amplification and analysis.

The aqueous two-phase systems composed of a pair of hydrophilic polymers were selected to develop two types of semi-permeable microcapsules. The first composition relied on dextran and acrylate-modified polyethylene glycol (PEGDA), which resulted in microcapsules with a PEGDA shell. These microcapsules were applied for single-bacterial cell analysis, including whole-genome amplification (WGA), cultivation, and phenotypic analysis. The second composition relied on dextran and gelatin methacrylate (GMA), which resulted in microcapsules with a GMA shell. These microcapsules opened much broader possibilities for single-cell research. As a proof-of-concept, the GMA microcapsules were used for cell type identification by multiplex RT-PCR and as biocompatible vessels for 3D cell cultivation. Furthermore, single-cell RNA sequencing (scRNA-Seq) of mammalian cells, as well as bacteria, was demonstrated using this composition.

Microcapsules presented in this work overcome the major constraints related to droplet-based microfluidics. It is anticipated that this work will become the basis of many other single-cell analysis workflows and expand the use of single-cell analysis approaches in laboratories with limited or no experience in microfluidics.

Study goal

Develop, characterize and apply semi-permeable hydrogel microcapsules for high-throughput complex single-cell analysis.

Objectives

1. Develop semi-permeable microcapsules using an aqueous two-phase system consisting of polyethylene glycol diacrylate (PEGDA) and dextran.
2. Evaluate cell isolation, cultivation, and nucleic acid amplification in PEGDA microcapsules.
3. Develop an alternative semi-permeable microcapsule composition using an aqueous two-phase system consisting of gelatin methacrylate (GMA) and dextran.
4. Assess GMA microcapsule stability and their use for mammalian cell isolation and nucleic acid retention.
5. Develop a novel multiplex single-cell RT-PCR assay using GMA microcapsules.
6. Validate GMA microcapsule use for whole transcriptome studies of single mammalian cells and bacteria.

Scientific novelty

Droplet-based microfluidics remains one of the most appealing tools for high-throughput single-cell isolation and analysis. However, from a critical point of view, the success of assay implementation is strongly influenced by the molecular biology approaches that need to be used to accomplish a particular analytical task. As a result, the broader use of droplet microfluidics technology becomes limited when complex multi-step reactions need to be incorporated into the water-in-oil format. This is particularly relevant for nucleic acid processing and analysis, where the completion of an assay requires several, in principle, incompatible steps (e.g., cell lysis and reverse transcription-polymerase chain reaction).

In this work, a practical solution allowing a high-throughput multi-step single-cell processing in a single laboratory tube is introduced for the first

time. This challenge was resolved by developing PEGDA and GMA microcapsules comprising a liquid core and a semi-permeable shell. The principle is easy to comprehend: the shell prevents encapsulated cells and high molecular weight biomolecules (e.g., gDNA, mRNA) from escaping the compartmentalization while simultaneously allowing the smaller molecules (e.g., enzymes, oligonucleotides, culture media components) to diffuse through. As a result, different types of enzymatic reactions and analyses can be conducted by simply transferring microcapsules from one reaction tube to another. In addition to the desired permeability, developed microcapsules demonstrate excellent stability under different chemical, physical, and mechanical treatments – features that allowed to conduct diverse molecular biology assays. The results of this work are reported in two research articles (44,45) and four patent applications, whereas one of the patent applications has been licensed already (46).

Defending statements

- Semi-permeable microcapsules can be generated by isolating a pair of hydrophilic polymers (PEGDA-dextran and GMA-dextran) in W/O droplets, followed by shell polymerization.
- Microcapsules retain encapsulated cells and their genetic material (gDNA, mRNA) while allowing smaller molecules (e.g., enzymes, oligonucleotides) to traverse the shell freely.
- Microcapsules are well-suited for conducting massively parallel single-cell analyses by complex multi-step molecular biology workflows.
- GMA microcapsules, in particular, provide a broadly applicable approach for conducting high-throughput single-cell nucleic acid analyses such as scRT-PCR and scRNA-Seq.

1. LITERATURE REVIEW

1.1. Single-cell analysis using droplet-based microfluidics

1.1.1. The concept of single-cell analysis

Most of what we know about biological systems has been revealed by modern molecular biology techniques studying populations of cells. For example, bulk RNA-Seq has been and remains a powerful tool for studying the molecular mechanisms of cancer development and is broadly used for cancer classification, biomarker discoveries, disease diagnosis, and optimizing therapeutic treatments (47,48). In addition, collective microbial cell analysis by metagenomics has allowed us to understand the human microbiome in health and disease (49,50) and explore the distinct environmental niches inhabited by cultivation recalcitrant microorganisms (51-53).

However, biological samples are heterogeneous and typically consist of tens or hundreds of distinct cell types at very different abundances (54). Delineating this cellular heterogeneity is important for our better understanding of biological systems. Unfortunately, conventional bulk-based cell assays become limited to measuring the global response from a population of cells under the assumption that the average phenotype and genotype readout represents a dominant feature of the sample (1,55). As a result, meaningful information about small but potentially relevant subpopulations may be hidden, particularly in cases where that subpopulation determines the behavior of the whole population (55). For example, tumors are heterogeneous dynamic systems undergoing continuous evolution. Their progression is determined by the interactions between cancerous cells and the tumor microenvironment (TME), composed of the extracellular matrix (ECM) and other non-transformed cell types, such as stromal and immune cells (56). Similarly, microbial samples obtained from marine and soil environments are composed of many different species, each having unique metabolic capabilities and roles in their niche (57). Consequently, single-cell analysis of these complex samples could provide a more complete snapshot of sample composition and cell-function relationship (**Figure 1.1**).

Overall, the choice between bulk and single-cell techniques mainly depends on the level of detail needed to answer the biological question. Sample complexity usually plays a defining role in making the decision. Single-cell analysis is often required for particularly heterogeneous samples, where the averaged readings would not accurately represent the sample.

With the increased interest and appreciation of single-cell analysis, new technological capabilities are needed to enable the efficient isolation of individual cells from a complex sample so they could be studied separately and collectively.

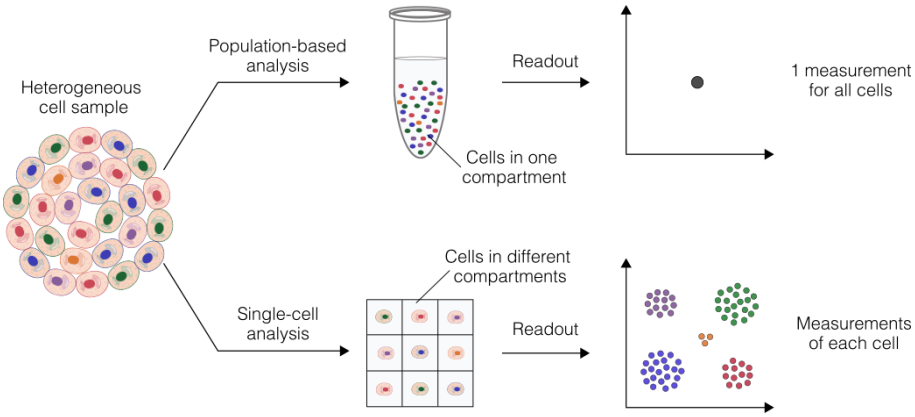

Figure 1.1. Comparison of the heterogeneous sample analysis using population-based (bulk) and single-cell analysis approaches. Applying a population-based analysis, all cells are pooled and processed in one compartment. In contrast, performing single-cell analysis, each cell in the sample is analyzed individually. As a result, this reveals sample diversity and rare cell types, which in the population-based analysis could remain undetected.

1.1.2. Main technologies for single-cell isolation

Cell isolation in separate reaction vessels is the first step toward single-cell analysis. Based on their operational principles, current cell isolation techniques can be classified into four main categories: (i) micromanipulation, (ii) fluorescence-activated cell sorting (FACS), (iii) laser capture microdissection (LCM), and (iv) microfluidics.

Micromanipulation (58) is the most commonly used and conceptually simple cell isolation technique. Sample partitioning is achieved in tubes or plate wells by simple mouth pipette (59) or using limited dilution series (60). However, these techniques are low-throughput and susceptible to errors, such as sample loss during handling and misidentification of a cell under a microscope. Semi-automated devices partially address these disadvantages for cell isolation, with which a skilled researcher can isolate approximately 50 cells per hour (61). A different approach, also considered micromanipulation relies on optical tweezers, which use a laser beam to capture and manipulate cells (62). Optical tweezers require high light intensities ($\sim 10^7$ W/cm^2) and high numerical aperture objectives (63). All these features restrict the ease of

operation, reduce the available working area, and damage sensitive cells (64). An improved optical manipulation technique termed optoelectronic tweezers (OET) requires about 100.000 times less power for manipulation, making the method appealing for working with live cells without damaging them (65). In addition, unlike optical tweezers, OET manipulations can be applied to hundreds or thousands of cells in parallel. This optofluidic technology was implemented by the Berkeley Lights company, which provides automated solutions for single-cell analysis, such as antibody discovery (66,67) or cell line development (68). However, the use of this platform outside the biotechnology industry has not been reported.

Fluorescence-activated cell sorting (FACS) is a process by which cells are sorted according to their light scattering and fluorescence characteristics into two or more containers as they flow through transiently formed aerosols (69,70). The main advantages of FACS-based sorting instruments are their accuracy, relatively broad multiplexing capabilities, and high throughput. Although sorting speeds can achieve up to 30 kHz, in practice, when working with fragile biological samples, the typical rates are in the range of 4-8 kHz. However, single-cell sorting is just the first step in the workflow, and the final assay duration will depend on the subsequent steps required to process sorted cells. In addition, because the FACS technique relies on fluorescently labeling cells expressing known biomarkers, its use for discovering new cell types and phenotypes is mainly limited.

Laser capture microdissection (LCM) is an automated sample isolation technique that enables the selection of specific cells from a heterogeneous population under a microscopic inspection (58,71,72). LCM techniques can be applied to histological specimens, living cells and cell cultures, plant material, chromosome spreads, forensic preparations, formalin-fixed paraffin-embedded (FFPE) samples, fresh-frozen tissues, and stained or unstained tissues (72). The most important advantages of LCM are its precision and the ability to retain information about the spatial location of sampled cells within a tissue. In addition, the morphology of the captured cells and the residual tissue is well preserved. The heat produced by the low-power laser does not affect the integrity of DNA, RNA, or proteins. Unfortunately, the minimum laser spot size of 7.5 μm limits the precision of isolating single cells (72). It creates significant challenges for capturing the cytoplasm content of a single cell without contamination with material from the neighboring cells. Also, because the section has to be of a single-cell width, DNA might be lost by partial nuclei dissection. For these reasons, LCM is less widely used for single-cell isolation than other methods.

Microfluidics uses miniaturized devices and controlled liquid streaming to isolate cells and biomolecules into pico- to nano-liter volume reaction vessels for the subsequent analysis steps at a high-throughput (8,73-75). Microfluidic systems can be categorized into three groups: (i) valve-based, (ii) microwell-based, and (iii) droplet-based microfluidics.

Valve-based microfluidics relies on microfluidic chips integrating embedded switching valves and peristaltic pumps that can switch on and off and thus move the fluids inside the microchannels (10,75). Valve-based methods provide a high degree of control over the fluids at the microscale. However, the high complexity of microfluidics devices and the limited number of reaction compartments that can be operated in parallel (~1.000) limits the broader use of these systems.

Microwells are miniaturized alternatives to 96-and 384-well plates aiming to achieve faster, cheaper, and more sensitive analysis methods (10,76-78). Microwells are usually produced by soft lithography or micromachining, and consist of thousands of 10-100 μm diameter wells (10). In a typical workflow, cells are flooded over a chip, and after their sedimentation, excess media is removed, leaving single cells partitioned among the individual wells. Like conventional plate systems, microwell-based technologies provide information about cell localization, which can be very useful when several measurements are performed on cells of interest (79). However, due to the technical implementation of sample and reagent partitioning, microwell systems are prone to cross-contamination between microwells (80). In addition, cell partitioning based on sedimentation is not accurate and is a time-consuming process.

Droplet-based microfluidics is characterized by the high-throughput formation of pico- to nano-liter volume water droplets suspended in inert and immiscible oil. In contrast to valve-based microfluidics and microwells, where the number of individual reactions is defined by the physical dimensions of the microfluidic chip, the droplet-based approaches provide virtually unlimited scalability (10). The number of reactions that can be conducted in droplets in parallel scales with emulsion volume. Aqueous solutions containing cells and biomolecules are injected into a microfluidics chip, forming a dispersed phase surrounded by the oil with a surfactant that acts as the continuous phase. The flows of these two immiscible phases are precisely controlled by microfluidic pumps and specially designed chips with molded or engraved microchannels (8). As a result, highly monodisperse aqueous droplets are produced as independent microreactors equivalent to wells in microtiter plates, yet the speed of 1.000-30.000 drops per second. To date, droplet-based microfluidics systems remain one of the most impactful and

appealing technological platforms for different single-cell genomics, transcriptomics, and epigenomics analyses (8,81,82).

1.1.3. The main principles of droplet-based microfluidics

Given the impact of droplet microfluidics technology on biological and biomedical sciences and the fact that this thesis makes extensive use of droplet microfluidics for single-cell analysis, it may be worth taking a brief look at the key aspects of this technology.

The first reports of this technology emerged in the early 2000s and were driven by the need for high-throughput analysis systems in life sciences, chemistry, biomaterials, and the pharmaceutical industry, amongst others (83). To date, droplet microfluidics evolved into one of the most appealing and impactful platforms for single-cell and molecule analysis (2,3,81,84). It is an interdisciplinary field where knowledge and advances in microfabrication, engineering, polymer chemistry, fluoro-chemistry, optics, biochemistry, and molecular biology come together to build new analytical tools for solving the challenges posed by complex biological sample analysis. The ultimate goal is to elucidate the differences between closely related cells and understand how these differences determine their function and fate.

Droplet-based single-cell analyses typically begin with an encapsulation, a process where the suspension cells are isolated in water-in-oil (W/O) droplets along with desirable assay reagents (**Figure 1.2**). Encapsulation of cells and assay reagents occurs in the microchannels of a microfluidics device under laminar flow conditions. This flow type ensures that different aqueous streams (e.g., one carrying cells and another carrying lysis reagents) are not mixed until the droplet formation occurs. After encapsulation, cells with assay reagents in droplets are physically and (bio)chemically isolated from each other and can be lysed and/or assayed.

The number of cells inside each droplet can be estimated using the Poisson distribution, in which the probability $P(X = x)$ of finding x cells per droplet is expressed by the equation $P(X = x) = e^{-\lambda} [\lambda^x / x!]$, with λ representing the mean number of cells per each droplet (85). As a result, droplet occupancy by cells (as well as by other bio-analytes, including DNA and RNA) can be tuned by changing the cell dilution in the aqueous phase. Intuitively, one could expect that the cell encapsulation with lambda value being 1 provides the most efficient way for cell isolation. However, the cell encapsulation process is entirely random, and this choice of the lambda value will result in 37 % of the droplets having no cells, 37 % having a single cell, 18.5 % having two cells, and 7.5 % having more than two cells. Such a high number of cell multiplets

(~25 %) will result in inaccurate analysis, where the results originating from several cells will be misinterpreted as obtained from a single cell. To avoid these events, droplet count is usually chosen an order of magnitude higher than the number of cells in the same volume, corresponding to lambda values around 0.1.

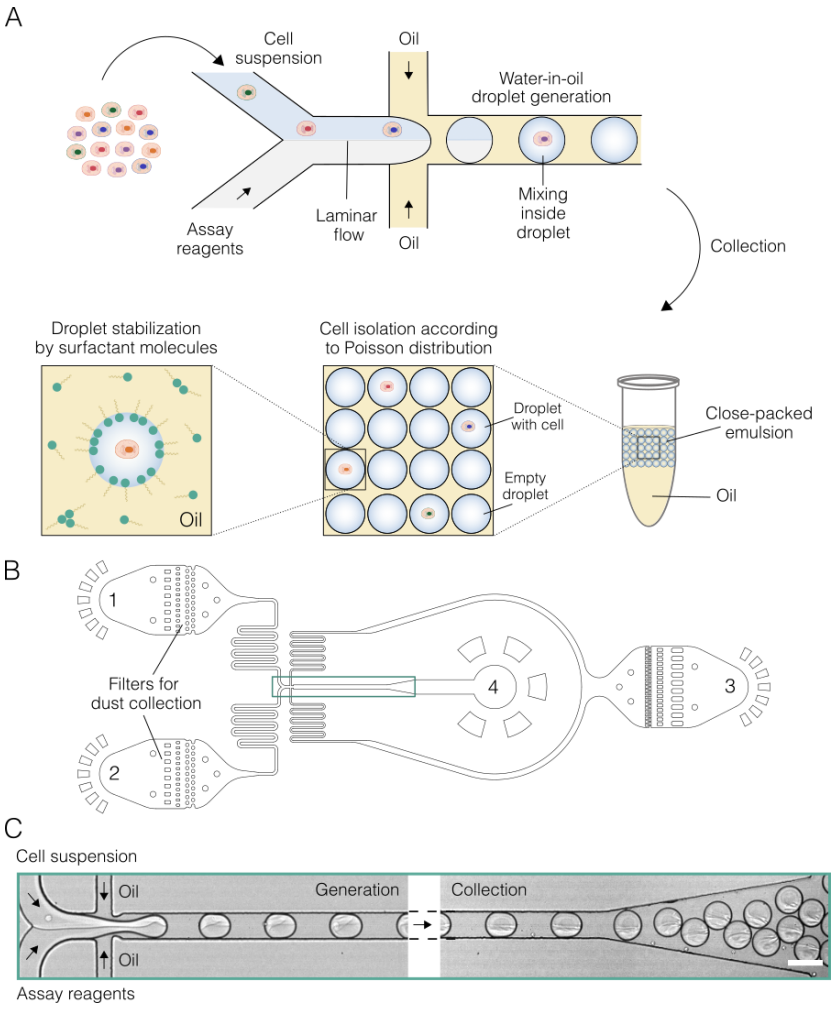

Figure 1.2. Cell isolation using droplet-based microfluidics. (**A**) Cell suspension and assay reagent encapsulation using a co-flow microfluidic device. Cells randomly distribute according to the Poisson distribution, while assay reagents distribute equality between all generated droplets. Immediately after encapsulation and during all analytical procedures, W/O droplets are stabilized by surfactant molecules. (**B**) Microfluidic chip schematic. Numbers indicate: 1 – inlet for cell suspension, 2 – inlet for assay reagents, 3 – inlet for droplet stabilization oil, and 4 – outlet for emulsion collection. (**C**) Digital micrographs showing droplet generation and collection. Black arrows indicate the direction of the flow. Scale bar, 100 µm.

Droplet stability and uniformity are other important features that should be considered aiming for efficient and accurate analysis. Uniformity and precise size control are achieved by the microfluidic devices and flow control by syringe pumps, while the surfactant molecules maintain droplet stability through all analytical procedures (85,86). A surfactant, usually supplied with the oil phase, partitions between the aqueous and oil phases so that the hydrophilic head faces the aqueous solution and the hydrophobic (or fluorophilic) tail faces the oil (**Figure 1.2, A**). In this way, the surfactant facilitates the interaction between two immiscible phases by reducing surface tension and stabilizes the emulsions by preventing the coalescence of individual droplets (87). Perfluorinated surfactants, such as perfluoropolyether-polyethylene glycol-perfluoropolyether (PFPE-PEG-PFPE) dissolved in fluorinated oils are the most common selection in the field of droplet microfluidics (88).

As mentioned above, the design of a microfluidic chip and the flow rates are the main factors defining the droplet generation process. Controlling the chip design and flow parameters, it is possible to have a wide range of droplet volumes, typically varying from 1 pl to 10 nl. The choice of a specific droplet volume should depend on the assay design and biological analyte. For example, performing single DNA molecule amplification, the preferred reaction volume is up to 10 pl (89,90). Smaller droplets result in increased stability and a higher number of compartments that can be generated per unit of time. For mammalian cell-based assays, the droplet volume typically ranges from 0.1 to 10 nl (10). An increased reaction volume (in the order of nano-liters) is often needed to elevate the inhibition of enzymatic reactions due to a crowded environment (10,91). For example, it was shown that the single-compartment RT-PCR assay might be inhibited by cell lysate itself when reaction volumes reach 1 nl (91-94). In other cases, larger droplet volumes might be needed to provide a sufficient amount of nutrients for cell growth (95). Due to these and other reasons, droplet volume should be carefully considered depending on the requirements of an assay.

1.1.4. Applications of droplet-based microfluidics to single-cell-omics

Single-cell analysis is one of the most exciting applications for droplet-based microfluidics. The past decade has seen the development of many techniques focusing on studying large numbers of individual cells (8,96). As a result, cells from heterogeneous samples can now be characterized at various informational levels with access to diverse molecular features and functions (**Figure 1.3**). A significant effort has been dedicated to cover the targeted and

untargeted "omic" analyses of single cells, and an excellent overview can be found in recent reviews (8,82). However, the detailed description of all these methods is outside the scope of this chapter. Therefore, only a few noticeable applications related to untargeted single-cell-omic analyses will be discussed in this section.

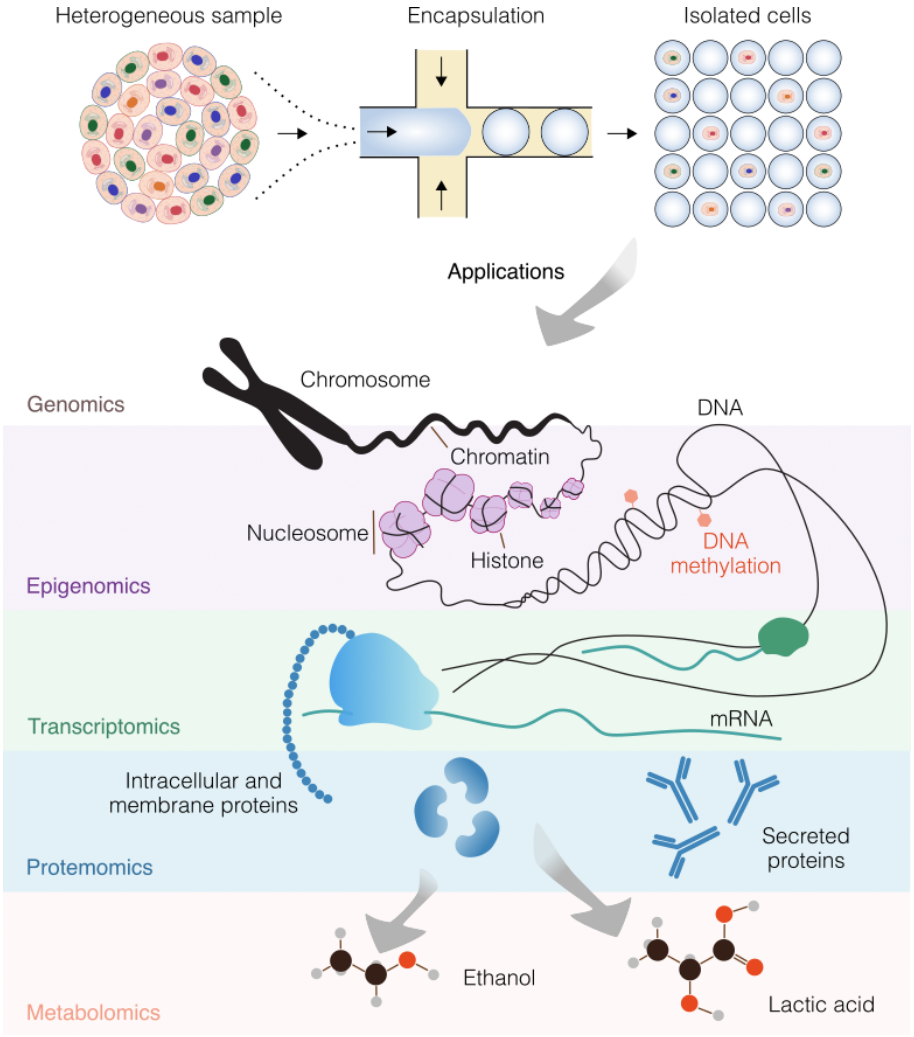

Figure 1.3. Schematic representation of droplet-based microfluidics applications to the diverse aspects of single-cell analysis. The schematic was adapted from the review article (8).

The untargeted single-cell-omic methods typically rely on sequencing as an information readout. One of the most significant breakthroughs in the field was the invention of genetic single-cell barcoding in droplets using beads with immobilized barcoding primers (2,3) or droplets with free-floating barcoding

primers (97). It was initially applied to single-cell RNA sequencing (scRNA-Seq). However, many molecular biology principles related to the barcoding of single cells are universal among different single-cell-omics and are briefly discussed in the following paragraphs.

Transcriptomics. Single-cell transcriptomics is the earliest and the most expanded field among other single-cell-omics. The principal steps and concepts of scRNA-Seq are shared among the different variations of this method, including the pioneering inDrops (2), Drop-Seq (3), and the widely commercialized version of 10X Genomics (98). The key aspect is the use of barcoding beads that are co-encapsulated with cells at conditions that droplets contain one cell and one bead. The beads can be hard spheres (Drop-Seq (3)), hydrogels (inDrops (2)), or dissolvable hydrogels (10X Genomics (98)). Each bead carries many copies (~10^6-10^9) of barcoding primers to capture transcriptomes from individual cells. The main characteristics of barcoding primers attached to the bead include: (i) poly(dT) region for polyadenylated mRNA capture, (ii) a unique molecular identifier (UMI) used to count unique mRNA molecules, (iii) a cell barcode used to identify individual cells, and (iv) a standard sequencing adapter that can also be used as a PCR handle. The key aspects of single-cell RNA sequencing using the 10X Genomics platform are presented in **Figure 1.4**.

Following encapsulation (**Figure 1.4, A**), oligonucleotides are released by DTT residing in the RT mix. The mRNA molecules released upon cell lysis are captured by their 3' end polyadenylated tail to the poly(dT) region on a barcoding DNA primer. The DNA strand is then extended by reverse transcriptase using the mRNA molecule as a template to yield a copy DNA (cDNA) molecule. A few cytosines are then added at the 3' end of the cDNA molecule by reverse transcriptase with the intrinsic terminal transferase activity. This short sequence is then used as an annealing site for the template switching oligo (termed TSO). This primer serves as a second template for the reverse transcription enzyme to synthesize the end of the cDNA molecule – a process known as template switching (**Figure 1.4, B**). The resultant products are chimeric, comprising a cDNA molecule covalently linked to a barcode and TSO sequence. After reverse transcription in droplets, the barcoded cDNA molecules are pooled and subjected to the amplification step. Because the TSO sequence is universal for all synthesized cDNA molecules, this site is used as a second adaptor for the PCR primer binding and cDNA library amplification. Amplified cDNA molecules are then used for the final library preparation steps (e.g., fragmentation, adaptor ligation) and are subjected to the Illumina sequencing instrument. Finally, the reads are demultiplexed based on the cell barcode DNA sequences, and gene counts are assigned to individual cells

(**Figure 1.4, C**). To this day, single-cell RNA sequencing remains one of the most important contributions to molecular biology. This technology has been fundamental to delineating cellular functions, discovering novel biomarkers, and much more (99-101).

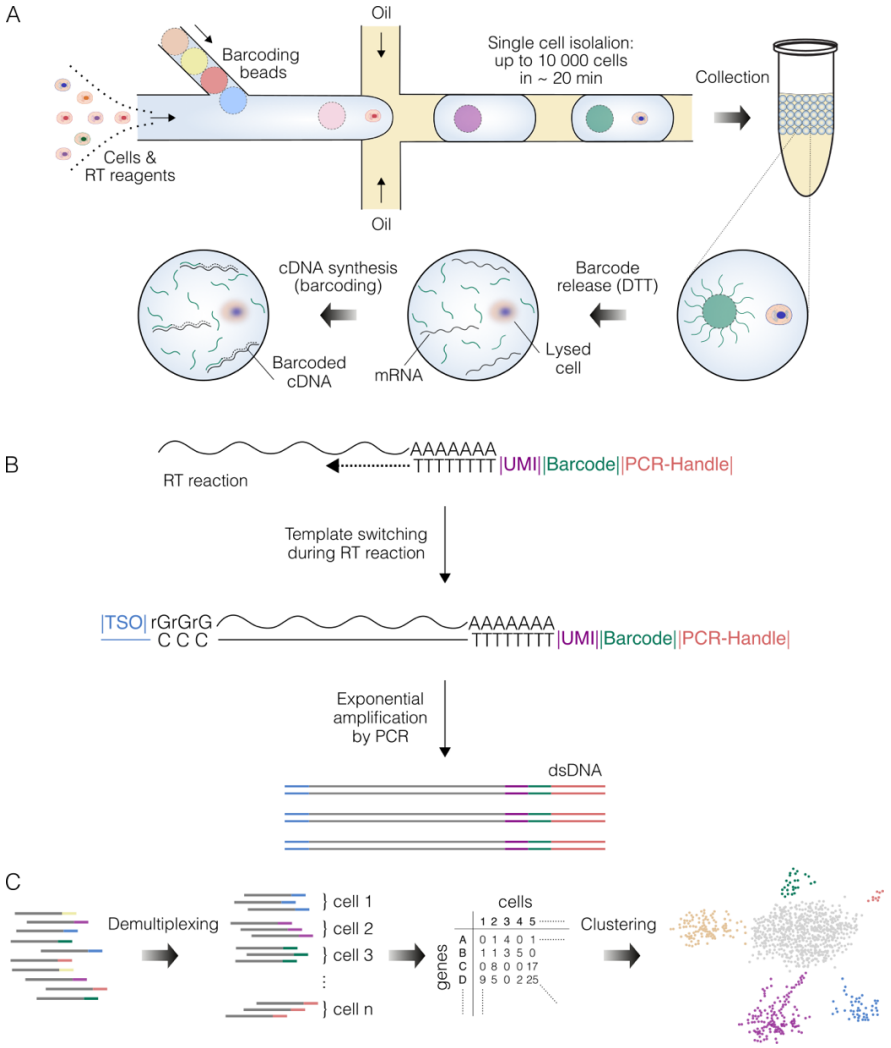

Figure 1.4. Single-cell RNA sequencing using 10X Genomics droplet microfluidics platform. (**A**) Schematic representation of cell and barcoding hydrogel bead loading in droplets followed by cell lysis and mRNA capture. (**B**) The molecular biology strategy used to amplify barcoded cDNA molecules. (**C**) The principle of read assignment to individual cells is based on the cell barcode sequence.

Epigenomics. Single-cell nucleic acid barcoding and sequencing have been extended to other cell modalities, such as chromatin profiling (102-105). In this area of research, one of the most noticeable developments has been the

adoption of transposase-accessible chromatin using sequencing (ATAC-Seq) (102). The method principle relies on nuclei isolation and treatment in bulk by transposase enzyme (Tn5) in order to preferentially fragment the DNA in open regions of the chromatin and to insert adapter sequences to the ends of these DNA fragments. Then, single transposed nuclei are encapsulated at a limiting dilution in droplets together with barcoding beads and PCR reagents. Barcoding beads are labeled with DNA primers containing a cell barcode sequence and a PCR handle. After emulsification, the droplets are thermo-cycled, allowing single-nucleus barcoding of the accessible DNA fragments. Finally, the genetic material is pooled and used to prepare libraries for next-gen sequencing.

Genomics. The first report demonstrating high-throughput single-cell genome sequencing (termed SiC-Seq) aimed to analyze ~50.000 environmental microbes (38). The principal strategy of the SiC-Seq approach relies on complex microfluidic operations where a single-cell derived DNA is fragmented and labeled with a barcode unique to that cell. To achieve this, a barcoding droplet library was first generated by encapsulating and PCR cycling of oligonucleotides with 15 random bases flanked by constant sequences. The resulting library was composed of ~10 million barcoding droplets. Next, the gDNA library (to be barcoded) was prepared by individual cell isolation in agarose beads, followed by lysis and gDNA purification. Then, agarose beads harboring purified gDNA were re-encapsulated in W/O droplets with the Nextera reaction mix to perform genome tagmentation. Having fragmented genomes, the droplets bearing agarose beads were merged with one droplet containing the PCR reagents and one barcoding droplet. The obtained merged droplets were thermo-cycled, adding the barcode sequences onto the genomic fragments using complementary PCR handles added by transposase. At this point, the spliced fragments contained both the P5 and P7 Illumina adaptors required for sequencing on the Illumina platforms. Unfortunately, this method has not found widespread applications due to the assay complexity and shallow sequencing results.

Proteomics. Accessing part of the cell proteome is another successful adaptation of genetically barcoded droplet libraries for single-cell analysis (106-108). Capturing proteins is inherently difficult because, unlike nucleic acids, proteins and peptides cannot be amplified or converted to "sequencable" libraries. Concomitantly two very similar methods termed Cellular Indexing of Transcriptomes and Epitopes by Sequencing (CITE-Seq) (106) and RNA Expression and Protein Sequencing (REAP-Seq) (108) were introduced. Both methods allow simultaneous single-cell transcriptome and proteome quantification by staining cells with DNA-labeled antibodies. Antibodies (Ab)

are conjugated to a DNA sequence containing (i) an antibody barcode, (ii) a PCR handle, (iii), and a poly(dA) tail. At first, cells are immunostained with DNA-Ab conjugates, followed by co-encapsulation in droplets with barcoding beads and lysis-RT reagents. After cell lysis, the poly(A) tail of the cellular mRNA and the poly(dA) tail of the DNA oligonucleotides conjugated to Abs anneal to the poly(dT) tail of the barcoding beads. During the RT step, the mRNA and the DNA-Ab conjugates are single-cell barcoded by the reverse transcriptase, amplified, and subjected to sequencing. As a proof-of-concept, CITE-Seq was designed to detect 13 proteins per cell in a single workflow simultaneously, and REAP-Seq allowed to detect up to 82 different proteins. Although CITE-Seq and REAP-Seq cannot assess the entire proteome of a single cell and are mainly limited to a panel of well-characterized surface markers, yet these techniques represent a significant step toward single-cell multi-omic analysis.

Droplet-based microfluidics has revolutionized our ability to study heterogeneous samples at the single-cell level. High-resolution data from single-cell sequencing provides entirely new insights into sample composition and cellular processes. Although significant progress in single-cell analysis technologies has been made, these technologies are not without limitations. Most current approaches are limited to mammalian cells, and high technical challenges appear when applying similar workflows to microorganisms. For example, applying analogous scRNA-Seq methods to bacteria requires harsh cell lysis to extract mRNA molecules efficiently. However, harsh lysis conditions are detrimental to the subsequent enzymatic reactions, and separating these two steps is required. In this context, it is worth mentioning the Drop-Seq protocol (3), where cell lysis is separated from the RT step by employing solid barcoding beads, which can be rinsed after capturing mRNA molecules before subjecting to the cDNA synthesis. However, cell and bead loading follow a double Poisson distribution, which limits assay throughput and cell capture efficiency (~1 % of generated droplets contain one cell and one bead). Furthermore, prokaryotic mRNA molecules lack a poly(A) tail, which needs a re-design of the mRNA capture strategy or additional steps for the RNA modification (109,110). Thus, biological systems that require more complex analysis workflows have a smaller chance to benefit from droplet-based microfluidics technology.

1.1.5. Multi-step reactions in water-in-oil droplets

Many molecular biology methods are built on sequential sample processing steps in order to initiate, modify, or terminate a reaction. Multi-

step operations are efficiently conducted in a bulk format using a regular laboratory pipette and tubes. However, transferring complex reactions to an emulsion-based format is challenging because the contents of droplets cannot be easily modified once they have formed. Implementing multi-step reactions might require complex fluidic operations such as droplet fusion (22,23), picoinjection (26), droplet reinjection (22,23), splitting (28), and sorting (13,22,23,111).

Multi-step sample processing is particularly common for nucleic acid analysis. For example, the previous section presented the single-cell genome sequencing approach (SiC-Seq) that used a very challenging experimental strategy (droplet reinjection and two merging steps). Another example of high methodological complexity is reverse transcription-PCR. When performed in a single compartment, the RT-PCR reaction follows the lysis step, which might be inhibitory or incompatible with the RT-PCR enzymes. It is well known that at concentrations of a single mammalian cell in a droplet (<5 nl), cell lysate is a potent inhibitor of RT-PCR (91-94). Some researchers suggested a strategy involving harsh cell lysis and post-lysis droplet dilution to avoid mammalian cell lysate inhibition of RT-PCR (112). To realize this strategy, droplet reinjection, fusion, splitting, and picoinjection were implemented in this workflow (**Figure 1.5**).

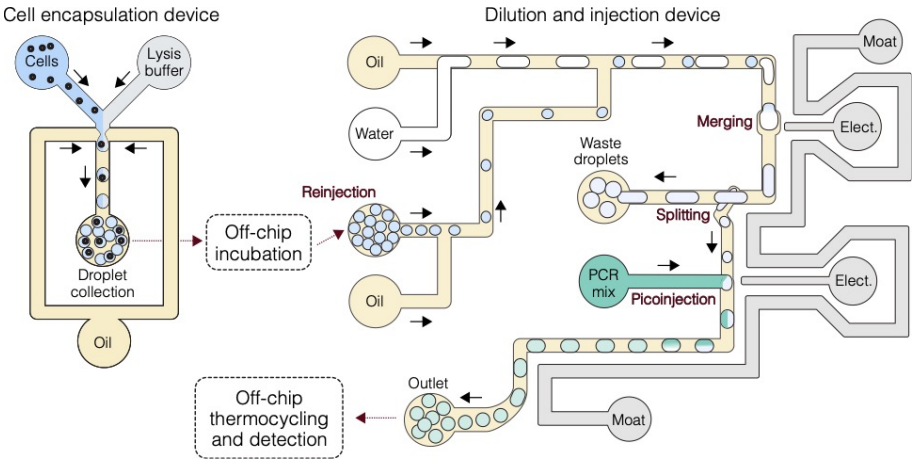

Figure 1.5. The workflow of a microfluidic platform used to conduct single-mammalian cell RT-PCR. Using a co-flow microfluidic device, cells were isolated with a lysis buffer containing proteinase K for off-chip thermal incubation. Following proteinase K inactivation, droplets were reinjected, and cell lysate was diluted upon merging with water droplets. After dilution, a portion of the lysate was split off and picoinjected with 2× RT-PCR reagents. Picoinjected droplets were collected into a tube, thermo-cycled, and analyzed under a fluorescence microscope. The schematic was adapted from the research article (112).

At first, a cell suspension was isolated into 34 pl droplets with lysis reagents (proteinase K) and lysed off-chip. Then the post-lysis emulsion was reinjected into a second microfluidic device, where droplets were merged with larger water droplets to achieve ~20-fold lysate dilution. Droplets were then split and further diluted by adding RT-PCR reagents before undergoing thermocycling and analysis. Since such proof-of-concept studies are built on complex microfluidic operations, they are unlikely to have practical usability. In addition, the strategy where post-lysis droplets are split and the smaller droplets are subjected to RT-PCR highlights a risk of missing very low abundance transcripts (<10 copies per cell).

For RT-PCR assays and alike, it would be advantageous to have a system where all three steps (lysis, reverse transcription, and PCR) are performed in one compartment and where all assay reagents are added at once at the beginning of droplet formation. Indeed, several systems were published in the last five years aiming to combine these steps by carefully optimizing the reaction composition (12,113,114). In one noticeable example, the authors used a recently engineered thermostable reverse transcription xenopolymerase (RTX) that enables both RT and PCR by a single enzyme (12,115). The authors confirmed that, in sharp contrast to commercially available one-step RT-PCR kits, RTX shows exceptional resistance in the presence of very high concentrations of mammalian cell lysates (~1 cell/500 pl). In another report, the inhibition of amplification at high lysate concentration was addressed by supplementing the RT-PCR mix with single-stranded DNA-binding protein (bacteriophage T7 gene 2.5 protein) (114).

The representative examples above show different strategies to achieve multi-step reactions in W/O droplets. From a technical point of view, single-compartment reactions using RTX enzyme or other multi-purpose enzymes and additives are more appealing because it eliminates complex microfluidic operations, yet finding enzymes or their combinations for conducting a desirable assay on cellular genetic material may not be that straightforward. Furthermore, performing different types of enzymatic reactions in one reaction buffer may lead to suboptimal conditions undermining the sensitivity. Therefore, the ability to modify droplet content easily should offer the much-needed flexibility of designing and performing diverse single-cell assays.

1.2. Hydrogel beads for single-cell isolation and analysis

1.2.1. Hydrogel bead production

Hydrogel beads represent a potential solution for overcoming some of the challenges relevant to multi-step analyte processing in W/O droplets. A hydrogel bead consists of a three-dimensional (3D) network of polymer chains that can swell in an aqueous solution and hold a large amount of water while maintaining its structure due to chemical or physical cross-linking of the individual polymer chains. There are multiple reports describing hydrogel bead production using droplet microfluidics technology (116-118). In a typical workflow, an aqueous phase containing a polymeric precursor is emulsified, and upon stimulus, polymer molecules are cross-linked to form a hydrogel mesh. Hydrogel beads are then recovered from the emulsion and suspended in a desirable assay solution. The resulting 3D hydrogel traps encapsulated cells (**Figure 1.6**) and enables reagent exchange with the external environment.

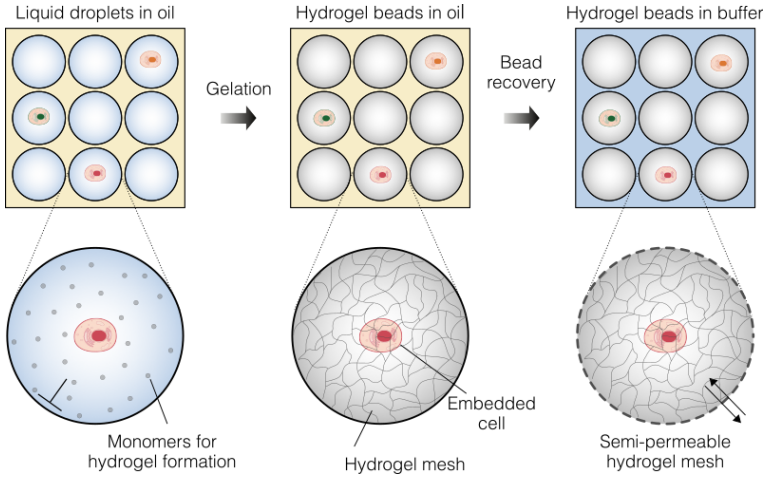

Figure 1.6. Single-cell isolation inside semi-permeable hydrogel beads. Cells are isolated in droplets with a hydrogel precursor, which forms a hydrogel mesh under a specific stimulus (e.g., temperature, radical initiators). Hydrogel beads are then recovered from the emulsion and can be subjected to the subsequent processing steps.

This section describes seven commonly used hydrogels, including naturally derived (agarose, alginate, gelatin, and hyaluronic acid) and synthetic (polyacrylamide and polyethylene glycol diacrylate).

Agarose is a biocompatible polysaccharide extracted from marine red algae (119). It is a linear polymer made up of the repeating units of agarobiose, from which it gets its name. One of the reasons for its widespread use is the

ability to form thermo-reversible hydrogels with gelation and melting points varying from 10-40 °C to 50-95°C, respectively, depending on its molecular weight, concentration, and the number of side groups (120). Agarose undergoes mild gelation through the formation of extensive intermolecular hydrogen bonds resulting in double helical structures that aggregate into thick bundles (121,122). The long-time use of agarose hydrogels in nucleic acid separation and bacterial culture makes it a very well-characterized material in terms of pore size and biocompatibility. Agarose is also widely used for making hydrogel beads and performing single-cell assays (31,123). However, temperature-induced gelation imposes practical limitations relying on elevated temperature during cell encapsulation, which can compromise cell viability (124).

Alginate is an unbranched anionic polysaccharide derived from brown seaweeds (125). It is a linear copolymer composed of D-mannuronic acid (M unit) and L-guluronic acid (G unit) and assembles into blocks with regions composed either homogeneously of M or G units or with alternating G and M units (126). Ca^{2+}-induced gelation is one of the most important functional properties of this polymer. The unique ability to chelate calcium ions comes from the molecular structure containing negatively charged glucuronic and mannuronic acid monomers. Carboxy acid moieties from 4 monomers can bind a calcium ion, and when calcium is bound to two polymer chains, they become crosslinked, forming a hydrogel. Interestingly, alginate hydrogels are also formed with many other divalent or trivalent cations (e.g., Ca^{2+}, Ba^{2+}, Cu^{2+}, Sr^{2+}, Zn^{2+}, Fe^{2+}, Mn^{2+}, Al^{3+}, and Fe^{3+}) (125). Biocompatibility and fast gelation make this polymer attractive in many hydrogel bead formation protocols for cell isolation and culture workflows (127,128). However, from the tissue engineering perspective, alginate hydrogels possess low mechanical strength, low compatibility with buffers having phosphate ions, and have poorly controlled degradation (129).

Gelatin is a protein obtained by the thermal denaturation of collagen, the main constituent of connective tissue. Depending on the processing conditions and its source, gelatin properties can vary, especially polymer molecular weight and the isoelectric point (IEP), which defines the two gelatin types. Type A gelatin is prepared by acidic hydrolysis and has an IEP at a pH of 8-9, while Type B gelatin is produced under alkaline hydrolysis conditions and has an IEP at a pH of 4-5 (130). Gelatin has many advantages over native collagen, including higher solubility and reversible thermo-gelation near 30 °C. Although the phase transition is compatible with live cell encapsulation, the inability to retain physical structure at elevated temperatures makes it impractical for many molecular biology applications.

To solve this problem, gelatin is often cross-linked using chemical, physical and enzymatic methods (130). Physical methods may include plasma (131) or UV treatment (132). Enzymatic methods mainly use transglutaminase, which primarily catalyzes the formation of isopeptide bonds between γ-carboxamide groups of glutamine residue side chains and the ε-amino groups of lysine residue side chains (133). In comparison, chemical cross-linking approaches are more diverse. Some approaches aim to cross-link gelatin chains by bridging free amine groups of lysine and hydroxylysine or free carboxylic acid residues of glutamic and aspartic acid (130). Examples of these cross-linking agents may be genipin (134) and aldehydes (formaldehyde, glutaraldehyde, glyceraldehyde) (135). Another group of crosslinkers, instead of being physically involved in the hydrogel mesh, activate carboxylic acid residues to react with free amine residues, resulting in the formation of an amide bond (135). One of the most popular crosslinkers includes the pair of 1-ethyl-3-(3-dimethyl aminopropyl) carbodiimide (EDC) and N-hydroxysuccinimide (NHS) (130). Another chemical cross-linking strategy is the introduction of reactive groups, which can be later cross-linked. A very common option uses methacrylates, which can be used to modify the type A or B gelatin (136) and produce hydrogels after the photopolymerization (137). There are several commonly used photoinitiators, with Irgacure 2959 being one of the earliest, which is increasingly being replaced with a more biocompatible lithium phenyl-2,4,6-trimethylbenzoylphosphinate (LAP), which can work at longer wavelengths of 405 nm (138). In addition to biocompatible hydrogel formation, the chemical properties of gelatin methacrylate also support cell adhesion and biocompatible degradation using collagenase (137).

Hyaluronic acid, similarly to gelatin, is also naturally derived, but it is a negatively charged polysaccharide and does not inherently exhibit thermo-gelation. Creating hyaluronic acid hydrogels requires covalent cross-linking, which can also be done using methacrylate-based chemistry (139). In many cases, this hydrogel is used to provide mechanical structure. However, hyaluronic acid hydrogels do not inherently support cell attachment and require chemical modification to promote cell adhesion (140). In contrast to gelatin, this polysaccharide is more hydrophilic and often has a high molecular weight, which makes it possible to form hydrogels at low mass fractions. Hyaluronic acid also has commercially available enzymes (hyaluronidase) for degradation under mild conditions, which plays an important role in recovering live cells embedded within hydrogel structures (141).

Polyacrylamide is one of the best-characterized hydrogel polymers due to its widespread use in molecular biology. It is a synthetic hydrogel produced from acrylamide monomers, in contrast to the other mentioned hydrogels

produced from existing polymer chains. Hydrogel formation from acrylamide monomers makes it possible to create well-defined polymer networks, which make polyacrylamide one of the most mechanically stable hydrogel materials (142). Polyacrylamide gel stiffness can be tuned by varying acrylamide concentration and the necessary linker, which is needed to cross-link the otherwise linear polyacrylamide chains. Bis-acrylamide is the most commonly used linker, in addition to di-thiol linkers, which result in a polyacrylamide gel soluble under reducing conditions (143). Such beads are important not only for the genetic droplet barcoding (2,86) but also for forming sacrificial core templates for the hydrogel microcapsule formation (33). Despite the advantages of polyacrylamide hydrogels, the high concentrations of acrylate monomers and radical polymerization induced by ammonium persulfate (APS) and tetramethylethylenediamine (TEMED) are toxic to cells. This prevents using such hydrogels in cases where cell viability has to be retained.

Polyethylene glycol diacrylate (PEGDA) is similar to polyacrylamide in many aspects, as it is also a synthetic and biologically inert material with well-defined characteristics. However, unlike polyacrylamide, PEGDA hydrogels are formed from pre-formed PEGDA polymers, which only need to be cross-linked. There is a wide variety of commercially available PEGDA length options, spanning the range of 0.25 kDa to 20 kDa. Lower molecular weight PEGDA polymers have issues with water solubility and biocompatibility (144). In contrast, higher molecular weight polymers form softer and less mechanically stable hydrogels due to the lower proportion of acrylate cross-links per chain length. Since ester bonds link the acrylate moieties at the ends of PEG polymers, these hydrogels can be dissolved under basic conditions (145). However, hydrolysis requires high pH values and elevated temperatures, which makes the process incompatible with live cell and RNA recovery. DNA, however, can withstand these conditions and be recovered from PEGDA hydrogel beads for the subsequent analysis steps (44). The availability and variety of PEGDA polymers and the option to use photochemical cross-linking (138) make this material one of the most popular and useful polymers for hydrogel bead formation.

1.2.2. Nucleic acid processing in hydrogel beads

Significant technical challenges in conducting multi-step reactions within W/O emulsions originate from the difficulties of altering droplet contents during the steps of a molecular biology protocol. Many hydrogel bead-based approaches have been developed as a potential solution to this challenge (32,146-149), with the key feature relying on cell isolation into a semi-

permeable hydrogel mesh so that several incompatible or interfering experimental steps could be performed independently of each other.

One of the most common hydrogel bead applications is nucleic acid preparation for the amplification step. In several studies, single-bacterial cells were isolated in polyacrylamide beads to conduct harsh lysis and several washing steps to get purified gDNA. Hydrogels harboring purified genomes were then re-encapsulated in W/O droplets with PCR reagents to conduct selected gene amplification (32,146,147). Polyacrylamide hydrogel matrix is dense enough to hold bacterial genomes in place but loose enough to allow enzymes and primers to diffuse through (150). In another example, the authors developed an agarose bead-based platform for high-throughput single-mammalian cell genetic analysis (148). At first, single cells were co-encapsulated with primer-functionalized beads in liquid agarose droplets. After temperature-induced gelation and hydrogel bead recovery, embedded cells were immersed into a lysis buffer containing sodium dodecyl sulfate (SDS) and proteinase K, followed by several washing steps. Next, agarose beads having purified genomes were transferred into a PCR mix with fluorescently labeled forward primers, re-emulsified, and thermo-cycled. During the multiplex PCR, fluorescent amplicons were concatenated on the primer-functionalized beads, then purified and used for the subsequent analysis steps.

Cell embedding in hydrogel beads has not only been used for cell permeabilization and genetic material purification. For example, some reports showed that hydrogel beads could be used as reaction vessels for gDNA amplification using the whole-genome amplification (WGA) technique of multiple displacement amplification (MDA) catalyzed by phi29 DNA polymerase (118,149). Worth noting that a typical bacterial cell contains only a few femtograms of DNA, making WGA a critical step for sequencing whole genomes from single cells (151,152). Fortunately, this technique has allowed researchers to assemble a significant portion of single genomes and provided important insights about sampled microbial communities (57,58,70).

Phi29 DNA polymerase can synthesize DNA strands that are up to 100 kb in length with an average length greater than 10 kb (153,154). Given these amplicon sizes, hydrogel mesh efficiently isolates the WGA synthesis product. In a recently published work (149), the authors presented a single bacterial cell genome sequencing platform named SAG-gel. The strategy

relies on bacteria isolation in agarose beads followed by cell lysis, washing steps, and WGA (**Figure 1.7**). The agarose beads containing single amplified genomes (SAGs) are then FACS-sorted into multi-well plates for re-amplifying genetic material and subjected to the downstream library preparation and sequencing steps. Single genome pre-amplification in hydrogels could be a beneficial step for improving overall assay efficiency. Specifically, it is known that SAG generation efficiency and quality strongly vary between the isolated cells, and pre-selection is usually required before the sequencing (70). Thus, SAG-gel and similar approaches could allow SAG selection at the first steps using fewer efforts and reduced reagent costs.

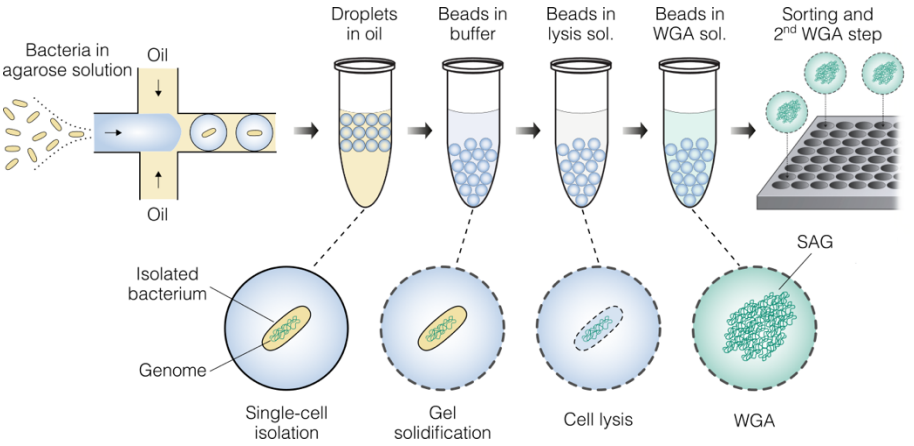

Figure 1.7. The SAG-gel approach for single-bacterial cell genome sequencing. Single-bacterial cells are encapsulated into ~40 µm microfluidic droplets with ultra-low melting temperature agarose solution. Collected droplets are solidified by cooling, and single cells are captured in an agarose matrix. Recovered microbeads are subjected to multi-step processing to initiate bacteria lysis, gDNA purification, and single-genome amplification. Finally, microbeads harboring amplified genomes are FACS-sorted into a multi-well plate for the subsequent analysis steps required for next-generation sequencing. The schematic was adapted from the research article (149).

1.2.3.Cell cultivation in hydrogel beads

In addition to nucleic acid processing, hydrogel beads also opened many opportunities for single-cell cultivation (31,36,155,156). It is particularly relevant in microbial ecology, where novel cell cultivation techniques are crucial for resurrecting yet unculturable bacteria (155-157) (**Figure 1.8**). Like W/O droplets, hydrogel beads allow the isolation of each member in the heterogeneous cell population to analyze them separately. Cell isolation in

distinct physical compartments allows separation of the fast-growing bacteria, which under the regular culture conditions, would outcompete the slower-growing bacteria hiding the initial sample diversity. This is often known as Simpson's paradox (158). In contrast to the immiscible oil phase surrounding the water droplets, hydrogel mesh provides a simple way for media replenishment, signaling molecule diffusion, and cell-cell communication among the microbial community members, which many bacteria require to complete some undetermined aspect of their life cycle (159). Furthermore, hydrogels suspended in an aqueous buffer are compatible with FACS instruments making it possible to select clones of interest based on their light scattering and fluorescence characteristics for the subsequent analysis steps (155,160,161).

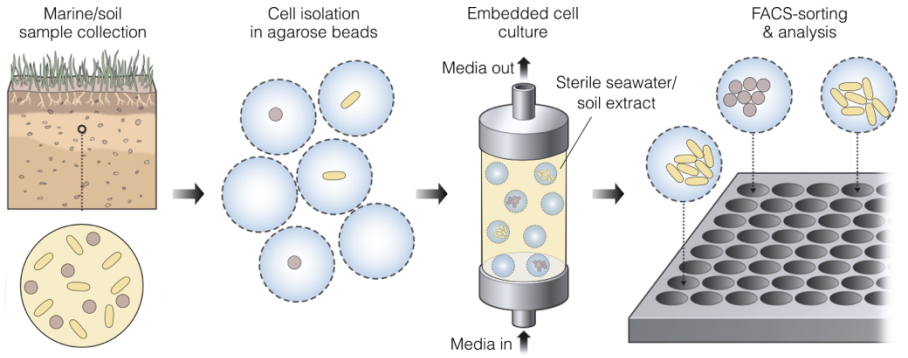

Figure 1.8. Representative scheme showing agarose bead implementation for bacteria culture from the environmental samples. Bacteria from marine or soil samples are isolated in semi-permeable agarose beads and then immersed in a continuous flow cultivation device. Agarose beads with evolved microcolonies are then FACS-sorted and used for the subsequent analysis steps (e.g., re-cultivation in 96-well plate, metabolite analysis, 16S rRNA sequencing). The schematic was adapted from the research article (155).

In addition to microbial cell re-cultivation or metabolic capability exploration, microcolonies evolved in hydrogel beads have also been directly applied for gDNA sequencing (161). As noted above, the WGA catalyzed by phi29 DNA polymerase is the most widely used reaction for amplifying genomes. Yet, the amplification of a single chromosome copy suffers from amplification biases and creates significant challenges in assembling complete genomes (70). On the other hand, since hydrogel beads support cell culture, they provide the means to expand hundreds to thousands of genetically identical cells (clones) per one hydrogel bead before initiating a WGA reaction (161). As a result, conducting WGA on isogenic microcolonies can

lead to larger assemblies and contigs and facilitate nearly complete genome recovery (161).

Isogenic colony sequencing has also been expanded to transcriptomic studies (29,30). Authors of the ICO-Seq method (30) combined the Drop-Seq barcoding strategy (3) with yeast expansion in agarose spheres to transcriptionally profile the microcolonies originating from single cells (30) (**Figure 1.9**).

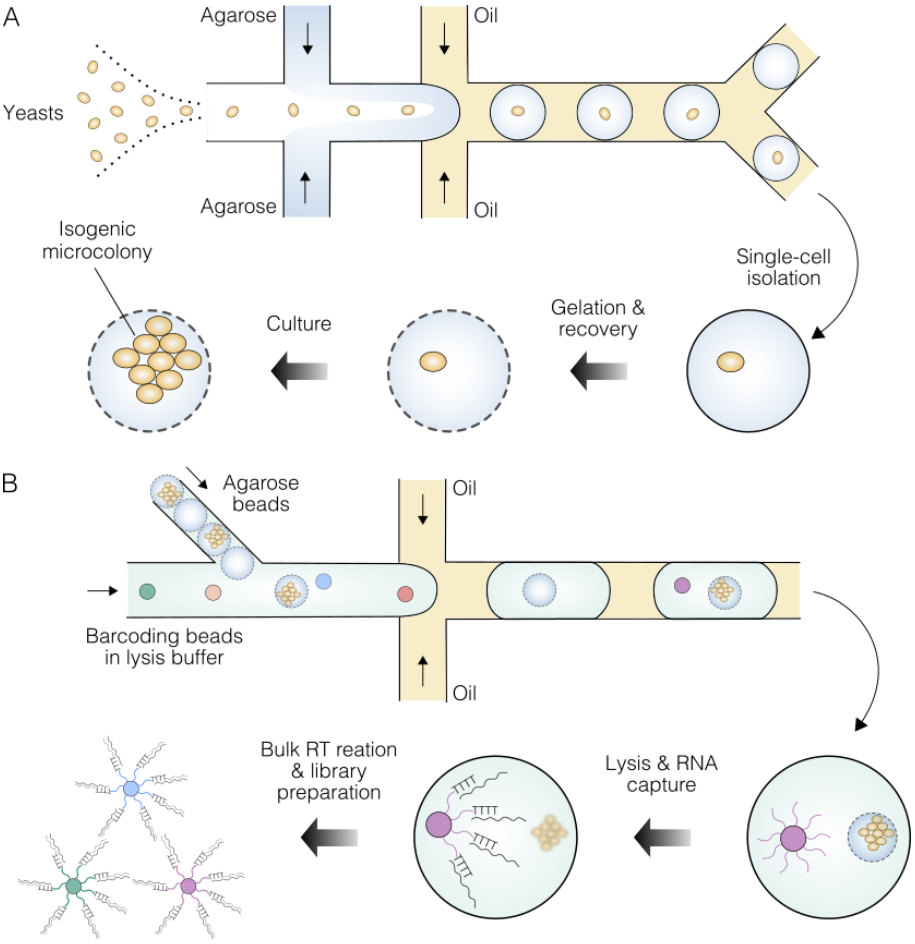

Figure 1.9. The workflow of isogenic yeast colony RNA sequencing (ICO-Seq). (**A**) Individual yeast cells are isolated in liquid agarose droplets, which are converted to semi-permeable hydrogel beads under cooling. Beads with single embedded cells are then immersed in culture media to generate isogenic microcolonies. (**B**) Yeast microcolony barcoding in droplets by co-encapsulation of agarose beads with lysis buffer and mRNA capturing beads, which are then purified and used to conduct bulk cDNA synthesis on bead surfaces.

Noteworthy, Drop-Seq and other scRNA-Seq technologies have been mainly developed and optimized for mammalian cells (2,3,98), which are larger and contain higher quantities of mRNA than yeast cells or other microorganisms. To provide a rough estimate of cell numbers needed for analysis, there are ~15.000 mRNA per yeast cell (30,162) and ~200.000 mRNA in a mammalian cell (30,58), so ~14 yeast cells yield mRNA quantities approximately equivalent to one mammalian cell. Therefore, the expansion of individual cells into isogenic colonies, followed by transcriptome barcoding and sequencing, may significantly improve the detection of low-copy number transcripts found in microorganisms.

In a more recent study, a similar approach, termed Clone-Seq, was applied to mammalian cells (29). The rationale of this technique was to minimize the confounding effects, such as cell cycle differences, technical variability, stochasticity, and low sensitivity, which all can strongly influence data quality and result interpretation. Similar to the ICO-Seq, the Clone-Seq workflow consists of three main steps: (i) single-cell isolation inside biocompatible and biodegradable hydrogel beads, (ii) clonal expansion of single cells within the hydrogel beads up to 60 cells, and (iii) single-clone RNA-Seq applying the inDrops platform (86), where each clone inside nanoliter droplets is uniquely barcoded. However, in contrast to ICO-Seq, hydrogel beads bearing cell clones are decomposed before the barcoding step, leaving highly cohesive and stable structures. Hence, Clone-Seq is limited to cells that remain physically connected after hydrogel decomposition. As expected, single-clone RNA-Seq showed roughly 10-times increased sensitivity compared to single-cells.

1.2.4. Challenges related to hydrogel bead-based systems

The polymer mesh of a hydrogel bead provides a physical barrier retaining cells and high molecular weight biomolecules, such as gDNA or phi29 polymerase amplicons generated during the WGA reaction. Also, hydrogel pores enable the diffusion and exchange of low molecular weight molecules necessary for cell culture and nucleic acid processing by different enzymatic reactions. Therefore, certain multi-step reactions can be conducted by moving hydrogel beads from one reaction buffer to another. These and other features make hydrogels an appealing alternative to regular W/O droplets when multi-step procedures are required for a specific experimental setup, and standard assay formats become impractical. Unfortunately, hydrogel bead-based systems are not without limitations.

Working with agarose – the most abundant polymer for hydrogel bead generation – requires an elevated temperature (~40-50 °C) to maintain molten

agarose in liquid format. Otherwise, polymer clogging and gelation can lead to polydisperse beads or even prematurely terminate the cell encapsulation process. While maintaining an elevated temperature during the encapsulation process represents a technical challenge, it can also be lethal to heat-sensitive cells (163).

Secondly, the poor cell retention in hydrogel spheres is well-documented (164-168). For example, microscopy analysis revealed that cells often tend to position themselves at the oil/water interface immediately after droplet formation (164). As a result, a significant fraction of the cells and their genetic material is lost upon hydrogel bead formation and the subsequent processing.

Finally, the uniform porosity of the entire hydrogel makes it challenging to achieve efficient enzymatic reactions and smaller molecule retention, including PCR amplicons. For that reason, many hydrogel bead-based methods include re-encapsulation in W/O droplets in order to complete the final nucleic acid analysis steps (32,146,147). These shortcomings complicate the workflows and can be challenging for users with limited expertise in microfluidics.

Overall, considering all the advantages and disadvantages of W/O droplets and hydrogel beads, there is an evident demand for simplified approaches to conduct multi-step cell processing workflows. As the next chapter reveals, hydrogel microcapsules overcome major limitations mentioned above and fulfill many requirements for multi-step single-cell assays.

1.3. Hydrogel microcapsules for single-cell isolation and analysis

1.3.1. Microcapsule production and application

Microcapsules, as a term, refer to liquid droplets surrounded by a semi-permeable hydrogel shell (membrane). Similar to hydrogel beads, the microcapsule's shell acts as a passive sieve – retaining encapsulated cells and high molecular weight molecules while allowing the smaller entities (such as proteins and oligonucleotides) to diffuse through. The first attempts to produce microcapsules were based on alginate polymerization in the presence of divalent metal cations (39,41,169). The representative scheme of alginate microcapsule production is depicted in **Figure 1.10**. Such microcapsules are typically produced by first encapsulating the cell suspension into water-in-air droplets surrounded by an alginate liquid shell and then solidifying the alginate shell upon reacting with cross-linking ions such as calcium or barium (169). In many of the reports, alginate microcapsules were used as biocompatible and elastic vessels for 3D cell culture (39,41,169-171). The

permeability of the hydrogel allows the free flow of nutrients into the microcapsule core to support cell proliferation. Some cell types, like epithelial cells, require contact with the extracellular matrix (ECM), which controls fundamental cell behaviors and characteristics such as proliferation, adhesion, migration, polarity, differentiation, and apoptosis (172). To fulfill these requirements, later reports showed alginate microcapsules supplemented with collagen (166,169) – the most abundant molecule comprising the ECM – to conduct colorectal cancer cell lines (CT26 and Caco-2) expansion into multicellular spheroids.

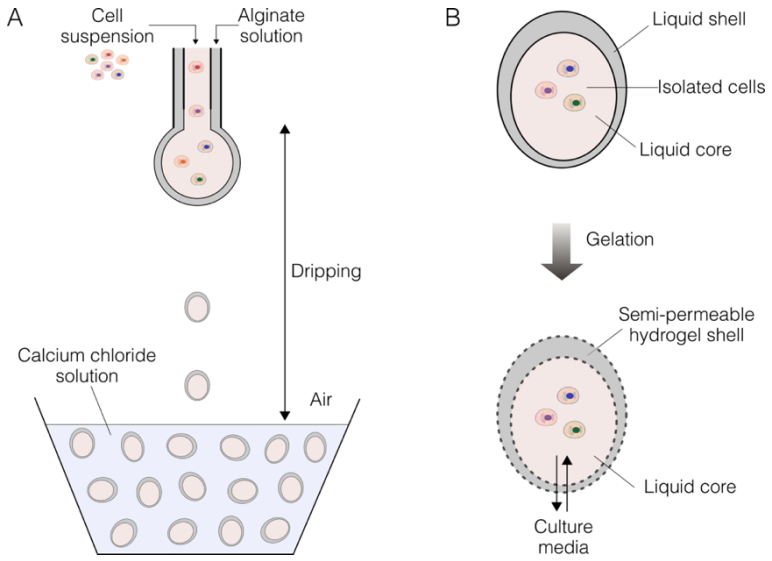

Figure 1.10. Alginate microcapsule production and characterization. (**A**) Co-extrusion of alginate and cell suspension solutions in the air followed by immersion of generated droplets in a gelling batch with calcium chloride. (**B**) After reaching a gelling bath, the liquid shell composed of alginate is transformed into a semi-permeable hydrogel membrane, which ensures isolated cell retention while allowing culture media replenishment. Note that microcapsules produced by this approach are elongated and have an irregular shape.

While alginate-based microcapsules have been used extensively and are stable in certain aqueous buffers, they suffer from poorly controllable stability in cell culture and physiological conditions (173). Gels based on alginate polymer are prone to dissolution due to the release of divalent ions into the surrounding media or due to an exchange reaction with monovalent cations (173). Alginate hydrogels also dissolve in the presence of phosphate ions, citrate, organic acids, and other molecules that can chelate the metal cations participating in the complexation (173). The microcapsules reported

by others are also sensitive to pH. For example, the calcium-alginate hydrogel may decompose upon lowering pH below 7.0 (174), which may occur during cell culture and harvesting due to the metabolic activity of encapsulated cells. As a result, alginate microcapsules found only limited use in specific environments.

Another microcapsule generation technique relies on a double-layer hydrogel bead formation (33,40,175), and the representative scheme is depicted in **Figure 1.11**. In one of the developed systems, microbial cells were isolated in polyacrylamide beads by co-encapsulating acrylamide and reversible cross-linker N,N′-bisacryloylcystamine (BAC) (33). Harsh lysis was applied to embedded bacteria to purify gDNA. The resulting post-lysis hydrogel beads were then isolated in liquid agarose droplets, and upon cooling the emulsion, beads were enveloped by a solid agarose layer. Double-layer hydrogel beads were recovered from the oil phase and subjected to the MDA reaction mix containing DTT. Disulfide linkages of BAC were broken in the presence of DTT, resulting in microcapsules with a liquid core and a semi-permeable agarose shell. Following MDA, microcapsules were enveloped by a second polyacrylamide hydrogel layer to retain PCR amplicons efficiently.

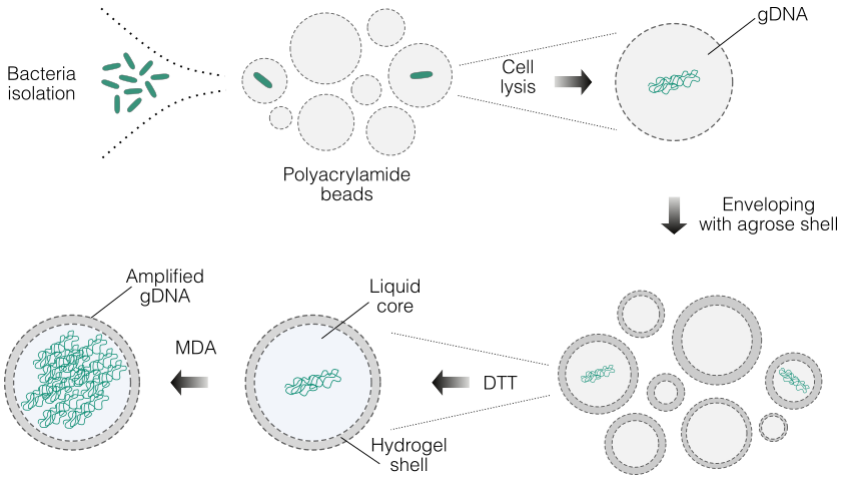

Figure 1.11. Microcapsule generation from double-layer hydrogel beads. Following DTT-soluble polyacrylamide bead generation, hydrogels are enveloped by an agarose shell resulting in double-layer hydrogel beads. By transferring these beads in a reaction mix comprising DTT, the hydrogel core dissolves, resulting in microcapsules with a liquid core and a semi-permeable hydrogel shell. Note that microcapsules produced by this approach are polydisperse and could have an uneven shell thickness.

While useful for some applications, this microcapsule generation approach has many limitations. First, polyacrylamide hydrogel formation usually occurs

via radical polymerization in the presence of ammonium persulfate and tetramethylethylenediamine, which are toxic for isolated cells. For that reason, cell fixation is conducted before the encapsulation step. Alternatively, polyacrylamide could be replaced by a more biocompatible hydrogel (e.g., gelatin), as demonstrated in another work, where cells were first isolated in gelatin beads followed by enveloping with alginate shell (40). Secondly, each hydrogel layer addition requires a new encapsulation round, which can be either time-consuming when microfluidic devices are used or result in polydisperse particles when applying the bulk emulsification technique (which was the case in this work). Altogether, this approach demonstrated a time-consuming and impractical strategy to generate microcapsules. As revealed in the following sections, simpler and more reliable microcapsule production can be achieved by implementing aqueous two-phase systems.

1.3.2. The concept of aqueous two-phase systems

Aqueous two-phase systems (ATPS), also known as aqueous biphasic systems (ABS), are formed when at least two water-soluble components are mixed in water above the critical concentrations, leading to the liquid-liquid phase separation (176-178). This phenomenon was first recognized by the microbiologist Martinus Beijerinck in 1896, who observed that a mixture of gelatin, agar, and water phase separated into two layers (179). Due to the formation of two immiscible aqueous layers, each phase is enriched in one of the phase-forming components. ATPS phases have a low interfacial tension (1-10 μN/m) and enhanced mass transport between the phases (176). This makes them frequently used for the extraction, separation, purification, and enrichment of proteins, membranes, viruses, enzymes, nucleic acids, and other biomolecules important for industry and academia (180). They are mainly used to replace the traditional liquid-liquid extraction procedures based on organic solvents (177).

ATPS can be generated by mixing a pair of hydrophilic polymers, a polymer with a salt, or two different salts, resulting in polymer-polymer, polymer-salt, and salt-salt systems, respectively (177). However, polymer-polymer systems are preferably used due to their excellent biocompatibility (180). Currently, several combinations of hydrophilic polymers were successfully employed for the formation of two-phase systems obtained from the mixing of: (**A**) two nonionic polymers, such as the well-known polyethylene glycol (PEG) and dextran; (**B**) one nonionic and an ionic polymer; and (**C**) two ionic polymers (charged polyelectrolytes) (**Figure 1.12**).

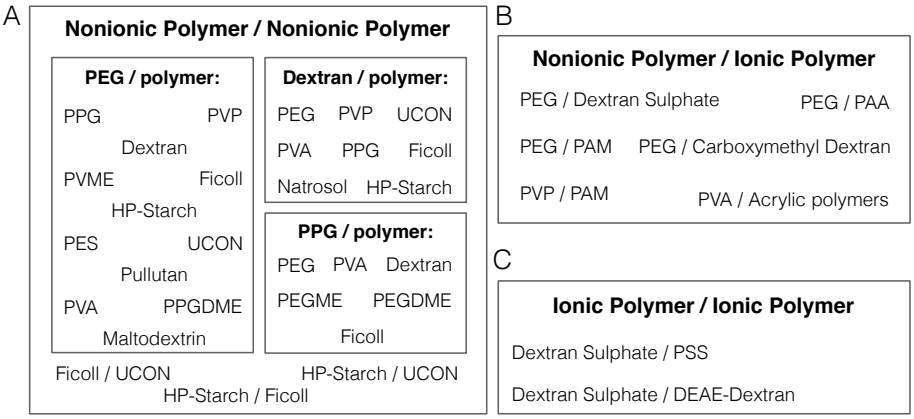

Figure 1.12. Representative examples of ATPSs composed of various polymer-polymer solutions: (**A**) two nonionic polymers, (**B**) one nonionic and an ionic polymer; and (**C**) two ionic polymers (charged polyelectrolytes). Acronyms indicate: PEG, polyethylene glycol; PEGME, polyethylene glycol methyl ether; PEGDME, polyethylene glycol dimethyl ether; PPG, polypropylene glycol; PPGDME, polypropylene glycol dimethyl ether; PVP, polyvinyl pyrrolidone; PVA, polyvinyl alcohol; PES, polyether sulfones; HP-starch, hydroxypropyl starch; PAA, polyacrylic acid; PAM, polyacrylamide; PSS, polystyrene sulfonate. The schematic was adapted from the book chapter (177).

ATPSs are usually described by the phase diagram (**Figure 1.13**), which is like a unique system fingerprint showing the potential working area under specific conditions (e.g., temperature and pH) (180). The phase diagram provides a set of valuable information about the system: (i) the concentrations of component 1 and component 2, which are necessary to create a biphasic system, (ii) the concentrations of phase components in the top (light) and bottom (heavy) phases, and (iii) ratio of the phase volumes (177).

The phase diagram comprises two phase-forming materials (components 1 and 2) and water (177). A solubility curve (termed binodal) divides the two-phase region (above the curve) from the single-phase region (below the curve). The composition of the phases in equilibrium is related by the tie-lines that connect two points on the binodal curve, which correspond to the concentration of components 1 and 2 in the top and bottom phases. For example, a, b, and c correspond to three ATPS solutions where the phases have the same equilibrium composition (177). Thus, moving along the same tie-line, the concentration of components 1 and 2 in the top (T (T_1, T_2) and bottom (B (B_1, B_2) phases remains unchanged, differing only in the phase volume ratios. From a purely practical point of view, phase volume ratio adjustment might be relevant when the analyte of interest needs to be concentrated in a minimal volume reaching the highest concentration. The

binodal curves are mainly determined by turbidimetric titration and cloud-point titration (177).

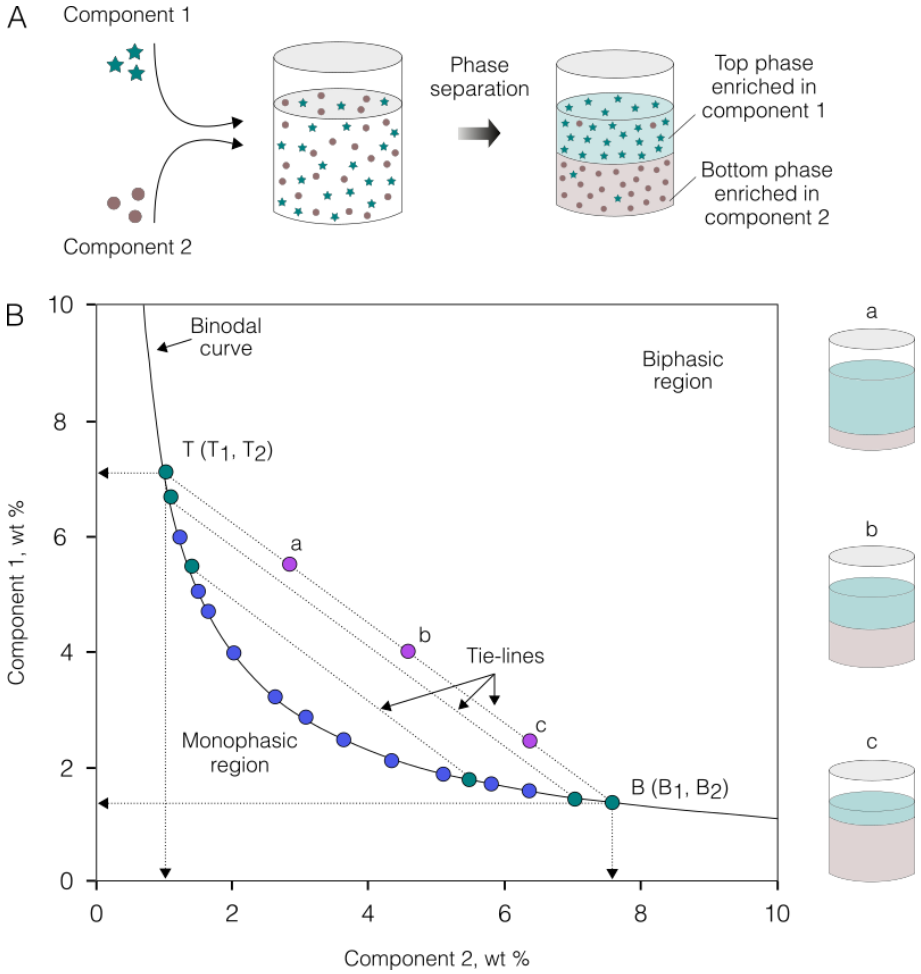

Figure 1.13. A schematic representation of ATPS formation and phase diagram. (**A**) Mixing component 1 and component 2 in an aqueous solution above the critical concentrations induces the formation of two phases: the top phase enriched in component 1 and the bottom phase enriched in component 2. (**B**) Any composition of concentrations of two phase-forming components above the binodal curve results in two separate phases. Point b represents an initial aqueous solution with defined weight fractions of the two components. A tie-line connects the points representing the compositions of the equilibrated top phase (T), bottom phase (B), and the initial point (b). Any polymer composition on the same tie-line (e.g., a, b, and c) will result in similar equilibrated top and bottom phases but with different volume ratios. The schematic was adapted from the book chapter (177).

1.3.3. ATPS-related microfluidic platforms

As mentioned above, ATPSs are mainly associated with liquid-liquid extraction platforms for recovery, concentration, and purification. However, partitioning and phase separation in bulk could be prolonged processes, leading to unacceptably long equilibrium times. This should be avoided, especially when working with sensitive biological samples, such as mammalian cells. These difficulties have been partly addressed through the transfer of ATPS to a microfluidic format (181-183). In the later work (183), the authors utilized a droplet-based microfluidic system to generate an ATPS in which aqueous droplets consist of two phases in the form of a double emulsion, with a PEG layer completely enveloping a dextran droplet. The authors revealed three important points: (i) phase separation and cell partitioning could be achieved in seconds, (ii) the cell surface properties dictate cell partitioning mode, and, more importantly, (iii) ATPS, composed of PEG and dextran form a core-shell structure, which became a starting point for semi-permeable microcapsule generation described in this thesis.

1.3.4. ATPS-based hydrogel microcapsules

Although different approaches for producing microcapsules have been reported (33,169,171,184-186), the use of two-phase polymer solutions provides a more convenient and reliable strategy to generate compartments with a core-shell topology. Before conducting this research, several microfluidic approaches based on ATPS were introduced (42,43,187). However, at the start of this work, there were no practical solutions that would demonstrate both the reliable microcapsule generation under physiological conditions and their application to multi-step biological workflows.

The use of microcapsules for single-cell analysis relies on the ability to produce controllable size monodisperse core-shell particles, which could effectively retain the isolated cells. To achieve that, the core and shell parts of a microcapsule need to be concentric to ensure that the core does not touch the shell creating a cup-like morphology (187,188). While this morphology can also be used for single-cell analysis (188), the inability to reliably enclose cells within the shell limits the broader applications of these particles. Also, to be practical in use, the shell surrounding the microcapsule core should retain high molecular weight biomolecules, such as gDNA, mRNA, and PCR amplicons, while allowing diffusion of smaller molecules (e.g., enzymes, oligonucleotides). High microcapsule stability under different chemical,

physical, and mechanical treatments, related to a specific assay, are prerequisite features.

The first report showing ATPS-based semi-permeable microcapsule generation, cell encapsulation, and amplification of nucleic acids originated during the course of this work (44,46) and is being discussed in greater details in the results section. The said microcapsules were based on a PEGDA-dextran system, where dextran forms the core and PEGDA forms the shell (**Figure 1.14**), and in contrast to other reports, were characterized by highly concentric core/shell structure. Interestingly, almost in parallel, another elegant system was published aiming to generate hydrogel microcapsules using a similar composition (189). In that work, dextran and two kinds of tetra-arm polyethylene glycol macromonomers were used to achieve phase separation resulting in a dextran-rich core and a tetra-PEG macromonomer-rich shell. Tetra-PEG macromonomers in the shell then became cross-linked via the end-coupling reaction, which converted ATPS droplets to semi-permeable microcapsules. Although being a very promising strategy, this and other later works (190) did not aim to explore biological applications, remaining unclear about the potential for single-cell research.

PEGDA microcapsules developed in this work were applied for whole-genome amplification, single bacterial culture, and metabolic activity screening of single-cell derived colonies. Other researchers recognized these microcapsules as a powerful tool for single-cell approaches in human microbiome research (191) and even space biology (192). In addition, others have adapted this approach to develop a high-throughput screening system (193).

Despite its initial success, the work reported in ref. (44) highlighted several limitations of the PEGDA microcapsules. These included the inability to break the shell under chemically mild conditions and mammalian cell partitioning at the water/oil interface resulting in their poor retention. In order to make microcapsule production applicable to mammalian cell analysis, culture, and recovery, an alternative strategy was developed (see results section). This new strategy was based on a biodegradable, polyampholyte polymer (gelatin methacrylate), which could be dissolved by simply adding collagenase enzyme to release the encapsulated cells without damaging them. Gelatin-based shells also provide encapsulated cells with a collagen-like matrix to adhere to and maintain their viability over long periods of time. Further details of using such microcapsules are provided in the results and discussion section.

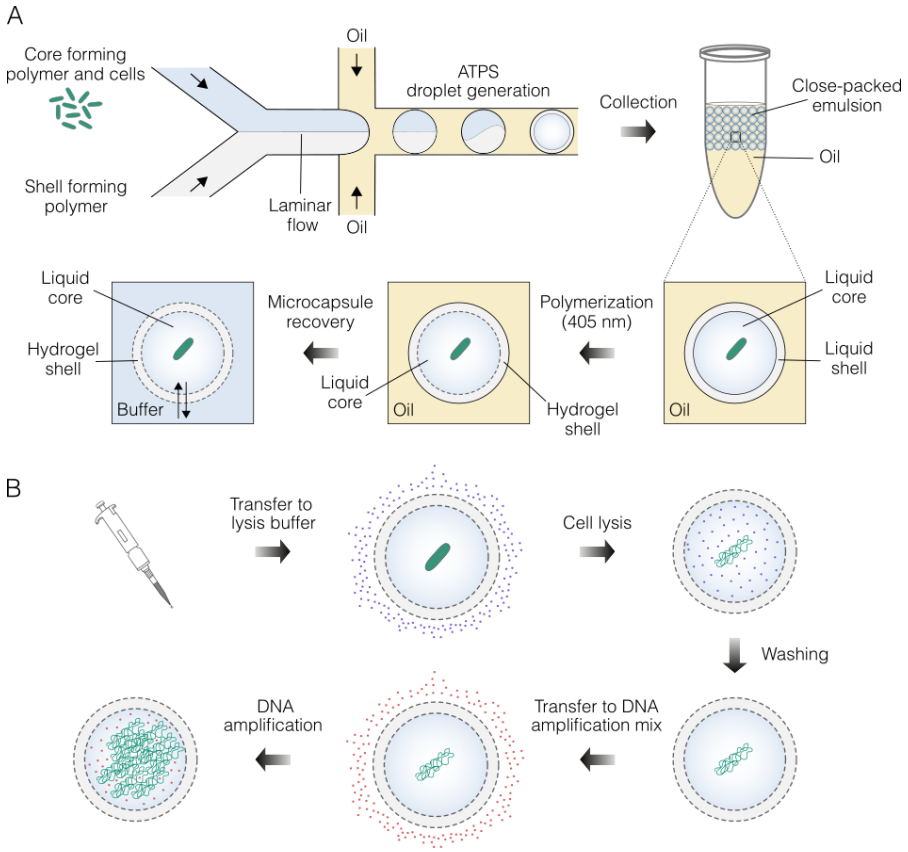

Figure 1.14. ATPS-based hydrogel microcapsule production, properties and applications. (**A**) The core and shell-forming polymers are infused via separate inlets using a co-flow microfluidic device. After encapsulation, two phases are formed: a liquid core enriched in dextran and a liquid shell enriched in PEGDA. The liquid shell is then converted to a semi-permeable hydrogel membrane by photopolymerization, and the resulting microcapsules are recovered from the oil phase and transferred to an aqueous buffer. (**B**) The hydrogel shell retains the isolated cells and high molecular weight biomolecules (e.g., gDNA, mRNA) while at the same time allowing the diffusion of smaller molecules (e.g., enzymes, culture media components). This selective permeability allows to perform different nucleic acid analyses on isolated species.

2. MATERIALS AND METHODS

2.1. PEGDA microcapsule generation and application

2.1.1. Fabrication and use of microfluidic devices

The polydimethylsiloxane (PDMS) microfluidic device having microchannels 20 μm height was obtained from Droplet Genomics (**Figure 2.1**).

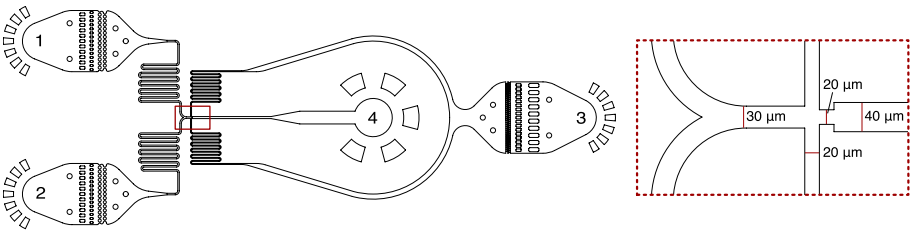

Figure 2.1. Microfluidic chip design used in this work to generate PEGDA microcapsules. Numbers indicate: 1 and 2 – inlets for aqueous phase injection, 3 – inlet for carrier oil injection, 4 – outlet for generated emulsion collection.

2.1.2. Aqueous two-phase system preparation

Aqueous two-phase systems (ATPSs) were prepared using 5.5 % (w/v) dextran, MW ~500k (Sigma-Aldrich, cat. no. D5251), 3 % (w/v) PEGDA, MW 8k (Fisher Scientific, cat. no. AA46801MD), 3 % (v/v) PEGDA, MW 575 (Sigma-Aldrich, cat. no. 437441-100ML), 0.1 % (w/v) lithium phenyl-2,4,6-trimethyl-benzoyl phosphinate (LAP) (Sigma-Aldrich, cat. no. 900889-5G) in 1x DPBS (Gibco, cat. no. 14190144). Other concentrations of PEGDA polymers could be used following **Table 2.1**. In all compositions tested, the concentrations of dextran and LAP were constant.

Table 2.1. Alternative microcapsule shell compositions and tested applications.

Composition	Tested application
3 % (w/v) PEGDA, MW 8K, 3 % (v/v) PEGDA, MW 575	Bacteria culture, MDA, PCR (≥567 bp)
2.5 % (w/v) PEGDA, MW 8k, 4 % (v/v) PEGDA, MW 575	Bacteria culture, MDA, PCR (≥567 bp)
2.1 % (w/v) PEGDA, MW 8k, 5 % (v/v) PEGDA, MW 575	PCR (≥567 bp)

The solutions containing all components were mixed and centrifuged at ≥10.000g for 30 min. to induce liquid-liquid phase separation. The bottom (dextran-rich) phase and upper (PEGDA-rich) phase were separated by pipetting. The dextran-rich phase was used to resuspend cells. Separated

phases were loaded onto a microfluidic device using a 1 ml syringe connected via 0.56 mm inner diameter PTFE tubing (Droplet Genomics, cat. no. DG-MT0.56-30) and encapsulated as described in section 2.1.4.

2.1.3. Microbial cell preparation

Escherichia coli strains (MG1655 and DH5α) were from the laboratory collection. *Rhodococcus rhodochrous* PY11 (DSM 101666), as well as pBHR68 and pTZ18R plasmids, were provided by Prof. Rolandas Meškys (Vilnius University Institute of Biochemistry, Lithuania). *Streptococcus mutans* UA159 was provided by Prof. Edita Sužiedėlienė (Vilnius University Institute of Biosciences, Lithuania).

For nucleic acid amplification *E. coli* MG1655, *R. rhodochrous* PY11, and *S. mutans* UA159 were used. Before *E. coli* MG1655 encapsulation, 5 µl of night cell culture were inoculated in 5 ml of Luria-Bertani (LB) broth (Invitrogen, cat. no. 12795027) and incubated for 2.5-3 hours at 37 °C and 220 rpm, resulting in OD600 value ~0.5. A 1 ml of fresh cell suspension was aliquoted, washed twice in Cell Washing Buffer comprised of 1x DPBS and 0.1 % Pluronic F-68 (Gibco, cat. no. 24040032), and concentrated 10-times in 1x DPBS. Then, 3 µl of concentrated bacterial suspension were combined with 47 µl of dextran-rich phase, resulting in ~30M cells/ml (detailed calculations are provided in **Table 2.2**). To encapsulate *R. rhodochrous* PY11 and *S. mutans* UA159, colonies were taken by scraping a plate, rinsed in Cell Washing Buffer, and resuspended in 1x DPBS. Cells were encapsulated at a limiting dilution following the calculations provided in **Table 2.2.**

Table 2.2. Calculations showing cell numbers used for encapsulations.

Specifications	**Numbers**
Droplet diameter	26-27 µm
Droplet volume	10 pl
Volume of loaded polymers (PEGDA and dextran)	100 µl (50 µl + 50 µl)
Number of generated droplets	100 µl/10 pl = 10M
Lambda value (λ)	0.3
Number of encapsulated cells	10M x 0.3 = 3M
3M bacterial cells should be added in 50 µl of dextran-rich phase	
Cell concentration in LB culture with OD600 of 0.5	1 x 10^8 cells/ml
Cell concentration of 10-times concentrated cell suspension	1 x 10^9 cells/ml
Volume of cell suspension needed for encapsulation	3 µl

For bacteria cultivation experiments, both *E. coli* MG1655 and DH5α were used. *E. coli* MG1655 cells were prepared using the same procedure as described above. DH5α cells were first transformed using $CaCl_2$ with pBHR68

plasmid, harboring three genes (*phaC*, *phaA*, and *phaB*) from the PHB synthesis pathway. As a negative control, DH5α transformed with pTZ18R vector was used. Colonies of transformed *E. coli* DH5α were taken by scraping a plate, rinsed in Cell Washing Buffer, and resuspended in 1x DPBS. Cells were encapsulated at a limiting dilution following the calculations provided in **Table 2.2.** Encapsulating DH5α, the dextran-rich phase was supplemented with 100 μg/ml ampicillin (Sigma-Aldrich, cat. no. A9518-5G).

2.1.4.PEGDA microcapsule generation and cross-linking

PEGDA microcapsules were generated on a microfluidics platform Onyx (Droplet Genomics) using a microfluidic device having a nozzle 20 μm deep and 20 μm wide (**Figure 2.1**). Typical flow rates were: 50 μl/h for the PEGDA-rich phase, 50 μl/h for the dextran-rich phase, and 250-500 μl/h for droplet stabilization oil (Droplet Genomics, cat. no. DG-DSO-20). Due to the increased viscosity of the biphasic system, droplet breakup by jetting mechanism could be observed, which could shift to the dripping mode by adjusting the flow rates of a system. The dilution of cells was chosen such that the majority of microcapsules would contain either 0 or 1 cell (occupancy ~0.1-0.3). The encapsulations were performed at room temperature for up to 30-60 min. The isolated cells were collected in a 1.5 ml tube prefilled with 200 μl of light mineral oil (Sigma-Aldrich, cat. no. M5904-500ML). Following cell encapsulation, the resulting ATPS droplets quickly formed a core-shell structure comprising a liquid core enriched in dextran and a liquid shell enriched in PEGDA. The ATPS droplets were immediately cross-linked by exposure to 365 nm wavelength light using High-Intensity UV Inspection Lamp (UVP, cat. no. 95-0127-01) for 2.5 min. In cases when isolated bacterial cells were used for cultivation, ATPS droplets were exposed to a 405 nm laser (Besram Technology Inc. module TEM00) at 1 W/cm^2 for 20 s or to a 405 nm light-emitting diode (LED) device (Droplet Genomics, cat. no. DG-BR-405) for 20 s as well.

After photopolymerization, the resulting microcapsules were recovered from the oil phase by applying an emulsion breaker (Droplet Genomics, cat. no. DG-EB-1) and 1ml of ice-cold Cell Washing Buffer. When embedded cells were used for culture experiments, microcapsules were kept in Cell Washing Buffer until transferred to culture media. When enzymatic reactions were performed, microcapsules were rinsed twice in a Washing Buffer comprised of 10 mM Tris-HCl [pH 7.5] (Invitrogen, cat. no. 15567027) and 0.05-0.1 % (v/v) Triton X-100 (Sigma-Aldrich, cat. no. X100-100M).

2.1.5.Single *E. coli* genome amplification

Following 2.1.2-2.1.4 sections, *E. coli* MG1655 cells were isolated in PEGDA microcapsules and subjected to lysis and MDA steps. Lysis of embedded bacteria was carried out in 1 ml lysis solution with a composition of 10 mM Tris-HCl [pH 7.5], 50 U/µl Ready-Lyse Lysozyme Solution (Lucigen, cat. no. R1804M), 200 µg/ml proteinase K (Invitrogen, cat. no. AM2546), 0.1 % (v/v) Triton X-100, 1 mM EDTA (Invitrogen, cat. no. 15575020). Closely packed microcapsule suspension occupied ~10 % (100 µl) of the final reaction volume. Cell lysis was performed for 30 min. at 37 °C followed by an additional 30 min. incubation at 50 °C. After lysis, microcapsules were rinsed 3-5 times in Washing Buffer.

Single-genome amplification (SGA) reaction was performed in a 100 µl MDA reaction mix containing 50 µl closely packed microcapsule suspension, 0.5 U/µl phi29 DNA polymerase (TFS, cat. no. EP0092), 0.002 U/µl pyrophosphatase (TFS, cat. no. EF0221), 25 µM exo-resistant random primers (TFS, cat. no. SO181), 1 mM dNTP mix (Invitrogen, cat. no. 18427013), 1 mM DTT (TFS, cat. no. R0861), 1x phi29 DNA polymerase reaction buffer (TFS, cat. no. EP0092), at 30 °C for 12-16 h. Post-SGA microcapsules were rinsed 3 times in Washing Buffer and used for microscopy analysis.

SGA in microcapsules was compared with two related systems – hydrogel beads and W/O droplets. For bacteria embedding in hydrogel beads, 12 % (v/v) PEGDA, MW 575 was co-encapsulated with 1x DPBS containing 3 M/ml cells resulting in 6 % (v/v) PEGDA droplets with a single bacterium inside. All procedures, including encapsulation, polymerization, particle recovery from the emulsion, lysis, and MDA were identical to the microcapsule workflow described above.

To perform *E. coli* lysis and MDA in droplets, bacteria were re-suspended in 10 mM Tris-HCl [pH 7.5] at 3 M/ml concentration and encapsulated at equal flow rates (50 µl/h) with 50 µl of 2x concentrated MDA reaction mix comprising 1 U/µl phi29 DNA polymerase, 0.004 U/µl pyrophosphatase, 100 U/µl Ready-Lyse Lysozyme Solution, 50 µM exo-resistant random primers, 2 mM dNTP mix, 2 mM DTT, 0.2 % (v/v) Triton X-100, and 2x phi29 DNA polymerase reaction buffer. Following encapsulation, bacteria lysis and MDA in droplets were performed at 30 °C for 12-16 h.

2.1.6.Single-genome amplification from gram-positive bacteria

This section is an extension of the previous experiment where SGA was performed on *E. coli* MG1655 cells. In this experiment, seven different lysis

conditions (one condition in W/O droplets and six conditions in microcapsules) were tested on two Gram-positive bacteria: *R. rhodochrous* PY11 and *S. mutans* UA159 (**Table 2.3**). Irrespectively to lysis condition, post-lysis microcapsules were washed 3-5 times in Washing Buffer and subjected to MDA. MDA conditions, including composition, reaction duration, and temperature, were the same as for *E. coli* and are detailed in section 2.1.5. Post-SGA microcapsules were rinsed 3 times in Washing Buffer and used for microscopy analysis.

Table 2.3. Lysis and SGA conditions tested on Gram-positive bacteria. Note that the pH value provided for Tris-HCl buffer corresponds to ~25 °C.

Cond.	Lysis-SGA	First step	Second step	Third step
Ref.	One-step in droplets	50 U/µl Ready-Lyse Lysozyme Solution, 0.1% (v/v) Triton X-100, 1× MDA reaction mix. Incubation for 12 h at 30 °C.	None	None
1.	One-step in microcap.	50 U/µl Ready-Lyse Lysozyme Solution, 0.1% (v/v) Triton X-100, 1× MDA reaction mix. Incubation for 12 h at 30 °C.	None	None
2.	Two-step in microcap.	50 U/µl Ready-Lyse Lysozyme Solution, 0.1% (v/v) Triton X-100, 1 mM EDTA, 10 mM Tris-HCl [pH 7.5]. Incubation for 30 min. at 37 °C.	Microcapsules washed and dispersed in 1x MDA mix for 12 h at 30°C.	None
3.	Two-step in microcap.	50 U/µl Ready-Lyse Lysozyme Solution, 0.1% (v/v) Triton X-100, 1 mM EDTA, 200 µg/ml proteinase K, 10 mM Tris-HCl [pH 7.5]. Incubation at 37 °C for 30 min. followed by 50 °C for 30 min.	Microcapsules washed and dispersed in 1x MDA mix for 12 h at 30°C.	None
4.	Three-step in microcap.	50 U/µl Ready-Lyse Lysozyme Solution, 0.1 % (v/v) Triton X-100, 1 mM EDTA, 10 mM Tris-HCl [pH 7.5]. Incubation for 30 min. at 37 °C.	Addition of 200 µg/ml proteinase K. Incubation for 30 min. at 50 °C.	Microcapsules washed and dispersed in 1x MDA mix for 12 h at 30°C.
5.	Three-step in microcap.	50 U/µl Ready-Lyse Lysozyme Solution, 0.1% (v/v) Triton X-100, 1 mM EDTA, 10 mM Tris-HCl [pH 7.5]. Incubation for 30 min. at 37 °C.	Addition of 200 µg/ml proteinase K and 1% (w/v) SDS. Incubation for 30 min. at 50 °C.	Microcapsules washed and dispersed in 1x MDA mix for 12 h at 30°C.
6.	Two-step in microcap.	0.5 M NaOH and 1% (w/v) SDS. Incubation at room temperature for 5 min.	Microcapsules washed and dispersed in 1x MDA mix for 12 h at 30°C.	None

2.1.7.Microcapsule-based PCR

Following 2.1.2-2.1.4 sections, *E. coli* MG1655 cells were isolated in PEGDA microcapsules and lysed using conditions detailed in 2.1.5 section. PCR in microcapsules was used to amplify the selected regions of *16S rRNA*, *kdsC*, and *ompA* genes corresponding to 320, 567, and 1050 bp fragments, respectively. PCR targeting each gene separately was conducted in a 50 µl reaction mix comprising 0.4 µM forward primer, 0.4 µM reverse primer (**Table 2.4**) and 1x KAPA HiFi HotStart ReadyMix (KAPA Biosystems, cat. no. KK2602). Closely packed microcapsule suspension occupied ~50 % of the final reaction volume. Each sample was thermally cycled through the following program: 95 °C (3 min.), 98 °C (20 s)/60 °C (15 s)/72 °C (30 s) for 35 cycles, and 72 °C (1 min.). Following thermal cycling, microcapsules were rinsed 3 times in Washing Buffer and used for the microscopy analysis.

Table 2.4. Sequences of PCR primers used to conduct PCR in PEGDA microcapsules.

Gene	Forward primer (5'→3')	Reverse primer (5'→3')	Product length
ompA	ATGAAAAAGACAGCTATCG CGATT	TTAAGCCTGCGGCTGAGTTA	1050 bp
kdsC	ATGAGCAAAGCAGGTGCGT C	TCATATCGATTGCCCTTTGG CTTCA	567 bp
16S rRNA	GTTAATACCTTTGCTCATTG A	ACCAGGGTATCTAATCCTGT T	320 bp

2.1.8.Scanning electron microscopy

PEGDA microcapsules were dispersed in water, frozen at -80 °C, and then freeze-dried. Lyophilized PEGDA microcapsules were coated with chromium. The surface morphology analysis was carried out in a dual-beam system of scanning electron microscope Helios Nanolab 650 equipped with an EDX spectrometer from Oxford Instruments.

2.1.9.Imaging of processed bacteria

Droplets, hydrogel beads, and microcapsules before and after lysis and after nucleic acid amplification were stained with 1× SYBR Green I dye (Invitrogen, cat. no. S7563) for 15 min. at room temperature. Stained hydrogels were then rinsed twice in Washing Buffer. The fluorescence intensity was recorded by layering the microcapsules, hydrogel beads, and droplets on a standard hemocytometer (Sigma-Aldrich, cat. no. 717805) and imaging using a Nikon Eclipse Ti microscope, Nikon Digital Sight DS-U3 camera, and CoolLED pE-300 illumination system. Imaging was performed

using the following settings: magnification – 10×, filter – FITC, gain – 1, 20 % intensity of blue light source used for excitation, and exposure times varied depending on the analysis step.

2.1.10. PEGDA microcapsule dissolution and DNA extraction

Microcapsules were dissolved in the presence of 1 M NaOH at 50 °C for 10 min. and then neutralized by adding an equimolar amount of 1 M acetic acid. PCR and MDA products were purified with Agencourt AMPure XP magnetic beads (Beckman Coulter, cat. no. A63881) using a 1.8x volume ratio and analyzed on 1 % agarose gel.

2.1.11. *E. coli* culture in microcapsules and droplets

Following 2.1.2-2.1.4 sections, *E. coli* MG1655 and DH5α cells were isolated in PEGDA microcapsules. Embedded cells were transferred into 30 × 15 mm Petri dishes prefilled with 2 ml of LB broth and incubated at 37 °C for 4-16 h. For transformed DH5α cells, LB broth was supplemented with 100 μg/ml ampicillin. To detect bacteria producing polyhydroxybutyrate (PHB), its synthesis in DH5α cells was induced by adding 1 mM isopropyl β-D-1-thiogalactopyranoside (IPTG) (TFS, cat. no. R1171) followed by incubation at 30 °C for 8 h.

For bacteria culture comparison, *E. coli* MG1655 cells were isolated in W/O droplets containing LB broth. The workflow of bacteria isolation in W/O droplets was similar to that described in the 2.1.5 section within a few modifications: instead of using 10 mM Tris-HCl [pH 7.5], cells were resuspended in LB broth and encapsulated with the second phase comprising LB broth as well.

2.1.12. Imaging of encapsulated bacteria

Microcapsules and droplets with *E. coli* MG1655 cells were stained with 1× SYBR Green I dye and analyzed under an epifluorescence microscope as described above. Microcapsules with *E. coli* DH5α microcolonies were stained for 10 min. with 0.5 μg/ml Nile red (Invitrogen, cat. no. N1142) and rinsed twice in Cell Washing Buffer. The fluorescence intensity was recorded using a Nikon Eclipse Ti microscope, Nikon Digital Sight DS-U3 camera, and CoolLED pE-300 illumination system. Imaging was performed using the following settings: magnification – 10×, filter – TXRED, gain – 1, exposure time – 100 ms, 40 % intensity of green light source for excitation. The second round of imaging was performed after lysis (**Table 2.3**, condition #3) without

the additional staining with Nile red and using the same settings to evaluate the changes in fluorescence signal. For dual *E. coli* DH5α imaging, microcapsules were stained repeatedly with Nile red and SYBR Green I dyes. Images were taken using the following settings: magnification – 10×, filters – FITC and TXRED, gain – 1, exposure time – 10 ms for FITC filter and 40 ms for TXRED, 20 % and 40 % intensity of blue and green light source for excitation, respectively.

2.1.13. Data analysis

Initial analysis of the microscopy data was carried out using Fiji software. Fluorescence data were obtained by manually outlining reaction compartments from brightfield images and then using these masks to segment fluorescence images. Data were analyzed and visualized using R (v.3.5.3) and R studio (v.1.1.463). Fluorescence was reported as logarithmic values. The local minimum was used to set the thresholds separating negative and positive events.

2.2. GMA microcapsule generation and application

2.2.1. Fabrication and use of microfluidic devices

The PDMS microfluidic devices having microchannels 40 µm and 20 µm heights were obtained from Droplet Genomics (**Figure 2.2**).

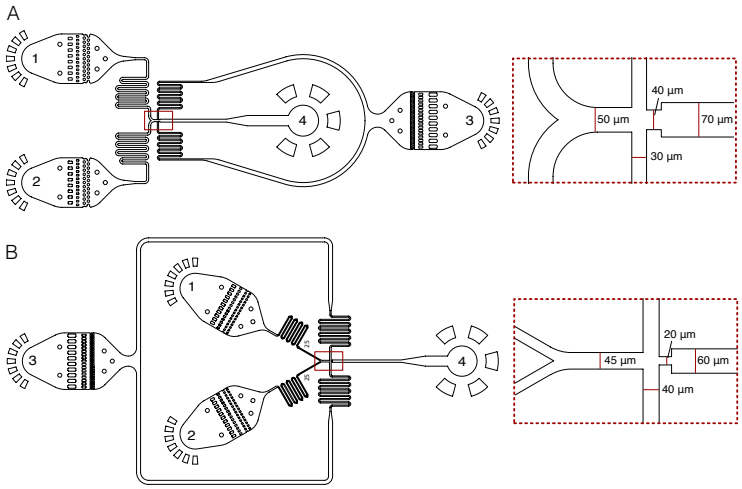

Figure 2.2. Microfluidic chip designs used in this work to generate 75-85 µm (**A**) and 60-65 µm (**B**) diameter GMA microcapsules. Numbers indicate: 1 and 2 – inlets for aqueous phase injection, 3 – inlet for carrier oil injection, 4 – outlet for generated emulsion collection.

2.2.2. Polymer solution preparation

The stock of shell-forming solution comprising 10 % (w/w) GMA (Sigma-Aldrich) dissolved in 1x DPBS was stored at 4 °C in 200 µl aliquots for up to 6 months. Before the experiment, the GMA solution was heated at 40 °C for 30 min., diluted down to 3% (w/v) in 1x DPBS buffer, and centrifuged at 10.000g for 10-15 min. at 37 °C to sediment the impurities originating from the GMA powder. The warm GMA solution was loaded onto a microfluidic device using a 1 ml syringe connected via 0.56 mm inner diameter PTFE tubing. The stock of core-forming solution comprising 30 % (w/w) dextran (Sigma-Aldrich, cat. no. D5251) dissolved in 1x DPBS was stored at 4 °C in 1 ml aliquots for up to 6 months. Before the experiment, the dextran solution was equilibrated at room temperature and diluted down to 15 % (w/v) with cell suspension in 1x DPBS. The dextran solution was loaded onto a microfluidic device using a 1 ml syringe connected via 0.56 mm inner diameter PTFE tubing.

2.2.3. Microcapsule generation and cross-linking

Following cell encapsulation, the resulting ATPS droplets quickly formed a core-shell structure comprising a liquid core enriched in dextran and a liquid shell enriched in GMA. The ATPS droplets were subjected to a two-step polymerization procedure. At first, the W/O droplets were incubated at 4 °C for 15-30 min. to solidify the GMA layer. The resulting intermediate microcapsules, having a liquid core and physically cross-linked GMA shell, were recovered from the oil phase by applying an emulsion breaker and released into Cell Washing Buffer. The suspension of intermediate microcapsules was incubated at room temperature for 5 min., mixed with a 0.1 % (w/v) LAP, and exposed to a low-energy 405 nm LED device for 20 s. The resulting microcapsules contained a liquid core enriched in dextran and a thin (~3 µm) membrane comprising chemically cross-linked polypeptides. Continuing procedures on ice, photopolymerized microcapsules were rinsed twice in Cell Washing Buffer and subjected to cell lysis or cell fixation in ethanol (see below).

2.2.4. Preparation of cells

K-562 (ATCC), HEK293 (ATCC), and NB-4 (kind gift by Dr. V.V. Borutinskaite, Vilnius University Institute of Biochemistry, Lithuania) cells were cultured in Iscove's Modified Dulbecco's Medium (Gibco, cat. no. 31980030), Dulbecco's Modified Eagle's Medium (Gibco, cat. no. 61965026),

and Roswell Park Memorial Institute (RPMI) 1640 Medium (Gibco, cat. no. 11875085), respectively, supplemented with 10 % fetal bovine serum (Gibco, cat. no. 10270-106) and 1x penicillin-streptomycin (Gibco, cat. no. 15140122) at 37 °C in the presence of 5 % CO_2. Cells were collected from a culture dish, washed once in ice-cold Cell Washing Buffer, and then in 1x DPBS. Before the encapsulation, cells were re-suspended in 15 % (w/v) dextran solution at a concentration of 0.1-0.2 M cells/100 µl when a 40 µm height microfluidic device was used. Using a 30 µm height microfluidic device, the final cell concentration in 15 % dextran solution was 0.6M/100 µl. All centrifugation steps were performed at 300g for 5 min. at 4 °C.

2.2.5.Preparation of PBMCs

PBMCs (ATCC, cat. no. PCS-800-011) were thawed from liquid nitrogen using RPMI 1640 Medium supplemented with 10 % fetal bovine serum. Thawed cells were washed twice in an ice-cold Cell Washing Buffer and resuspended in 1x DPBS at a concentration of 12M cells/ml. All centrifugation steps were performed at 300g for 7-10 min. at 4 °C.

2.2.6.Cell encapsulation

Cell isolation in microcapsules was performed on a microfluidics platform Onyx using a microfluidic device having a nozzle 40 µm deep and 40 µm wide (**Figure 2.2**). Typical flow rates were: 250 µl/h for GMA solution, 100 µl/h for dextran solution with cells, and 700 µl/h for droplet stabilization oil. NB4 and PBMC isolation in microcapsules was performed using a microfluidic device having a nozzle 30 µm deep and 20 µm wide. Typical flow rates were: 125 µl/h for GMA solution, 50 µl/h for dextran solution with cells, and 700-800 µl/h for droplet stabilization oil. The dilution of cells was chosen such that the majority of microcapsules would contain either 0 or 1 cell (occupancy ~0.1). The encapsulations were performed at room temperature for up to 30 min. The emulsion was collected in a 1.5 ml tube prefilled with 200 µl of light mineral oil.

2.2.7.Cell fixation in ethanol

To fix the encapsulated cells, the microcapsules were suspended in 70 % (v/v) ice-cold ethanol and stored at -20 °C until further analysis. To rehydrate the fixed cells, the tube with microcapsules was equilibrated on ice for 5 min., centrifuged at 2000g for 2 min. at 4 °C, and then washed once in ice-cold Rehydration Buffer (3x SSC buffer (Invitrogen, cat. no. 15557044)

supplemented with 0.04% BSA, 1 mM DTT and 0.2 U/µl RiboLock RNase Inhibitor (Thermo Fisher Scientific, cat. no. EO0381)). Ethanol fixed cells were permeabilized in a mild-lysis buffer as described below.

2.2.8.Cell lysis

The harsh lysis of encapsulated cells was performed by suspending microcapsules in 1 ml GeneJET RNA Purification Kit Lysis Buffer (TFS, cat. no. K0732) supplemented with 40 mM DTT. Microcapsules were washed in GeneJET Lysis Buffer 3-times, with 1 to 5 min. incubation between the washes. After lysis, the microcapsules were rinsed 5-times in Washing Buffer. During the washes, the centrifugation steps were performed at 2000g for 2 min. at 4 °C.

The mild lysis of encapsulated cells was performed by suspending microcapsules in 1 ml buffer containing 10 mM Tris-HCl [pH 7.5], 0.6 % (v/v) Igepal CA-630 (Sigma-Aldrich, cat. no. I8896-50ML), 40 mM DTT and 10 mM EDTA. The microcapsules were incubated at room temperature for 15 min., rinsed 3-times in Washing Buffer, and then added to the RT reaction mix. During the washes, the centrifugation steps were performed at 2000g for 2 min. at 4 °C.

2.2.9.Genomic DNA depletion

Genomic DNA depletion was performed in a 200 µl DNase I reaction mix containing 100 µl closely packed microcapsule suspension, 0.05 U/µl DNase I (TFS, cat. no. K2981), 0.2 U/µl RiboLock RNase Inhibitor, and 1x DNase I Buffer with $MgCl_2$, at 37 °C for 20 min. Then, additional 5 U of DNase I enzyme were added and incubated for 10 min. at 37 °C. The microcapsules were rinsed 3-5-times in Washing Buffer and then subjected to reverse transcription reaction.

2.2.10. Reverse transcription

Copy DNA synthesis was performed in 200 µl Maxima H Minus RT reaction mix containing 100 µl closely packed microcapsule suspension, 5 µM oligo$(dT)_{21}$ primer (IDT), 0.5 mM dNTP mix, 5 U/µl Maxima H Minus reverse transcriptase (TFS, cat. co. EP0751), 0.2 U/µl RiboLock RNase inhibitor and 1x RT buffer, at 50 °C for 60 min. Every 20 min. microcapsules were briefly dispersed. After cDNA synthesis, the RT enzyme was heat inactivated at 85 °C for 5 min. Then, microcapsules were rinsed 3-times in Washing Buffer and subjected to multiplex PCR. For capturing low abundance transcripts

(e.g., *PML-RARα*), 2.5 µM oligo(dT)$_{21}$ primer was combined with 2.5 µM random hexamer primer (TFS, cat. no. SO142). The RT reaction was initiated by preincubating the reaction mixture at room temperature for 10 min. followed by incubation at 50 °C for 60 min.

2.2.11. Multiplex PCR

Multiplex PCR was performed in a 100 µl reaction mix containing ~50 µl closely packed microcapsule suspension, 0.5 µM forward and 0.5 µM reverse primer (**Table 2.5**), and 1x Phire Tissue Direct PCR master mix (TFS, cat. no. F170L). Samples were thermally cycled through the following program: 98 °C (5 min.), 98 °C (5 s)/64 °C (5 s)/72 °C (20 s) for 30 cycles, 72 °C (1 min.). For capturing low abundance transcripts, at first, the preamplification was performed by 10-cycles of PCR. Then microcapsules were washed twice in Washing Buffer and subjected to 30-cycles PCR using the same conditions as indicated above. Following thermal cycling, microcapsules were treated with 100 U Exonuclease I (NEB, cat. no. M0293L) for 15 min. at 37 °C, rinsed 3-times in Washing Buffer, and used for the subsequent microscopy and flow cytometry analysis.

Table 2.5. Sequences of PCR primers used to conduct multiplex RT-PCR.

Name	**Sequence (5'→3')**	**Product length**
555-*YAP*-forward	Alexa Fluor 555-CCCTCGTTTTGCCATGAACC	584 bp
YAP-reverse	CCAGTGTTCCAAGGTCCACA	
488-*PTPRC*-forward	Alexa Fluor 488-ACATTGCTGCACAAGGTCCCAG	532 bp
PTPRC-reverse	AACCATCAGGCATCTCTGTCGC	
647-*ACTB*-forward	Alexa Fluor 647-ATTCCTATGTGGGCGACGA	607 bp
ACTB-reverse	AATGGTGATGACCTGGCCG	
647-*B2M*-forward	Alexa Fluor 647-AGCAGCATCATGGAGGTTTGA	513 bp
B2M-reverse	CCAGATTAACCACAACCATGCC	
647-*TBP*-forward	Alexa Fluor 647-GCGCAAGGGTTTCTGGTTTG	539 bp
TBP-reverse	TTTGCAGCTGCGGTACAATC	
555-*PML-RARα*-forward	Alexa Fluor 555-AGCGCGACTACGAGGAGAT	688 bp
PML-RARα-reverse	CTGCTGCTCTGGGTCTCAAT	
546-*BCR-ABL*-forward	Alexa Fluor 546-GAAGTGTTTCAGAAGCTTCTCC	417 bp
BCR-ABL-reverse	GTTTGGGCTTCACACCATTCC	

2.2.12. Post-RT-PCR microcapsule staining

Optional. To identify microcapsules with isolated cells in the separate channel than PCR amplicons, post-RT-PCR microcapsules were immersed in a Washing Buffer containing 300 nM of 4',6-diamidino-2-phenylindole dihydrochloride-DAPI (Invitrogen, cat. no. D1306) and incubated in the dark

on ice for 10 min. Then microcapsules were washed 3-times in Washing Buffer and used for the subsequent microscopy and flow cytometry analysis.

2.2.13. Fluorescence microscopy analysis

The fluorescence intensity was recorded by layering the microcapsules on a standard hemocytometer and imaging them under a Nikon Eclipse Ti-E microscope with DAPI, GFP, RFP, and Cy5 fluorescence filter sets. Imaging settings were kept the same per experiment with an exposure time of 400 ms and the gain value set at 1.0. The microscope objective was CFI Plan Fluor 10x (N.A. 0.30, W.D. 16.0 mm). For each analysis, at least 10 brightfield and fluorescence images (~200 microcapsules per image) were recorded with Nikon DS-Qi2 digital camera.

2.2.14. Flow cytometry

The microcapsules were washed twice in Washing Buffer, filtered through a 100 µm cell strainer (Corning, cat. no. 431752), and loaded onto the Partec CyFlow Space and BD FACSAria III FACS instruments. The microcapsules were detected using forward scatter, side scatter, and fluorescence channels and by recording signal area. Isolated cells in microcapsules were detected by measuring signal height in the DAPI channel on the BD FACSAria III FACS instrument.

2.2.15. RT-qPCR

Bulk RT-qPCR was conducted using the QuantStudio-1 real-time PCR system (TFS). The total RNA from K-562, HEK293, NB-4, and PBMCs were extracted using the GeneJET RNA Purification kit (TFS, cat. no. K0732). The gDNA traces were depleted by RapidOut DNA removal kit (TFS, cat. no. K2981). cDNA synthesis was performed in 50 µl Maxima H Minus RT reaction mix comprising 40 ng/µl total RNA (with PBMCs, final RNA concentration was 5 ng/µl), 5 µM oligo$(dT)_{21}$ primer, 0.5 mM dNTP mix, 5 U/µl Maxima H Minus reverse transcriptase, 2 U/µl RiboLock RNase inhibitor, and 1x RT Buffer, at 50 °C for 30 min. After cDNA synthesis, the RT enzyme was heat inactivated at 85 °C for 5 min. Then, cDNA material was diluted 10-fold in nuclease-free water and used directly for qPCR. qPCR was performed in 10 µl reaction volume comprising 2 µl cDNA, 5 µl 2x Maxima SYBR Green/ROX qPCR master mix (TFS, cat. no. K0221), and 3 µl of 1 µM forward/reverse primer mix (**Table 2.6**). Each sample had three technical replicates. Samples were thermally cycled through the following program:

95 °C (10 min.), 95 °C (15 s)/60 °C (30 s)/72 °C (60 s) for 40 cycles, and the number of threshold cycles (Ct) for each marker gene was recorded using software provided with the QuantStudio-1 instrument.

Table 2.6. Sequences of PCR primers used to conduct quantitative PCR.

Name	Sequence (5'→3')	Product length
YAP-forward	CCCTCGTTTTGCCATGAACC	584 bp
YAP-reverse	CCAGTGTTCCAAGGTCCACA	
PTPRC-forward	ACATTGCTGCACAAGGTCCCAG	532 bp
PTPRC-reverse	AACCATCAGGCATCTCTGTCGC	
ACTB-forward	ATTCCTATGTGGGCGACGA	607 bp
ACTB-reverse	AATGGTGATGACCTGGCCG	
B2M-forward	AGCAGCATCATGGAGGTTTGA	513 bp
B2M-reverse	CCAGATTAACCACAACCATGCC	
TBP-forward	GCGCAAGGGTTTCTGGTTTG	539 bp
TBP-reverse	TTTGCAGCTGCGGTACAATC	
PML-RARα-forward	AGCGCGACTACGAGGAGAT	688 bp
PML-RARα-reverse	CTGCTGCTCTGGGTCTCAAT	
BCR-ABL-forward	GAAGTGTTTCAGAAGCTTCTCC	417 bp
BCR-ABL-reverse	GTTTGGGCTTCACACCATTCC	

2.2.16. Double-stranded DNA retention in microcapsules

GeneRuler Low Range DNA ladder (TFS, cat. no. SM1191) was mixed with 30 % (w/w) dextran at a ratio 1:1 and encapsulated using the standard procedure described above. Following DNA encapsulation, the emulsion was transferred to 4 °C for 60 min. 30 µl aliquot of an emulsion was removed from the tube, broken, and treated with 0.5 µl of 20 mg/ml proteinase K (TFS, cat. no., EO0491) for 10 min. at 37 °C. Then 10 µl of sample were combined with 2 µl of Gel Loading Dye, Purple (6x) (NEB, cat. no. B7024S) and analyzed on 3% agarose gel in 1x TAE buffer. This sample was considered as a control, since no DNA loss was expected. The remaining (~ 150 µl) of emulsion was converted to microcapsules as follows. The physically cross-linked (intermediate) microcapsules were released from the W/O emulsion by adding 50 µl of emulsion breaker, washed once in 1 ml ice-cold Cell Washing Buffer and pelleted at 500g for 2 min. at 4 °C. 30 µl aliquot of physically cross-linked microcapsules was combined with 1 ml of ice-cold Cell Washing Buffer and incubated on ice for 30 min. Then, the microcapsules were rinsed twice in ice-cold Cell Washing Buffer, pelleted by centrifugation and treated with 0.5 µl of 20 mg/ml proteinase K at 37 °C for 10 min. Next, 10 µl of the treated sample were combined with 2 µl of Gel Loading Dye, Purple (6x) and analyzed on 3 % agarose gel in 1x TAE buffer. The remaining (physically cross-linked) microcapsules were dispersed in 1 ml of ice-cold Cell Washing Buffer

supplemented with photo-initiator (0.1% (w/v) LAP) and cross-linked by a 20 s exposure to a 405 nm LED device. Photopolymerized microcapsules were rinsed once in Cell Washing Buffer and then divided into 4 tubes at equal 30 µl portions. 1 ml of Cell Washing Buffer was added to each tube and microcapsule suspensions were incubated for 30 min. at different temperatures: 4 °C, 22 °C, 50 °C, and 70 °C. Then, the microcapsules incubated on ice (4 °C) were rinsed twice in an ice-cold Cell Washing Buffer and pelleted by centrifugation. The microcapsules incubated at 22-70 °C were rinsed twice in room temperature Cell Washing Buffer and pelleted by centrifugation. 30 µl of microcapsule suspension from each tube were treated with 0.5 µl of 20 mg/mL proteinase K and incubated at 37 °C for 10 min. Finally, 10 µl of each treated sample were combined with 2 µl of Gel Loading Dye, Purple (6x) and analyzed on 3% agarose gel in 1x TAE buffer. In an alternative approach, a photoinitiator was added at the beginning of ATPS droplet generation (final concentration 0.1 %) and photopolymerized after temperature-induced gelation, omitting cured microcapsule storage in an aqueous buffer. The remaining steps were identical to those described above.

2.2.17. RNA leakage among microcapsules

To investigate RNA leakage, blank microcapsules (without cells) were immersed in 200 µl Maxima H Minus RT reaction mixture containing 5 µM oligo$(dT)_{21}$ primer, 0.5 mM dNTP mix, 5 U/µl Maxima H Minus reverse transcriptase, 0.2 U/µl RiboLock RNase inhibitor, 1x RT Buffer, 5 ng/µl total RNA purified from K-562 cells, and 5 ng/µl total RNA purified from HEK293 cells. Microcapsules occupied half of the final reaction volume (100 µl). RT step was conducted at 50 °C for 60 min. Every 20 min. microcapsules were briefly dispersed. After cDNA synthesis, the RT enzyme was heat inactivated at 85 °C for 5 min. Then, microcapsules were rinsed 3-times in Washing Buffer and subjected to multiplex PCR targeting *ACTB*, *PTPRC*, and *YAP*. The post-RT-PCR microcapsules (n ~1000) were analyzed under the epifluorescence microscope.

2.2.18. Time-lapse of microcapsule decomposition

400 µl of diluted microcapsule suspension in Cell Washing Buffer was transferred into one well of a 12-well cell culture plate (Corning, cat. no., 10253041), fixed on the Nikon Eclipse Ti microscope, and left for sedimentation for 2 min. Then, 20 µl of collagenase A (final concentration 1 mg/ml) or 4 µl of proteinase K (final concentration 0.2 mg/ml) were added,

and decomposition was recorded every 5 s using a Nikon Digital Sight DS-U3 camera.

2.2.19. Mammalian cell culture in microcapsules

A549 (ATCC) and Jurkat (ATCC) cells were cultured in DMEM and RPMI 1640 media, respectively, supplemented with 10 % fetal bovine serum and 1x penicillin-streptomycin at 37 °C in the presence of 5 % CO_2. Cells were collected from a culture dish and washed twice in complete culture medium. Before the encapsulation, cells were mixed with 30 % (w/w) dextran solution at a ratio 1:1. Cell concentration in dextran solution was 0.2 M cells/100 µl. Cell isolation in microcapsules was performed on a microfluidics platform Onyx using a microfluidic device having a nozzle 40 µm deep and 40 µm wide (**Figure 2.2, A**) as detailed in section 2.2.6.

Following cell encapsulation, the W/O droplets were incubated at 4 °C for 15-30 min. to solidify the GMA layer. The resulting intermediate microcapsules were recovered from the oil phase by applying an emulsion breaker and released into 400 µl Cell Washing Buffer and 500 µl complete culture media. The suspension of intermediate microcapsules was incubated at room temperature for 5 min., mixed with a 0.1 % (w/v) LAP, and exposed to a low-energy 405 nm LED device for 20 s. Continuing procedures on ice, photopolymerized microcapsules were rinsed 3-times in complete culture media. Photopolymerized microcapsules were transferred to a 60 x 15 mm Petri dish (Cat. no., CLS430166), prefilled with 5 ml of complete culture media, and incubated at 37 °C in the presence of 5 % CO_2. Embedded cells/spheroids were passaged every 3-4 days. To do this, microcapsule suspension was loaded through a 40 µm cell strainer (Corning, cat. no., 352340) and rinsed with 5 ml of complete culture media. Then, keeping a cell strainer in an inverted position, microcapsules were recovered into a new Petri dish using 5 ml of a complete culture medium.

2.2.20. Data analysis

Cell retention in microcapsules. To evaluate K-562 and Jurkat cell retention, 34 bright-field images were recorded for each cell sample: 17 images for W/O droplets and 17 images for microcapsules. Each image contained at least 100 microcapsules. For each image, the occupancy (lambda value, λ) of cells was estimated. Then, distribution normality was verified by applying Lilliefors (Kolmogorov-Smirnov) normality test. The calculated p-values were 0.4283 (K-562) and 0.7784 (Jurkat), which confirmed a normal data distribution. Then F-test for homogeneity of variance was applied. The

calculated p-values were 0.0282 (K-562) and 0.7868 (Jurkat). Assuming equal variance between cell occupancy in droplets and microcapsules, an independent sample t-test was performed for the Jurkat sample and a Welch t-test for the K-562 sample (under a two-sided alternative hypothesis). Occupancy measurements were visualized using Python 3.7.6, Pandas framework, and Seaborn library.

DNA retention in microcapsules. DNA fragment retention was quantified by measuring the DNA band intensity on an agarose gel. Each DNA fragment retention value was averaged from three independent measurements and analyzed using a Fiji software package. The measurements were visualized using Python 3.7.6, Pandas framework, and Seaborn library.

Microscopy analysis of post-RT-PCR microcapsules. Microcapsules from bright-field images were analyzed using a Python script. Microcapsules were outlined using the Hough circle transform and the masks were used to crop and measure mean and max fluorescence from the images obtained using corresponding DAPI, GFP, RFP filters. Measurements were processed and visualized using Python 3.7.6, Pandas framework, and Seaborn library.

Flow cytometry data analysis. Flow cytometry data were analyzed and visualized using FCS Express 7 software (version 7.12.0005). The post-RT-PCR microcapsules after harsh lysis were analyzed using the Partec CyFlow Space FACS instruments. The gating process was performed in the following manner: 1) gating the microcapsules based on forward *vs.* side scatter signal, 2) gating *ACTB* positive events based on Alexa Fluor 647 *vs.* side scatter signal, 3) analyzing *PTPRC* and *YAP* marker abundance based on Alexa Fluor 488 *vs.* Alexa Fluor 555 signal. All measurements were performed by analyzing the signal area. Note that due to the spillover of Alexa Fluor 488 to the Alexa Fluor 555 channel and the imperfect compensation process, the *PTPRC*-positive population showed increased intensity in Alexa Fluor 555 channel when measurements were performed using Partec CyFlow Space FACS instrument.

The post-RT-PCR microcapsules after mild lysis on NB-4 and PBMCs were analyzed using the BD FACSAria III FACS instrument. The gating process was performed in the following manner: 1) gating the microcapsules with isolated cells based on Alexa Fluor 488 (*PTPRC*) signal area *vs.* DAPI-stained nuclei fluorescence signal height, 2) gating *PML-RARα* positive events based on Alexa Fluor 488 signal area *vs.* Alexa Fluor 555 signal area.

Sensitivity, specificity, and positive/negative predictive values. The microcapsules carrying a cell and being positive for one of the marker genes (*ACTB*, *B2M*, *TBP*, *PTPRC*, *YAP*) were counted as true positives. The microcapsules carrying no cells and showing no fluorescence were counted as

true negatives. The false positives were microcapsules lacking cells but being fluorescent for one of the marker genes. The false negatives were microcapsules with cells displaying no signal for any marker gene. The following statistical values were defined as:

$$\text{Sensitivity} = (\text{TruePos}/(\text{TruePos} + \text{FalseNeg})) \times 100\%;$$
$$\text{Specificity} = (\text{TrueNeg}/(\text{TrueNeg} + \text{FalsePos})) \times 100\%;$$
$$\text{PPV} = (\text{TruePos}/(\text{TruePos} + \text{FalsePos})) \times 100\%;$$
$$\text{NPV} = (\text{TrueNeg}/(\text{TrueNeg} + \text{FalseNeg})) \times 100\%.$$

2.3. Single-cell RNA sequencing

2.3.1. Fabrication and use of microfluidic devices

The PDMS microfluidic device used for RNA barcoding experiments was obtained from Droplet Genomics (**Figure 2.3**).

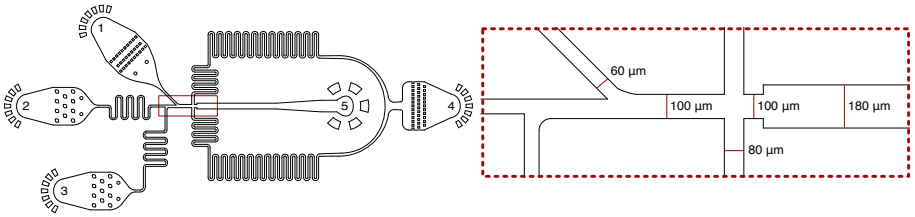

Figure 2.3. Microfluidic chip design used in this work to perform RNA barcoding. Numbers indicate: 1 – inlet for barcoding bead injection, 2 – inlet for RT reaction mix injection, 3 – inlet for microcapsule injection, 4 – inlet for carrier oil injection and 5 – outlet for generated emulsion collection.

2.3.2. Preparation of mammalian cells

K-562 and NIH-3T3 cells (from the ATCC collection) were cultured in IMDM and DMEM media, respectively, supplemented with 10 % fetal bovine serum and 1x penicillin-streptomycin at 37 °C in the presence of 5 % CO_2. Cells were collected from a culture dish, washed twice in an ice-cold Cell Washing Buffer, and re-suspended in 1x DPBS at a concentration of 4 M/ml. All centrifugation steps were performed at 300g for 5 min. at 4 °C. K-562 and NIH-3T3 cell suspensions were mixed at equal volumes and then diluted in 15 % (w/v) dextran solution at a concentration of 0.2 M cells/100 µl. Cell isolation in GMA microcapsules was performed on a 40 µm height microfluidic device as described in sections 2.2.3 and 2.2.6.

Isolated cells were subjected to harsh lysis, as described in section 2.2.8, followed by gDNA depletion, as detailed in section 2.2.9. The microcapsules were washed twice in Washing Buffer and filtered through a 100 µm cell

strainer. Before the barcoding step, microcapsules were washed 3-times in Hydrogel Loading Buffer with a composition of 1x Maxima H Minus RT reaction buffer and 0.6 % Igepal CA-630, closely packed, and loaded onto a microfluidic device (**Figure 2.3**) using a 1 ml syringe connected via 0.56 mm inner diameter PTFE tubing.

2.3.3. Preparation of bacterial cells

Bacteria used in this experiment were from the laboratory collection. A single colony of *E. coli* MG1655 and *B. subtilis* 23857 was inoculated into separate tubes with 5 ml LB broth and cultivated overnight at 30 °C and 220 rpm. Then, 5 µl of night *E. coli* culture and 50 µl of night *B. subtilis* culture were inoculated into separate tubes with 5 ml of fresh LB broth and incubated at 30 °C and 220 rpm for ~4-5 h. 1 ml of each culture was then aliquoted, washed twice in Cell Washing Buffer, and resuspended in 1x DPBS at OD600 ~2.0. 2.5 µl of *E. coli* suspension and 2.5 µl of *B. subtilis* suspension were combined with 95 µl of 15 % (w/v) dextran solution. Bacteria isolation in microcapsules was performed on a microfluidics platform Onyx using a microfluidic device having a nozzle 20 µm deep and 20 µm wide (**Figure 2.1**). Typical flow rates were: 50 µl/h for 3 % (w/v) GMA solution, 20 µl/h for 15 % (w/v) dextran solution with cells, and 400 µl/h for droplet stabilization oil. The dilution of cells was chosen such that most microcapsules would contain either 0 or 1 cell (occupancy ~0.1). The encapsulations were performed at room temperature for ~1 h. The emulsion was collected in a 1.5 ml tube prefilled with 200 µl of light mineral oil and subjected to a two-step polymerization procedure as detailed in section 2.2.3.

Microcapsules with isolated bacteria were resuspended in 2 ml of LB media and incubated at 30 °C for 30 min. Note that the incubation time could be adjusted to control the number of cells per microcapsule. After the incubation, the microcapsules were collected in a 1.5 ml tube, spun down at 1000g for 2 min., and subjected to a lysis step.

2.3.4. Bacteria lysis and gDNA depletion

To lyse the encapsulated bacteria, microcapsules were first washed once in 1 ml buffer containing 10 mM Tris-HCl, pH [7.5], 100 mM NaCl, 1mM EDTA, and 0.1 % Triton X-100. Microcapsules were then centrifuged at 1000g for 2 min., and the supernatant was replaced with lysis buffer containing 10 mM Tris-HCl, pH [7.5], 100 mM NaCl, 1mM EDTA, 0.1 % Triton X-100, and 50 U/µl Ready-Lyse Lysozyme Solution (Lucigen, cat. no.

R1810M). After incubation at room temperature for 15 min., microcapsules were centrifuged and immersed in 1 ml GeneJET RNA Purification Kit Lysis Buffer supplemented with 40 mM DTT. Following 5 min. incubation at room temperature, the microcapsules were washed 4-5 times with Washing Buffer. During the washes, centrifugations were performed at 2000g for 2 min. at 4 °C. Finally, microcapsules were resuspended in 70 % ice-cold ethanol and stored at -20 ºC until further analysis.

To rehydrate the fixed cells, the tube with microcapsules was equilibrated on ice for 5 min., centrifuged at 2000g for 2 min. at 4 °C, and then washed 3-times in Washing Buffer. The supernatant was aspirated and closely packed microcapsules were subjected to the gDNA depletion step described in section 2.2.9. After gDNA depletion, the microcapsules were rinsed 3-5-times in Washing Buffer and then subjected to the polyadenylation step.

2.3.5.RNA polyadenylation

RNA polyadenylation was performed in 200 µl Poly(A) polymerase reaction mix (NEB, cat. no. M0276L) containing 100 µl closely packed microcapsule suspension, 1 mM ATP, 0.4 U/µl *E.coli* Poly(A) polymerase, and 1x Reaction Buffer, at 37 °C for 30 min. Every 15 min., microcapsules were briefly dispersed. After RNA polyadenylation, the microcapsules were washed twice in Washing Buffer and filtered through a 70 µm cell strainer (Corning, cat. no. 431751). Before the barcoding step, microcapsules were washed 3-times in Hydrogel Loading Buffer, packed, and loaded onto a microfluidic device using a 1 ml syringe connected via 0.56 mm inner diameter PTFE tubing.

2.3.6.Barcoding hydrogel bead preparation

Barcoding hydrogel beads (86) (DG) were washed 3-times in Hydrogel Loading Buffer, packed, and loaded onto a microfluidic device using a 1 ml syringe connected via 0.56 mm inner diameter PTFE tubing.

2.3.7.Reverse transcription mix preparation

For mammalian cell barcoding, 150 µl of RT reaction mix, comprising 25 µM TSO (IDT) (**Table 2.7**), 1 mM dNTP mix, 20 U/µl Maxima H Minus RT enzyme, 4 U/µl RiboLock RNase inhibitor, 0.6 % Igepal CA-630, and 1x RT buffer, were prepared and loaded onto a microfluidic device using a 1 ml syringe connected via 0.56 mm inner diameter PTFE tubing. To decompose the GMA shell, the RT mix was supplemented with 0.8 mg/µl

collagenase A (Roche, cat. no. 10103586001). For bacteria barcoding, 150 µl of RT reaction mix, comprising 1.5 µM TSO, 0.75 mM dNTP mix, 15 U/µl Maxima H Minus RT enzyme, 3 U/µl RiboLock RNase inhibitor, 0.45 % Igepal CA-630, and 1x RT buffer, were prepared. An ice-filled glove was used to cool the RT mix during the encapsulation (86).

Table 2.7. DNA oligonucleotide sequences used in scRNA-Seq experiments. Asterix indicates phosphorothioate modification.

Name	Sequence (5'→3')
Reverse transcription and template switching	
TSO	AAGCAGTGGTATCAACGCAGAGTACATrGrGrG
cDNA amplification	
PCR1-p5	TACGGCGACCACCGAGATC
PCR1-tso	AAGCAGTGGTATCAACGCAGAG
Adapter ligation	
Ligation adapter is a duplex DNA	5Phos-GATCGGAAGAGCACACGTCTGAACTCCAGTCAC-3ddC
	5AmMC6-GCTCTTCCGATCT
Indexing PCR	
P5 indexing primer	AATGATACGGCGACCACCGAGATCTACAC
P7 index 6	CAAGCAGAAGACGGCATACGAGATCAGTGGGTGACTGGAGTTCAG ACGTG*T
P7 index 7	CAAGCAGAAGACGGCATACGAGATGTTGTCGTGACTGGAGTTCAG ACGTG*T
P7 index 8	CAAGCAGAAGACGGCATACGAGATTGACAAGTGACTGGAGTTCAG ACGTG*T
P7 index 13	CAAGCAGAAGACGGCATACGAGATACTCTAGTGACTGGAGTTCAG ACGTG*T
P7 index 14	CAAGCAGAAGACGGCATACGAGATCGAGATGTGACTGGAGTTCAG ACGTG*T
P7 index 15	CAAGCAGAAGACGGCATACGAGATGAGTCCGTGACTGGAGTTCAG ACGTG*T

2.3.8.RNA barcoding

RNA barcoding was conducted using the microfluidic device design presented in **Figure 2.3**. The infusion flow rates used for mammalian cells were: 250 µl/h – RT mix, 100 µl/h – BHBs, 100 µl/h – microcapsules, and 400 µl/h – droplet stabilization oil. The emulsion was collected in a 1.5 ml tube prefilled with 200 µl of light mineral oil on ice. The infusion flow rates used for bacteria were: 200 µl/h – RT mix, 40 µl/h – BHBs, 10 µl/h – microcapsules, and 500 µl/h – droplet stabilization oil. The emulsion was collected in a 1.5 ml tube prefilled with 200 µl of light mineral oil on ice.

During the barcoding step, droplets need to be carefully observed to identify BHB doublets. To avoid these events, the bead flow rate should be adjusted by 10-20 µl/h until no more doublets are observed. Microcapsule

doublets are tolerated since the fraction of positive microcapsules is less than 20 %.

2.3.9.Reverse transcription

The barcoding DNA primers were released from the BHBs by exposing the emulsion under a UV lamp for 7 min. The emulsion was aliquoted corresponding to ~3000 cells and transferred to 42 °C for 60 min., followed by RT enzyme inactivation at 85 °C for 5 min. After the RT step, the emulsion was broken by adding 10 µl emulsion breaker, diluted to 100 µl with 1x RT Buffer, and treated with 1 µl of dextranase (Sigma-Aldrich, cat. no. D0443-50ML) at 37 °C for 5 min. To dissolve microcapsule shells, the post-RT mix was treated with 1 µl of 20 mg/ml proteinase K and incubated at 37 °C for 10 min. Hydrogel beads were then separated from the barcoded cDNA molecules with Zymo Spin-IC column (Zymo, cat. no. C1004-250) by centrifugation at 1000g for 5 min.

2.3.10. cDNA purification and amplification

The barcoded cDNA molecules were purified twice with 0.8x AMPure magnetic beads (Beckman Coulter, cat. no. A63880) and eluted in 20 µl of water. cDNA amplification was performed in a 50 µl reaction mix comprising 20 µl barcoded cDNA, 0.5 µM of forward/reverse PCR primers (**Table 2.7**), and 1x Kapa HiFi 2X Ready Mix (KAPA, cat. no. KK2602). Samples were thermally cycled through the following program: 98 °C (3 min.), 98 °C (15 s)/67 °C (20 s)/72 °C (1 min.) for 13 cycles with mammalian cells and 24 cycles with bacteria, and 72 °C (1 min.). Post-PCR samples were purified twice with 0.6x AMPure magnetic beads, eluted into 20 µl of water, and subjected to fragmentation.

2.3.11. Library fragmentation and adapter ligation

DNA fragmentation was carried out in a 17.5 µl reaction mix comprising ~50 ng amplified DNA, 1.75 µl NEBNext Ultra FS Reaction buffer (NEB, cat. no. E7805S), 0.5 µl NEBNext Ultra FS Enzyme mix, and water to 17.5 µl. The mammalian cell library was fragmented at 37 °C for 8 min. and the bacterial cell library - for 6 min., followed by incubation for 30 min. at 65 °C. After fragmentation, double size selection (0.6x-0.8x AMPure) was performed. Specifically, 92.5 µl water were added, and then 66 µl AMPure beads. 160 µl of the unbound fraction were taken and supplemented with 20 µl

AMPure, followed by a regular purification workflow. DNA was eluted in 17.5 µl water and subjected to a ligation reaction.

Adapter ligation was performed in a 34.25 µl reaction mix comprising 17.5 µl fragmented DNA, 15 µl NEBNext Ultra II Ligation Master Mix, 0.5 µl NEBNext Ultra II Ligation Master Enhancer, and 1.25 µl of 1.5 µM ligation adapter (**Table 2.7**). Ligation was carried out at 20 °C for 15 min. After the ligation, the total volume was brought to 100 µl by adding water and purified with 0.8x AMPure. The product was eluted in 40 µl water.

2.3.12. Final library amplification and indexing

Indexing PCR was conducted in a 50 µl reaction mix comprising 20 µl adapter-ligated DNA, 0.5 µM P5 and 0.5 µM P7 indexing PCR primers (**Table 2.7**), and 1x Kapa HiFi 2X Ready Mix. Samples were thermally cycled through the following program: 95 °C (3 min.), 98 °C (20 s)/54 °C (30 s)/72 °C (20 s) for 11 cycles, and 72 °C (1 min.). Following PCR, double size selection (0.6x-0.8x AMPure) was performed. Purified DNA was eluted in 14 µl water. Library quality was verified on the Agilent BioAnalyzer HS DNA chip (Agilent, cat. no. 5067-4626).

2.3.13. Sequencing and data analysis

Sequencing of mammalian cell libraries was performed on the NextSeq Illumina instrument using NextSeq 500/550 High Output Kit v2.5 (75 cycles) (Illumina, cat. no. 20024906) and the following cycling settings: Read 1 – 16 cycles, Read 2 – 62 cycles, i5 read – 8 cycles, i7 read – 6 cycles. Sequencing of bacterial cell libraries was conducted using Illumina MiSeq Reagent Kit v3 (150 cycles) (Illumina, cat. no. MS-102-3001) on MiSeq Illumina instrument using the following cycling settings: Read 1 – 16 cycles, Read 2 – 134 cycles, i5 read – 8 cycles, i7 read – 6 cycles.

The solo-in-drops pipeline (https://github.com/jsimonas/solo-in-drops), was used to obtain cell × gene expression matrices. Since a cell barcode of the current CapDrop and inDrops protocols is split into two reads (Index 1 and Read 1), the solo-in-drops pipeline, firstly, demultiplexes sequencing information into 3 reads per library and combines the cell barcode halves and UMI into a single fastq file. Then, the combined cell barcode fastq together with the transcript fastq are passed to the STARsolo, which performs error correction and demultiplexing of cell barcodes, transcript read alignment and annotation, UMI deduplication and quantification of gene expression per cell. Secondary analysis was done using the Scanpy framework.

3. RESULTS AND DISCUSSION

This chapter reveals the unfolding of semi-permeable microcapsule technology from the concept to high-throughput single-cell analysis. It is organized into four major sections. Section 3.1 provides results of the early work on PEGDA microcapsule development in the context of single-bacterial cell analysis. In section 3.2, another microcapsule system, comprised of GMA, is introduced and applied for cell type identification using multiplex RT-PCR. Section 3.3 presents GMA microcapsule application to single-cell RNA sequencing in order to analyze the whole transcriptomes of single-mammalian and single-bacterium cells. Finally, section 3.4 discusses the presented results, their impact, and their relevance to state-of-the-art.

3.1. Microcapsules comprising PEGDA-based shell

3.1.1. Development strategy of PEGDA microcapsules

The overall development strategy of semi-permeable microcapsules used in this work is summarized in **Figure 3.1**. At first, an aqueous two-phase system (ATPS) consisting of PEGDA and dextran was selected for the generation of microcapsules comprising a core/shell structure. Although not limited, this selection was motivated by the fact that PEGDA and dextran remain among the most popular and well-described polymers for the generation of aqueous biphasic systems (180).

Having selected specific polymer candidates for the ATPS formation, the next step was to evaluate phase separation, which was conducted in bulk format. These experiments were necessary to screen polymer molecular weights and concentrations at which liquid-liquid phase separation may occur. In addition, bulk polymerization tests were conducted. For example, polymerization attempts of each separated phase provided valuable information about the fluidity and stiffness of dextran-rich and PEGDA-rich phases. As a starting point, the lowest concentrations were chosen, at which phase separation would still occur (while volumes of both phases remain similar). The concentration was also chosen such that the resulting PEGDA phase would form a stiff hydrogel and the dextran phase would behave as a liquid.

Once the conditions for liquid-liquid phase separation were established, the next step was the characterization of phase separation within W/O droplets and polymer partitioning topology. ATPS droplets having a core-shell structure were predicted to form well-centered microcapsules. In contrast, the Janus structure and concave shape particles were obtained, indicating that

additional physico-chemical parameters have to be adjusted. At the same time, it was necessary to identify which polymer would be enriched in the core and the shell because the results obtained in bulk format with bottom and top phases do not translate directly into W/O format with corresponding core and shell layers. One of the most convenient ways to determine phase positioning is the fluorescence staining of ATPS droplets. FITC-labelled dextran distribution between the core and shell layers was followed microscopically, revealing that the dextran phase forms a core. Microscopy analysis was applied to evaluate microcapsule quality since the characteristic core and shell geometry can be clearly visualized. The microcapsule uniformity, size, concentricity, shell thickness, and stability under different experimental conditions were evaluated before moving to single-cell assay workflows.

Although the microcapsule generation strategy was exemplified using PEGDA and dextran, a similar workflow can be applied to other aqueous two-phase systems.

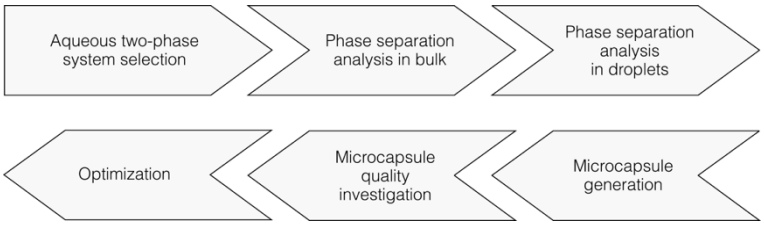

Figure 3.1. The strategy used to develop semi-permeable microcapsules.

3.1.2. PEGDA microcapsule generation

To produce PEGDA microcapsules, ATPS droplets were first generated using a 20 μm deep co-flow microfluidic device at a throughput of 1700 droplets/s by infusing the PEGDA-rich phase and the dextran-rich phase (**Figure 3.2, A**). To achieve the right balance between microcapsule uniformity, concentricity, and mechanical stability, the ATPS comprising a blend of longer (MW 8k) and shorter (MW 575) PEGDA polymers and dextran (MW ~500k) (see *Materials and Methods*) were selected. Whereas the longer PEGDA was required for efficient phase separation, the shorter PEGDA was added to increase shell stiffness and improve microcapsule mechanical stability by increasing the cross-linking events (194).

Following droplet generation, the PEGDA and dextran phases quickly phase-separated (within seconds), forming a liquid shell enriched in PEGDA and a liquid core enriched in dextran (**Figure 3.2, B**). To solidify the PEGDA shell, ATPS droplets were exposed to 365 or 405 nm light in the presence of a light-activated photo-initiator. The resulting microcapsules contained a

liquid-like core enriched in dextran and solidified hydrogel shell enriched in PEGDA (**Figure 3.2, C**). Using FITC-dextran (MW ~500k), it was estimated that upon reaching the equilibrium, the core of ATPS droplets comprised ~9.6 % (w/v) dextran. Considering similar PEGDA partitioning, the shell should comprise ~11 % (w/v) PEGDA. The core of microcapsules became cloudy after the photopolymerization, presumably due to the presence of residual PEGDA and the formation of a weak hydrogel mesh.

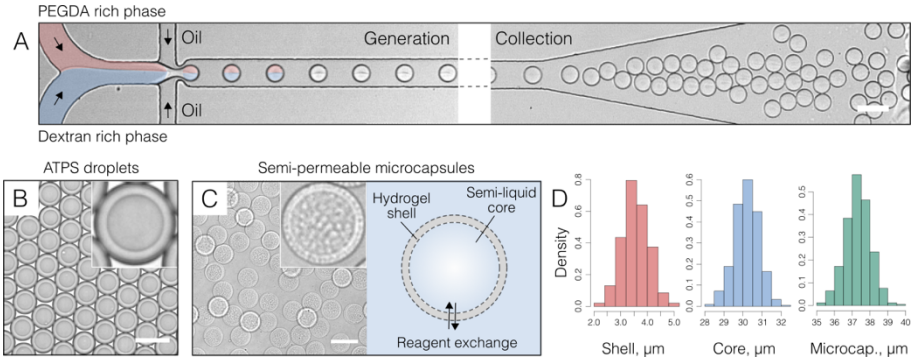

Figure 3.2. Semi-permeable microcapsule generation using ATPS composed of PEGDA and dextran. (**A**) ATPS droplet generation using a co-flow microfluidics device. (**B**) Liquid-liquid phase separation in droplets resulting in dextran-rich core and PEGDA-rich shell. (**C**) Recovered microcapsules from the emulsion, where PEGDA formed a firm hydrogel shell, and the dextran phase formed the semi-liquid core. (**D**) Histograms, derived from >100 measurements (compartments), indicate shell thickness (3.56 ± 0.48 µm), core (30.2 ± 0.6 µm), and overall microcapsule diameter (37.3 ± 0.7 µm). Scale bars, 50 µm.

One of the biggest challenges while implementing PEGDA microcapsule formation based on an ATPS was an inconsistent and non-uniform shell formation. It was observed that using high molecular weight PEGDA polymers (e.g., 10k, 20k) or increasing PEGDA (MW 8k) concentration, the microcapsule core tends to migrate towards the outer oil interphase before shell polymerization, leading to a concave particle topology. Similar topology has also been observed in the previous work (187). As a result, a significant fraction of microcapsules contained uneven or ruptured shells. Since the microcapsule shell uniformity depends on the concentricity of ATPS droplets, it was postulated that the density mismatch between the core and shell phases was driving the core off-center before complete shell polymerization. To verify this hypothesis, ATPS solutions were prepared using 3 % (w/v) and 6 % (w/v) of longer PEGDA (MW 8k), while the shorter PEGDA (MW 575) and dextran concentrations remained the same. The measurements of PEGDA and

dextran phases revealed a higher density mismatch when PEGDA (MW 8k) concentration was increased from 3 % (w/v) to 6 % (w/v) (**Figure 3.3, A)**. As expected, microcapsules originating from the density-imbalanced ATPS resulted in defective and concave particle topology (**Figure 3.3, B)**. Thus, reducing the density difference between the two aqueous phases enabled a consistent generation of monodisperse and concentric ATPS-based microcapsules (**Figure 3.3, C)** – a prerequisite feature for efficient cell isolation and different assay developments.

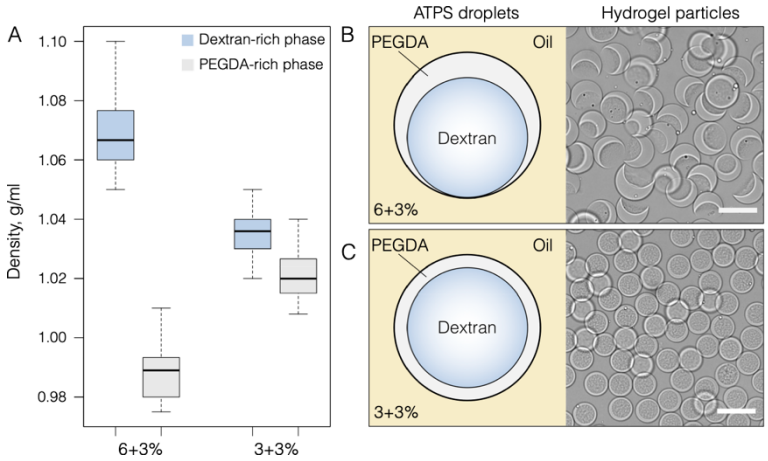

Figure 3.3. The effect of density differences between the two aqueous phases for microcapsule concentricity. (**A**) Boxplots showing the density of PEGDA (shell) and dextran (core) phases after the ATPS formation. (**B**) Microcapsules were prepared using the composition of 6% (w/v) PEGDA (MW 8k) and 3% (v/v) PEGDA (MW 575), while in (**C**) 3% (w/v) PEGDA (MW 8k) and 3% (v/v) PEGDA (MW 575) were used. Boxplots are derived from 25 measurements of each sample. Scale bars, 50 μm.

3.1.3. Single *Escherichia coli* genome amplification

Having established PEGDA microcapsule production, verifying this system's applicability for analyzing nucleic acids from single bacterial cells was the next step. Specifically, multiple displacement amplification (MDA) reaction catalyzed by phi29 DNA polymerase was conducted to investigate single-genome amplification (SGA) from individual *Escherichia coli* MG1655 cells. For comparison, *E. coli* cells were also isolated in two other microfluidic formats – W/O droplets and hydrogel beads (**Figure 3.4, A**). For each assay format, individual *E. coli* cells were isolated in ~20 picoliter (pl) volume droplets together with reagents required for lysis/SGA reaction, hydrogel bead, or microcapsule generation (see *Materials and Methods*). SGA

in microcapsules and hydrogel beads was performed in two steps – cell lysis and MDA reaction. In the droplet format, however, these two steps were combined into a single reaction by loading lysis and MDA reagents from the start of droplet generation. Noteworthy, lysis conditions resulting in efficient *E. coli* disruption and nucleic acid release that are compatible with enzymatic steps were carefully optimized in the laboratory.

After encapsulation, the observed occupancy by *E. coli* cells in each assay followed Poisson distribution with a mean lambda value being ~0.17 and ~0.18 for droplets and beads, respectively. In microcapsules, the occupancy by *E. coli* cells was slightly higher, with a median lambda value of ~0.23. The small increase in lambda value could be attributed to the viscous high molecular weight dextran, which reduced cell sedimentation during the encapsulation process and, as a result, gave higher cell occupancy. While the bacteria encapsulation process in droplets, beads, and microcapsules showed relatively similar output (e.g., lambda values were similar), significant differences emerged after the cell lysis step (**Figure 3.4, B**). If the number of positive compartments in W/O droplets remained similar before and after cell lysis, the hydrogel beads lost ~55 % of the isolated cells' gDNA. In microcapsules, the gDNA loss was ~15 %. Microscopy analysis revealed that such a notable drop in occupancy in hydrogel beads could be attributed to the bacteria's tendency to localize at the hydrogel/oil interface (**Figure 3.4, A**), which has been shown in previous reports as well (34,35). Therefore, due to the cell partitioning, the gDNA released during the lysis step becomes susceptible to diffusion out of the hydrogel mesh and eventual loss. In microcapsules, however, the presence of hydrogel-shell prevented most cells from reaching the outer (oil) phase, thereby improving the retention of cells or their lysate.

Fluorescence measurements of post-SGA compartments revealed that SGA reaction from individual *E. coli* cells was more efficient in microcapsules than in hydrogel beads or droplets (**Figure 3.3, C**). The increased SGA reaction yield in microcapsules over hydrogel beads could be attributed to the liquid-like core, which does not interfere with the synthesis of long DNA molecules (>10 kb) generated by phi29 DNA polymerase. However, in hydrogel beads, the newly synthesized DNA molecules are embedded in the hydrogel mesh and physically confined, thereby causing less efficient enzymatic replication. In support of this notion, the SGA reaction yield in W/O droplets (liquid state) was ~2-times higher than in beads (hydrogel state), as shown in **Figure 3.4, C** (green and blue boxplots).

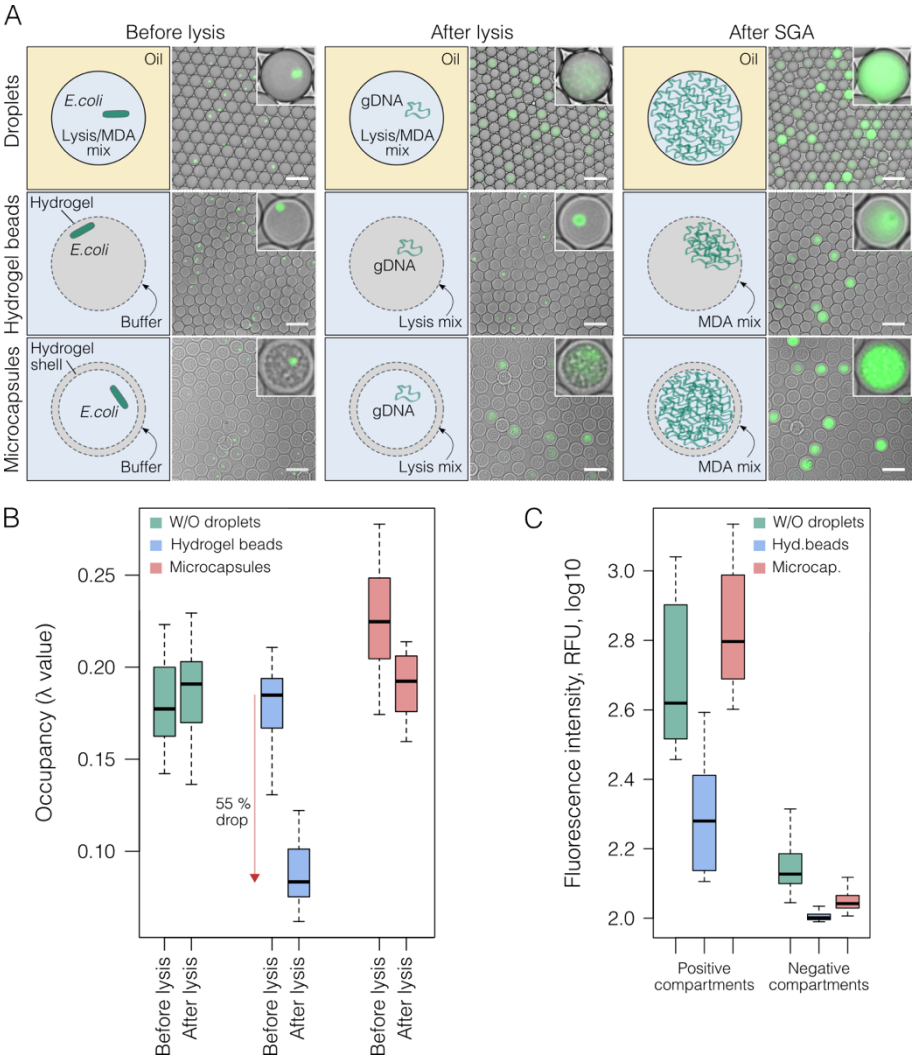

Figure 3.4. Comparison of *E. coli* isolation and SGA efficiency in W/O droplets, PEGDA hydrogel beads, and PEGDA microcapsules. (**A**) Schematics show each assay with corresponding digital images before cell lysis, after cell lysis, and after SGA reaction. (**B**) Lambda value (occupancy) measurements after *E. coli* encapsulation and lysis. Boxplots were derived by analyzing >450 compartments from each sample. (**C**) Boxplots represent mean fluorescence intensity in positive and negative (empty) post-SGA compartments. Boxplots were derived by measuring the fluorescence of 558 droplets, 511 hydrogel beads, and 491 microcapsules. Scale bars, 50 µm.

Comparing the DNA amplification efficiency in microcapsules *vs.* W/O droplets (**Figure 3.4, C,** red and green boxplots), PEGDA microcapsules showed a small reaction improvement. It could be attributed to the exchange

of reaction components through the semi-permeable membrane. In the microcapsule-based assay, the amount of MDA reagents (such as dNTPs, oligonucleotides, and DNA polymerase) is not limited to particle volume (195) but could be continuously replenished through the semi-permeable membrane. Alternatively, these results could also be explained by a more efficient bacteria lysis: the microcapsules were suspended in a lysis buffer containing lysozyme and proteinase K enzymes before DNA amplification. In the droplet assay, the use of proteinase K is prohibitive because of incompatibility with SGA.

3.1.4. Gram-positive bacteria lysis and SGA efficiency

Gram-positive bacteria usually require harsher lysis conditions (196) that are either inhibitory or harmful to the subsequent enzymatic steps. Therefore, it was anticipated that the differences in SGA reaction efficiency between microcapsules and W/O droplets would be even more pronounced. To verify this, *Rhodococcus rhodochrous* PY11 and *Streptococcus mutans* UA159 bacteria were separately isolated in PEGDA microcapsules and subsequently subjected to different lysis-SGA conditions provided in **Table 3.1**. Tested lysis-SGA conditions could be categorized into three groups: one-step, two-step, and three-step. In a one-step reaction, lysis and MDA reagents were introduced simultaneously, mimicking the droplet-based format (condition #Ref. and condition #1). In a two-step workflow, lysis and MDA were separated by post-lysis microcapsule washing in a neutral buffer before transferring them to the DNA amplification reaction. Similarly, lysis and MDA steps were separated in a three-step workflow, and a more complex lysis strategy involving two stages was applied.

Out of the six conditions tested, the three-step workflow with two lysis stages (lysozyme-induced lysis at 37 ºC for 30 min. followed by proteinase K and SDS treatment at 50 ºC for 30 min.) generated the highest number of positive reactions (**Table 3.1**, condition #5): 84 % for *S. mutans* and 99 % for *R. rhodochrous*. In the second place, alkaline solution and SDS-induced lysis (condition #6) generated 33 % positive reactions for *S. mutans* and 48 % positive reactions for *R. rhodochrous*. Noteworthy, the alkali-induced lysis is widely used with environmental samples (57), and microcapsule compatibility with these harsh lysis conditions could bring advantages to single-cell genomics research. For comparison, the one-step lysis-SGA approach in W/O droplets and microcapsules (condition #Ref. and condition #1) generated only 25 %

positive reactions for *S. mutans* and 4-8 % positive reactions for *R. rhodochrous*.

These results confirmed that regular W/O systems do not provide efficient means of amplifying single bacterial genomes and should be replaced by microcapsules that offer efficient release and clean-up of genetic material before the amplification step.

Table 3.1. Lysis conditions and SGA reaction efficiency for *R. rhodochrous* and *S. mutans* bacteria. Post-MDA microcapsules were stained with SYBR Green I and analyzed under an epifluorescence microscope to identify positive reactions. For each tested condition, >600 microcapsules were analyzed.

Cond.	Lysis-SGA	First step	Second step	Third step	Reaction efficiency
Ref.	One-step in droplets	50 U/µl Ready-Lyse Lysozyme Solution, 0.1% (v/v) Triton X-100, 1× MDA reaction mix. Incubation for 12 h at 30 °C.	None	None	25 % (*Strep.*) 8 % (*Rhod.*)
1.	One-step in microcap.	50 U/µl Ready-Lyse Lysozyme Solution, 0.1% (v/v) Triton X-100, 1× MDA reaction mix. Incubation for 12 h at 30 °C.	None	None	25 % (*Strep.*) 4 % (*Rhod.*)
2.	Two-step in microcap.	50 U/µl Ready-Lyse Lysozyme Solution, 0.1% (v/v) Triton X-100, 1 mM EDTA, 10 mM Tris-HCl [pH 7.5, 25 °C]. Incubation for 30 min. at 37 °C.	Microcapsules washed and dispersed in 1x MDA mix for 12 h at 30 °C.	None	26 % (*Strep.*) 3 % (*Rhod.*)
3.	Two-step in microcap.	50 U/µl Ready-Lyse Lysozyme Solution, 0.1% (v/v) Triton X-100, 1 mM EDTA, 200 µg/ml proteinase K, 10 mM Tris-HCl [pH 7.5, 25 °C]. Incubation at 37 °C for 30 min. followed by 50 °C for 30 min.	Microcapsules washed and dispersed in 1x MDA mix for 12 h at 30 °C.	None	20 % (*Strep.*) 58 % (*Rhod.*)
4.	Three-step in microcap.	50 U/µl Ready-Lyse Lysozyme Solution, 0.1% (v/v) Triton X-100, 1 mM EDTA, 10 mM Tris-HCl [pH 7.5, 25 °C]. Incubation for 30 min. at 37 °C.	Addition of 200 µg/ml proteinase K. Incubation for 30 min. at 50 °C.	Microcapsules washed and dispersed in 1x MDA mix for 12 h at 30°C.	15 % (*Strep.*) 57 % (*Rhod.*)
5.	Three-step in microcap.	50 U/µl Ready-Lyse Lysozyme Solution, 0.1% (v/v) Triton X-100, 1 mM EDTA, 10 mM Tris-HCl [pH 7.5, 25 °C]. Incubation for 30 min. at 37 °C.	Addition of 200 µg/ml proteinase K and 1% (w/v) SDS. Incubation for 30 min. at 50 °C.	Microcapsules washed and dispersed in 1x MDA mix for 12 h at 30°C.	84 % (*Strep.*) 99 % (*Rhod.*)
6.	Two-step in microcap.	0.5 M NaOH and 1% (w/v) SDS. Incubation at room temperature for 5 min.	Microcapsules washed and dispersed in 1x MDA mix for 12 h at 30 °C.	None	33 % (*Strep.*) 48 % (*Rhod.*)

3.1.5.Single-cell PCR

In addition to whole-genome amplification, specific target detection by PCR plays a crucial role in microbiology and ecology for identifying and annotating bacterial communities (32,146,147). To make PCR possible in PEGDA microcapsules, several requirements must be fulfilled. At first, microcapsules must remain stable and intact under an extreme temperature regime (from 4 ºC to 98 ºC). Secondly, the microcapsule shell must provide an efficient physical barrier for retaining gDNA and smaller molecular weight nucleic acids.

To evaluate PEGDA microcapsule retention capacity, 320, 567, and 1050 bp DNA fragments were generated by PCR following their diffusion between the particles. As illustrated in **Figure 3.5**, the occupancy value after PCR had a stable region when DNA amplicons were 567 bp (blue) or 1050 bp (green). Selecting fluorescence threshold value 0.1 resulted in 0.683, 0.215, and 0.170 occupancy for 320, 567, and 1050 bp amplicons, respectively. Taking into account cell occupancy value before PCR (0.176), it could be concluded that dsDNA fragments ≥567 bp were efficiently retained inside PEGDA microcapsules. Smaller DNA fragments (320 bp size) diffused between the microcapsules, as witnessed by the appearance of low fluorescence compartments and increased post-PCR occupancy value.

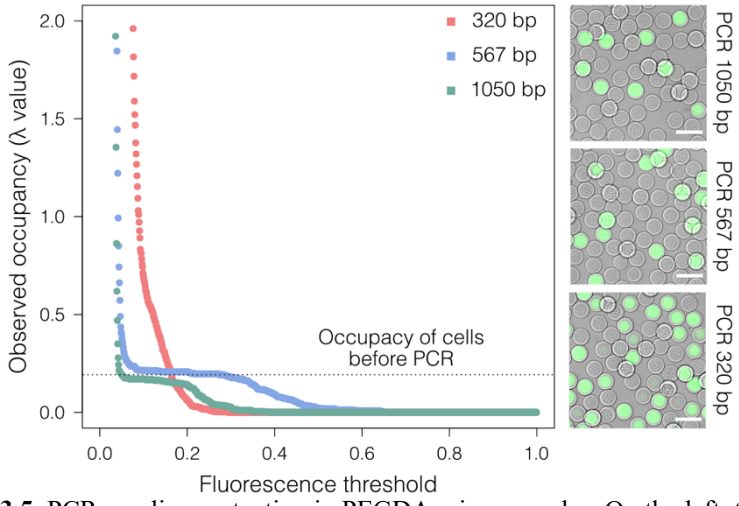

Figure 3.5. PCR amplicon retention in PEGDA microcapsules. On the left, the knee plot shows how the lambda value corresponds to different fluorescence threshold values. The knee plot was derived by measuring the fluorescence of >800 microcapsules for each sample. On the right, merged images showing the microcapsules after the synthesis of different length PCR amplicons: 1050, 567, and 320 bp. Scale bars, 50 μm.

Using the Kratky–Porod equation (197), it was estimated that PCR fragments (320, 567, and 1050 bp) have radii of gyration on the order of 26, 40, and 60 nm. Considering these values and diffusivity results, it can be approximated that the average pore size of the PEGDA hydrogel shell is ~60 nm. Scanning electron microscopy analysis revealed an average pore size of 55 ± 31 nm.

3.1.6. Bacteria culture and phenotypic analysis

In addition to nucleic acid amplification and analysis, a large variety of microbiology assays would benefit from a system that enables phenotypic bacterial cell characterization. This commonly requires a continuous bacterial cell culture, induced gene expression, and the following analysis of proteins or metabolites. All these steps in combination are significant challenges for W/O emulsions. Meanwhile, semi-permeable microcapsules combine a scalable and high-throughput cell isolation methodology with the standard molecular biology workflows. This section demonstrates this notion by performing the synthesis and detection of a bacterial metabolite polyhydroxybutyrate (PHB) in isogenic colonies originating from single isolated *E. coli* cells.

To investigate whether the PEGDA microcapsules could be used as microreactors for single isolated bacterium cultivation, *E. coli* MG1655 cells were encapsulated, transferred to LB growth medium, and allowed to expand within microcapsules for 4 hours at 37 ºC (**Figure 3.6, A**). As a reference, bacterial cells were encapsulated in W/O droplets containing LB growth medium and cultivated for 4 hours at 37 ºC (**Figure 3.6, B**). Following SGA results presented in sections 3.1.3 and 3.1.4, it was anticipated that the diffusion of growth media through the semi-permeable hydrogel shell would ensure extended cell growth until the entire microcapsule core is filled with bacteria mass. In contrast, in the droplet case, the critical cell mass would be limited by the available nutrients within a droplet. Microscopy analysis revealed that in microcapsules, a single bacterial cell expanded into a colony of ~90 cells, while in W/O droplets, micro-colonies reached ~30 cells (**Figure 3.6, C**).

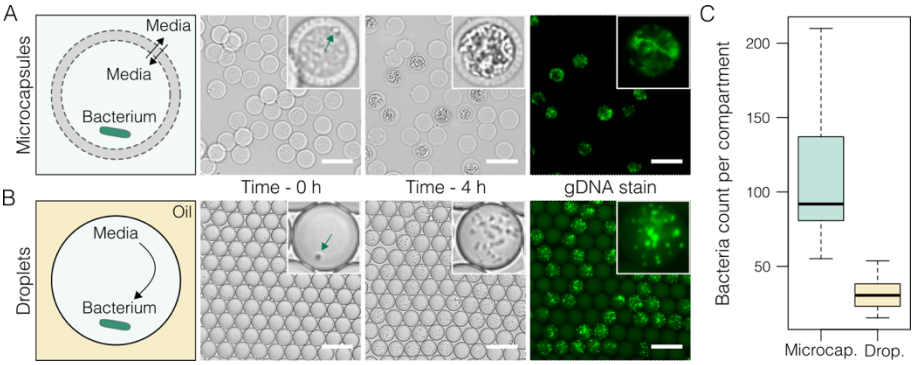

Figure 3.6. Comparison of *E. coli* MG1655 microcolony formation in PEGDA microcapsules and W/O droplets. Left: schematics depicting microcapsule-based (**A**) and droplet-based (**B**) assays. Digital images show bacteria growth in microcapsules (**A**) and in droplets (**B**) at 0 and 4 hours of cell culture at 37 °C. The green arrows indicate a single bacterium at time 0. Fluorescent images were obtained after staining with SYBR Green I dye. (**C**) Boxplots show bacteria counts after 4 hours of incubation in microcapsules and droplets. Boxplots were derived by measuring 20 droplets and 30 microcapsules. Scale bars, 50 μm.

Having shown the growth of *E. coli* and isogenic colony formation, microcapsules were then applied to the phenotypic analysis of bacteria that produce polyhydroxybutyrate (PHB) – an environmentally important biodegradable plastic (198-200). To demonstrate that such analysis is possible using semi-permeable PEGDA microcapsules, *E. coli* (DH5α) strain was transformed with the pBHR68 vector, harboring genes (*phaC*, *phaA,* and *phaB*) for PHB synthesis (201). Transformed bacterial cells were then loaded in PEGDA microcapsules, cultivated into micro-colonies for 6 hours, and then PHB synthesis was induced by adding isopropyl β-D-1-thiogalactopyranoside (IPTG). After 8 hours of induction, PHB formation was verified in live cells using Nile Red dye, which stains PHB granules (202) (**Figure 3.7, A,** Live culture). Unfortunately, it was noticed that Nile Red, being a lipophilic dye, also binds to the cell membrane yielding a highly fluorescent signal in both positive and negative control samples (**Figure 3.7, B,** Live culture). To circumvent the background fluorescence resulting from non-specific staining, cell membranes were dissolved in a lysis buffer containing lysozyme and proteinase K. This additional step increased the analytical sensitivity of positive-to-negative clones by approximately 10-fold (**Figure 3.7, C**).

Having confirmed the discrimination of PHB producers from negative clones, the next step was to identify the most efficient microcolonies synthesizing PHB. Taking into account only the intensity of Nile Red is inaccurate since the fastest-growing clones can outcompete the slower

growers with a higher PHB synthesis potential. To overcome this limitation, Nile Red dye was combined with SYBR Green I for dual PHB and gDNA staining. This additional staining allowed the normalizing of PHB synthesis levels to bacteria count (**Figure 3.8**).

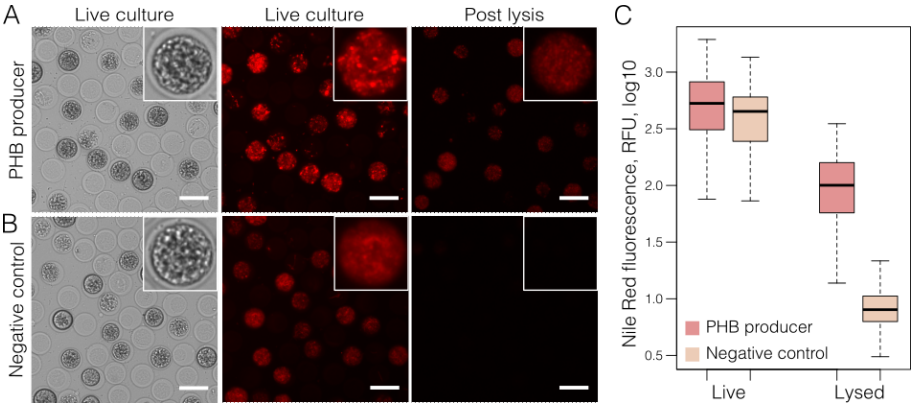

Figure 3.7. Detection of PHB-producing microcolonies based on Nile Red staining. (**A**) Microcolonies producing PHB – DH5α-pBHR68 and (**B**) negative control – DH5α-pTZ18R were analyzed before and after cell lysis using Nile Red staining. (**C**) Boxplots show relative PHB levels using Nile Red dye on live and lysed cells. Boxplots were derived by measuring >100 microcapsules for each assay. Scale bars, 50 µm.

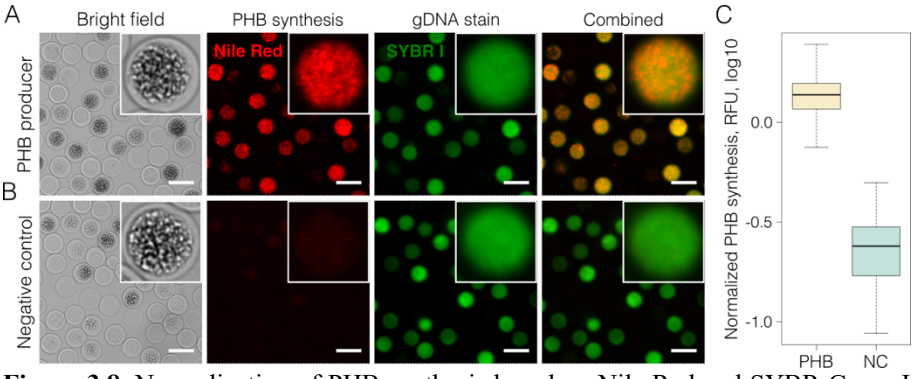

Figure 3.8. Normalization of PHB synthesis based on Nile Red and SYBR Green I dual staining. (**A**) Microcolonies producing PHB – DH5α-pBHR68 and (**B**) negative control – DH5α-pTZ18R were analyzed after cell lysis step and after staining with Nile Red and SYBR Green I. (**C**) Boxplots show normalized PHB synthesis levels of positive (yellow) and negative (green) clones. The ratio of Nile red to SYBR Green I was used for normalizing the PHB levels to bacteria count. Boxplots were derived from 107 and 78 measurements of positive and negative microcolonies, respectively. Scale bars, 50 µm.

Working with Gram-negative and Gram-positive bacteria laid the groundwork for cell culture and performing molecular biology protocols where separate steps are not compatible if done together (lysis and SGA). The next step was expanding this methodology to new cell types and other multi-step workflows.

3.1.7. Mammalian cell isolation in PEGDA microcapsules

So far, this work has presented the development and use of PEGDA-based semi-permeable microcapsules for single-bacterial genotypic and phenotypic analysis. However, to be broadly applicable to diverse research areas, microcapsules should also enable efficient mammalian cell isolation and analysis. When attempting to isolate single-mammalian cells in PEGDA-based microcapsules, several unexpected challenges appeared. First, because mammalian cells are far larger than typical bacterial cells, the microcapsules have to be >40 µm, preferably ≥60 µm. However, PEGDA microcapsules of such size have reduced concentricity and tend to lose the encapsulated cells. Furthermore, mammalian cells showed a preference to partition at the interphase between the PEGDA and dextran and, in some cases, cross the shell entirely. To overcome these issues, modified compositions consisting of medium-length PEGDA polymers (e.g., MW 2k and MW 3.4k) were developed. Although an improved concentricity of larger microcapsules (≥60 µm) could be achieved, the retention of mammalian cells remained poorly controlled and inefficient (**Figure 3.9**).

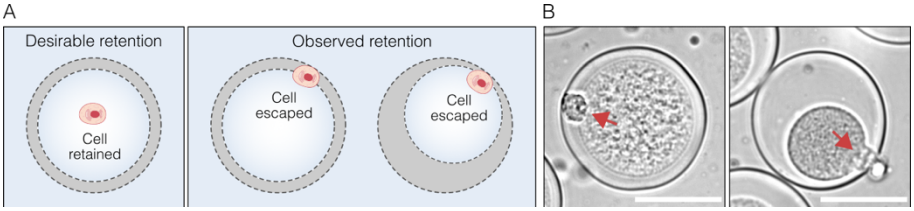

Figure 3.9. Mammalian cell (K-562) isolation in PEGDA-based microcapsules. (**A**) Schematic representation of the desirable and observed cell partitioning. (**B**) Micrographs of PEGDA microcapsules with isolated K-562 cells. Cells were isolated in microcapsules having different shell thicknesses. Scale bars, 50 µm.

These disappointing results encouraged a search for new polymers to generate ATPS-based microcapsules tailored for efficient mammalian cell retention. As revealed in the next chapter, the missing features were fulfilled by replacing PEGDA with gelatin methacrylate (GMA).

3.2. Microcapsules comprising GMA-based shell

3.2.1.GMA microcapsule generation and their stability assessment

To produce microcapsules comprising the GMA-based shell, the ATPS droplets were first generated by infusing GMA and dextran (MW ~500k) solutions, with cells being suspended in the dextran solution at a desirable density (**Figure 3.10, A**). Following droplet generation, the GMA and dextran phases separated into a liquid shell enriched in GMA and a liquid core enriched in dextran (**Figure 3.10, B**). To convert the liquid droplets to microcapsules, the semi-permeable shell was formed in a two-step process. First, the liquid shell layer was solidified by simply cooling the droplets to 4 ºC for 30 min. Next, the intermediate microcapsules (having physically cross-linked shell) were recovered from the emulsion and covalently cross-linked in an aqueous buffer under a brief exposure to 405 nm light in the presence of a light-activated photo-initiator (see *Materials and Methods*). This two-step polymerization procedure, where the physical gelation of microcapsules is followed by a covalent cross-linking, ensured a highly reproducible generation of intact and highly uniform microcapsules (**Figure 3.10, C).**

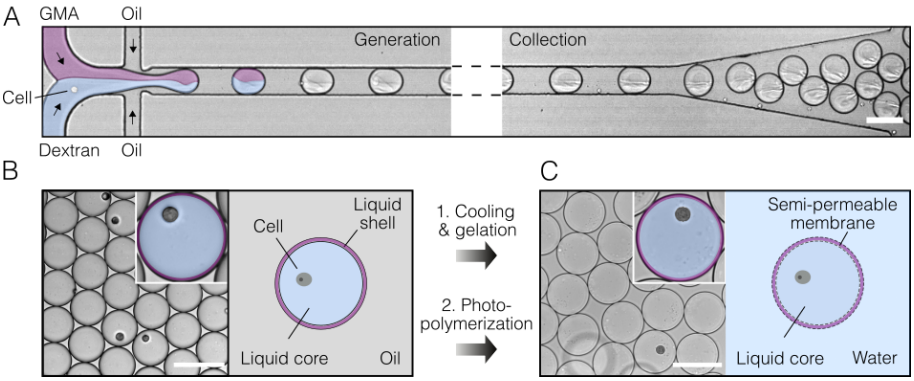

Figure 3.10. GMA microcapsule generation and cell isolation. (**A**) Cell encapsulation and collection off-chip. A mixture of cells is encapsulated in ATPS droplets comprising a liquid core enriched in dextran and a liquid shell enriched in GMA and collected off-chip into a tube. (**B**) The liquid shell of collected droplets is converted to a semi-permeable membrane in a two-step process. At first, the liquid shell is gelled by cooling and then covalently cross-linked by photo-polymerization (**C**). Scale bars, 100 μm.

Having established a protocol for GMA microcapsule production, the next step was investigating their stability under different chemical, physical, and mechanical treatments. Considering the protein-based shell material, the GMA microcapsules were expected to be less stable than PEGDA. At first, microcapsule stability was verified by immersing particles in the widely used buffers, including 1x DPBS [pH 7.4], 1x HBSS [pH ~6], 1x SSC [pH 7.0], and 10 mM Tris-HCl [pH 7.5], at room temperature. Results presented in **Figure 3.11** indicate that regardless of buffer composition, GMA-based microcapsules remained intact without any detectable swelling or shrinking. It is worth mentioning that GMA microcapsules stored in 10 mM Tris-HCl buffer over 10 months at 4 ºC also retained high stability. Furthermore, as illustrated in **Figure 3.18**, these microcapsules were stable under extreme temperature regimes used during PCR cycling. Centrifugation and vortexing between the experimental steps also did not have any adverse effects.

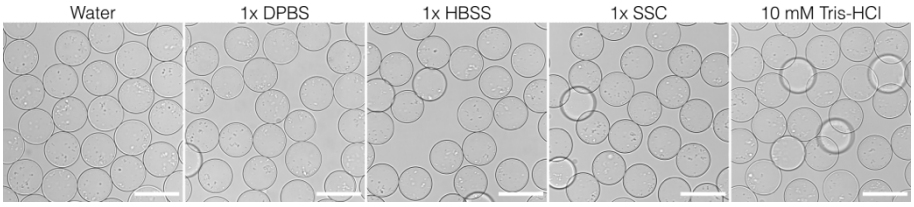

Figure 3.11. GMA microcapsule stability in different aqueous solutions. Bright-field microscopy images were taken after microcapsule incubation at room temperature for 60 min. in MQ-water, 1x Dulbecco's phosphate-buffered saline (DPBS) buffer, 1x Hanks' Balanced Salt Solution (HBSS) buffer, 1x saline-sodium citrate (SSC) buffer, and 10 mM Tris-HCl. Scale bars, 100 µm.

Maintaining microcapsule integrity as they are suspended in alcohols and other polar solvents, or keeping them intact in a frozen state, could also offer an important advantage. For example, many nucleic acid processing protocols rely on a step where genetic material is stored at -20 ºC or -80 ºC prior to analysis, or cells are preserved using alcohol and acetone-based fixation (203,204). Thus, microcapsules supporting isolated cell and nucleic acid storage in these organic solvents would facilitate many analytical steps. To verify GMA microcapsule compatibility with freezing in alcohols and acetone, particles were suspended in 70 % ethanol, 90 % methanol, and 90 % acetone and stored at -20 ºC or -80 ºC overnight. Results in **Figure 3.12** show that microcapsules remained intact without aggregation and clumping in all tested conditions (except for a few sticky microcapsules after storage in acetone), confirming that they are suitable for frozen sample preservation. While the longest incubation time that would be safe for microcapsule storage

was not verified, it was noticed that GMA microcapsules remained stable after several months at -20 ºC in 70 % ethanol.

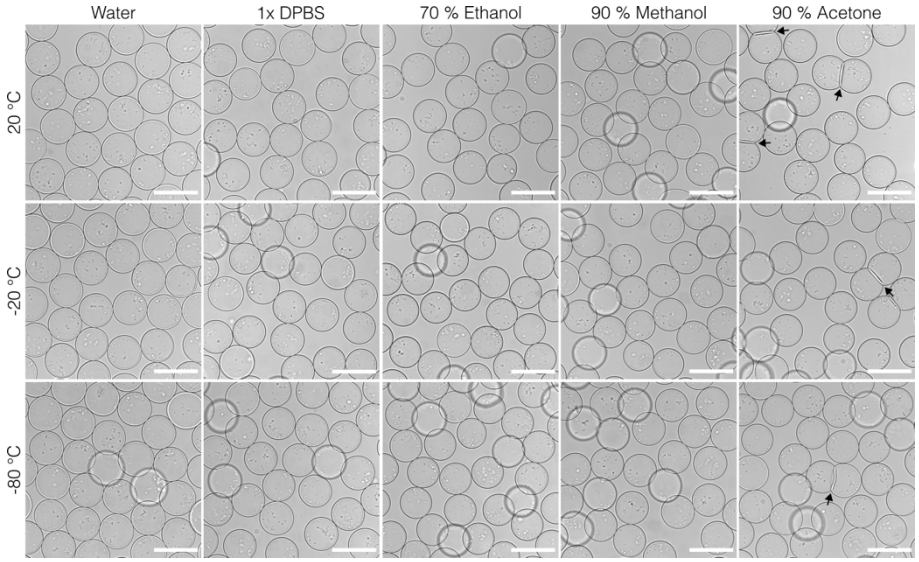

Figure 3.12. GMA microcapsule stability in different polar solvents and freezing conditions. Bright-field microscopy images of the microcapsules in different polar solvents at room temperature (top row), after freezing at -20 °C for 16 hours (middle row), and after freezing at -80 °C for 16 hours (bottom row). Microcapsules incubated with ethanol, methanol, and acetone were rinsed once in 1x DPBS before imaging. Black arrows show sticky microcapsules after storage in acetone. Scale bars, 100 μm.

Finally, the shell composed of gelatin polypeptide implies sensitivity to proteolytic enzymes. A few minutes of incubation at room temperature were sufficient to dissolve microcapsules immersed in 1x DPBS buffer containing proteinase K or collagenase A (**Figure 3.13**). These results are important for several reasons. First, they indicate that gelatin-based microcapsules cannot be used in workflows that require proteases (e.g., cell lysis step using proteinase K). On the other hand, mild and biocompatible conditions provided by trypsin and collagenase enable the straightforward release of both the encapsulated cells and processed nucleic acids. These results demonstrate the advantages of this composition over PEGDA microcapsules, as dissolving the PEGDA shell requires heating in an alkaline solution – a condition detrimental to cells, RNA, and protein molecules.

Altogether these results confirmed that the developed GMA-based microcapsules remain uniform in size and intact under various experimental conditions such as freezing, thawing, high-speed centrifugation, and in the presence of different salts and solvents. However, to be applicable for cell-

based analysis, these microcapsules must first retain isolated mammalian cells efficiently – a property that was difficult to achieve using PEGDA microcapsules.

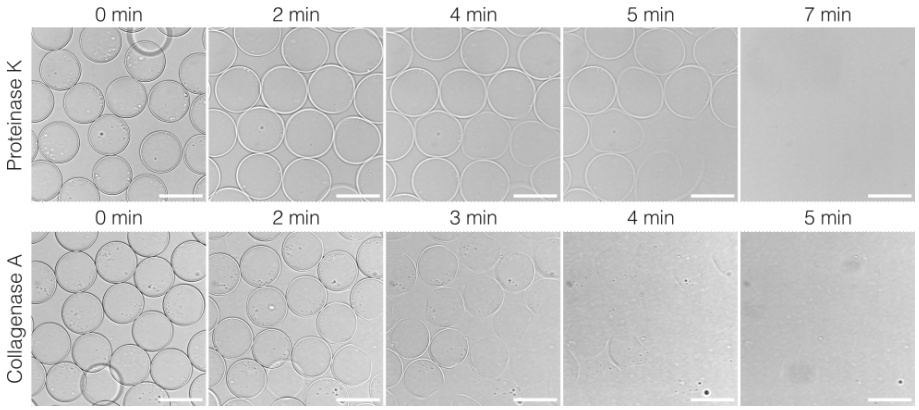

Figure 3.13. GMA microcapsule decomposition by proteolytic enzymes. Bright-field microscopy images of the microcapsules immersed in 1x DPBS supplemented with 0.2 mg/ml proteinase K (top row) or 1 mg/ml collagenase A (bottom row). Scale bars, 100 μm.

3.2.2. Mammalian cell and nucleic acid retention

To evaluate mammalian cell encapsulation and retention efficiency, human hematopoietic malignant cells K-562 and Jurkat were loaded into 75.0 ± 1.5 μm size microcapsules with a 3.0 ± 0.2 μm-thick shell. Cell numbers were quantified microscopically immediately after encapsulation (in W/O droplets) and after forming the microcapsules. No significant difference was detected ($p = 0.2613$ and $p = 0.7906$ for K-562 and Jurkat samples, respectively), confirming that compartmentalized cells were efficiently retained during microcapsule generation (**Figure 3.14**). These results were also supported by the more thorough inspection of the isolated cells under the microscope, which revealed that mammalian cells preferably localize in the dextran phase without detectable bias towards the dextran-GMA interphase. These results are in sharp contrast to PEGDA-based microcapsules. Hence, microcapsules, composed of dextran and GMA, are optimal for mammalian cell workflows as cell loss is minimal or none.

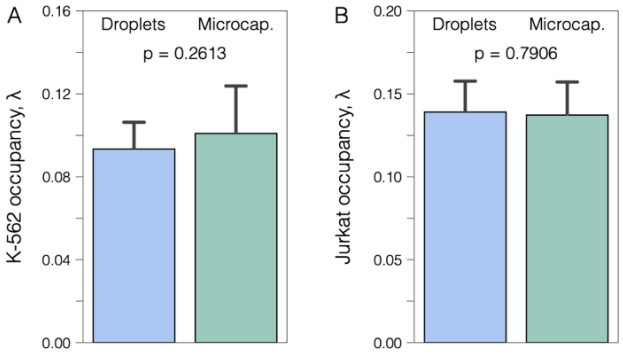

Figure 3.14. Mammalian cell retention in GMA-based microcapsules. (**A**) Barplots show K-562 cell occupancy in droplets and microcapsules. Independent sample Welch's t-test showed that there is no statistically significant difference in cell occupancy between droplets and microcapsules (two-sided alternative hypothesis, n = 17, p = 0.2613). (**B**) Barplots show Jurkat cell occupancy in droplets and microcapsules. Independent sample t-test showed that there is no statistically significant difference in cell occupancy between droplets and microcapsules (two-sided alternative hypothesis, n = 17, p = 0.7906).

Furthermore, by combining efficient cell retention with biocompatible GMA microcapsule generation, isolated cells retained their viability and could be expanded to spheroids (**Figure 3.15**). Having isolated cells in a microcapsule suspension, a consistent increase in cell quantity was observed. It took 5 to 10 days for cells to fill the microcapsule core, with the differences explained by different cell cycle durations. For example, fast-growing Jurkat cells filled the microcapsule core in approximately 5 days, while for a slower grower – A549 cells – it took twice as long.

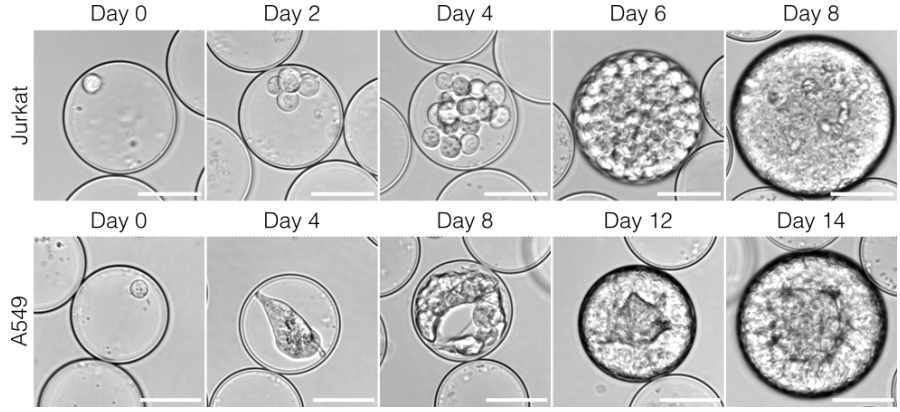

Figure 3.15. Long-term mammalian cell retention and cultivation in GMA microcapsules. Top row: micrographs show single isolated Jurkat cell cultivation for 8 days. Bottom row: micrographs show single isolated A549 cell cultivation for 14 days. Scale bars, 50 μm.

While efficient cell isolation and retention are mandatory for conducting single-cell assays, the retention of nucleic acids is crucial for many diverse applications based on nucleic acid amplification and analysis. Therefore, GMA microcapsules must also ensure that PCR amplicons and nucleic acid molecules released from the lysed cells are efficiently retained during the multi-step molecular biology procedures. To experimentally verify the permeability and retention of the nucleic acid molecules within microcapsules, dsDNA fragments ranging from 25 to 700 bp were encapsulated, and microcapsules were incubated at temperatures ranging from 4 to 70 ºC for 30 min. Then the microcapsules were washed in a neutral pH buffer to remove all unretained DNA molecules, and the retained DNA molecules were extracted by dissolving the shell (see *Materials and Methods*). The results shown in **Figure 3.16, A**, indicated that DNA fragments up to 100 bp freely traversed the microcapsule membrane, while DNA fragments over 300 bp were fully retained. The molecular weights of these polynucleotides correspond to ~60 kDa and 180 kDa, respectively. Interestingly, DNA retention slightly increased when photopolymerization was performed in the emulsion format after the temperature-induced gelation (**Figure 3.16, B**) and indicated that GMA microcapsules with only physical cross-links have a higher permeability to nucleic acids.

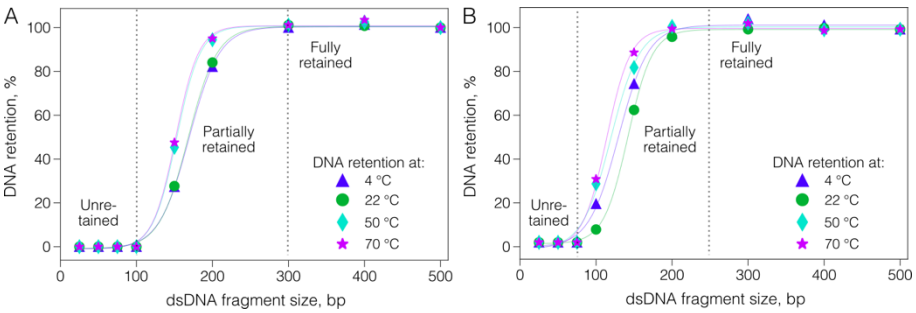

Figure 3.16 DNA retention in GMA microcapsules at different temperatures after 30 min. incubation. (**A**) DNA retention was tested in microcapsules prepared using a two-step approach, where physically gelled microcapsules were dispersed in an aqueous buffer and then photopolymerized. (**B**) DNA retention was tested in microcapsules prepared by co-encapsulating the photo-initiator in ATPS droplets. ATPS droplets were cooled down to induce physical gelation and then photopolymerized in W/O droplets. Solid lines serve only for visual guidance.

Considering the typical oligonucleotide length of 20-50 nt (12–30 kDa), the molecular weight of M-MLV reverse transcriptase (71 kDa) and Taq DNA polymerase (94 kDa), and their compact globular protein structure, microcapsules with such permeability are well-suited for conducting parallel

enzymatic reactions, such as reverse transcription (RT) and PCR on thousands of single-cells by simply dispersing microcapsules in a suitable reaction mix. Microcapsule uniformity, stability, efficient cell retention, and semi-permeability made it possible to develop a multiplex RT-PCR assay for cell type identification, which in this work was named RNA cytometry.

3.2.3. High-throughput nucleic acid analysis in individual cells

The overall concept of microcapsule-based single-cell RNA cytometry is summarized in **Figure 3.17**. At first, the individual cells are isolated in semi-permeable microcapsules and are lysed by dispersing the particles in an appropriate lysis buffer. Upon lysis, the nucleic acid molecules longer than 300 bp are preferably retained within the microcapsules, while smaller biomolecules are removed by dialysis. Therefore, RNA and DNA molecules contained within the individual cells can be efficiently purified and retained. Once the nucleic acids are purified, the microcapsules are transferred to the RT-PCR reaction mix to initiate cDNA synthesis, followed by multiplex PCR. During PCR, the fluorescently labeled primers in the reaction mix cross the membrane by diffusion and are incorporated into the PCR amplicons, making cell-containing microcapsules fluorescent. Thus, using a multiplex panel of fluorescently labeled PCR primers, the expression of the selected genes of interest can be digitally profiled in thousands of individual cells. Finally, microcapsules are inspected using microscopy or flow cytometry-based analysis.

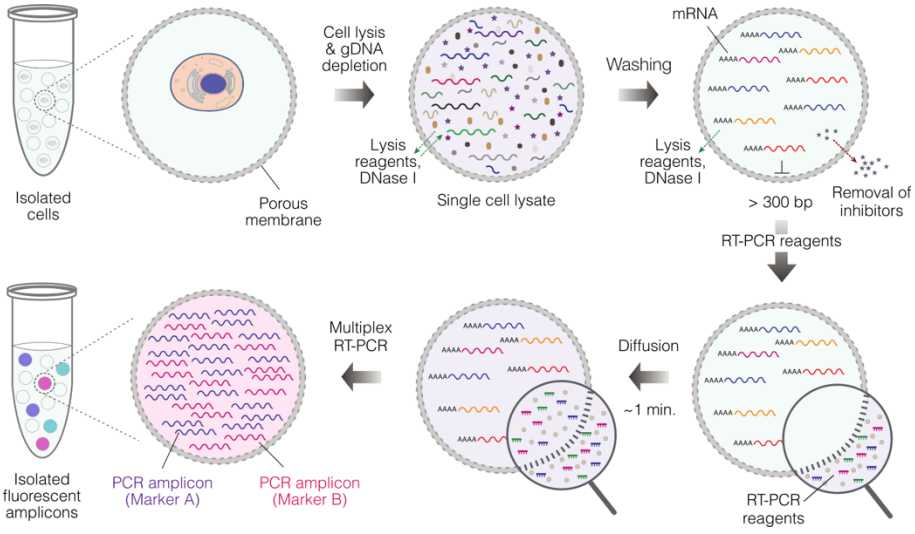

Figure 3.17. The concept of performing single-cell RNA cytometry using GMA microcapsules.

3.2.4. Cell type identification based on digital RT-PCR readout

To demonstrate the digital profiling of individual human cells based on their gene expression, hematopoietic malignant cells (K-562) and human embryonic kidney cells (HEK293) were mixed at an equal ratio. Having this sample, cells were encapsulated at limiting dilution such that each microcapsule, on average, would contain no more than one cell. As a reference, K-562 and HEK293 cells were encapsulated separately. The isolated cells were first lysed by dispersing microcapsules in a chaotropic lysis mix, followed by gDNA depletion by DNase I to obtain the microcapsules with purified total RNA derived from single cells (see *Materials and Methods*). This multi-step processing was implemented for several reasons. First, efficient cell lysis is critical for releasing genetic material completely. Secondly, the depletion of gDNA increases the RT-PCR signal specificity by preventing co-amplification of gDNA. Third, rigorous washing of the post-lysis microcapsules in an aqueous buffer with non-ionic detergents removes the lysis reagents, nucleases, and intracellular inhibitors originating from the cell lysate itself (91,94,113,205,206).

Microcapsules harboring purified total RNA derived from single cells were dispersed in the RT reaction mix to convert mRNA molecules to copy DNA (cDNA) (see *Materials and Methods*). To identify individual cells based on their gene expression profile, the post-RT microcapsules were then transferred into a PCR reaction mix comprising fluorescently labeled primers targeting cell type-specific and universal markers. The cDNA of transcripts encoding protein tyrosine phosphatase receptor type C (*PTPRC*) was chosen as K-562 specific target, and the cDNA of transcripts encoding Yes-associated protein 1 (*YAP*) was selected as HEK293 specific target. Whereas the cDNA of β-actin (*ACTB*) was chosen as a universal marker. The target-specific PCR primers were fluorescently labeled at 5'-end with fluorophores emitting light at different wavelengths to identify amplified nucleic acids based on the fluorescence signal. During the PCR step, fluorescently labeled oligonucleotides diffuse from the bulk solution into the microcapsule core and, upon annealing to the target DNA region, get incorporated into PCR amplicons, thereby converting an amplified DNA into a fluorescent product (**Figure 3.18**). The fluorescent probes would only label microcapsules harboring the target template (e.g., *PTPRC*, *YAP*, or *ACTB*), while empty microcapsules would remain blank. When a given cell simultaneously expresses two genes, the microcapsules become fluorescent in two channels. Given the differential expression of *PTPRC* and *YAP* and the ubiquitous expression of *ACTB*, it was anticipated that microcapsules containing K-562

cells would be identified by *PTPRC* and *ACTB* signal (cyan), while HEK293 would be identified by *YAP* and *ACTB* signal (magenta). The microscopy analysis confirmed that K-562 and HEK293 cells could indeed be identified by the fluorescence profile of the amplified markers (**Figure 3.18, B and C**).

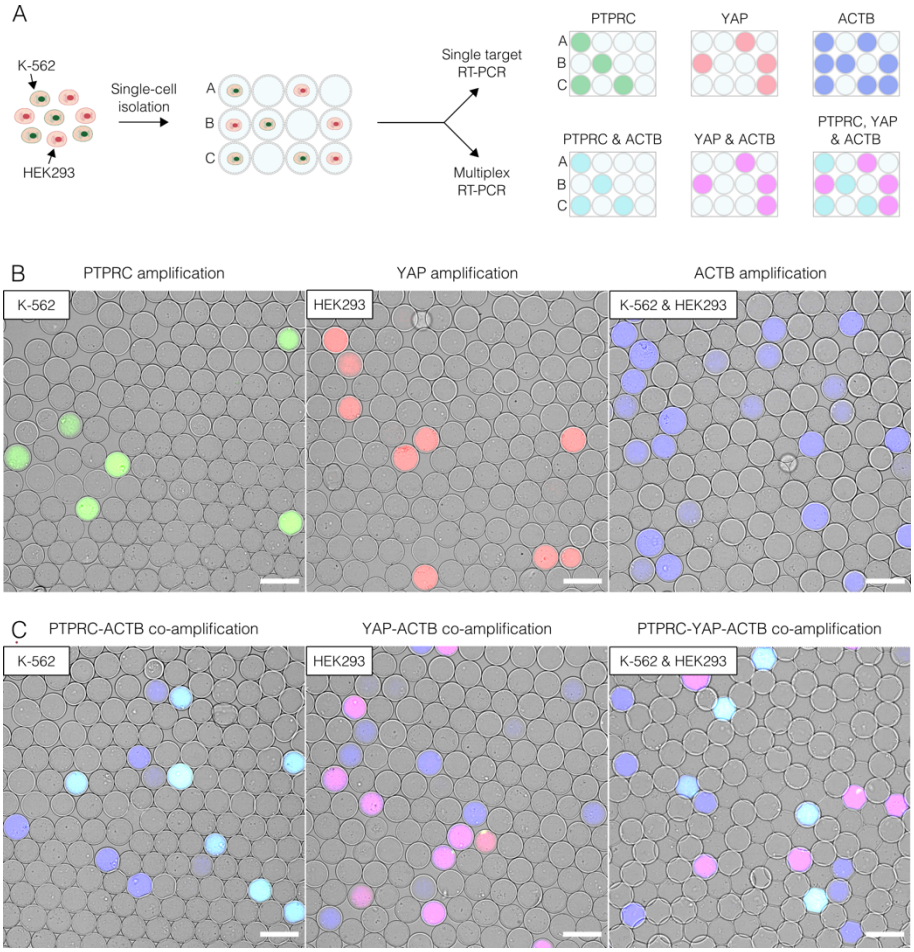

Figure 3.18. Gene expression profiling in individual cells using microcapsule-based RT-PCR. (**A**) Schematic of the experimental design. The mixture of K-562 and HEK293 cells was isolated in microcapsules, lysed, treated with DNase I, and subjected to uniplex RT-PCR or multiplex RT-PCR assay using fluorescently labeled primers targeting the transcripts of interest (*PTPRC*, *YAP*, and *ACTB*). Post-RT-PCR microcapsules were then analyzed by layering them on a hemocytometer and recording their fluorescence. (**B**) Merged images of microcapsules after RT-PCR targeting one transcript of interest: *PTPRC* (green), *YAP* (red), or *ACTB* (blue). (**C**) Merged images of microcapsules after multiplex RT-PCR simultaneously targeting two or three transcripts of interest: *PTPRC* and *ACTB* (cyan), *YAP* and *ACTB* (magenta) or *PTPRC*, *YAP* and *ACTB* (cyan/magenta). Scale bars, 100 μm.

These results confirmed that GMA-based microcapsules support single-cell RT-PCR assay enabling cell-type identification based on their digital gene expression signature. Furthermore, as shown in the next section, the microcapsules are also compatible with standard flow cytometry instruments making it possible to perform high-throughput particle analyses in a time-efficient manner.

3.2.5. Post-RT-PCR microcapsule analysis by flow cytometry

Flow cytometry could provide a high-throughput approach for analyzing post-RT-PCR microcapsule samples. Towards this goal, microcapsule samples carrying amplified material from K-562 cells, HEK293 cells, and a mixture of both were loaded onto the Partec Cyflow Space FACS instrument to perform flow cytometry (**Figure 3.19**). As a proof of concept, up to 30.000 microcapsules were analyzed per experiment, although the total microcapsule count was not limited and could be easily scaled up. Microcapsules were analyzed by sequentially gating the distribution of flow cytometry events in the forward *vs.* side scatter plot (**Figure 3.19,** Microcapsule gate), the fluorescence of Alexa Fluor 647 *vs.* side scatter plot (Actin gate), and Alexa Fluor 488 *vs.* Alexa Fluor 555 intensity plot (Cell marker gate). This enabled precise quantification of cell-type-specific marker expression and identification of different cell types in the population.

The results summarized in **Table 3.2** show a very close agreement between the flow cytometry and epifluorescence microscopy measurements. The microcapsules carrying K-562 cells were *PTPRC* positive (3.19 % and 3.63 % events for microscopy and flow cytometry analysis, respectively), whereas those with HEK293 cells were *YAP* positive (4.84 % and 5.46 % events for microscopy and flow cytometry analysis, respectively), approaching the theoretical number of microcapsules with cells (~5-6 %). The microcapsules prepared with a mixture of K-562 and HEK293 cells showed two distinct populations either positive for the *PTPRC* or *YAP* marker. K-562 and HEK293 co-encapsulation events were rare (0.02–0.15 %) and followed the Poisson distribution. Dedicating one channel for a cell type-specific marker gene and one for a ubiquitously expressed gene facilitated the digital profiling of single cells. For instance, 99.07 % of *PTPRC*-positive events were also positive for the *ACTB* marker in the sample containing K-562 cells, and 94.57 % of *YAP*-positive events were also positive for the *ACTB* marker in the sample containing HEK293 cells.

Altogether, these results confirmed that post-RT-PCR microcapsules and their fluorescence can be detected using flow cytometry, which significantly reduces the time required to complete the analysis.

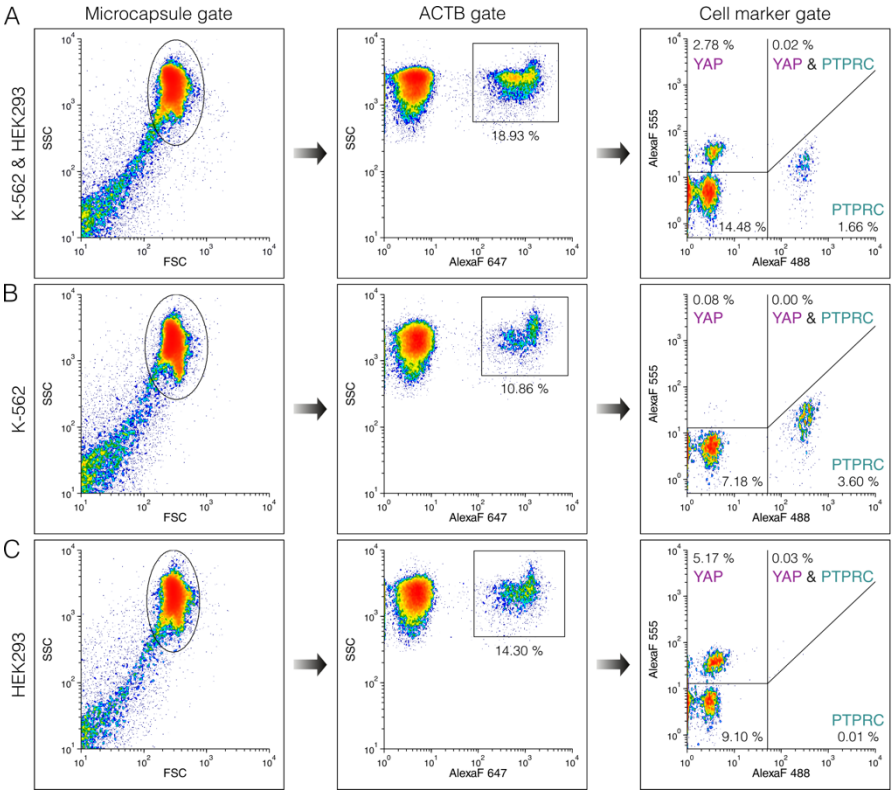

Figure 3.19. Flow cytometry of post-RT-PCR microcapsule samples. Scatter plots show three microcapsule samples containing a mixture of K-562 and HEK293 cells (**A**), K-562 cells (**B**), and HEK293 cells (**C**). The microcapsules were first gated based on forward *vs.* side scatter signal (Microcapsule gate). The resulting sub-population was then gated by *ACTB* marker expression (Actin gate), and finally, the expression of *PTPRC* and *YAP* markers was evaluated based on the fluorescence scatter plot (Cell marker gate). The percentages indicate the total events.

Table 3.2. Comparative analysis of the multiplex single-cell RT-PCR results using flow cytometry and epifluorescence microscopy.

Sample	Total counts	ACTB	YAP	YAP & ACTB	PTPRC	PTPRC & ACTB	YAP & PTPTC	YAP, PTPTC & ACTB
Microscopy analysis								
K-562	2822	285 (10.1%)	3 (0.11%)	3 (0.11%)	90 (3.19%)	90 (3.19%)	2 (0.07%)	2 (0.07%)
HEK293	2128	272 (12.78%)	103 (4.84%)	102 (4.79%)	0 (0.0%)	0 (0.0%)	0 (0.0%)	0 (0.0%)
K-562 & HEK293	2006	361 (18.0%)	69 (3.44%)	68 (3.39%)	36 (1.79%)	36 (1.79%)	3 (0.15%)	3 (0.15%)
Flow cytometry analysis								
K-562	23628	2565 (10.86%)	84 (0.36%)	18 (0.08%)	858 (3.63%)	850 (3.60%)	1 (<0.01%)	1 (<0.01%)
HEK293	19574	2800 (14.30%)	1069 (5.46%)	1011 (5.17%)	1 (<0.01%)	1 (<0.01%)	6 (0.03%)	6 (0.03%)
K-562 & HEK293	31061	5881 (18.93%)	940 (3.03%)	863 (2.78%)	524 (1.69%)	516 (1.66%)	6 (0.02%)	5 (0.02%)

Both flow cytometry and microscopy analyses showed that there is a subpopulation with a fluorescent signal corresponding to the *ACTB* target alone and lacking *PTPCR* and *YAP* expression. A fraction of *ACTB*-positive events (**Table 3.2**, 3rd column) was approximately 3-times higher than the number of target-specific *YAP* (4th column) or *PTPRC* (6th column) events. Considering the significant excess of *ACTB*-positive events compared to the number of loaded cells, it was postulated that these false-positive events might represent ambient RNA molecules that were present in the initial cell suspension (before the isolation) due to premature cell lysis. These observations were supported by the previous reports showing that scRT-PCR in W/O droplets leads to increased positive counts compared to the actual number of cells (112,207). In addition, ambient mRNA molecules released during cell preparation and encapsulation were identified as the most likely source of these events (114). In this context, accurate detection of false-positive events is important for any future diagnostic and biological applications as these events may create undesirable artifacts in nucleic acid quantification and analysis. As shown in the next section, an independent fluorescence readout was required to efficiently discriminate the true-positive and false-positive events and simultaneously identify the cells lacking the expression of the cell-specific marker gene.

3.2.6. Discrimination of true-positive and false-positive events

Accurate differentiation of the fluorescent microcapsules that carry a cell (true-positive events) from the fluorescent microcapsules that lack a cell but happen to have ambient mRNA molecules (false-positive events) might be challenging since the end-point fluorescent signal can be indistinguishable

between these events. For example, results presented in **Figure 3.18, C** show that separation of the microcapsules that contain cells and those that contain cell-free RNA is difficult, if not impossible, to achieve. To overcome this analytical drawback, the microcapsule-based multiplex scRT-PCR approach presented in section 3.2.4 was slightly changed by modifying cell lysis conditions. It was postulated that using mild-lysis conditions, cell nuclei would retain their compact structure during all reaction steps and, as a result, could be used as a reference to identify the microcapsules with the isolated cells irrespective of their transcriptional activity.

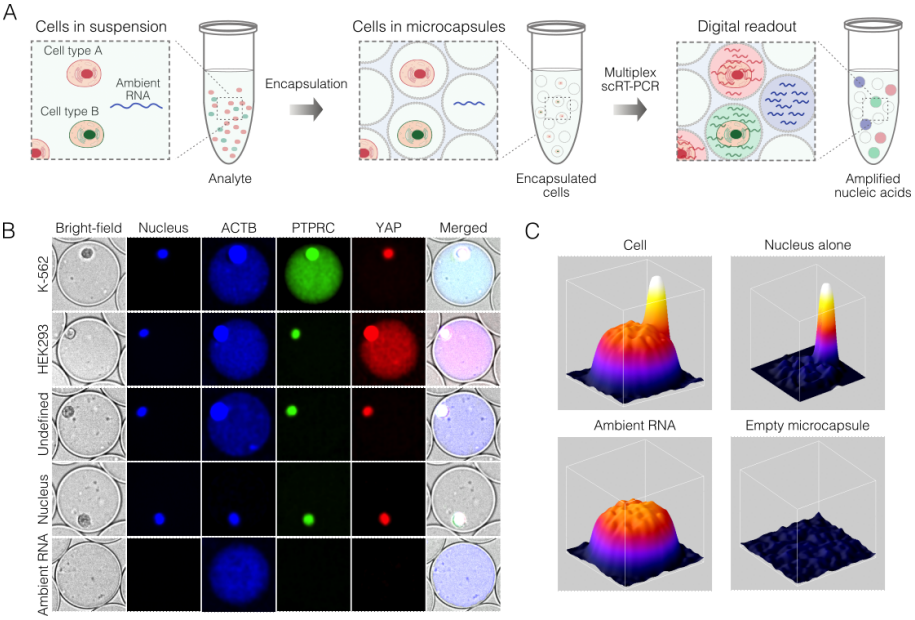

Figure 3.20. Detection of true/false-positive and true/false-negative events after single-cell multiplex RT-PCR in microcapsules. (**A**) Illustration of an experimental scheme where a typical biological analyte comprising cells and ambient RNA is isolated in microcapsules, subjected to multiplex RT-PCR, and evaluated by fluorescence imaging. (**B**) Representative microscopy images of the microcapsules after multiplex scRT-PCR targeting *ACTB*, *PTPRC*, and *YAP* markers. (**C**) 3D fluorescence profiles of microcapsules in the Alexa Fluor 647 (*ACTB*) channel correspond to a cell with amplicons, a nucleus alone, amplified ambient RNA, and an empty microcapsule. The heat colors indicate pixel intensity.

To verify this approach, the mixture of K-562 and HEK293 cells was isolated in microcapsules, fixed in ice-cold ethanol, and permeabilized in mild-lysis conditions using non-ionic detergent (see *Materials and Methods*). The microcapsules were then subjected to regular multiplex RT-PCR. Digital analysis of post-RT-PCR samples revealed that using mild-lysis conditions,

cell nuclei not only remained intact but also emitted a characteristic and spatially confined fluorescence in all channels (Alexa Fluor 647 (*ACTB*), Alexa Fluor 488 (*PTPRC*), and Alexa Fluor 555 (*YAP*)), presumably due to the non-specific uptake of fluorescently labeled PCR probes (**Figure 3.20, B and C**). However, the fluorescence emitted from the nuclei could be enhanced by staining with a DAPI dye, which was relevant when working with smaller primary cells, such as PBMCs. In contrast, the fluorescence of PCR amplicons was uniformly distributed across the entire microcapsule volume. Therefore, measuring the fluorescence profile of the entire microcapsule provides a straightforward approach to correctly identifying the microcapsules that carry cells and separating them from the microcapsules with cell-free nucleic acid molecules (**Figure 3.21**).

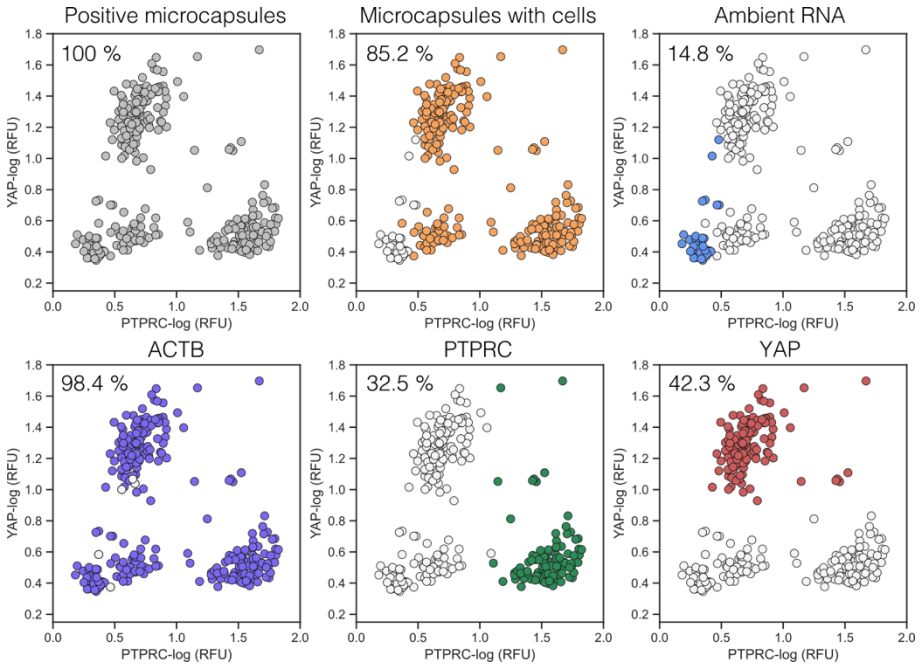

Figure 3.21. Microscopy-based characterization of a sample comprising a mixture of K-562 and HEK293 cells. Grey color shows microcapsules that exhibit any fluorescent signal; orange color shows microcapsules that contain a cell; blue color shows microcapsules that exhibit RT-PCR signal lacking a cell; purple, green, and red colors show microcapsules positive for *ACTB*, *PTPRC*, and *YAP* marker, respectively. Each plot is represented by >300 counts.

Taking advantage of this analytical feature, cell-free RNA levels were evaluated in a sample with co-encapsulated K-562 and HEK293 cells for three housekeeping genes, including *ACTB*, β-2-microglobulin (*B2M*), and TATA-

box binding protein (*TBP*). It was anticipated that highly-abundant *ACTB* transcript would have an increased contamination level as more RNA molecules would be released prematurely by the compromised cells. As expected, the number of cell-free microcapsules displaying a fluorescent signal for the *ACTB* marker constituted 16 % of all positive *ACTB* counts but dropped to 0.8 % when targeting the *TBP* gene (**Figure 3.22**). Based on the literature reports, *TBP* is being expressed at ~10 copies per cell (208), and qPCR results showed ~60 times lower expression levels compared to the *ACTB* gene. Furthermore, being able to identify and quantify the true/false positives and true/false negatives made it possible to evaluate the statistical characteristics of the multiplex RT-PCR assay. The assay specificity was in the range of 97.71-99.93 %. The sensitivity was estimated to be 98.65 % for *ACTB* and 92.57 % for *YAP* when analyzing HEK293 cells and 98.37 % for *ACTB* and 71.74 % for *PTPRC* when analyzing K-562 cells. The cell-type specific markers *YAP* and *PTPRC* displayed very high positive predictive values (PPVs), 98.56 % and 99.25 %, respectively. Negative predictive values (NPVs) were also very high, 99.60 % and 98.23 %, respectively. However, it is worth noting that these values are not fixed and depend on sample quality, cell type, physiological state, or target selection (as revealed in the following paragraph).

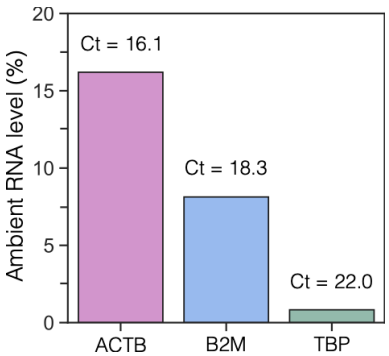

Figure 3.22. The ambient RNA levels for *ACTB*, *B2M*, and *TBP* housekeeping genes in a mixture containing K-562 and HEK293 cells. The ambient RNA levels were determined by performing multiplex RT-PCR and recording the fraction of the cell-free microcapsules positive for a given housekeeping gene. The percentage on Y-axis is expressed as $(n_1/(n_1 + n_2)) \times 100$ %, where n_1 is cell-free microcapsules positive for a given housekeeping gene and n_2 is microcapsules with cells positive for a housekeeping gene. The average Ct values were obtained from three independent bulk RT-qPCR experiments. The sensitivity of *ACTB*, *B2M*, and *TBP* marker detection was 98.68 %, 95.76 %, and 97.54 %, respectively.

Digital profiling of the microcapsules with co-isolated K-562 and HEK293 cells uncovered a subpopulation that lacked detectable levels of *PTPRC* or *YAP* markers yet expressed high levels of a housekeeping gene. To better understand the origin of these cells, multiplex scRT-PCR was repeated on each cell line independently. In agreement with FACS results (209), this experiment revealed a bimodal *PTPRC* gene expression distribution in K-562 cells (**Figure 3.23**), which are known to differentiate into the erythroid lineage that lacks *PTPRC* gene expression (210). However, a limited degree of bimodality may be caused by transcriptional bursts (211), cell cycle dependence (212), and stochastic effects (213). All of them may give rise to cells that appear to lack a transcript of interest at a given moment in time. In addition, compromised cell viability could also result in a bimodal distribution, which might be the case for *YAP* expression in HEK293 cells.

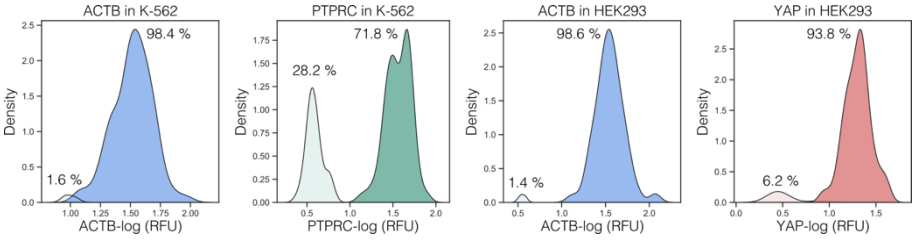

Figure 3.23. Digital profiling of K-562 and HEK293 cells for *ACTB*, *PTPRC*, and *YAP* gene expression. Kernel density estimate (KDE) plots represent the fluorescence distribution in microcapsules after multiplex RT-PCR targeting for *ACTB* (blue), *PTPRC* (green), and *YAP* (red) transcripts in individual cell lines. For *ACTB* profiling, all microcapsules harboring nuclei were plotted, while for *PTPRC* and *YAP* profiling, only microcapsules bearing nuclei and being positive for *ACTB* were selected and plotted.

3.2.7. Leukemia cell discrimination from PBMCs

To demonstrate the potential use of the developed microcapsule technology for biomedical applications, primary human cell profiling was conducted. For that purpose, previously-frozen peripheral blood mononuclear cells (PBMCs) were isolated in microcapsules and subjected to scRT-PCR targeting the commonly used blood cell marker *PTPRC* (also known as CD45). Considering the well-established fact that PBMCs are positive for the *PTPRC* marker, it was expected to achieve a >95 % detection rate. The microscopy-based analysis of the post-RT-PCR microcapsules revealed that only 77.2 % of the encapsulated cells were positive for the *PTPRC* marker (**Figure 3.24**). Profiling PBMCs for another ubiquitous marker (*B2M*) showed a similar detection rate (74.6 %). These numbers, however, matched the

fraction of viable cells (~77 %) very closely, as determined by trypan blue staining, pointing out that cell detection rate by scRT-PCR correlates with cell viability.

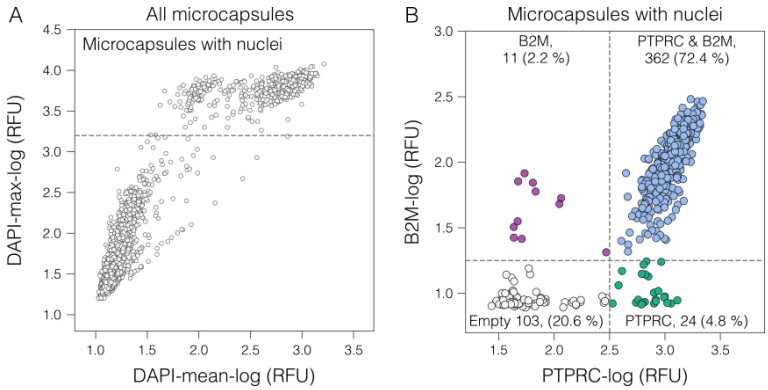

Figure 3.24. ScRT-PCR output from thawed PBMCs. (**A**) The strategy used to identify microcapsules with isolated cells was based on DAPI peak intensity. The scatter plot is represented by 4000 counts. (**B**) *PTPRC* and *B2M* marker detection in microcapsules with nuclei. The scatter plot is represented by 500 counts.

After confirming RT-PCR product generation from primary human cells, PMBCs were spiked with acute promyelocytic leukemia cells (NB-4), and the pooled sample was used to identify the leukemic cells based on the expression of the fused gene *PML-RARα*. It was shown previously that NB-4 cells and primary leukemia samples have a similar *PML-RARα* expression level (214). Single-cell multiplex RT-PCR was applied as an alternative to the standard method where instead of analyzing individual cells, the total RNA is extracted from the blood sample and subjected to cancer diagnostics by bulk RT-PCR (214,215). The results presented in **Figure 3.25** indicate that individual leukemia cells were identified in the mixture of PBMCs using microscopy (**A**) and flow cytometry analysis (**B**), although the fraction of detected NB-4 cells appeared ~2-fold lower than the theoretical prognosis.

To better understand this discrepancy, the expression level of *PML-RARα* transcript in NB-4 cells was quantified using qPCR. This experiment showed that *PML-RARα* expression was ~200-fold lower than for *PTPRC* or *TBP*, which roughly translates to less than 1 copy of *PML-RARα* transcript per cell, on average. Therefore, it is reasonable to assume that not all NB-4 cells were expressing *PML-RARα* at a given moment in time, thus explaining the difference in the observed counts. In this context, it is worth noting that digital profiling of another fusion transcript (*BCR-ABL*) in K-562 (expressed at

approximately 40 copies per cell on average (216)) resulted in a 98.6 % detection rate (**Figure 3.26**).

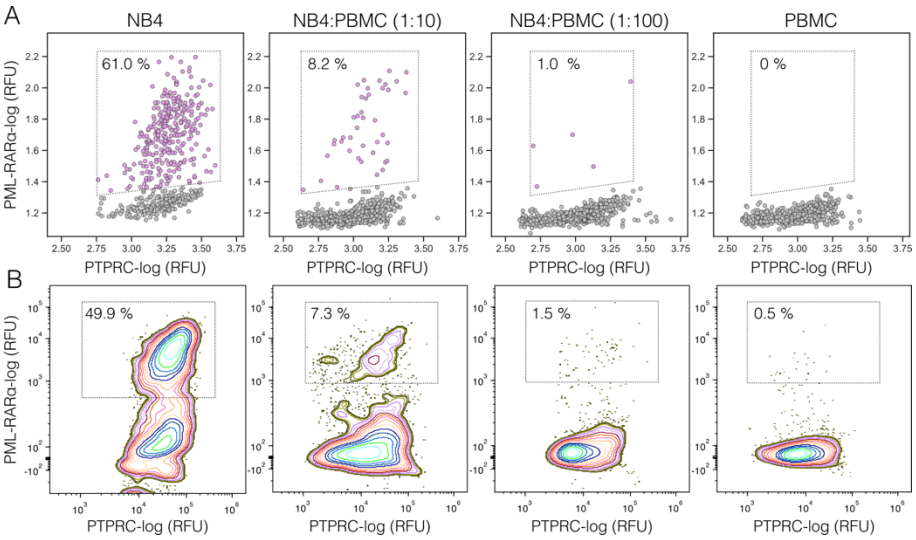

Figure 3.25. RNA cytometry of acute promyelocytic leukemia cells and human peripheral blood mononuclear cells (PBMCs). (**A**) Microscopy-based and (**B**) flow cytometry-based analysis of human PBMCs spiked with different dilutions of NB-4 cells. The multiplex scRT-PCR targeted *PTPRC* (CD45) and *PML-RARα* transcripts. The PBMCs were detected by the expression of a marker gene *PTPRC*; the NB-4 cells were quantified by recording the co-expression of *PTPRC* and *PML-RARα*. The percentages depict the fraction of the total counts. The scatter plots are represented by 500 (**A**) and ~4000 (**B**) counts.

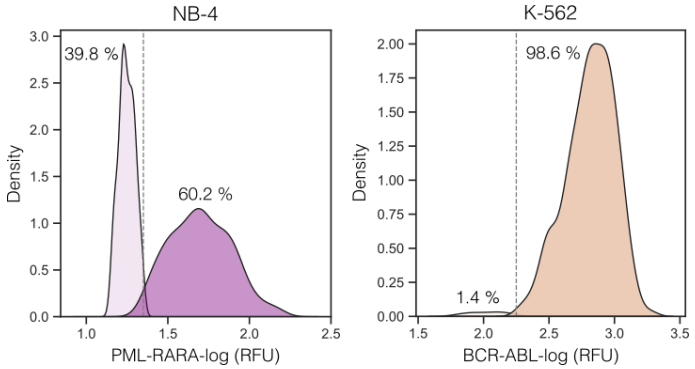

Figure 3.26. Digital profiling of NB-4 and K-562 cells for *PML-RARα* and *BCR-ABL* gene expression. KDE plots represent the fluorescence distribution in microcapsules after multiplex RT-PCR targeting for *PML-RARα* (purple) and *BCR-ABL* (orange) transcripts in individual cell lines. For fusion transcript distribution analysis, all microcapsules harboring nuclei and being positive for housekeeping gene (*B2M*), were selected and plotted.

Altogether, the RNA cytometry concept presented in this study offers a practical and easily customizable approach for rapid and highly sensitive digital profiling of thousands of individual cells and is advantageous over the existing droplet and plate-based RT-PCR platforms. More importantly, GMA microcapsules are not limited to the RT-PCR assay and can be easily extended to diverse molecular biology applications. As presented in the following section, it can be applied to single-cell RNA sequencing.

3.3. Single-cell RNA sequencing

3.3.1. The strategy used to capture single-cell transcriptomes

As shown in the previous section, the GMA microcapsules can be used to release the genetic material after extracting it from the individual cells and processed through multiple buffers and biochemical reactions. Based on these results, it was anticipated that microcapsules developed in this work could provide an advantage over existing droplet-based and plate-based single-cell RNA sequencing (scRNA-Seq) approaches, where cell lysis and mRNA barcoding are performed in the same reaction under suboptimal conditions, and in the presence of intracellular inhibitors (e.g. RNases).

To demonstrate microcapsule implementation for scRNA-Seq, the workflow depicted in **Figure 3.27** was pursued. Similar to scRT-PCR, cells at a limiting dilution were isolated in microcapsules and subjected to harsh lysis by dispersing the microcapsules in a chaotropic lysis mix, followed by gDNA depletion in the presence of DNase I (**Figure 3.27**, **A).** The microcapsules bearing the purified total RNA from single cells were subjected to inDrops platform (2,86) to conduct the mRNA barcoding step. Briefly, GMA microcapsules were loaded in W/O droplets along with barcoding hydrogel beads and reverse transcription reagents. The semi-permeable nature of the microcapsule shell permits reverse transcription reagents and barcoding DNA primers to diffuse into the microcapsule core, followed by polyadenylated RNA capture on the poly(dT) region and cDNA synthesis initiation (**Figure 3.27**, **B**). After this step, cDNA molecules were labeled with cell-specific barcodes and could be pooled together for the subsequent library preparation and sequencing.

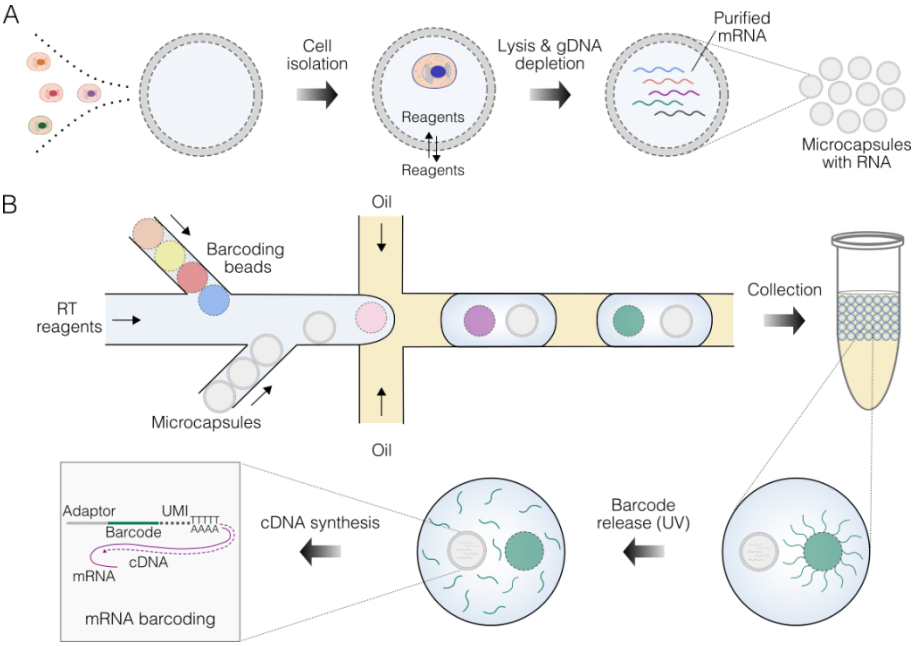

Figure 3.27. Single-cell RNA sequencing strategy using GMA microcapsules. (**A**) Single-cell isolation in microcapsules followed by mRNA purification. (**B**) Microcapsule loading in W/O droplets with barcoding beads and reverse transcription reagents. Following barcode release, oligonucleotides traverse the semi-permeable shell and initiate cDNA synthesis inside the microcapsule core.

3.3.2. Analysis of mammalian cell transcriptomes

The first attempts to validate microcapsules for whole transcriptome analysis were addressed using cultured mammalian cell lines. As a model system, a mixture containing an even ratio of mouse NIH-3T3 and human K-562 cells was isolated in GMA microcapsules, followed by harsh lysis and gDNA depletion. Then, microcapsules containing RNA molecules were loaded into W/O droplets to conduct mRNA barcoding (the workflow termed CapDrop). In parallel, the scRNA-Seq library was prepared by supplementing the reverse transcription reaction with collagenase A to decompose the GMA shell, which might also enhance mRNA capture efficiency (the workflow termed CapDrop + ColA). As a reference, the standard inDrops protocol, where single cells were loaded in droplets without using the microcapsules, was also included.

Comparative analysis revealed that single-cell processing (lysis and RNA purification) in microcapsules before the barcoding step increased transcript and gene counts by approximately 1.5-fold (**Table 3.3**). An improved mRNA capture could be attributed to a more efficient mRNA release under harsh lysis

conditions in microcapsules and subsequent washes to remove RNases and other intracellular inhibitors that might be present in a cell lysate.

Table 3.3. Comparative analysis of the mean and median values of transcripts (UMI) and gene counts after scRNA-Seq using CapDrop, CapDrop + ColA, and inDrops. All three samples showed similar sequencing saturation (0.336-0.386).

Sample	Mean UMI	Median UMI	Mean genes	Median genes
CapDrop	12012	11659	2953	2882
CapDrop + ColA	12157	11678	3011	2920
InDrops	7637	7000	2051	1988

The second aspect of CapDrop and inDrops method evaluation was the analysis of barcoding specificity. A cell with more than 80 % of all reads aligned to the human genome was classified as a K-562 cell, and a cell with more than 80 % of all reads aligned to the mouse genome was classified as a NIH-3T3 cell. The remaining cells (barcodes, BCs) were identified as multiplets as they had a significant fraction of reads belonging to both cell lines. As expected, CapDrop showed a similar cell doublet ratio as inDrops – 8.12% *vs.* 6.52% (**Figure 3.28**, **A**).

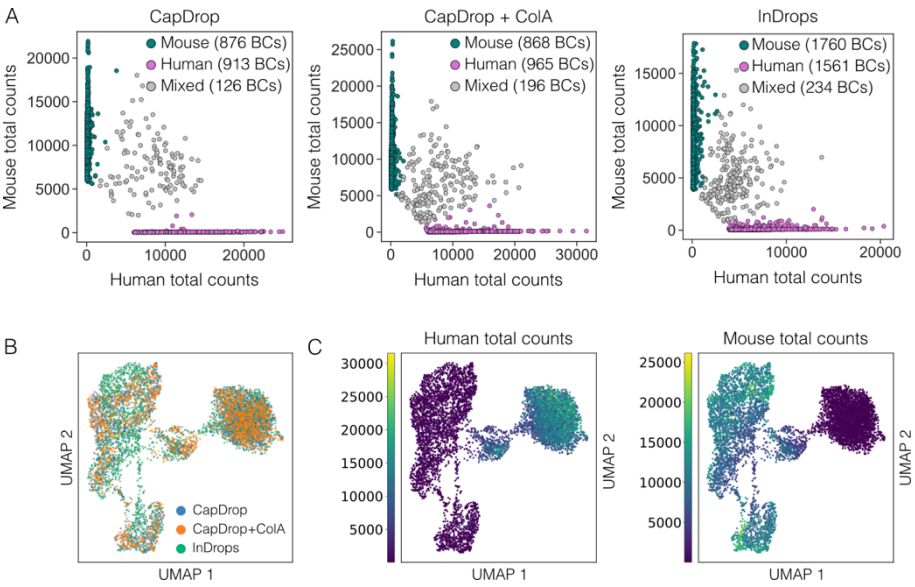

Figure 3.28. RNA sequencing results from individual K-562 and NIH-3T3 cells. (**A**) Scatter plots show species mixing events from three workflows: (i) CapDrop, (ii) CapDrop + ColA, and (iii) inDrops. (**B**) UMAP plot shows single-cell transcriptomes derived from three methodologies distributions between the formed clusters. (**C**) UMAP plots show human and mouse count distribution between the clusters.

Furthermore, projecting the single-cell transcriptomes on Uniform Manifold Approximation and Projection (UMAP) showed homogeneous transcriptome distribution for all three methodologies and confirmed that there were no obvious differences between CapDrop and inDrops (**Figure 3.28**, **B and C**). The results also showed that GMA shell decomposition by collagenase A during the reverse transcription step did not have any clear effect on UMI and gene capture.

Having confirmed that microcapsule-based single-cell RNA sequencing faithfully captures nucleic acids derived from single cells without obvious biases, CapDrop was applied to a more challenging biological sample – bacterial cells, which is introduced in the next section.

3.3.3. Analysis of bacterial cell transcriptomes

In contrast to mammalian scRNA-Seq, bacterial cell profiling has many more challenges, including low RNA content, lack of mRNA polyadenylation, and a resistant cell envelope. Due to these reasons, the scRNA-Seq strategy for mammalian cells presented in **Figure 3.27** was not optimal and had to be modified to enable bacterial cell analysis. At first, a two-step lysis approach was conducted, where lysozyme-induced lysis was followed by a treatment in the chaotropic reagent (see *Materials and Methods*). Secondly, to capture RNA molecules via the poly(dT) region located on the barcoding primer, microcapsules with total purified RNA were subjected to the polyadenylation step. As a result, all RNA molecules, including highly abundant ribosomal RNAs, were labeled with polyA tail.

To demonstrate RNA sequencing from individual bacterial cells, *E. coli* MG1655 and *B.subtilis* 23857 were mixed at an equal ratio and encapsulated at a limiting dilution such that each microcapsule, on average, would contain no more than one cell. As a reference, either *E. coli* MG1655 or *B. subtilis* 23857 cells were encapsulated separately. The isolated cells were subjected to multi-step processing, including two-step lysis, gDNA depletion, and RNA polyadenylation. Microcapsules bearing polyadenylated RNA molecules were then loaded onto inDrops platform to conduct RNA barcoding, followed by library construction and sequencing (see *Materials and Methods*). As a proof-of-concept, ~3000 positive microcapsules from each sample were barcoded.

The first question that had to be answered from the sequencing results was barcoding specificity. Similar to mammalian cell sequencing and data analysis, a threshold of 80 % gene counts was used to assign cell identity for every demultiplexed barcode. Although not-equal representation of the two species occurred, the results revealed that 92 % of barcodes were assigned to

one species, and 8 % remained as multiplets (**Figure 3.29**, **A**, first scatter plot). Interestingly, the sample with separate species isolation in microcapsules and mixing before the barcoding (**Figure 3.29**, **A**, second scatter plot) showed a very similar multiplet frequency (8.5 %), which confirms that multiplets were not originated from the *E. coli* and *B. subtilis* co-encapsulation events or physical cell interaction. Independent *E. coli* and *B. subtilis* sequencing (**B**) indicated that the assignment to the corresponding species was highly specific, and just a few discrepancies occurred in the *B. subtilis* sample, where 0.2 % barcodes were assigned to *E. coli,* and 0.6 % were assigned to both bacterial species. These results confirmed that most of the multiplets could be explained by the co-occurrence of the same barcode and/or co-encapsulation of two or more microcapsules with one barcode during the cDNA synthesis step.

To evaluate UMI counts in each species, the sample prepared by cell co-encapsulation was selected (**Figure 3.29**, **A**, first scatter plot). Using the knee plot, cells bearing more than 100 UMIs were selected (**C**), and then the distributions of total counts (**D**), rRNA counts (**E)**, and mRNA counts were plotted (**F**). As expected, more than 80 % UMIs originated from rRNA barcoding.

Sequencing reads enriched in rRNA are undesirable and have to be reduced, aiming to capture mRNA and extract biologically meaningful information more efficiently. In a recently published work, this limitation was overcome by 5S, 16S, and 23S rRNA depletion using blocking primers, which prevented rRNA polyadenylation and the subsequent amplification (217). In addition, RNA capture efficiency is strongly influenced by template switching during the reverse transcription step. Template switching is known to be biased to RNA molecules having a 5'-terminal 7-methylguanylate (m^7G) cap, which is present in eukaryotic but not prokaryotic mRNA molecules (218). In contrast, prokaryotic mRNA molecules have a 5'-terminal triphosphate group, which could be modified to (m^7G) cap by Vaccinia virus Capping Enzyme (218). Another possible strategy is a randomly primed second-strand synthesis after reverse transcription to append a second oligonucleotide handle for whole transcriptome amplification (219). In this way, those mRNA molecules that were successfully reverse transcribed but to which a second oligonucleotide handle was not appended due to inefficient template switching would not be lost and would participate in the next steps of library preparation. In conclusion, these additional RNA processing steps should be prioritized in order to increase single-cell RNA sequencing quality. It is anticipated that the unique features provided by microcapsules developed in this work, and the proof-of-concept study revealed in this chapter, will pave the way to achieving this ultimate goal.

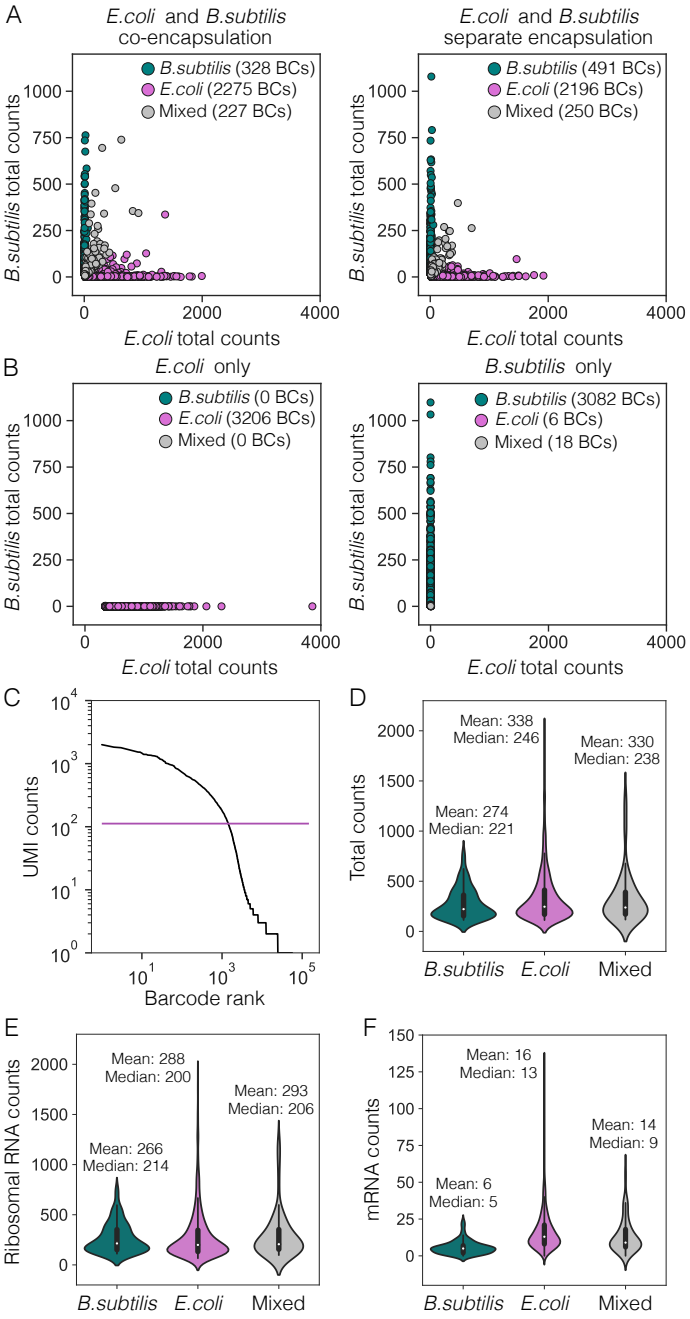

Figure 3.29. RNA sequencing results from individual *E.coli* MG1655 and *B. subtilis* 23857 cells. (**A**) Scatter plots represent species mixing events after barcoding bacteria mixture and (**B**) after barcoding each species separately. (**C**) Knee plot of the sample with co-encapsulated *E. coli* and *B. subtilis*. Cells bearing >100 UMIs were selected for plotting the distribution of total counts (**D**), ribosomal RNA counts (**E**), and mRNA counts (**F**).

3.4. Discussion

Multi-step analyte processing is highly common in biological and biochemical sciences, where reagents need to be added or replaced at a specific step of the workflow. This is particularly relevant for nucleic acid analysis, where cell disruption and nucleic acid purification must take place prior to the amplification and analysis. Such multi-step analyses represent one of the biggest challenges for droplet microfluidics technology, which is largely built on single-step reactions, where all the reagents are combined at once during the cell encapsulation. Although sophisticated technological solutions exist for conducting multi-step reactions, these are not readily available to regular molecular biology laboratories and require highly specialized expertise.

This thesis aimed to provide a simple and practical solution for performing a high-throughput single-cell analysis compatible with a broad range of molecular biology protocols. This was achieved by creating semi-permeable microcapsules that enable efficient isolation and retention of single cells as well as their nucleic acids through multi-step workflow procedures. These unique compartments are based on a conceptually simple principle, where a plurality of cells are isolated in a plurality of aqueous two-phase system droplets having a liquid core and a liquid shell. Upon a stimulus (cooling and/or photopolymerization), the liquid shell is converted to an elastic hydrogel shell, completely enveloping the liquid core. Once the cells are isolated within the microcapsules, multi-step reactions can be performed by simply changing aqueous solutions in which microcapsules are dispersed. Microcapsules featuring biocompatibility, thermostability, chemical stability in different buffers, high uniformity, and semi-permeable shells should open new possibilities for performing single-cell research.

Even though the concept and several methods for producing hydrogel microcapsules were published before and during this work (33,39-43,189,190), the applications of such microcapsules for single-cell analysis were not pursued as the works focused mostly on fundamental physical and chemical research (42,43,189,190). Meanwhile, the works focusing on single-cell analysis were limited by the complex and inefficient microcapsule generation restricting their further use (33,40). In this context, alginate-based microcapsules represent one of the most efficient systems (39), even if it is limited to cell cultivation.

This study introduced two hydrogel microcapsule compositions based on PEGDA and GMA hydrogel shells. In both cases, the shells envelop the dextran-based core, where isolated cells reside, and assays/reactions occur.

Microcapsules developed in this work share many common features. First, PEGDA and GMA hydrogel shells ensure that microcapsules retain large entities (e.g., cells, gDNA, dsDNA ≥600 bp. and ≥300 bp., respectively), while allowing smaller molecules (e.g., proteins, oligonucleotides) to traverse the hydrogel membrane. Second, both compositions demonstrate high stability during a variety of laboratory treatments, such as pipetting, vortexing, centrifugation, PCR cycling, and freezing. However, the different compositions gave rise to important functional differences. For example, PEGDA microcapsule diameter is limited to 40–60 μm, and the generation of larger concentric microcapsules becomes very challenging to achieve. In contrast, GMA microcapsule diameter can be adjusted to 150-200 μm while retaining excellent concentricity. Another major difference was observed in cell retention. While in GMA microcapsules, cells preferably localize in the dextran core, in PEGDA microcapsules, cells partition at the PEGDA/dextran interphase. Finally, one of the most significant differences is the decomposition of microcapsules. Dissolving PEGDA microcapsules can only be achieved in a strong alkaline solution at elevated temperatures. GMA microcapsules, on the other hand, can also be decomposed using proteinase K, trypsin, or collagenase. Taking into account these differences, it can be concluded that PEGDA microcapsules are beneficial for bacterial cell analysis, while GMA microcapsules represent a more universal tool for isolating and analyzing diverse cell types.

Four single-cell assays – single-genome amplification, multiplex RT-PCR, RNA sequencing, and cultivation – were implemented to demonstrate microcapsule use and superiority in corresponding research areas. In the first part of this study, sequential reactions on Gram-positive and Gram-negative bacteria were conducted in PEGDA microcapsules to obtain single amplified genomes (SAGs). In the case of *R. rhodochrous* and *S. mutans* bacteria, efficient SAG generation was possible only by applying a two-step lysis protocol, where lysozyme-induced lysis was followed by the treatment with proteinase K and SDS. Such harsh lysis conditions are not compatible with the W/O droplet technologies. Although hydrogel beads, in principle, are suitable for multi-step reactions and conditions required for efficient cell lysis, poor isolated bacterial cell retention and lower DNA yield after MDA limit their use. As a result, PEGDA microcapsules provide an advantageous solution for genome amplification, especially for difficult-to-lyse bacteria. As yet another example, it was demonstrated that individual *E. coli* cells maintain their physiological activity in microcapsules and can be expanded into isogenic microcolonies for the subsequent phenotypic analysis. In general microcapsule-based phenotypic screening is possible when the molecules of

interest are either retained within the bacteria or, because of their size, remain trapped in the microcapsule core, which was the case with the PHB granules (220). In some cases, cell cultivation in microcompartments is accompanied by cell recovery required for downstream analysis steps, such as recultivation (155). Unfortunately, retrieving live cells from PEGDA microcapsules is difficult, if not impossible, to achieve.

An alternative microcapsule composition comprising a GMA-based shell was introduced to enable mammalian cell isolation and analysis. These microcapsules were applied for digital profiling of human leukemia cells, embryonic kidney cells, and primary PBMCs using a multiplex RT-PCR assay. Before the analysis, it was anticipated that harsh lysis followed by gDNA depletion would result in the highest assay efficiency. Even though bright fluorescent partitions specific to a given cell type were generated, it was observed that microcapsules with cells and microcapsules with ambient RNA generated nearly the same fluorescence intensity, highlighting the risk of accurately quantifying cells based on the gene expression of a single marker. This limitation could be overcome by targeting two genes simultaneously (e.g., one ubiquitously and one differentially expressed gene), yet at the cost of increased assay multiplexing. As yet another analytical strategy, it was shown that using mild-lysis conditions, nuclei remained intact during all analytical procedures and provided a convenient way to differentiate true-positive events (cells) from false-positive events (cell-free nucleic acids) in the post-RT-PCR sample.

The microcapsule-based scRT-PCR assay specificity was particularly high (99.12 ± 0.89%) with all target probes used in this work, although the sensitivity varied from 71 % to 98 % depending on the gene marker, cell type, and primers used. It was estimated that targeting genes expressed at low to medium levels (10 to 40 copies per cell) reduced the false positive (ambient RNA) levels down to ~0.8 % while retaining high assay sensitivity (97.54 %). The detection of transcripts that are expressed at very low levels (e.g., 1 copy per cell) was also successfully achieved, although it may need further optimizations, one of which may involve using targeted RT primers (221).

An important advantage of the microcapsule-based technique reported in this work is that nucleic acids encoded by single cells can be efficiently purified under a variety of lysis conditions leading to improved enzymatic reactions. Also, the compatibility of microcapsules with freezing in alcohols allows isolated samples to be stored for longer periods. The ability to entirely replace microcapsule content at any given step in a protocol should make microcapsules broadly applicable to different formats of multiplexing, including *in situ* hybridization and imaging (222).

The post-RT-PCR microcapsule analysis was performed using flow cytometry and epifluorescence microscopy without any clear discrepancies between these approaches. In cases where time is a limiting factor and a high number of cells needs to be analyzed (n >10.000), flow cytometry provides an optimal option. On the other hand, the results of microscopy analysis are easier to interpret, especially during assay development. Although not used in this study, imaging flow cytometry for post-RT-PCR microcapsule analysis could, in principle, provide the most appealing option by combining imaging data with the throughput of flow cytometry.

The multiplex scRT-PCR assay developed in this study could be expanded to other research areas, such as analysis of gene isoforms (223), clinically relevant marker expression (224), or genetic aberrations (214,215,225,226). It could quantitively assess the distribution and frequency of somatic mutations in a panel of cancer-driving genes and benefit cancer diagnostics (227-229). Microcapsule-based overlap extension RT-PCR could also be applied for natively paired sequencing of B and T cell receptors to understand adaptive immunity in health and disease (12,91,113,205,206,230,231).

The applicability of GMA microcapsules can be extended beyond RT-PCR, as demonstrated in the last part of this study. RNA molecules originating from a single mammalian and bacterial cell can be barcoded and sequenced to obtain the whole transcriptome-encoded information. The experimental strategy using microcapsules sharply contrasts with the existing droplet-based scRNA-Seq platforms (2,98), where cell lysis and reverse transcription steps are performed in a single compartment highlighting the risk of suboptimal conditions. This is exemplified by approximately a 1.5-fold increase in gene and transcript counts when single-cell lysis and RNA purification were done in microcapsules. Although bacterial cell RNA sequencing results showed a very shallow transcriptome profiling, it still remains a highly promising strategy pending further optimizations. It is anticipated that the rRNA depletion (217) and more efficient mRNA capture and amplification (218,219) would improve mRNA sequencing results. Also, considering the time required for cell isolation in microcapsules and rapid bacterial mRNA turnover, it is important to perform cell fixation step before the encapsulation (232). In addition, GMA microcapsules being biocompatible, provide an option to cultivate single bacterial cells into isogenic colonies. As shown in some literature reports, isogenic colony RNA-sequencing bypassed low RNA content and significantly increased UMI counts per cell (29,30). Moreover, the microcapsules presented in this work could be used with an alternative barcoding option based on a combinatorial split-and-pool process (233,234). Due to the selective permeability of the microcapsule shell, the short

barcoding oligonucleotides can be delivered during the several rounds of nucleic acid barcoding reactions while also ensuring the retention of longer (barcoded) nucleic acids inside the core.

In conclusion, the semi-permeable microcapsule concept that is reported in this doctoral thesis provides the basis for a variety of single-cell assays that could be built and adapted for various research goals. It can be anticipated that these novel compartments will eventually benefit diagnostics, cell biology, and biomedicine.

CONCLUSIONS

1. Semi-permeable microcapsules have been developed using an aqueous two-phase system consisting of PEGDA and dextran.
2. PEGDA microcapsules were found to efficiently retain bacterial cells and allow genomic DNA amplification, cultivation, and assessment of metabolic activity.
3. The localization of mammalian cells between the outer and inner phases in PEGDA microcapsules makes the isolation and analysis of these cells impractical and inefficient.
4. An aqueous two-phase system consisting of GMA and dextran can be used as an alternative composition of semi-permeable microcapsules.
5. Microcapsules with a GMA shell exhibit efficient cell and nucleic acid retention ($\geq$ 300 bp), stability, and biocompatibility, making them suitable for the analysis of nucleic acids from single mammalian cells.
6. Single-cell RT-PCR in GMA microcapsules provides an accurate and sensitive method for the analysis of single cells against target genes.
7. GMA microcapsules have enabled the development of a new method for the whole transcriptome analysis of single mammalian and bacterial cells.

LIST OF PUBLICATIONS AND PERSONAL CONTRIBUTIONS

Publications included in this thesis

- **Leonaviciene, G**.; Leonavicius, K.; Meskys, R.; Mazutis, L., Multi-step processing of single cells using semi-permeable capsules. Lab Chip 2020, 20 (21), 4052-4062.
  In this work, I planned and performed the experiments, analyzed the data, prepared the figures, and contributed to the writing of the manuscript.

- **Leonaviciene, G**. and Mazutis, L., RNA cytometry of single-cells using semi-permeable microcapsules. Nucleic Acid Research 2022, gkac918.
  In this work, I planned and performed the experiments, analyzed the data, prepared the figures, and contributed to the writing of the manuscript.

Publications not included in this thesis

- Simutis, K.; **Stonyte, G**.; Mazutis, L., Antibody discovery using microfluidic systems. In *Microfluidics for Pharmaceutical Applications* (2019) 337-351 William Andrew Publishing.
  In this work, I collected references related to droplet-based microfluidics approaches used for antibody-secreting cell screening and natively paired sequencing of B cell T cell receptors. I also contributed to the preparation of figures and writing.

LIST OF PATENT APPLICATIONS AND PERSONAL CONTRIBUTIONS

Patent applications included in this thesis

- Mazutis, L.; **Stonyte, G**.; Leonavicius, K.; Zelvyte, A., Systems and methods for encapsulation and multi-step processing of biological samples. PCT/IB2020/057266. 2020.
  In this work, I planned and performed the experiments, analyzed data, prepared the figures, and contributed to the writing.

- Mazutis, L.; **Leonaviciene, G**., Microcapsules comprising biological samples, and methods for use of same. 2021.
  In this work, I planned and performed the experiments, analyzed data, prepared the figures, and contributed to the writing.

- Mazutis, L.; **Leonaviciene, G**., Microcapsules comprising biological samples, and methods for use of same. 2021.
  In this work, I planned and performed the experiments, analyzed data, prepared the figures, and contributed to the writing.

- Mazutis, L.; **Leonaviciene, G**.; Goda, K., Methods for processing and/or barcoding nucleic acids. 2021.
  In this work, I contributed to the planning and performing of the experiments. I also contributed to the preparation of figures and writing.

Poster presentations at international conferences

- **Leonaviciene, G**.; Leonavicius, K.; Meskys, R.; Mazutis, L., Multi-Step Processing of Single-Bacteria Using Semi-Permeable Capsules. SCGS Workshop, USA. 2019.

- **Leonaviciene, G**.; Leonavicius, K.; Meskys, R.; Mazutis, L., Multi-Step Processing of Single-Bacteria Using Semi-Permeable Capsules. The COINS, Lithuania. 2021.

ACKNOWLEDGMENTS

I would like to express my gratitude to all the people who supported me during the long and winding journey of my PhD. I could not have taken this journey without the support from my supervisor Prof. Dr. Linas Mažutis, who introduced me to the field of droplet microfluidics, set my scientific direction, and guided my decisions along the way. I am thankful for your trust in my abilities and for providing this rewarding, once-in-a-lifetime experience. I would also like to extend my gratitude to all the lab members for making the lab feel like a second home. Thank you for all the daily stimulating conversations and the relaxing atmosphere when it was most needed during the plentiful challenges of scientific research.

This journey could not have been completed without my defense panel: Prof. Dr. Kęstutis Sužiedėlis, Assoc. Prof. Dr. Aušra Sasnauskienė, Dr. Mindaugas Zaremba, Dr. Remigijus Skirgaila and Prof. Dr. Skirmantas Kriaučionis. Thank you all for dedicating your time to evaluate my doctoral thesis. I am extremely grateful to Dr. Mindaugas Zaremba and Dr. Remigijus Skirgaila, who took their time to thoroughly review my thesis and provide valuable feedback at the final stages of writing up. I would also like to acknowledge the help of the VU Life Sciences Center Team in developing my interpersonal skills and assisting me with the academic administrative requirements involved in the long process of PhD studies.

Finally, I am extremely grateful to my family and friends for their understanding of the risks and time commitments involved in undertaking a PhD project. It was your trust and support that maintained my motivation high. I am especially thankful to my husband Karolis for his love, unwavering support, and inspiring ideas.

SANTRAUKA

Įvadas

Biologinėms sistemoms, sudarytoms net iš nedidelio ląstelių skaičiaus, yra būdingas heterogeniškumas. Šio heterogeniškumo atskleidimas yra svarbus uždavinys siekiant suprasti ląstelių savybes, funkcijas ir jų tarpusavio skirtumus (1). Išsamiam biologinio mėginio charakterizavimui dažnai prireikia nepriklausomai išanalizuoti tūkstančius ląstelių, o tai tampa praktiška tik tuomet, kai taikomi didelio našumo analizės metodai (2-5).

Lašeliais paremtos mikroskysčių technologijos yra vienos iš plačiausiai taikomų didelio našumo sistemų, kurios leidžia atlikti ~10^6 reakcijų vieno eksperimento metu (6-9). Analizės principas remiasi tuo, jog pavienės ląstelės ar biomolekulės yra izoliuojamos į pikolitro-nanolitro tūrio vandens lašelius ir analizuojamos taikant įvarius molekulinės biologijos metodus. Tarp svarbiausių mikroskysčių technologijų taikymų būtų galima išskirti šiuos: antikūnų repertuaro analizė (10-12), įvairios atrankos sistemos (13-16), kryptinga baltymų evoliucija (17,18), skaitmeninė PGR (19) bei pavienių ląstelių sekoskaita (8,20,21).

Nepaisant plataus taikymo ir reikšmingo indėlio gyvybės mokslų srityje, mikroskysčių technologijoms būdingi tam tikri esminiai trūkumai. Didžioji dalis molekulinės biologijos metodų yra sudaryti iš kelių nepriklausomai atliekamų etapų/reakcijų, kurių atskyrimas yra svarbus bendram proceso efektyvumo užtikrinimui. Pavyzdžiui, norint padauginti ląstelių genetinę medžiagą, pirmiausia atliekamas ląstelių ardymas ir nukleorūgščių gryninimas ir tik po to išgryninta DNR ar RNR perkeliama į nukleorūgščių padauginimo reakcijas. Tokiu būdu užtikrinama, jog sąlygos, kurios reikalingos efektyviam nukleorūgščių išgryninimui, neslopintų tolimesnių fermentinių reakcijų. Tačiau šias kelių etapų reakcijas yra itin sudėtinga perkelti į lašelių formatą, kadangi lašelių turinio pakeitimas jau po jų formavimo yra techniškai sudėtingas procesas, o reagentų pašalinimas yra neįmanomas. Pakopinių reakcijų atlikimas lašeliuose kai kuriais atvejais yra įmanomas taikant įvairias skysčių manipuliacijas: lašelių grąžinimą į lustą (22-24), suliejimą (22-25), piko-injekcijas (26,27) ir lašelių dalijimą (28). Vis dėlto, šiuos procesus yra itin sunku atlikti molekulinės biologijos laboratorijose dėl reikalingų specializuotų darbo su mikroskysčiais įgūdžių.

Hidrogelinės mikrosferos suteikia alternatyvų ir paprastesnį būdą taikyti tam tikras kelių etapų molekulinės biologijos metodikas. Jų panaudojimo principas remiasi pavienių ląstelių izoliavimu porėtame hidrogeliniame tinkle ir po to sekančiu hidrogelinių sferų pernešimu tarp skirtingų reakcijos/analizės

mišinių. Dėl tankaus hidrogelinio tinklo ląstelės ir didelės molekulinės masės molekulės (pvz., genominė DNR) lieka fiziškai izoliuotos, o analizei naudojami reagentai difuzijos būdu keliauja į ir iš hidrogelinės sferos. Būtų galima išskirti dvi pagrindines hidrogelinių mikrosferų panaudojimo kryptis: pavienių ląstelių kultivavimas (29-31) ir nukleorūgščių paruošimas padauginimui, kuomet taikomos griežtos ląstelių ardymo sąlygos ir po jų seka bent keletas praplovimo etapų (32,33). Pastarasis taikymas yra itin aktualus dirbant su mikroorganizmais, kadangi metodai, į kuriuos įeina bakterijų lizė, išlieka iššūkiu sėkmingam mikrobiologinių aplikacijų perkėlimui į lašelių formatą (32). Vis dėlto, nepaisant reikšmingo postūmio derinant pakopines reakcijas su didelio našumo pavienių ląstelių analize, didžioji dalis hidrogelinėmis sferomis paremtų metodų susiduria su sunkumais, kurie užkerta kelią platesniam ir efektyvesniam šios sistemos panaudojimui. Visų pirma, hidrogelinių mikrosferų formavimo metu dalis ląstelių yra prarandama dėl jų polinkio lokalizuotis tarp vandens ir alyvos fazių (34-37). Taip pat, tolygus hidrogelinės mikrosferos porėtumas priverčia rinktis tarp fermentinių reakcijų efektyvumo ir izoliuotų molekulių išlaikymo. Dėl šios priežasties dalis iki šiol publikuotų darbų atlieka hidrogelinių mikrosferų patalpinimą į vandens lašelius tam, kad būtų užbaigti paskutinieji analizės etapai (32,38). Taigi, atsižvelgiant tiek į vandens lašelių, tiek į hidrogelinių mikrosferų savybes, buvo akivaizdu, jog reikia universalesnės sistemos, leidžiančios paprasčiau atlikti sudėtingas molekulinės biologijos reakcijas su pavienėmis ląstelėmis.

Rezultatai pateikti šiame darbe pristato naujo tipo mikrokompartmentų (mikrokapsulių), kurių skiriamasis bruožas yra skystas lašelio pavidalo vidus, apsuptas plonu hidrogelio apvalkalu, išvystymą ir taikymą. Hidrogelinis apvalkalas veikia kaip selektyviai pralaidi membrana: sulaikomos izoliuotos ląstelės ir didelės molekulinės masės molekulės, o mažos molekulės (pvz., fermentai, oligonukleotidai, mitybinės terpės komponentai) gali difuzijos būdu patekti į mikrokapsulės vidų. Dėl šio selektyvaus pralaidumo mikrokapsulės yra tinkamos atlikti pakopines reakcijas pernešant jas tarp atitinkamų reakcijos mišinių naudojant įprastą laboratorinę pipetę ir mėgintuvėlius. Nors keletas mikrokapsulių paruošimo metodų buvo pristatyti anksčiau (33,39-43), nė vienas iš jų nebuvo tinkamas sudėtingiems molekulinės biologijos tyrimams, paremtais nukleorūgščių padauginimu ir analize.

Vandeninės dvifazinės sistemos, sudarytos iš hidrofilinių polimerų, buvo pasirinktos kuriant dviejų tipų selektyviai pralaidžias mikrokapsules. Pirmoji sistema buvo sudaryta iš dekstrano ir polietilenglikolio diakrilato (PEGDA), kurie atitinkamai suformavo mikrokapsulės vidinę dalį ir apvalkalą. Šios

mikrokapsulės buvo pritaikytos pavienių bakterijų viso genomo padauginimui, kultivavimui ir fenotipinei analizei. Antroji sistema rėmėsi dekstrano ir želatinos metakrilato (ŽMA) panaudojimu formuojant mikrokapsules su ŽMA apvalkalu. Ši alternatyvi mikrokapsulių sistema atvėrė daug platesnes pavienių ląstelių tyrimų galimybes. ŽMA mikrokapsulės buvo pritaikytos ląstelių tipui identifikuoti taikant daugybinę AT-PGR, RNR barkodavimui ir sekoskaitai iš pavienių žinduolių ląstelių bei bakterijų.

Šiame darbe išvystytos mikrokapsulių sistemos padeda išspręsti pagrindinius apribojimus, susijusius su lašelių pagrindu veikiančiomis mikroskysčių technologijomis. Dėl šios priežasties yra tikimasi, kad šis darbas taps svarbiu pagrindu atliekant tolimesnius tyrimus pavienių ląstelių lygmenyje bei dėl nesudėtingo naudojimo ras pritaikymą laboratorijose, turinčiose ribotą patirtį mikroskysčių srityje.

Tikslas

Išvystyti, charakterizuoti ir pritaikyti selektyviai pralaidžias hidrogelines mikrokapsules didelio našumo kompleksinei pavienių ląstelių analizei.

Uždaviniai

1. Panaudojant vandeninę dvifazinę sistemą, sudarytą iš polietilenglikolio diakrilato (PEGDA) ir dekstrano, sukurti selektyviai pralaidžias mikrokapsules.
2. Įvertinti ląstelių izoliavimą, kultivavimą ir nukleorūgščių analizę PEGDA mikrokapsulėse.
3. Panaudojant vandeninę dvifazinę sistemą, sudarytą iš želatinos metakrilato (ŽMA) ir dekstrano, sukurti alternatyvią selektyviai pralaidžių mikrokapsulių sistemą.
4. Įvertinti ŽMA mikrokapsulių stabilumą bei jų tinkamumą žinduolių ląstelių izoliavimui bei nukleorūgščių išlaikymui.
5. Pritaikyti ŽMA mikrokapsules pavienių žinduolių ląstelių daugybinei AT-PGR.
6. Įvertinti ŽMA mikrokapsulių tinkamumą pavienių žinduolių ląstelių ir bakterijų viso transkriptomo tyrimuose.

Mokslinis naujumas

Lašeliais paremtos mikroskysčių technologijos išlieka vienu iš dažniausių pasirinkimų atliekant didelio našumo pavienių ląstelių analizę. Tačiau konkretaus taikymo (aplikacijos) įgyvendinimo sėkmė dažnai priklauso nuo molekulinės biologijos metodų, kurie reikalingi kuriamai aplikacijai išvystyti. Tais atvejais, kai reikalingos daugiapakopės reakcijos, neretai platesnis šių technologijų panaudojimas tampa ribotas. Tai ypač aktualu vykdant nukleorūgščių analizę, kuomet tyrimui atlikti reikia kelių sunkiai suderinamų etapų: ląstelių lizės ir nukleorūgščių padauginimo.

Šiame darbe pristatomas praktiškas ir inovatyvus sprendimas, leidžiantis atlikti didelio našumo kompleksinę pavienių ląstelių analizę naudojant įprastas laboratorines metodikas. Tai buvo pasiekta sukūrus PEGDA ir ŽMA mikrokapsules, sudarytas iš skysto vandens lašelį primenančio vidaus ir jį gaubančio selektyviai pralaidaus hidrogelinio apvalkalo. Mikrokapsulių panaudojimo principas gan paprastas: hidrogelinis apvalkalas sulaiko izoliuotas ląsteles ir didelės molekulinės masės biomolekules (pvz., gDNR, iRNR), o mažesnės molekulės (pvz., fermentai, oligonukleotidai, mitybinės terpės komponentai) juda difuzijos būdu. Todėl įvairių tipų fermentines reakcijas ir analizes galima atlikti perkeliant mikrokapsules iš vieno reakcijos mėgintuvėlio į kitą. Be selektyvaus pralaidumo mikrokapsulės pasižymi itin geru stabilumu veikiant įvairiems cheminiams, fizikiniams ir mechaniniams veiksniams. Visos šios savybės leido atlikti įvairius pavienių ląstelių tyrimus. Šio darbo rezultatai pateikti dviejuose moksliniuose straipsniuose ir keturiose patentinėse paraiškose, iš kurių viena yra licenzijuota.

Disertacijoje pristatomi teiginiai

- Selektyviai pralaidžios mikrokapsulės gali būti paruošiamos izoliuojant hidrofilinių polimerų – PEGDA-dekstrano ir ŽMA-dekstrano – porą lašeliuose ir atliekant išorinio sluoksnio polimerizaciją.
- Mikrokapsulės išlaiko izoliuotas ląsteles ir jų genetinę medžiagą (gDNR, iRNR), o mažesnės molekulės (pvz., fermentai, oligonukleotidai) difuzijos būdu pereina per hidrogelinį apvalkalą.
- Mikrokapsulės yra tinkamos didelio našumo pavienių ląstelių analizei atlikti, kuomet reikalingos sudėtingos ir daugiapakopės molekulinės biologijos metodikos.
- ŽMA mikrokapsulės turi plačias taikymo galimybes atliekant pavienių ląstelių nukleorūgščių analizę AT-PGR ir RNR sekoskaitos metodais.

PEGDA mikrokapsulių išvystymas ir taikymas

Vandeninių dvifazinių sistemų paruošimas

Vandeninės dvifazinės sistemos (ATPS) buvo ruošiamos naudojant 5,5 % (m/V) dekstrano, MM ~500k (Sigma-Aldrich, kat. nr. D5251), 3 % (m/V) PEGDA, MM 8k (Fisher Scientific, kat. nr. AA46801MD), 3 % (V/V) PEGDA, MM 575 (Sigma-Aldrich, kat. nr. 437441-100ML), 0,1 % (m/V) ličio fenil-2,4,6-trimetil-benzoilfosfinato (LAP) (Sigma-Aldrich, kat. nr. 900889-5G) ir 1x DPBS (Gibco, kat. nr. 14190144). Tirpalai su visais komponentais buvo sumaišyti ir 30 min. centrifuguojami ≥10 000g greičiu, kad įvyktų greitesnis fazių atsiskyrimas. Apatinė (praturtinta dekstranu) ir viršutinė (praturtinta PEGDA) fazės buvo atskirtos ir laikomos tamsoje iki inkapsuliacijos pradžios. Ląstelėms suspenduoti buvo naudojama dekstrano fazė (koncentracija siekė 3 M/ml).

Mikrokapsulių paruošimas

PEGDA mikrokapsulės buvo generuojamos naudojant Onyx prietaisą (DG) ir lustą su 20 µm gylio ir 20 µm pločio kanalais. Naudoti tėkmės greičiai: 50 µl/val. - PEGDA praturtintai fazei, 50 µl/val. - dekstrano praturtintai fazei su ląstelėmis ir 250-500 µl/val. - lašelių stabilizavimo alyvai (DG, kat. nr. DG-DSO-20). Ląstelių skiedimas buvo parinktas toks, kad daugumoje mikrokapsulių būtų 0 arba 1 ląstelė (lambda vertė ~0,1-0,3). Inkapsuliavimas buvo atliekamas kambario temperatūroje iki 30-60 min. Emulsija su izoliuotomis ląstelėmis buvo surinkta į 1,5 ml mėgintuvėlį, pripildytą 200 µl mineralinės alyvos (Sigma-Aldrich, kat. nr. M5904-500ML). ATPS lašeliai iš karto po inkapsuliacijos buvo apšviesti 2.5 min. 365 nm bangos ilgio šviesa naudojant UV lempą (UVP, kat. nr. 95-0127-01). Tais atvejais, kai buvo atliekamas bakterijų kultivavimas, ATPS lašeliai 20 sek. buvo apšviesti 405 nm bangos ilgio lazeriu (Besram Technology Inc. modulis TEM00) arba 405 nm LED prietaisu (DG, kat. nr. DG-BR-405). Po fotopolimerizacijos gautos mikrokapsulės buvo išgrynintos iš emulsijos naudojant emulsijos ardymo reagentą (DG, kat. nr. DG-EB-1) ir 1 ml atšaldyto ląstelių plovimo buferinio tirpalo, kurio sudėtis 1x DPBS ir 0.1% Pluronic F-68 (Gibco, kat. nr. 24040032). Kuomet izoliuotos ląstelės buvo naudojamos kultivavimui, mikrokapsulės buvo laikomos ląstelių plovimo buferiniame tirpale iki kol buvo perkeltos į mitybinę terpę. Atliekant fermentines reakcijas, mikrokapsulės buvo du kartus praplautos plovimo buferiniu tirpalu, kurio

sudėtis 10 mM Tris-HCl [pH 7,5] (Invitrogen, kat. nr. 15567027) ir 0,05-0,1 % (V/V) Triton X-100 (Sigma-Aldrich, kat. nr. X100-100M).

Pavienių E. coli genomų padauginimas

Po *E. coli* MG1655 ląstelių izoliavimo į PEGDA mikrokapsules buvo atliekamas bakterijų lizavimas ir gDNR padauginimas. Bakterijų lizavimas buvo atliekamas 1 ml lizavimo mišinyje, kurio sudėtis 10 mM Tris-HCl [pH 7,5], 50 U/µl lizocimo (Lucigen, kat. nr. R1804M), 200 µg/ml proteinazės K (Invitrogen, kat. nr. AM2546), 0,1 % (V/V) Triton X-100 ir 1 mM EDTA (Invitrogen, kat. nr. 15575020). Mikrokapsulės sudarė ~10 % (100 µl) galutinio reakcijos tūrio. Ląstelių lizė buvo atliekama 30 min. 37 °C temperatūroje ir po to dar 30 min. 50 °C temperatūroje. Po lizės mikrokapsulės buvo praplautos 3-5 kartus plovimo buferiniame tirpale.

Pavienių genomų padauginimas (angl., *single-genome amplification-SGA*) buvo atliekamas 100 µl MDA (angl., *multiple displacement amplification*) reakcijos mišinyje, kuriame buvo 50 µl mikrokapsulių suspensijos, 0,5 U/µl phi29 DNR polimerazės (TFS, kat. nr. EP0092), 0,002 U/µl pirofosfatazės (TFS, kat. nr. EF0221), 25 µM egzonukleazėms atsparių atsitiktinių pradmenų (TFS, kat. nr. SO181), 1 mM dNTP mišinio (Invitrogen, kat. nr. 18427013), 1 mM DTT (TFS, kat. nr. R0861) ir 1x phi29 DNR polimerazės buferinio tirpalo (TFS, kat. nr. EP0092). Reakcija buvo atliekama 30 °C temperatūroje 12-16 val. Po padauginimo mikrokapsulės buvo 3 kartus praplautos plovimo buferiniu tirpalu ir naudotos mikroskopinei analizei.

Pavienių genomų padauginimas mikrokapsulėse buvo palygintas su hidrogelinėmis sferomis ir lašeliais. Izoliuojant bakterijas į hidrogelines sferas, vienodais tėkmės greičiais (50 µl/val.) buvo inkapsuliuojami 12 % (V/V) PEGDA, MM 575 ir 1x DPBS, kuriame buvo 3 M/ml *E. coli* MG1655 ląstelių. Alyvos tėkmės greitis buvo 250 µl/val. Po inkapsuliacijos buvo gauti 6 % (V/V) PEGDA lašeliai su pavienėmis bakterijomis. Visi etapai, įskaitant inkapsuliavimą, polimerizaciją, dalelių gryninimą iš emulsijos, lizavimą ir MDA reakciją, buvo identiški anksčiau aprašytam mikrokapsulių metodui.

Norint atlikti pavienių *E. coli* genomų padauginimą lašeliuose, lizės ir MDA etapai buvo apjungti. Bakterijos buvo suspenduotos 10 mM Tris-HCl [pH 7,5] buferiniame tirpale iki 3 M/ml koncentracijos ir inkapsuliuotos vienodais tėkmės greičiais (50 µl/val.) su 50 µl 2x koncentruotu MDA reakcijos mišiniu, kurio sudėtis buvo: 1 U/µl phi29 DNR polimerazės, 0,004 U/µl pirofosfatazės, 100 U/µl lizocimo, 50 µM egzonukleazėms atsparių atsitiktinių pradmenų, 2 mM dNTP mišinio, 2 mM DTT, 0,2 % (V/V) Triton X-100 ir 2x phi29 DNR polimerazės buferinio tirpalo. Po

inkapsuliavimo bakterijų lizės ir MDA etapai lašeliuose buvo atlikti 12-16 val. 30 °C temperatūroje.

Pavienių gramteigiamų bakterijų genomų padauginimas

Šiame eksperimente su dviem gramteigiamų bakterijų rūšimis (*Rhodococcus rhodochrous* PY11 ir *Streptococcus mutans* UA159) buvo išbandytos septynios skirtingos lizės-SGA sąlygos (viena sąlyga lašeliuose ir šešios sąlygos mikrokapsulėse). Nepriklausomai nuo taikytų lizės sąlygų, po lizės mikrokapsulės buvo 3-5 kartus praplautos plovimo buferiniu tirpalu ir perkeltos į MDA reakcijos mišinį. MDA sąlygos, įskaitant reakcijos komponentų sudėtį ir koncentracijas, reakcijos trukmę ir temperatūrą, buvo tokios pat kaip ir atliekant eksperimentus su *E. coli*. Po SGA mikrokapsulės buvo 3 kartus praplautos plovimo buferiniu tirpalu ir naudotos mikroskopinei analizei.

1 lentelė. Lizės ir SGA sąlygos, išbandytos su gramteigiamomis bakterijomis. Pastaba, jog nurodytos Tris-HCl buferinio tirpalo pH vertės įvertintos esant ~25 °C.

Sąlyga	Lizė-SGA	Pirmas žingsnis	Antras žingsnis	Trečias žingsnis
Kontr.	Vieno žingsnio lašeliuose	50 U/µl lizocimo, 0,1% (V/V) Triton X-100, 1× MDA reakcijos mišinys. 12 val./30 °C.	Netaikytas	Netaikytas
1.	Vieno žingsnio mikrokapsulėse	50 U/µl lizocimo, 0,1% (V/V) Triton X-100, 1× MDA reakcijos mišinys. 12 val./30 °C.	Netaikytas	Netaikytas
2.	Dviejų žingsnių mikrokapsulėse	50 U/µl lizocimo, 0,1% (V/V) Triton X-100, 1 mM EDTA, 10 mM Tris-HCl [pH 7,5]. 30 min./37 °C.	Mikrokapsulės praplautos ir perkeltos į 1x MDA mišinį. 12 val./30 °C.	Netaikytas
3.	Dviejų žingsnių mikrokapsulėse	50 U/µl lizocimo, 0,1% (V/V) Triton X-100, 1 mM EDTA, 200 µg/ml proteinazės K, 10 mM Tris-HCl [pH 7,5]. 30 min./37 °C ir 30 min./50 °C.	Mikrokapsulės praplautos ir perkeltos į 1x MDA mišinį. 12 val./30 °C	Netaikytas
4.	Trijų žingsnių mikrokapsulėse	50 U/µl lizocimo, 0,1% (V/V) Triton X-100, 1 mM EDTA, 10 mM Tris-HCl [pH 7,5]. 30 min./37 °C.	Papildymas 200 µg/ml proteinazės K. 30 min./50 °C.	Mikrokapsulės praplautos ir perkeltos į 1x MDA mišinį. 12 val./30 °C.
5.	Trijų žingsnių mikrokapsulėse	50 U/µl lizocimo, 0,1% (V/V) Triton X-100, 1 mM EDTA, 10 mM Tris-HCl [pH 7,5]. 30 min./37 °C.	Papildymas 200 µg/ml proteinazės K ir 1% (m/V) NDS. 30 min./50 °C.	Mikrokapsulės praplautos ir perkeltos į 1x MDA mišinį. 12 val./30 °C.
6.	Dviejų žingsnių mikrokapsulėse	0,5 M NaOH ir 1% (m/V) NDS. 5 min./21 °C	Mikrokapsulės praplautos ir perkeltos į 1x MDA mišinį. 12 val./30 °C.	Netaikytas

Bakterijų kultivavimas

E. coli MG1655 ir DH5α ląstelės buvo izoliuotos į PEGDA mikrokapsules, kaip aprašyta aukščiau, ir perkeltos į 30 × 15 mm Petri lėkšteles su 2 ml LB terpės. Izoliuotos ląstelės buvo inkubuojamos 37 °C temperatūroje 4-16 val. Transformuotoms DH5α ląstelėms LB terpė buvo papildyta 100 μg/ml ampicilino. Norint aptikti polihidroksibutiratą (PHB) sintetinančias bakterijas, jo sintezė DH5α ląstelėse buvo indukuota pridėjus 1 mM izopropil β-D-1-tiogalaktopiranozido (IPTG) (TFS, kat. nr. R1171) ir inkubuojant 30 °C temperatūroje 8 val.

Mikroskopinė analizė

Lašeliai, hidrogelinės sferos ir mikrokapsulės prieš ir po lizės bei po nukleorūgščių padauginimo buvo dažomi 1× SYBR Green I dažu (Invitrogen, kat. nr. S7563) 15 min. kambario temperatūroje. Po dažymo hidrogelinės sferos ir mikrokapsulės buvo du kartus praplautos plovimo buferiniame tirpale. Mėginiai buvo perkelti ant standartinio hemocitometro (Sigma-Aldrich, kat. nr. 717805) ir šviesaus lauko bei fluorescencijos vaizdai buvo registruojami mikroskopu Nikon Eclipse Ti ir Nikon Digital Sight DS-U3 kamera. Mikroskopinė analizė atlikta naudojant šiuos parametrus: didinimas - 10×, filtras - FITC, stiprinimas - 1, sužadinimui naudotas 20 % mėlynos šviesos šaltinio intensyvumas, o išlaikymas keitėsi priklausomai nuo analizės etapo.

Mikrokapsulės ir lašeliai su *E. coli* MG1655 mikrokolonijomis buvo nudažyti 1× SYBR Green I dažu ir analizuojami epifluorescenciniu mikroskopu kaip aprašyta aukščiau. Mikrokapsulės su *E. coli* DH5α mikrokolonijomis buvo 10 min. dažomos su 0,5 μg/ml Nile Red dažu (Invitrogen, kat. nr. N1142), du kartus praplautos ląstelių plovimo buferiniu tirpalu ir analizuotos epifluorescenciniu mikroskopu naudojant šiuos parametrus: didinimas - 10×, filtras - TXRED, stiprinimas - 1, išlaikymas - 100 ms, 40 % žalios šviesos šaltinio sužadinimo intensyvumas. Antrasis mikroskopijos etapas atliktas po lizės (1 lentelė, sąlyga Nr. 3) be papildomo dažymo Nile Red dažu ir naudojant tuos pačius parametrus. Atliekant PHB kiekio normalizavimą, mikrokapsulės buvo pakartotinai nudažytos Nile Red ir SYBR Green I dažais. Mikroskopinė analizė atlikta naudojant šiuos parametrus: didinimas - 10×, filtrai - FITC ir TXRED, stiprinimas - 1, išlaikymas - 10 ms FITC filtrui ir 40 ms TXRED filtrui, atitinkamai 20 % ir 40 % mėlynos ir žalios šviesos šaltinio intensyvumas sužadinimui. Šviesaus lauko ir fluorescencijos vaizdai buvo registruojami mikroskopu Nikon Eclipse Ti ir Nikon Digital Sight DS-U3 kamera.

Duomenų analizė

Pirminė mikroskopijos duomenų analizė atlikta Fiji programine įranga. Šviesaus lauko mikroskopijos nuotraukose buvo apvestos mikrokapsulės, hidrogelinės sferos ir lašeliai. Gautos kaukės buvo panaudotos fluorescencijos vaizdams segmentuoti ir išgauti vidutinį fluorescencjos intensyvumą. Antrinė duomenų analizė atlikta naudojant R (v. 3.5.3) ir R studio (v. 1.1.463).

ŽMA mikrokapsulių išvystymas ir taikymas

Mikrokapsulių generavimas ir ląstelių inkapsuliavimas

Ląstelių izoliavimas ŽMA mikrokapsulėse atliktas naudojant Onyx prietaisą (DG) ir mikroskysčių lustą su 40 µm gylio ir 40 µm pločio kanalais. Naudoti tėkmės greičiai: 250 µl/val. - 3 % (m/V) ŽMA tirpalui (Sigma-Aldrich), 100 µl/val. - 15 % (m/V) dekstrano tirpalui (Sigma-Aldrich, kat. nr. D5251) su ląstelėmis ir 700 µl/val. - lašelių stabilizavimo alyvai. NB4 ir PKVL izoliavimas atliktas naudojant 30 µm gylio ir 20 µm pločio mikroskysčių lustą. Naudoti tėkmės greičiai: 125 µl/val. - 3 % (m/V) ŽMA tirpalui, 50 µl/val. - 15 % (m/V) dekstrano tirpalui su ląstelėmis ir 700-800 µl/val. - lašelių stabilizavimo alyvai. Ląstelių skiedimas buvo pasirinktas toks, kad daugumoje mikrokapsulių būtų 0 arba 1 ląstelė (lambda vertė ~0,1). Inkapsuliacijos buvo atliekamos kambario temperatūroje iki 30 min. Emulsija buvo renkama į 1,5 ml mėgintuvėlį, pripildytą 200 µl mineralinės alyvos. ATPS lašeliai buvo paversti mikrokapsulėmis per du etapus. Iš pradžių lašeliai 15-30 min. buvo inkubuojami 4 °C temperatūroje, kad ŽMA apvalkalas sukietėtų. Tarpinės mikrokapsulės buvo išskirtos iš alyvos fazės naudojant emulsijos ardymo reagentą ir ląstelių plovimo buferinį tirpalą. Tarpinių mikrokapsulių suspensija 5 min. buvo inkubuojama kambario temperatūroje, tada sumaišyta su 0,1 % (m/V) LAP ir 20 sek. veikiama mažos energijos 405 nm LED prietaisu. Tęsiant procedūras lede, mikrokapsulės buvo du kartus praplautos ląstelių plovimo buferiniame tirpale. Po šio etapo sekė ląstelių lizė arba ląstelių fiksavimas etanolyje (žr. toliau).

Ląstelių fiksavimas etanolyje

Mikrokapsulės su izoliuotomis ląstelėmis buvo suspenduotos 70 % (V/V) atšaldyto etanolio tirpale ir laikomos -20 °C temperatūroje iki sekančių analizės etapų. Prieš analizę mėgintuvėlis su mikrokapsulėmis buvo inkubuojamas ant ledo 5 min. ir mikrokapsulės centrifuguojamos 2 min. 2000g greičiu 4 °C temperatūroje. Pašalinus etanolį, mikrokapsulės buvo praplautos 1 ml rehidratacijos buferiniame tirpale, kurio sudėtis: 3x SSC (Invitrogen, kat. nr. 15557044), 0,04 % BSA, 1 mM DTT ir 0,2 U/µl RNazių

slopiklio RiboLock (TFS, kat. nr. EO0381). Po šio etapo sekė ląstelių lizė nejoniniu detergentu (žr. toliau).

Ląstelių lizavimas

Izoliuotų ląstelių lizavimas, taikant griežtas sąlygas, buvo atliktas mikrokapsules suspenduojant 1 ml GeneJET lizės buferiniame tirpale (TFS, kat. nr. K0732), papildytu 40 mM DTT. Mikrokapsulės buvo praplautos GeneJET lizės buferiniame tirpale 3 kartus ir tarp plovimų inkubuojant nuo 1 iki 5 min. Po lizės mikrokapsulės buvo 5 kartus praplautos plovimo buferiniu tirpalu (10 mM Tris-HCl [pH 7,5] ir 0,1 % (V/V) Triton X-100). Tarp atskirų etapų mikrokapsulių centrifugavimas atliktas 2000g greičiu 2 min. 4 °C temperatūroje.

Ląstelių lizė švelniomis sąlygomis buvo atlikta mikrokapsules suspenduojant 1 ml buferinio tirpalo, kurio sudėtis: 10 mM Tris-HCl [pH 7,5], 0,6 % (V/V) IGEPAL CA-630 (Sigma-Aldrich, kat. nr. I8896-50ML), 40 mM DTT ir 10 mM EDTA. Mikrokapsulės buvo 15 min. inkubuojamos kambario temperatūroje ir 3 kartus praplautos plovimo buferiniu tirpalu. Tarp atskirų etapų mikrokapsulių centrifugavimas atliktas 2000g greičiu 2 min. 4 °C temperatūroje.

Genominės DNR pašalinimas

Genominė DNR buvo pašalinta 200 µl DNazės I reakcijos mišinyje, kuriame buvo 100 µl mikrokapsulių suspensijos, 0,05 U/µl DNazės I (TFS, kat. nr. K2981), 0,2 U/µl RNazių slopiklio RiboLock ir 1x DNazės I buferinio tirpalo su $MgCl_2$. Mikrokapsulės buvo inkubuojamos 37 °C temperatūroje 20 min. Po to papildomai įdėti 5U DNazės I fermento ir 10 min. inkubuota 37 °C temperatūroje. Mikrokapsulės po gDNR pašalinimo buvo 3-5 kartus praplautos plovimo buferiniu tirpalu.

Atvirkštinė transkripcija (AT)

kDNR sintezė buvo atliekama 200 µl Maxima H Minus AT reakcijos mišinyje, turinčiame 100 µl mikrokapsulių suspensijos, 5 µM oligo$(dT)_{21}$ pradmens (IDT), 0,5 mM dNTP mišinio, 5 U/µl Maxima H Minus atvirkštinės transkriptazės (TFS, kat. nr. EP0751), 0,2 U/µl RiboLock RNazių slopiklio ir 1x AT buferinio tirpalo. Reakcija buvo atliekama 50 °C temperatūroje 60 min. Kas 20 min. mikrokapsulės buvo išmaišomos jas pipetuojant. Po kDNR sintezės AT fermentas buvo inaktyvuojamas karščiu (85 °C/5 min.) ir mikrokapsulės praplautos 3 kartus plovimo buferiniu tirpalu.

Norint detektuoti retus transkriptus (pvz., *PML-RARα*), 2,5 µM oligo$(dT)_{21}$ pradmens buvo sumaišoma su 2,5 µM atsitiktiniais heksamerais (TFS, kat. nr.

SO142). kDNR sintezė buvo inicijuojama reakcijos mišinį inkubuojant 10 min. kambario temperatūroje ir tuomet perkeliant į 50 °C temperatūrą 60 min.

Daugybinė PGR

PGR buvo atliekama 100 µl reakcijos mišinyje, kuriame buvo ~50 µl mikrokapsulių suspensijos, 0,5 µM tiesioginio ir 0,5 µM atvirkštinio pradmens (**2 lentelė**) ir 1x Phire Tissue Direct PGR mišinio (TFS, kat. nr. F170L). kDNR padauginimas buvo vykdomas naudojant šią ciklinimo programą: 98 °C (5 min.), 98 °C (5 sek.)/64 °C (5 sek.)/72 °C (20 sek.) 30 ciklų, 72 °C (1 min.). Po PGR mikrokapsulės 15 min. 37 °C temperatūroje buvo inkubuojamos su 100 U egzonukleazės I (NEB, kat. nr. M0293L) ir 3 kartus praplautos plovimo buferiniu tirpalu.

Norint detektuoti retus transkriptus, padauginimas buvo atliktas dviem etapais: pirmiausia naudojant 10 ciklų, o po to 30 ciklų. Po pirmojo padauginimo etapo mikrokapsulės buvo praplautos plovimo buferiniu tirpalu. Po antrojo PGR etapo mikrokapsulės 15 min. 37 °C temperatūroje buvo inkubuojamos su 100 U egzonukleazės I ir 3 kartus praplautos plovimo buferiniu tirpalu.

2 lentelė. PGR pradmenų sekos.

Pavadinimas	**Seka (5'→3')**	**Produkto ilgis**
555-*YAP*-tiesioginis	Alexa Fluor 555-CCCTCGTTTTGCCATGAACC	584 bp
YAP-atvirkštinis	CCAGTGTTCCAAGGTCCACA	
488-*PTPRC*-tiesioginis	Alexa Fluor 488-ACATTGCTGCACAAGGTCCCAG	532 bp
PTPRC-atvirkštinis	AACCATCAGGCATCTCTGTCGC	
647-*ACTB*-tiesioginis	Alexa Fluor 647-ATTCCTATGTGGGCGACGA	607 bp
ACTB-atvirkštinis	AATGGTGATGACCTGGCCG	
647-*B2M*-tiesioginis	Alexa Fluor 647-AGCAGCATCATGGAGGTTTGA	513 bp
B2M-atvirkštinis	CCAGATTAACCACAACCATGCC	
647-*TBP*-tiesioginis	Alexa Fluor 647-GCGCAAGGGTTTCTGGTTTG	539 bp
TBP-atvirkštinis	TTTGCAGCTGCGGTACAATC	
555-*PML-RARα*-tiesioginis	Alexa Fluor 555-AGCGCGACTACGAGGAGAT	688 bp
PML-RARα-atvirkštinis	CTGCTGCTCTGGGTCTCAAT	
546-*BCR-ABL*-tiesioginis	Alexa Fluor 546-GAAGTGTTTCAGAAGCTTCTCC	417 bp
BCR-ABL-atvirkštinis	GTTTGGGCTTCACACCATTCC	

Branduolių dažymas po AT-PGR

Po AT-PGR mikrokapsulės buvo perkeltos į plovimo buferinį tirpalą su 300 nM 4',6-diamidino-2-fenilindolo dihidrochloridu-DAPI (Invitrogen, kat. nr. D1306) ir 10 min. inkubuotos tamsoje ant ledo. Po to mikrokapsulės buvo 3 kartus praplautos plovimo buferiniu tirpalu ir naudotos tolimesnei mikroskopinei analizei ar tėkmės citometrijai.

Mikroskopinė analizė

Mikrokapsulių suspensija (~10-15 µl) buvo perkelta ant standartinio hemocitometro ir tuomet šviesaus lauko ir fluorescencijos vaizdai buvo registruojami mikroskopu Nikon Eclipse Ti-E ir Nikon DS-Qi2 kamera. Naudoti fluorescencijos filtrai: DAPI, GFP, RFP ir Cy5. Kiekvieno eksperimento metu naudoti vienodi parametrai: išlaikymas - 400 ms, stiprinimas - 1,0. Mikroskopo objektyvas buvo CFI Plan Fluor 10x (N.A. 0,30, 16,0 mm).

Tėkmės citometrija

Mikrokapsulės buvo du kartus praplautos plovimo buferiniu tirpalu ir praleistos per 100 µm dydžio sietelį (Corning, kat. nr. 431752). Tėkmės citometrija buvo atlikta dviem instrumentais: Partec CyFlow Space ir BD FACSAria III. Mikrokapsulių analizei be branduolių buvo naudotas Partec CyFlow Space, o mikrokapsulėms su branduoliu - BD FACSAria III. Mikrokapsulių populiacija buvo aptikta analizuojant priekinės ir šoninės šviesos išbarstymą. Siekiant atskirti mikrokapsules su branduoliu, buvo fiksuojamas signalo aukštis DAPI kanale. Visais kitais atvejais fiksuotas signalo plotas.

Tėkmės citometrijos duomenų analizė

Tėkmės citometrijos duomenys buvo analizuojami ir vizualizuojami naudojant FCS Express 7 programinę įrangą (versija 7.12.0005). Rezultatai, gauti su Partec CyFlow Space prietaisu, buvo analizuojami taikat šią strategiją: 1) mikrokapsulių identifikavimas pagal priekinį ir šoninį šviesos išbarstymą, 2) *ACTB* teigiamų mikrokapsulių skirstymas pagal Alexa Fluor 647 ir šoninės sklaidos signalą, 3) mikrokapsulių su *PTPRC* ir *YAP* žymenimis analizė pagal Alexa Fluor 488 (*PTPRC*) ir Alexa Fluor 555 (*YAP*) signalus.

Rezultatai, gauti su BD FACSAria III prietaisu, buvo analizuojami taikant kiek kitokią strategiją: 1) mikrokapsulių su izoliuotomis ląstelėmis identifikavimas pagal Alexa Fluor 488 (*PTPRC*) signalo plotą ir DAPI signalo aukštį, 2) *PML-RARα* teigiamų įvykių identifikavimas pagal Alexa Fluor 488 (*PTPRC*) ir Alexa Fluor 555 signalus (*PML-RARα*).

Jautrumas, specifiškumas ir teigiama/neigiama prognozavimo vertės

Mikrokapsulės, kuriose yra branduolys ir kurios yra teigiamos vienam iš žymenų (*ACTB*, *B2M*, *TBP*, *PTPRC*, *YAP*), buvo vertinamos kaip teisingai teigiamos (TT). Mikrokapsulės, kuriose nebuvo branduolių ir kurios nerodė fluorescencijos, buvo laikomos teisingai neigiamomis (TN). Klaidingai teigiamos (KT) buvo mikrokapsulės, kuriose nebuvo branduolių, bet kurios

turėjo fluorescencinį signalą vienam iš žymenų. Klaidingai neigiamos (KN) buvo mikrokapsulės su branduoliais, kuriose nei vienas pasirinktas žymuo nerodė detektuojamo fluorescencijos signalo. Statistinių charakteristikų skaičiavimas:

Jautrumas = ((TT)/((TT+) KN))×100 %;

Specifiškumas = ((TN)/((TN+) KT))×100 %;

PPV = ((TT)/((TT+) KT))×100%;

NPV = ((TN)/((TN+) KN))×100%.

Pavienių ląstelių RNR sekoskaita

Žinduolių ląstelių izoliavimas ir paruošimas barkodavimui

K-562 ir NIH-3T3 ląstelių izoliavimas vienodu santykiu į ŽMA mikrokapsules buvo atliktas remiantis aukščiau pateikta metodika. Ląstelių skiedimas buvo pasirinktas toks, kad daugumoje mikrokapsulių būtų 0 arba 1 ląstelė (lambda vertė ~0,1). Izoliuotoms ląstelėms buvo taikytos griežtos lizės sąlygos chaotropiniais reagentais ir gDNR pašalinimas remiantis aukščiau pateikta metodika. Po gDNR pašalinimo mikrokapsulės buvo 2 kartus praplautos plovimo buferiniu tirpalu ir praleistos per 100 µm dydžio sietelį. Prieš barkodavimo etapą mikrokapsulės buvo 3 kartus praplautos 1x Maxima H Minus AT reakcijos buferiniu tirpalu, papildytu 0,6 % Igepal CA-630.

Bakterijų izoliavimas ir paruošimas barkodavimui

E. coli MG1655 ir *B. subtilis* 23857 izoliavimas ŽMA mikrokapsulėse buvo atliekamas naudojant Onyx prietaisą ir mikroskyscių lustą su 20 µm gylio ir 20 µm pločio kanalais. Naudoti tėkmės greičiai: 50 µl/val. - 3 % (m/V) ŽMA tirpalui, 20 µl/val. - 15 % (m/V) dekstrano tirpalui su ląstelėmis ir 400 µl/val. - lašelių stabilizavimo alyvai. Ląstelių skiedimas buvo pasirinktas toks, kad daugumoje mikrokapsulių būtų 0 arba 1 ląstelė (lambda vertė ~0,1). Inkapsuliavimas buvo atliekamas kambario temperatūroje ~1 valandą. Emulsija buvo renkama į 1,5 ml mėgintuvėlį, pripildytą 200 µl mineralinės alyvos. ATPS lašelių polimerizacija buvo atlikta taikant aukščiau aprašytą metodiką. Po inkapsuliavimo mikrokapsulės buvo suspenduotos 2 ml LB terpės ir 30 °C temperatūroje inkubuotos 30 min. Po inkubacijos mikrokapsulės buvo surinktos į 1,5 ml mėgintuvėlį centrifuguojant 1000g greičiu 2 min. 4 °C temperatūroje.

Mikrokapsulės buvo praplautos 1 ml buferinio tirpalo, kurio sudėtis 10 mM Tris-HCl, pH [7,5], 100 mM NaCl, 1 mM EDTA ir 0,1 % Triton X-100. Pašalinus supernatantą, mikrokapsulės buvo perkeltos į 1 ml lizavimo tirpalą, kurio sudėtis buvo: 10 mM Tris-HCl, pH [7,5], 100 mM NaCl, 1 mM EDTA,

0,1 % Triton X-100 ir 50 U/µl lizocimo (Lucigen, kat. nr. R1810M). Po 15 min. inkubavimo kambario temperatūroje supernatantas buvo pašalintas ir mikrokapsulės buvo perkeltos į 1 ml GeneJET lizės buferinį tirpalą, turintį 40 mM DTT, ir inkubuotos 5 min. kambario temperatūroje. Po lizės mikrokapsules buvo praplautos 4-5 kartus plovimo buferiniu tirpalu. Tarp atskirų etapų ir praplovimų mikrokapsulės buvo nusukamos 1000-2000g greičiu 2 min. 4 °C temperatūroje. Mikrokapsulės buvo suspenduotos šaltame 70 % etanolyje ir laikomos -20 °C temperatūroje iki kitų analizės etapų.

Norint rehidratuoti fiksuotas ląsteles, mėgintuvėlis su mikrokapsulėmis buvo perkeltas ant ledo ir 5 min. inkubuotas. Etanolis buvo pašalintas centrifuguojant mikrokapsules 2000g greičiu 2 min. 4 °C temperatūroje ir 3 kartus praplaunant plovimo buferiniu tirpalu. Kitame etape buvo atliktas gDNR pašalinimas taikant anksčiau aprašytą metodiką. Po gDNR pašalinimo mikrokapsulės buvo 3-5 kartus praplautos plovimo buferiniu tirpalu ir perkeltos į poliadenilinimo reakciją.

RNR poliadenilinimas buvo atliekamas 200 µl poly(A) polimerazės reakcijos mišinyje (NEB, kat. nr. M0276L), kuriame buvo 100 µl mikrokapsulių suspensijos, 1 mM ATP, 0,4 U/µl *E. coli* poly(A) polimerazės ir 1x reakcijos buferinio tirpalo, ir inkubuojant 37 °C temperatūroje 30 min. Kas 15 min. mikrokapsulės buvo išmaišomos jas pipetuojant. Po RNR poliadenilinimo mikrokapsulės buvo 2 kartus praplautos plovimo buferiniu tirpalu ir perleistos per 70 µm sietelį (Corning, kat. nr. 431751). Prieš barkodavimo etapą mikrokapsulės buvo 3 kartus praplautos 1x Maxima H Minus AT reakcijos buferiniu tirpalu, papildytu 0,6 % Igepal CA-630.

Atvirkštinės transkripcijos mišinio paruošimas

Vienai barkodavimo reakcijai su žinduolių ląstelėmis atlikti buvo paruošta 150 µl AT reakcijos mišinio, sudaryto iš 25 µM TSO (IDT) (**3 lentelė**), 1 mM dNTP mišinio, 20 U/µl Maxima H Minus AT fermento, 4 U/µl RiboLock RNazių slopiklio, 0,6 % Igepal CA-630 ir 1x AT buferinio tirpalo. Inkapsuliavimo metu AT mišiniui šaldyti buvo naudojama ledu užpildyta pirštinė (86).

Vienai barkodavimo reakcijai su bakterijomis atlikti buvo paruošta 150 µl AT reakcijos mišinio, sudaryto iš 1,5 µM TSO, 0,75 mM dNTP mišinio, 15 U/µl Maxima H Minus AT fermento, 3 U/µl RiboLock RNazių slopiklio, 0,45 % Igepal CA-630 ir 1x AT buferinio tirpalo. Inkapsuliavimo metu AT mišiniui šaldyti buvo naudojama ledu užpildyta pirštinė.

3 lentelė. Sekoskaitos eksperimentuose naudotos DNR oligonukleotidų sekos. Žvaigždutė žymi tiofosfatinę modifikaciją.

Pavadinimas	Seka (5'→3')
Atvirkštinė transkripcija ir matricos perjungimas	
TSO	AAGCAGTGGTATCAACGCAGAGTACATrGrGrG
kDNR padauginimas	
PGR1-p5	TACGGCGACCACCGAGATC
PGR1-tso	AAGCAGTGGTATCAACGCAGAG
Adapterių ligavimas	
Ligavimo adapteris	5Phos-GATCGGAAGAGCACACGTCTGAACTCCAGTCAC-3ddC
	5AmMC6-GCTCTTCCGATCT
Indeksavimas ir galutinis bibliotekos padauginimas	
P5 indeksas	AATGATACGGCGACCACCGAGATCTACAC
P7 indeksas 6	CAAGCAGAAGACGGCATACGAGATCAGTGGGTGACTGGAGTTCAG ACGTG*T
P7 indeksas 7	CAAGCAGAAGACGGCATACGAGATGTTGTCGTGACTGGAGTTCAG ACGTG*T
P7 indeksas 8	CAAGCAGAAGACGGCATACGAGATTGACAAGTGACTGGAGTTCAG ACGTG*T
P7 indeksas 13	CAAGCAGAAGACGGCATACGAGATACTCTAGTGACTGGAGTTCAG ACGTG*T
P7 indeksas 14	CAAGCAGAAGACGGCATACGAGATCGAGATGTGACTGGAGTTCAG ACGTG*T
P7 indeksas 15	CAAGCAGAAGACGGCATACGAGATGAGTCCGTGACTGGAGTTCAG ACGTG*T

Pavienių ląstelių RNR barkodavimas

Barkoduojantys rutuliukai (86) buvo gauti iš Droplet Genomics. Prieš barkodavimo etapą hidrogeliai buvo 3 kartus praplauti 1x Maxima H Minus AT reakcijos buferiniu tirpalu, papildytu 0,6 % Igepal CA-630. Barkodavimo eiga ir mikroskyščių lusto dizainas buvo perimti iš ankstesnių darbų (86). Naudoti skysčių tėkmės greičiai su žinduolių ląstelėmis: 250 µl/val. - AT mišinys, 100 µl/val. - barkoduojantys rutuliukai, 100 µl/val. - mikrokapsulės ir 400 µl/val. - lašelius stabilizuojanti alyva. Naudoti skysčių tėkmės greičiai su bakterijomis: 200 µl/val. - AT mišinys, 40 µl/val. - barkoduojantys rutuliukai, 10 µl/val. - mikrokapsulės ir 500 µl/val. - lašelius stabilizuojanti alyva. Emulsija buvo renkama lede, į 1,5 ml mėgintuvėlį, pripildytą 200 µl mineralinės alyvos. Po inkapsuliacijos mėgintuvėlis su emulsija buvo apšviestas UV lempa 7 min., kad būtų nukabinti barkoduojantys pradmenys. Emulsija buvo išdalinta į PGR mėgintuvėlius po ~3000 ląstelių. AT reakcija vykdyta 42 °C temperatūroje 60 min., po kurios sekė fermento inaktyvavimas (85 °C/5 min.). Po AT etapo emulsija buvo suardyta ir reakcijos produktas praskiestas iki 100 µl su 1x AT buferiniu tirpalu. Į praskiestą AT produktą buvo įdėtas 1 µl dekstranazės (Sigma-Aldrich, kat. nr. D0443-50ML) ir inkubuota 5 min. 37 °C temperatūroje. Po veikimo dekstranaze mikrokapsulių apvalkalas buvo ištirpintas įdedant 1 µl 20 mg/ml proteinazės K ir inkubuojant

10 min. 37 °C temperatūroje. Hidrogeliniai rutuliukai buvo pašalinti perleidžiant AT produktą per Zymo Spin-IC kolonėlę (Zymo, kat. nr. C1004-250) ir centrifuguojant 1000g greičiu 5 min.

kDNR gryninimas ir padauginimas

kDNR molekulės buvo 2 kartus išvalytos su 0,8x AMPure magnetiniais rutuliukais (Beckman Coulter, kat. nr. A63880) ir eliucija atlikta su 20 µl vandens. kDNR padauginimas buvo atliktas 50 µl reakcijos mišinyje, kurį sudarė 20 µl barkoduotos kDNR, 0,5 µM tiesioginio ir 0,5 µM atvirkštinio pradmens (**3 lentelė**, kDNR padauginimas) ir 1x Kapa HiFi 2X Ready Mix (KAPA, kat. nr. KK2602). Mėginiai buvo ciklinami naudojant šią programą: 98 °C (3 min.), 98 °C (15 sek.)/67 °C (20 sek.)/72 °C (1 min.) 13 ciklų mėginiams su žinduolių ląstelėmis ir 24 ciklai mėginiams su bakterijomis ir 72 °C (1 min.). Po PGR padauginta DNR buvo 2 kartus išvalyta su 0,6x AMPure magnetiniais rutuliukais ir eliucija atlikta su 20 µl vandens.

Bibliotekos fragmentavimas ir adapterių ligavimas

DNR fragmentavimas buvo atliekamas 17,5 µl reakcijos mišinyje, kurį sudarė ~50 ng padaugintos DNR, 1,75 µl NEBNext Ultra FS reakcijos buferinio tirpalo (NEB, kat. nr. E7805S), 0,5 µl NEBNext Ultra FS fermentų mišinio ir vandens iki 17,5 µl galutinio tūrio. Žinduolių ląstelių biblioteka buvo fragmentuojama 8 min. 37 °C temperatūroje, o bakterijų - 6 min. 37 °C temperatūroje, po kurių sekė 30 min. inkubacija 65 °C temperatūroje. Po fragmentavimo atlikta dviguba dydžio atranka (0,6x-0,8x AMPure). Pirmiausia buvo įpilta 92,5 µl vandens, tada 66 µl AMPure magnetinių dalelių. Buvo paimta 160 µl tirpalo be dalelių ir jis papildytas 20 µl AMPure magnetinėmis dalelėmis. Po to atliktas įprastas gryninimo procesas. DNR eliucija atlikta 17,5 µl vandens ir perkelta į ligavimo reakciją.

Adapterio ligavimas atliktas 34,25 µl reakcijos mišinyje, kurį sudarė 17,5 µl fragmentuotos DNR, 15 µl NEBNext Ultra II Ligation Master Mix, 0,5 µl NEBNext Ultra II Ligation Master Enhancer ir 1,25 µl 1,5 µM adapterio (**3 lentelė**). Ligavimas buvo atliekamas 20 °C temperatūroje 15 min. Po ligavimo bendras tūris buvo padidintas iki 100 µl įpilant vandens ir atliktas gryninimas su 0,8x AMPure. Eliucija atlikta 40 µl vandens.

Galutinis bibliotekos padauginimas ir indeksavimas

Indeksavimo PGR buvo atliekama 50 µl reakcijos mišinyje, kurį sudarė 20 µl DNR produkto po ligavimo, 0,5 µM indeksavimui skirto P5 ir 0,5 µM P7 PGR pradmens (**3 lentelė**) ir 1x Kapa HiFi 2X Ready Mix. Mėginiai buvo ciklinami naudojant šią programą: 95 °C (3 min.), 98 °C (20 sek.)/54 °C

(30 sek.)/72 °C (20 sek.) 11 ciklų ir 72 °C (1 min.). Po PGR atlikta dviguba dydžio atranka (0,6x-0,8x AMPure). Eliucija buvo atlikta 14 µl vandens. Bibliotekos kokybė buvo patikrinta naudojant Agilent BioAnalyzer HS DNR lustą (Agilent, kat. nr. 5067-4626).

Sekoskaita ir duomenų analizė

Žinduolių ląstelių bibliotekų sekoskaita atlikta naudojant NextSeq Illumina instrumentą ir NextSeq 500/550 High Output Kit v2.5 (75 ciklai) reagentų rinkinį (Illumina, kat. nr. 20024906). Naudoti šie nuskaitymo ilgiai: pirmas nuskaitymas - 16 ciklų, antras nuskaitymas - 62 ciklai, i5 nuskaitymas - 8 ciklai, i7 nuskaitymas - 6 ciklai. Bakterijų ląstelių bibliotekų sekoskaita atlikta naudojant MiSeq Illumina instrumentą ir Illumina MiSeq Reagent Kit v3 (150 ciklų) reagentų rinkinį (Illumina, kat. nr. MS-102-3001). Naudoti šie nuskaitymo ilgiai: pirmas nuskaitymas - 16 ciklų, antras nuskaitymas - 134 ciklai, i5 nuskaitymas - 8 ciklai, i7 nuskaitymas - 6 ciklai. Ląstelių x genų matricoms gauti buvo naudojamas ,,solo-in-drops‘‘ programų paketas (https://github.com/jsimonas/solo-in-drops). Antrinė analizė atlikta naudojant Scanpy programų paketą.

REZULTATAI IR JŲ APTARIMAS

PEGDA mikrokapsulių išvystymas ir taikymas

PEGDA mikrokapsulių paruošimas

Polimerai, formuojantys vandeninę dvifazinę sistemą (ATPS) – PEGDA ir dekstranas, buvo inkapsuliuoti ~1700 lašelių per sekundę greičiu naudojant 20 µm aukščio mikroskysčių lustą (**1 pav., A**). Norint pasiekti tinkamą balansą tarp mikrokapsulių monodispersiškumo, tinkamo centravimo ir mechaninio stabilumo, buvo pasirinkta kompozicija, sudaryta iš ilgesnio (MM 8k) ir trumpesnio (MM 575) PEGDA polimerų mišinio ir dekstrano (MM ~500k). Ilgesnis PEGDA buvo reikalingas efektyviam fazių atsiskyrimui, o trumpesnis PEGDA buvo pridėtas siekiant užtikrinti apvalkalo standumą ir mikrokapsulių mechaninį stabilumą, padidinant kryžminio susiuvimo dažnį (194). Po ATPS lašelių susidarymo PEGDA ir dekstrano fazės atsiskyrė, suformuodamos skystą apvalkalą, praturtintą PEGDA, ir skystą vidinę dalį, praturtintą dekstranu (**1 pav., B**). Naudojant FITC žymėtą dekstraną (MM ~500k), apskaičiuota, kad, pasiekus pusiausvyrą, ATPS lašelių vidinę dalį sudarė ~9,6 % (m/V) dekstrano. Esant panašiam PEGDA pasiskirstymui, apvalkalą turėtų sudaryti ~11 % (m/V) PEGDA. Norint skystą PEGDA apvalkalą paversti hidrogeliu (**1 pav., C**), ATPS lašeliai buvo

veikiami 365 arba 405 nm šviesa, esant fotoiniciatoriui. Gautos mikrokapsulės buvo išgrynintos iš alyvos ir toliau naudojamos pavienių ląstelių tyrimuose.

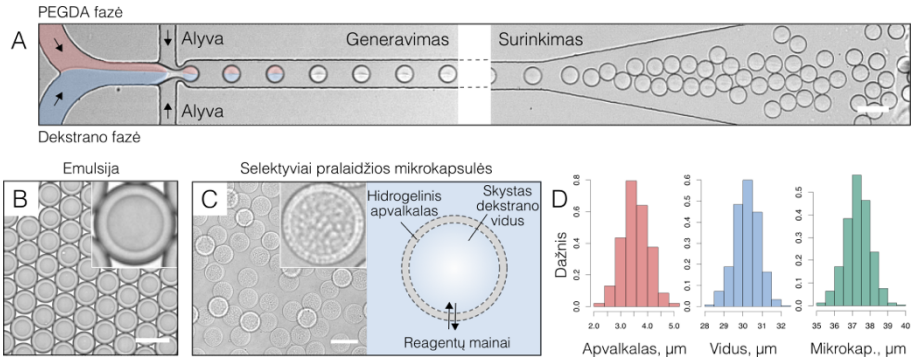

1 pav. Selektyviai pralaidžių mikrokapsulių paruošimas naudojant vandeninę dvifazinę sistemą, sudarytą iš PEGDA ir dekstrano. (**A**) ATPS lašelių generavimas naudojant bendros tėkmės mikroskysčių lustą. (**B**) Vandeninių fazių atsiskyrimas lašeliuose, kuomet susidaro dekstranu praturtintas vidus ir PEGDA praturtintas apvalkalas. (**C**) Mikrokapsulės, kuriose PEGDA sudarė tvirtą hidrogelinį apvalkalą, o dekstrano fazė – pusiau skystą vidinę dalį. (**D**) Histogramos, gautos iš >100 matavimų, rodo apvalkalo storį (3,56 ± 0,48 µm), vidinį (30,2 ± 0,6 µm) ir bendrą mikrokapsulės skersmenį (37,3 ± 0,7 µm). Skalė – 50 µm.

Vienas iš didžiausių iššūkių formuojant PEGDA mikrokapsules ATPS pagrindu buvo netolygus apvalkalo formavimasis. Pastebėta, jog naudojant didelės molekulinės masės PEGDA polimerus (pvz., 10k, 20k) arba didinant PEGDA (MM 8k) koncentraciją, mikrokapsulės vidinė dalis migruoja link alyvos. To pasekoje po polimerizacijos gaunamos netaisyklingos formos ir įtrūkusios dalelės, kurios buvo stebėtos ir ankstesniuose darbuose (187). Kadangi mikrokapsulės apvalkalo vientisumas priklauso nuo dekstrano ir PEGDA fazių centravimo, buvo iškelta prielaida, kad dėl dekstrano ir PEGDA fazių tankių neatitikimo vidinė dalis nusėda dar iki įvykstant apvalkalo polimerizacijai. Siekiant tai patikrinti, buvo paruošti du vandeninių dvifazinių sistemų bandiniai, iš kurių pirmasis turėjo 3 % (m/V), o antrasis 6 % (m/V) ilgesniojo PEGDA (MM 8k) polimero. Trumpesniojo PEGDA (MM 575) ir dekstrano koncentracijos išliko nepakitusios, atitinkamai 3 % (V/V) ir 5,5 % (m/V). Atlikus atsiskyrusių fazių tankių matavimus, nustatyta, jog didesnis tankių skirtumas atsiranda kuomet PEGDA (MM 8k) koncentracija buvo padidinta nuo 3 % (m/V) iki 6 % (m/V) (**2 pav., A**). Kaip ir tikėtasi, mikrokapsulių, susidariusių iš ATPS, kurių tankiai nebuvo suderinti, struktūra buvo netinkama ir vidinė dalis nebuvo išlaikoma (**2 pav., B**). Remiantis šiais rezultatais, galima teigti, jog, sumažinus tankių skirtumus tarp PEGDA ir

dekstrano fazių, buvo galima paruošti tinkamai centruotas mikrokapsules (**2 pav., C**), kas yra būtina savybė siekiant efektyviai izoliuoti ląsteles ir atlikti įvairius tyrimus.

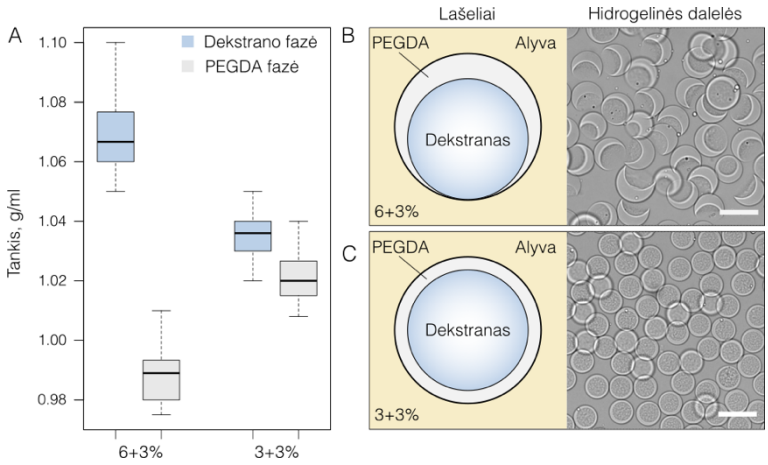

2 pav. Dviejų vandeninių fazių tankių skirtumų poveikis mikrokapsulių centravimui. (**A**) Stačiakampė diagrama, rodanti PEGDA (apvalkalo) ir dekstrano (vidinės dalies) fazių tankį po fazių atsiskyrimo. Diagramos sudarytos iš 25 kiekvieno mėginio matavimų. (**B**) Mikrokapsulės, paruoštos naudojant 6 % (m/V) PEGDA (MM 8k) ir 3 % (V/V) PEGDA (MM 575) polimerų mišinį. (**C**) Mikrokapsulės, paruoštos naudojant 3 % (m/V) PEGDA (MM 8k) ir 3 % (V/V) PEGDA (MM 575) polimerų mišinį. Skalė – 50 μm.

Pavienių *Escherichia coli* ląstelių genomų padauginimas

Sukūrus PEGDA mikrokapsulių paruošimo protokolą, kitas žingsnis buvo įvertinti, ar ši sistema gali būti naudojama pavienių bakterijų nukleorūgščių analizei atlikti. Tuo tikslu buvo pasirinktas pavienių *E. coli* genomų padauginimas (angl. *single-genome amplification – SGA*) taikant padauginimą daugybiniu nustūmimu (angl., *multiple displacement amplification – MDA*), kurį katalizuoja phi29 DNR polimerazė. Palyginimui *E. coli* ląstelės taip pat buvo izoliuotos į kitas dvi mikroskysčių sistemas – vandens lašelius alyvoje bei hidrogelinius rutuliukus (**3 pav., A**). Pavienės *E. coli* ląstelės buvo izoliuotos ~20 pikolitrų (pl) tūrio lašeliuose kartu su reagentais reikalingais lizės/SGA reakcijai, hidrogelinių mikrosferų ir mikrokapsulių paruošimui. Pavienių genomų padauginimas mikrokapsulėse ir hidrogeliniuose rutuliukuose buvo atliktas dviem etapais. Pirmiausia izoliuotos ląstelės buvo lizuotos ir, praplovus hidrogelines daleles, perkeltos į mėgintuvėlį su DNR padauginimo reagentais. Tuo tarpu, lašeliuose šie du etapai buvo sujungti į vieną reakciją ląsteles patalpinant į vandens lašelius kartu su lizės ir MDA reagentais. Pažymėtina, kad laboratorijoje buvo optimizuotos lizės sąlygos,

užtikrinančios veiksmingą *E. coli* suardymą, kuris suderinamas su po to sekančiais fermentiniais etapais.

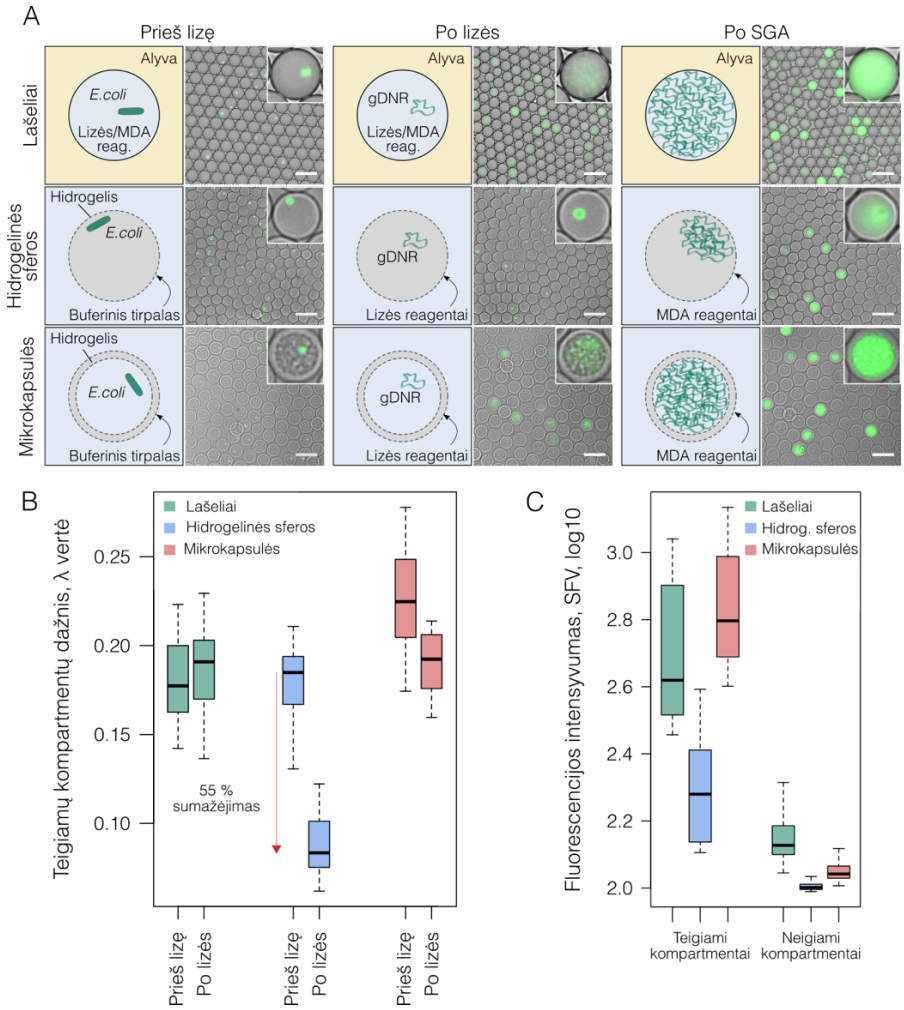

3 pav. *E. coli* izoliavimo ir genomų padauginimo efektyvumo palyginimas vandens lašeliuose, PEGDA hidrogelinėse sferose ir PEGDA mikrokapsulėse. (**A**) Schemos ir mikroskopinės analizės nuotraukos, vaizduojančios kiekvieną iš sistemų prieš bakterijų lizavimą, po lizavimo ir po DNR padauginimo. (**B**) Lambda verčių matavimai po *E. coli* inkapsuliavimo ir lizės. Stačiakampės diagramos sudarytos išanalizavus >450 kompartmentų kiekviename mėginyje. (**C**) Stačiakampės diagramos rodo fluorescencijos intensyvumą teigiamuose ir neigiamuose (tuščiuose) kompartmentuose po SGA. Stačiakampės diagramos sudarytos išmatavus 558 lašelių, 511 hidrogelinių rutuliukų ir 491 mikrokapsulių fluorescenciją. Skalė – 50 µm.

Po inkapsuliavimo *E. coli* ląstelės kiekviename iš reakcijos formatų buvo pasiskirsčiusios pagal Puasono skirstinį, o lambda reikšmė siekė 0,17 ir 0,18

atitinkamai lašeliams ir rutuliukams. Mikrokapsulių atveju *E. coli* ląstelių dažnis buvo šiek tiek didesnis ir lambda reikšmė siekė 0,23. Nedidelį lambda vertės padidėjimą galima paaiškinti klampiu didelės molekulinės masės dekstranu, kuris inkapsuliavimo metu sumažino ląstelių sedimentaciją ir dėl to didesnis ląstelių skaičius pateko į lašelius. Nors bakterijų inkapsuliavimo į lašelius, hidrogelinius rutuliukus ir mikrokapsules rezultatai buvo palyginti panašūs (lambda reikšmės buvo panašios), atlikus ląstelių lizavimą, buvo pastebėti reikšmingi skirtumai (**3 pav., B**). Vandens lašeliuose teigiamų reakcijų skaičius išliko panašus prieš ląstelių lizavimą ir po jo, tačiau hidrogeliniuose rutuliukuose buvo prarasta ~55 % izoliuotų ląstelių genetinės medžiagos. Mikrokapsulių atveju ląstelių genetinės medžiagos praradimas sudarė ~15 %. Mikroskopinė analizė parodė, kad tokį žymų sumažėjimą hidrogeliniuose rutuliukuose galima paaiškinti ląstelių polinkiu lokalizuotis tarp hidrogelio ir alyvos fazių (**3 pav., A**), kuris buvo stebėtas ir ankstesniuose darbuose (34,35). Tuo tarpu, mikrokapsulių hidrogelinis apvalkalas užtikrino, kad didžioji dalis ląstelių ir jų genetinė medžiaga liktų išlaikyta po lizavimo.

Fluorescencijos matavimai po pavienių genomų padauginimo parodė, kad SGA reakcija buvo efektyvesnė mikrokapsulėse nei hidrogeliniuose rutuliukuose ar lašeliuose (**3 pav., C**). Didesnė SGA reakcijos išeiga mikrokapsulėse, palyginus su hidrogeliniais rutuliukais, gali būti susijusi su skystu mikrokapsulės vidumi, kuris netrukdo phi29 DNR polimerazei sintetinti ilgų DNR molekulių (>10 kb). Tuo tarpu, hidrogeliniuose rutuliukuose naujai sintetinamos DNR molekulės įsiterpia į hidrogelio tinklelį ir yra fiziškai apribotos, kas gali daryti įtaką DNR padauginimo efektyvumui. Šią prielaidą patvirtina tai, kad SGA reakcijos išeiga lašeliuose buvo ~2 kartus didesnė nei hidrogeliniuose rutuliukuose. Lyginant DNR padauginimo efektyvumą mikrokapsulėse ir lašeliuose, PEGDA mikrokapsulėse padaugintos DNR kiekis buvo didesnis. Tai galima paaiškinti nepertraukiamu reakcijos komponentų (dNTP, oligonukleotidų ir DNR polimerazės) papildymu per pusiau pralaidžią mikrokapsulės membraną. Tuo tarpu, lašeliuose reakcijos komponentų kiekis yra fiksuotas ir apribotas lašelio tūriu (195). Tačiau neatmetama galimybė, jog efektyvesnis DNR padauginimas įvyko dėl griežtesnių lizavimo sąlygų taikytų mikrokapsulėse, kas galėjo turėti įtakos gDNR prieinamumui.

Gramteigiamų bakterijų lizavimas ir SGA efektyvumas

Gramteigiamoms bakterijoms lizuoti paprastai reikia griežtesnių lizės sąlygų (196), kurios gali arba slopinti, arba būti nesuderinamos su po to sekančiais fermentiniais etapais. Todėl tikėtasi, kad SGA reakcijos efektyvumo skirtumai taikant sąlygas, tinkančias lašelių formatui, ir taikant

sąlygas, suderinamas su mikrokapsulėmis, bus dar ryškesni. Siekiant tai įvertinti, *Rhodococcus rhodochrous* PY11 ir *Streptococcus mutans* UA159 bakterijos buvo atskirai izoliuotos į PEGDA mikrokapsules, išdalintos lygiomis dalimis į atskirus mėgintuvėlius, iš kurių kiekvienai taikytos skirtingos lizės ir SGA sąlygos, pateiktos **4 lentelėje**. Šiame eksperimente taikytas lizės ir SGA sąlygas galima suskirstyti į tris grupes: vieno, dviejų ir trijų žingsnių. Atliekant vieno žingsnio reakciją, lizės ir MDA reagentai buvo įnešami vienu metu. Dviejų žingsnių reakcijose lizės ir MDA etapai buvo atskirti mikrokapsules praplaunant neutraliame buferiniame tirpale. Analogiškai, lizės ir MDA etapai buvo atskirti trijų žingsnių reakcijose. Tačiau šiuo atveju lizės etapas buvo kompleksiškesnis ir turėjo dvi lizavimo stadijas. Kiekvienai taikytai sąlygai buvo įvertintas įvykusių genomų padauginimo reakcijų skaičius. Iš šešių tikrintų sąlygų daugiausia teigiamų reakcijų gauta taikant trijų žingsnių strategiją su dviem lizės etapais (lizocimo inicijuota lizė 37 ºC temperatūroje 30 min. ir po to sekantis inkubavimas su proteinaze K ir NDS 50 ºC temperatūroje 30 min.): 84 % su *S. mutans* ir 99 % su *R. rhodochrous* bakterijomis (**4 lentelė,** sąlyga nr. 5). Antroje vietoje efektyviausiai veikė šarminė lizė ir NDS (sąlyga nr. 6). Tai leido išgauti 33 % teigiamų reakcijų su *S. mutans* ir 48 % su *R. rhodochrous*. Pažymėtina, kad bakterijų lizavimas veikiant šarmu plačiai naudojamas tiriant aplinkos mėginius (57). PEGDA mikrokapsulių suderinamumas su šiomis griežtomis lizės sąlygomis galėtų suteikti daug privalumų pavienių ląstelių genomikos tyrimuose. Palyginimui, taikant vieno žingsnio lizės-SGA metodą lašeliuose ir mikrokapsulėse (kontrolinė sąlyga ir sąlyga nr. 1) gauta tik 25 % teigiamų reakcijų su *S. mutans* ir 4-8 % teigiamų reakcijų su *R. rhodochrous*. Šie rezultatai patvirtino, kad PEGDA mikrokapsulės yra tinkamos analizuojant pavienių mikroorganizmų genetinę medžiagą, kadangi reagentai reikalingi efektyviam bakterijų suardymui neturi įtakos mikrokapsulių stabilumui ir yra pašalinami prieš mikrokapsulių perkėlimą į MDA reakcijos mišinį. Kaip parodyta sekančiame skyrelyje, PEGDA mikrokapsulių panaudojimas gali būti išplėstas atliekant bakterijų kultivavimą.

4 lentelė. *R. rhodochrous* PY11 ir *S. mutans* UA159 bakterijų lizės sąlygos ir SGA reakcijos efektyvumas. Po MDA mikrokapsulės buvo nudažytos SYBR Green I dažu ir analizuotos epifluorescenciniu mikroskopu. Kiekvienai tiriamai sąlygai buvo išanalizuota >600 mikrokapsulių ir lašelių.

Sąlyga	Lizė-SGA	Pirmas žingsnis	Antras žingsnis	Trečias žingsnis	Reakcijos efektyvumas
Kontr.	Vieno žingsnio lašeliuose	50 U/µl lizocimo, 0,1% (V/V) Triton X-100, 1× MDA reakcijos mišinys. 12 val./30 °C.	Netaikytas	Netaikytas	25% (*Strep.*) 8% (*Rhod.*)
1.	Vieno žingsnio mikrokap.	50 U/µl lizocimo, 0,1% (V/V) Triton X-100, 1× MDA reakcijos mišinys. 12 val./30 °C.	Netaikytas	Netaikytas	25% (*Strep.*) 4% (*Rhod.*)
2.	Dviejų žingsnių mikrokap.	50 U/µl lizocimo, 0,1% (V/V) Triton X-100, 1 mM EDTA, 10 mM Tris-HCl [pH 7,5, 25 °C]. 30 min./37 °C.	Mikrokap. praplautos ir perkeltos į 1x MDA mišinį. 12 val./30 °C.	Netaikytas	26% (*Strep.*) 3% (*Rhod.*)
3.	Dviejų žingsnių mikrokap.	50 U/µl lizocimo, 0,1% (V/V) Triton X-100, 1 mM EDTA, 200 µg/ml proteinazės K, 10 mM Tris-HCl [pH 7,5, 25 °C]. 30 min./37°C ir 30 min./50°C.	Mikrokap. praplautos ir perkeltos į 1x MDA mišinį. 12 val./30 °C	Netaikytas	20% (*Strep.*) 58% (*Rhod.*)
4.	Trijų žingsnių mikrokap.	50 U/µl lizocimo, 0,1% (V/V) Triton X-100, 1 mM EDTA, 10 mM Tris-HCl [pH 7,5, 25 °C]. 30 min./37 °C.	Papildymas 200 µg/ml proteinazės K. 30 min./50 °C.	Mikrokap. praplautos ir perkeltos į 1x MDA mišinį. 12 val./30 °C.	15% (*Strep.*) 57% (*Rhod.*)
5.	Trijų žingsnių mikrokap.	50 U/µl lizocimo, 0,1% (V/V) Triton X-100, 1 mM EDTA, 10 mM Tris-HCl [pH 7.5, 25 °C]. 30 min. /37 °C.	Papildymas 200 µg/ml proteinazės K ir 1% (m/V) NDS. 30 min./50 °C.	Mikrokap. praplautos ir perkeltos į 1x MDA mišinį. 12 val./30 °C.	84% (*Strep.*) 99% (*Rhod.*)
6.	Dviejų žingsnių mikrokap.	0,5 M NaOH ir 1% (m/V) NDS. 5 min./21 °C	Mikrokap. praplautos ir perkeltos į 1x MDA mišinį. 12 val./30 °C.	Netaikytas	33% (*Strep.*) 48% (*Rhod.*)

Bakterijų kultivavimas ir fenotipinė analizė

Be genomų padauginimo ir analizės, sistema, leidžianti fenotipiškai analizuoti pavienes bakterijas, būtų vertinga atliekant įvairesnius mikrobiologinius tyrimus. Mikroorganizmų fenotipinei analizei atlikti dažnai prireikia bakterijų kultivavimo, genų raiškos indukcijos ir po to sekančios metabolitų analizės. Visų šių etapų įgyvendinimas vandens lašeliuose yra didelis iššūkis. Tuo tarpu, selektyviai pralaidžios mikrokapsulės leidžia suderinti didelį analizės našumą kartu su kelių etapų analizės metodais. Šioje dalyje mikrokapsulių panaudojimas parodytas atliekant bakterijų metabolito polihidroksibutirato (PHB) sintezę ir nustatymą izogeninėse kolonijose, kilusiose iš pavienių izoliuotų *E. coli* ląstelių.

Siekiant įvertinti, ar PEGDA mikrokapsulės gali būti naudojamos pavienių bakterijų kultivavimui, *E. coli* MG1655 ląstelės buvo izoliuotos ir mikrokapsulės perkeltos į auginimo lėkštelę su LB mitybine terpe (**4 pav., A**). Palyginimui *E. coli* MG1655 ląstelės buvo izoliuotos vandens lašeliuose su LB mitybine terpe (**4 pav., B**). Abiejose sistemose ląstelės buvo kultivuojamos 4 valandas 37 ºC temperatūroje. Remiantis rezultatais, gautais atlikus pavienių genomų padauginimą, buvo tikimasi, jog nepertraukiamas mitybinių medžiagų patekimas per hidrogelinį apvalkalą užtikrins ilgesnį ląstelių augimą iki kol visa mikrokapsulės vidinė dalis bus užpildyta bakterijomis. Tuo tarpu, lašeliuose galutinį ląstelių skaičių ribotų lašelio viduje esančios mitybinės medžiagos. Atlikus mikroskopinę analizę, ši prielaida buvo patvirtinta: mikrokapsulėse pavienės bakterijos išaugo į mikrokolonijas, kuriose ląstelių skaičius siekė ~90, o lašeliuose mikrokolonijas sudarė ~30 ląstelių (**4 pav., C**).

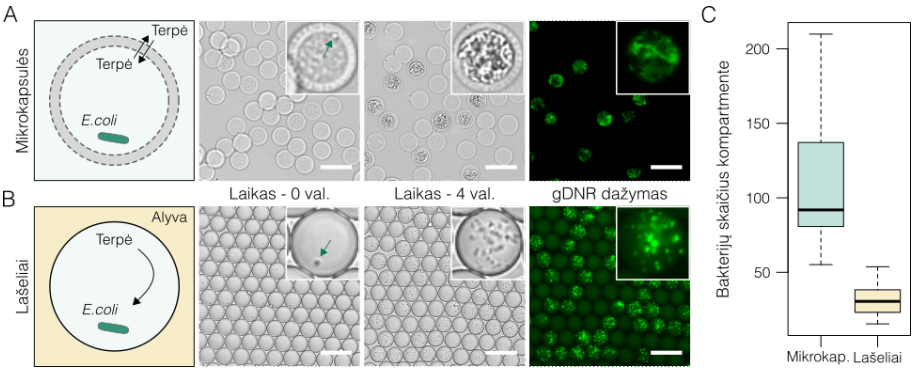

4 pav. *E. coli* MG1655 mikrokolonijų formavimosi PEGDA mikrokapsulėse ir lašeliuose palyginimas. Kairėje: mikrokapsulių (**A**) ir lašelių (**B**) eksperimentinės schemos. Viduryje: mikroskopinės analizės nuotraukos, kuriose matomas bakterijų augimas mikrokapsulėse (**A**) ir lašeliuose (**B**) inkubuojant 37 °C temperatūroje 4 valandas. Žalios rodyklės rodo pavienes bakterijas iš karto po izoliavimo. Fluorescenciniai vaizdai gauti po dažymo SYBR Green I dažu. (**C**) Stačiakampės diagramos rodo bakterijų skaičių po 4 valandų auginimo mikrokapsulėse ir lašeliuose. Stačiakampės diagramos sudarytos išmatavus 20 lašelių ir 30 mikrokapsulių. Skalė – 50 μm.

Patvirtinus, jog *E. coli* gali būti kultivuojamos PEGDA mikrokapsulėse, sekančiame etape mikrokapsulės buvo panaudotos bakterijų, sintetinančių biodegraduojamą plastiką – polihidroksibutiratą (PHB) (198-200), identifikavimui. Tuo tikslu *E. coli* DH5α ląstelės buvo transformuotos su pBHR68 vektoriumi, turinčiu PHB sintezės genus (*phaC*, *phaA* ir *phaB*) (201). Transformuotos bakterijos buvo izoliuotos į PEGDA mikrokapsules,

6 valandas kultivuotos ir tada PHB sintezė buvo indukuota pridedant izopropil-β-D-1-tiogalaktopiranozido (IPTG). Po 8 valandų inkubavimo su IPTG PHB susidarymas buvo patikrintas gyvose ląstelėse naudojant Nile Red dažą, kuris, remiantis literatūros duomenimis, nudažo PHB granules (202) (**5 pav., A**). Atlikus dažymą ir mikroskopinę analizę, buvo pastebėta, kad Nile Red, būdamas lipofilinis dažas, taip pat jungiasi prie ląstelės membranos. Dėl šios priežasties tiek teigiami, tiek neigiami mėginiai turėjo aukštą fluorescencijos signalą, kuris neleido patikimai identifikuoti PHB sintetinančių bakterijų (**5 pav., B**). Siekiant sumažinti šį nespecifinį fluorescencijos signalą, mikrokapsulės su išaugintomis mikrokolonijomis buvo perkeltos į lizavimo mišinį, turintį lizocimo, proteinazės K ir nejoninio detergento, ir analizuotos pakartotinai. Šis papildomas etapas padidino fluorescencinio signalo skirtumą tarp teigiamų ir neigiamų klonų apie 10 kartų (**5 pav., C**).

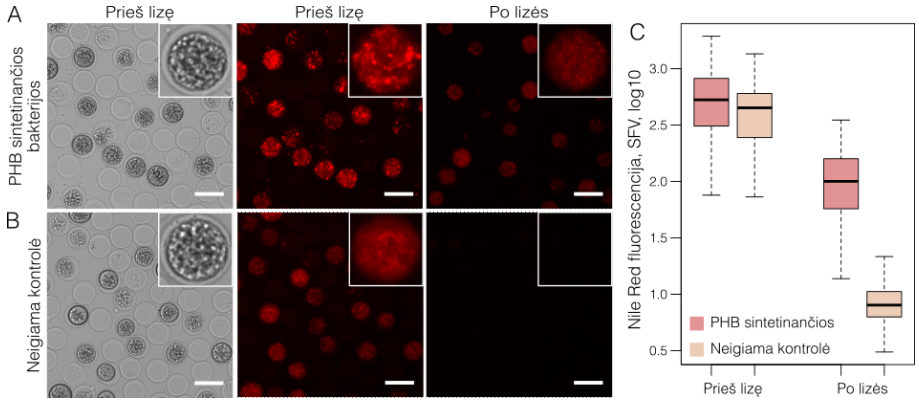

5 pav. PHB sintetinančių mikrokolonijų detekcija taikant dažymą Nile Red. (**A**) PHB sintetinančios mikrokolonijos ir (**B**) neigiama kontrolė buvo analizuotos prieš ir po ląstelių lizės. (**C**) Stačiakampės diagramos rodo santykinį PHB kiekį remiantis fluorescencijos signalo intensyvumu gyvose ir lizuotose mikrokolonijose. Stačiakampės diagramos sudarytos išmatavus >100 mikrokapsulių kiekvienai sąlygai. Skalė – 50 μm.

Įvertinus, jog PHB sintetinančias bakterijas galima atskirti nuo neigiamų klonų, kitas žingsnis buvo nustatyti, kurios mikrokolonijos PHB sintezę vykdo efektyviausiai. Kuomet atsižvelgiama tik į rezultatus, gautus po dažymo su Nile Red, iškyla rizika klaidingam įvertinimui, nes sparčiausiai augantys klonai gali užgožti lėčiau augančius, tačiau turinčius didesnį PHB sintezės potencialą. Siekiant išvengti šio netikslumo, lizuotoms mikrokolonijoms buvo taikytas dažymas tiek su Nile Red, tiek su SYBR Green I. Šis dvigubas dažymas leido normalizuoti PHB sintezės lygį pagal bakterijų skaičių (**6 pav.)**

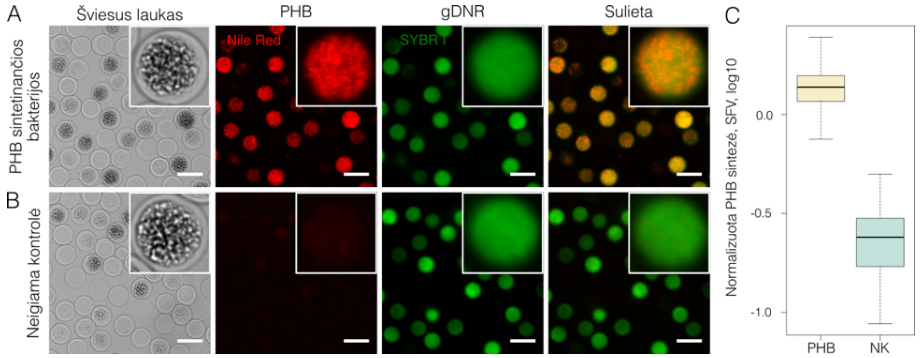

6 pav. PHB kiekio normalizavimas mikrokapsulėse. (**A**) PHB sintetinančios mikrokolonijos ir (**B**) neigiama kontrolė (NK) buvo analizuotos po ląstelių lizės ir dažymo Nile Red ir SYBR Green I dažais. (**C**) Stačiakampės diagramos rodo normalizuotus teigiamų (geltona spalva) ir neigiamų (žalia spalva) klonų PHB sintezės lygius. PHB kiekiui normalizuoti naudotas Nile Red ir SYBR Green I fluorescencijos santykis. Stačiakampės diagramos sudarytos išmatavus 107 teigiamas ir 78 neigiamas mikrokolonijas Skalė – 50 µm.

Rezultatai, gauti atliekant ląstelių nukleorūgščių padauginimą ir kultivavimą, patvirtino, jog PEGDA mikrokapsulės yra tinkama ir patogi sistema kompleksinei pavienių bakterijų analizei atlikti. Sekantis etapas buvo išplėsti mikrokapsulių taikymus analizuojant žinduolių ląsteles bei taikant kitas molekulinės biologijos metodikas. Kaip parodyta sekančiuose skyreliuose, tai buvo pasiekta sukūrus naują mikrokapsulių sistemą.

Želatinos metakrilato mikrokapsulių išvystymas ir taikymas

Želatinos metakrilato mikrokapsulių paruošimas

Mikrokapsulės, turinčios želatinos metakrilato (ŽMA) apvalkalą, buvo ruošiamos inkapsuliuojant želatinos metakrilato ir dekstrano (MM ~500k) tirpalus ir formuojant vandeninius dvifazinius lašelius (žr. medžiagas ir metodus). Kaip ir su PEGDA mikrokapsulėmis, ląstelės atitinkama koncentracija buvo suspenduojamos dekstrano fazėje (**7 pav., A**). Po lašelių susiformavimo ŽMA ir dekstrano fazės atsiskyrė, sudarydamos skystą apvalkalą, praturtintą ŽMA, ir skystą vidinę dalį, praturtintą dekstranu (**7 pav., B**). Norint paversti lašelius mikrokapsulėmis, selektyviai pralaidus apvalkalas buvo formuojamas dviem etapais. Pirmiausia skystas apvalkalo sluoksnis buvo sukietintas atšaldant lašelius 4 ºC temperatūroje 30 minučių. Po šio etapo tarpinės mikrokapsulės buvo išgrynintos iš emulsijos ir perkeltos į buferinį tirpalą, kur atliktas cheminis kryžminis susiuvimas veikiant 405 nm bangos ilgio šviesai ir fotoiniciatoriui. Šis dviejų etapų polimerizacijos

protokolas užtikrino stabilių, vienodo dydžio ir centruotų mikrokapsulių paruošimą. (**7 pav., C**).

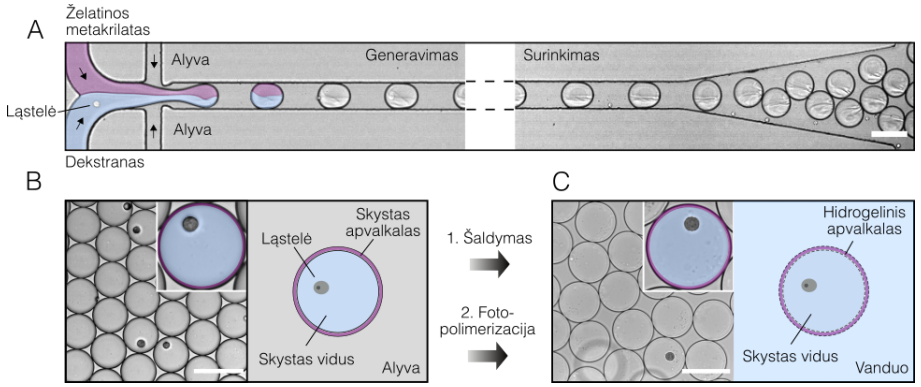

7 pav. ŽMA mikrokapsulių generavimas ir ląstelių izoliavimas. (**A**) Ląstelių suspensija inkapsuliuojama į vandeninius dvifazinius lašelius, sudarytus iš skystos vidinės dalies, praturtintos dekstranu, ir skysto apvalkalo, praturtinto ŽMA (**B**). Surinktų lašelių skystas apvalkalas paverčiamas selektyviai pralaidžia membrana taikant dviejų žingsnių polimerizaciją. Pirmiausia, atšaldant emulsiją, skystas apvalkalas paverčiamas hidrogeliu, po kurio seka cheminis kryžminis susiuvimas vykdant fotopolimerizaciją (**C**). Skalė – 100 μm.

Ląstelių tipų identifikavimas taikant AT-PGR

Siekiant įvertinti ŽMA mikrokapsulių tinkamumą pavienių žinduolių ląstelių tyrimuose, buvo pasirinkta atlikti atvirkštinės transkripcijos polimerazės grandininę reakciją (AT-PGR), kurios produktas leistų identifikuoti pavienes ląsteles pagal pasirinktų žymenų raišką. Tuo tikslu vienodu santykiu buvo sumaišytos K-562 ir HEK293 ląstelės ir inkapsuliuotos remiantis Puasono statistika taip, kad kiekvienoje mikrokapsulėje vidutiniškai patektų ne daugiau kaip viena ląstelė. Palyginimui atskirai buvo inkapsuliuotos K-562 ir HEK293 ląstelės. Izoliuotos ląstelės buvo lizuojamos perkeliant mikrokapsules į chaotropinį buferinį tirpalą, po kurio sekė mikrokapsulių praplovimai ir gDNR pašalinimas veikiant DNaze I. Tokiu būdu buvo gautos mikrokapsulės su išgryninta RNR iš pavienių ląstelių. Šis mėginio paruošimo būdas buvo pasirinktas dėl kelių priežasčių. Visų pirma, veiksminga ląstelių lizė yra labai svarbi norint efektyviai išgauti nukleorūgštis. Antra, gDNR pašalinimas padidina AT-PGR signalo specifiškumą, nes užkerta kelią gDNR padauginimui. Trečia, mikrokapsulių praplovimas po lizės yra būtinas siekiant pašalinti lizės reagentus bei slopiklius, esančius ląstelių lizate (91,94,113,205,206).

Mikrokapsulės su išgryninta visumine RNR buvo perkeltos į AT reakcijos mišinį, kuriame iRNR molekulės buvo paverstos kopijine DNR (kDNR). Siekiant identifikuoti ląsteles pagal jų genų raiškos profilį, mikrokapsulės po AT buvo perkeltos į daugybinės PGR mišinį, turintį pradmenis specifiškus ląstelių tipo ir universaliems žymenis. K-562 ląstelėms buvo pasirinktas *PTPRC* žymuo (angl., *protein tyrosine phosphatase receptor type C*), o HEK293 ląstelėms – *YAP* žymuo (angl., *Yes-associated protein 1*). Beta-aktinas (*ACTB*) buvo pasirinktas kaip universalus žymuo, kurio raiška būdinga abiem ląstelių linijoms. PGR tiesioginių pradmenų 5'-galas buvo pažymėtas fluorescencinėmis žymėmis, kurių emisija įvyksta ties skirtingais bangos ilgiais: Alexa Fluor 488 (*PTPRC* pradmuo), Alexa Fluor 555 (*YAP* pradmuo) ir Alexa Fluor 647 (*ACTB* pradmuo). PGR etapo metu žymėti oligonukleotidai difunduoja iš pagrindinio tirpalo į mikrokapsulės vidų ir, įvykus prisilydimui prie specifinio DNR regionio, yra įtraukiami į PGR produktus. (**8 pav.**). Tokiu būdu pagal fluorescencijos signalą galima identifikuoti iš pavienių ląstelių padaugintus žymenis. Atsižvelgiant į skirtingą *PTPRC* ir *YAP* raišką ir universalią *ACTB* raišką, buvo tikimasi mikrokapsules su K-562 ląstelėmis identifikuoti pagal *PTPRC* ir *ACTB* signalą (žydra spalva), o HEK293 – pagal *YAP* ir *ACTB* signalą (purpurinė spalva). Mikroskopinė analizė patvirtino, jog K-562 ir HEK293 ląstelės, iš tiesų, gali būti identifikuojamos pagal padaugintų žymenų fluorescencijos profilį (**8 pav., B ir C**).

Gauti rezultatai patvirtino, kad ŽMA mikrokapsulės yra tinkamos pavienių ląstelių izoliavimui ir analizei atliekant AT-PGR, kas leidžia identifikuoti ląstelių tipus pagal pasirinktų žymenų raišką. Be to, kaip parodyta kitame skyrelyje, šios mikrokapsulės yra suderinamos su tėkmės citometriją, kas leidžia paspartinti didelės apimties dalelių analizę.

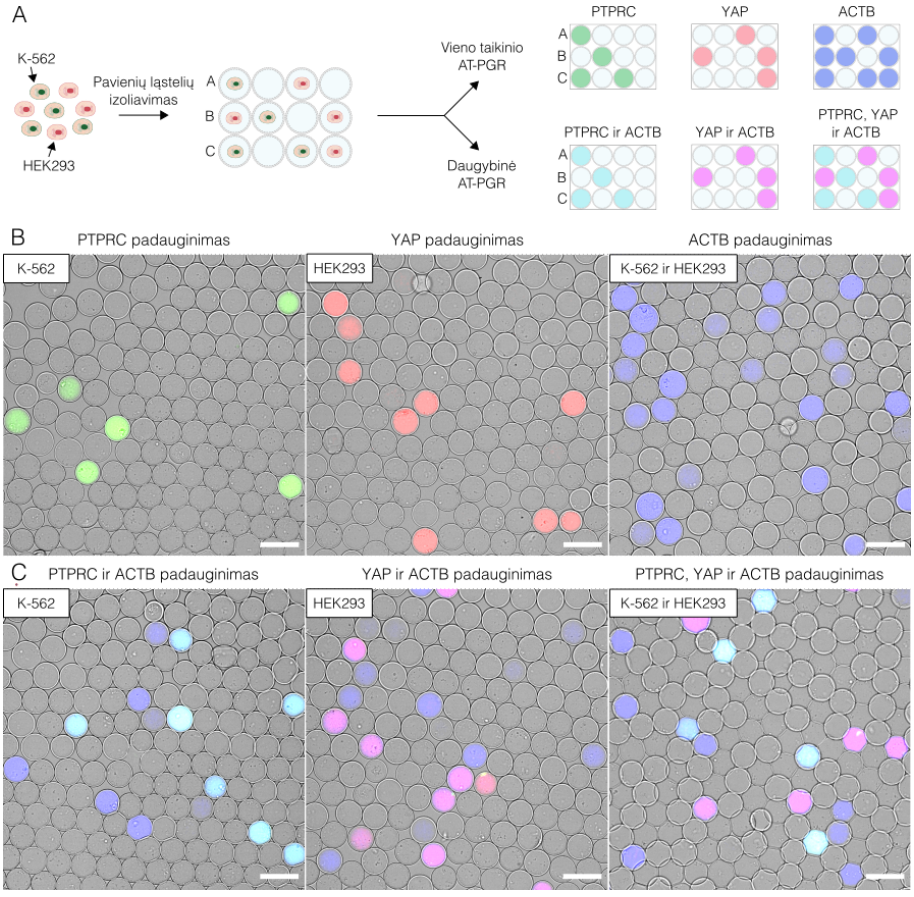

8 pav. Ląstelių tipų identifikavimas atliekant AT-PGR mikrokapsulėse. (**A**) Eksperimento schema. K-562 ir HEK293 ląstelių mišinys izoliuojamas mikrokapsulėse ir atliekamas vieno žymens arba kelių žymenų (daugybinė) AT-PGR. Pasirinktų žymenų padauginimui naudojami fluorescencine žyme pažymėti pradmenys specifiški *PTPRC*, *YAP* ir *ACTB*. Po AT-PGR įvertinama mikrokapsulių fluorescencija. (**B**) Mikroskopijos nuotraukos po AT-PGR, kuomet buvo padaugintas vienas iš žymenų: *PTPRC* (žalia spalva), *YAP* (raudona spalva) ir *ACTB* (mėlyna spalva). (**C**) Mikroskopijos nuotraukos po daugybinės AT-PGR, kai vienu metu buvo atliekamas dviejų arba trijų žymenų padauginimas: *PTPRC* ir *ACTB* (žydra spalva), *YAP* ir *ACTB* (purpurinė spalva), *PTPRC*, *YAP* ir *ACTB* (žydra ir purpurinė spalvos). Skalė – 100 µm.

Mikrokapsulių po AT-PGR analizė tėkmės citometrija

Mikroskopija yra patogus ir tikslus būdas analizuoti mikrokapsules po AT-PGR. Tačiau tais atvejais, kai reikia išanalizuoti didelį mikrokapsulių skaičių (>10 000), šis būdas tampa nepraktiškas. Dėl šios priežasties buvo siekiama įvertinti, ar tėkmės citometrija gali būti naudojama kaip alternatyvus būdas mikrokapsulių analizei. Tuo tikslu mikrokapsulės su K-562 ląstelėmis, HEK293 ląstelėmis ir jų mišiniu buvo analizuotos Partec CyFlow Space tėkmės citometru (**9 pav.**). Vieno eksperimento metu buvo išanalizuota iki 30 000 mikrokapsulių, tačiau galutinis mikrokapsulių skaičius nėra ribojamas ir gali būti padidintas. Atliekant tėkmės citometriją, mikrokapsulės buvo identifikuojamos pagal priekinės ir šoninės sklaidos grafiką, kur buvo stebimas lokalizuotas matavimų/dalelių židinys. Pasirinkta mikrokapsulių populiacija toliau buvo analizuojama pagal Alexa Fluor 647 fluorescencijos ir šoninės sklaidos grafiką, kas leido identifikuoti *ACTB* teigiamas mikrokapsules. Galiausiai, *ACTB* teigiamos mikrokapsulės buvo analizuojamos pagal Alexa Fluor 488 ir Alexa Fluor 555 fluorescenciją, kas leido identifikuoti *PTPRC* ir *YAP* teigiamas populiacijas ir nustatyti pradinį mėginį sudarančias ląsteles.

5 lentelėje pateikti rezultatai rodo, kad tėkmės citometrijos ir mikroskopijos rezultatai yra labai panašūs. Mikrokapsulės su K-562 ląstelėmis buvo teigiamos pagal *PTPRC* signalą: 3,19 % buvo gauti atliekant mikroskopinę analizę ir 3,63 % - naudojant tėkmės citometriją. Mikrokapsulės su HEK293 ląstelėmis buvo teigiamos pagal *YAP* signalą: 4,84 % buvo gauti atliekant mikroskopinę analizę ir 5,46 % – naudojant tėkmės citometriją, kas atitiko teorinį ląstelių dažnį mikrokapsulėse (~5-6 %). Mikrokapsulės su K-562 ir HEK293 ląstelių mišiniu buvo teigiamos arba pagal *PTPRC*, arba *YAP* signalą. Dviejų skirtingų ląstelių izoliavimo į tą pačią mikrokapsulę įvykiai buvo reti (0,02-0,15 %) ir atitiko Puasono skirstinį. Svarbu paminėti, jog 99,07 % *PTPRC* teigiamų mikrokapsulių buvo teigiami *ACTB* signalui mėginyje su K-562 ląstelėmis, o 94,57 % *YAP* teigiamų mikrokapsulių buvo teigiami *ACTB* signalui mėginyje su HEK293 ląstelėmis. Šie rezultatai patvirtino, jog izoliuotų ląstelių identifikavimas galimas naudojant ląstelės tipui specifinių bei universalių žymenų raiškos kombinaciją.

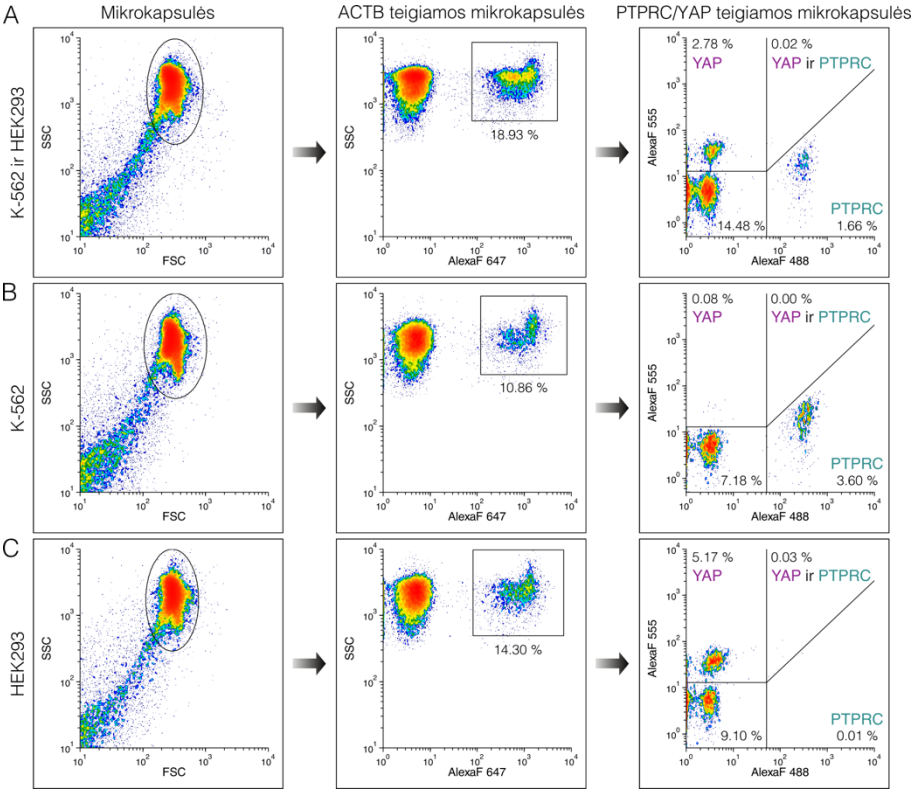

9 pav. Mikrokapsulių po AT-PGR analizė tėkmės citometrija. Tėkmės citometrijos duomenų grafikuose pavaizduoti trys mikrokapsulių mėginiai: K-562 ir HEK293 ląstelių mišinys (**A**), K-562 ląstelės (**B**) ir HEK293 ląstelės (**C**). Mikrokapsulės buvo identifikuotos pagal priekinės ir šoninės sklaidos signalą. Tuomet pasirinkta populiacija buvo suskirstyta pagal *ACTB* žymens raišką ir galiausiai pagal *PTPRC* ir *YAP* žymenų raišką. Procentai rodo dalį nuo visų mikrokapsulių skaičiaus.

5 lentelė. AT-PGR rezultatų palyginimas naudojant tėkmės citometriją ir mikroskopiją.

Mėginys	**Matavimų skaičius**	**ACTB**	**YAP**	**YAP ir ACTB**	**PTPRC**	**PTPRC ir ACTB**	**YAP ir PTPRC**	**YAP, PTPRC ir ACTB**
Mikroskopija								
K-562	2822	285 (10.1%)	3 (0.11%)	3 (0.11%)	90 (3.19%)	90 (3.19%)	2 (0.07%)	2 (0.07%)
HEK293	2128	272 (12.78%)	103 (4.84%)	102 (4.79%)	0 (0.0%)	0 (0.0%)	0 (0.0%)	0 (0.0%)
K-562 ir HEK293	2006	361 (18.0%)	69 (3.44%)	68 (3.39%)	36 (1.79%)	36 (1.79%)	3 (0.15%)	3 (0.15%)
Tėkmės citometrija								
K-562	23628	2565 (10.86%)	84 (0.36%)	18 (0.08%)	858 (3.63%)	850 (3.60%)	1 (<0.01%)	1 (<0.01%)
HEK293	19574	2800 (14.30%)	1069 (5.46%)	1011 (5.17%)	1 (<0.01%)	1 (<0.01%)	6 (0.03%)	6 (0.03%)
K-562 ir HEK293	31061	5881 (18.93%)	940 (3.03%)	863 (2.78%)	524 (1.69%)	516 (1.66%)	6 (0.02%)	5 (0.02%)

Tiek tėkmės citometrija, tiek mikroskopinė analizė parodė, kad yra trečia teigiamų mikrokapsulių populiacija, kurios fluorescencinis signalas atitinka *ACTB* žymenį, bet nedetektuojami nei *PTPRC*, nei *YAP* signalai. *ACTB* teigiamų įvykių skaičius (**5 lentelė**, 3 stulpelis) buvo maždaug 3 kartus didesnis nei *YAP* (4 stulpelis) ar *PTPRC* (6 stulpelis) įvykių skaičius. Atsižvelgiant į didelį *ACTB* teigiamų mikrokapsulių skaičių, kuris viršija izoliuotų ląstelių skaičių, buvo padaryta prielaida, kad šie klaidingai teigiami įvykiai galėjo atsirasti dėl laisvai plaukiojančių iRNR molekulių, kurių buvo pradinėje ląstelių suspensijoje (prieš izoliavimą) dėl išankstinės ląstelių lizės. Šie pastebėjimai sutampa su ankstesniais tyrimais, rodančiais, jog atliekant pavienių ląstelių AT-PGR lašeliuose, teigiamų lašelių skaičius yra didesnis nei izoliuotų ląstelių kiekis (112,207). Be to, kaip labiausiai tikėtinas šių įvykių šaltinis buvo įvardintos iRNR molekulės, atsiradusios dėl nedidelio kiekio besilizuojančių ląstelių mėginio paruošimo ir inkapsuliavimo metu (114). Klaidingai teigiamų įvykių atsiradimas dažnai yra neišvengiamas atliekant nukleorūgščių padauginimą. Dėl šios priežasties buvo svarbu rasti būdą, kaip tokius įvykius aptikti, kad būtų išlaikomas analizės tikslumas. Kaip parodyta sekančiame skyrelyje, norint atskirti teisingai teigiamus ir klaidingai teigiamus įvykius, reikėjo įvesti papildomą žymenį, nepriklausantį nuo ląstelės genų raiškos aktyvumo.

Teisingai teigiamų ir klaidingai teigiamų įvykių atskyrimas

Tikslus fluorescuojančių mikrokapsulių atskyrimas, kuriose buvo izoliuota ląstelė (teisingai teigiami įvykiai), nuo mikrokapsulių, į kurias pateko neląstelinė iRNR (klaidingai teigiami įvykiai), gali būti sudėtingas, kadangi fluorescencinio signalo intensyvumo tarp šių įvykių gali būti neįmanoma atskirti. Pavyzdžiui, 8 pav. C dalyje pateikti rezultatai rodo, kad atskirti mikrokapsules, kuriose buvo izoliuotos ląstelės, nuo mikrokapsulių, kuriose buvo izoliuotos neląstelinės iRNR, gali būti itin sunku ir netikslu. Siekiant išspręsti šį analitinį trūkumą, praeitame skyrelyje pristatytas daugybinės AT-PGR mikrokapsulėse metodas buvo modifikuotas pakeičiant ląstelių ardymo sąlygas. Buvo padaryta prielaida, kad, taikant švelnias lizės sąlygas, ląstelių branduoliai turėtų išlaikyti savo kompaktišką struktūrą visų analizės etapų metu ir juos būtų galima panaudoti kaip papildomą žymenį identifikuojant mikrokapsules su izoliuotomis ląstelėmis.

Norint įvertinti šios strategijos tinkamumą, K-562 ir HEK293 ląstelių mišinys buvo izoliuotas mikrokapsulėse, fiksuotas atšaldytame etanolyje ir ląstelės permeabilizuotos naudojant nejoninį detergentą (žr. medžiagas ir metodus). Po šių etapų sekė daugybinė AT-PGR taikant tokias pat sąlygas kaip nurodyta praeitame skyrelyje. Mikroskopinė analizė parodė, kad,

naudojant švelnias lizės sąlygas, ląstelių branduoliai po AT-PGR išlaikė savo struktūrą bei turėjo aiškiai identifikuojamą fluorescencijos signalą visuose kanaluose (Alexa Fluor 647 (*ACTB*), Alexa Fluor 488 (*PTPRC*) ir Alexa Fluor 555 (*YAP*)) galimai dėl nespecifinio PGR pradmenų įsisavinimo (**10 pav., B**). Taip pat, branduolių fluorescencijos signalą buvo galima sustiprinti naudojant mėlynai fluorescuojantį DAPI dažą, kas buvo svarbu analizuojant nedidelio dydžio periferinio kraujo vienbranduoles ląsteles (PKVL). Tuo tarpu, PGR produktų fluorescencija buvo tolygiai pasiskirsčiusi visame mikrokapsulės vidinės dalies tūryje. Taigi, mikrokapsulės fluorescencijos profilio matavimas suteikė paprastą būdą nustatyti mikrokapsules su ląstelėmis ir atskirti jas nuo mikrokapsulių, kuriose buvo padauginta neląstelinė iRNR. (**10 pav., C**).

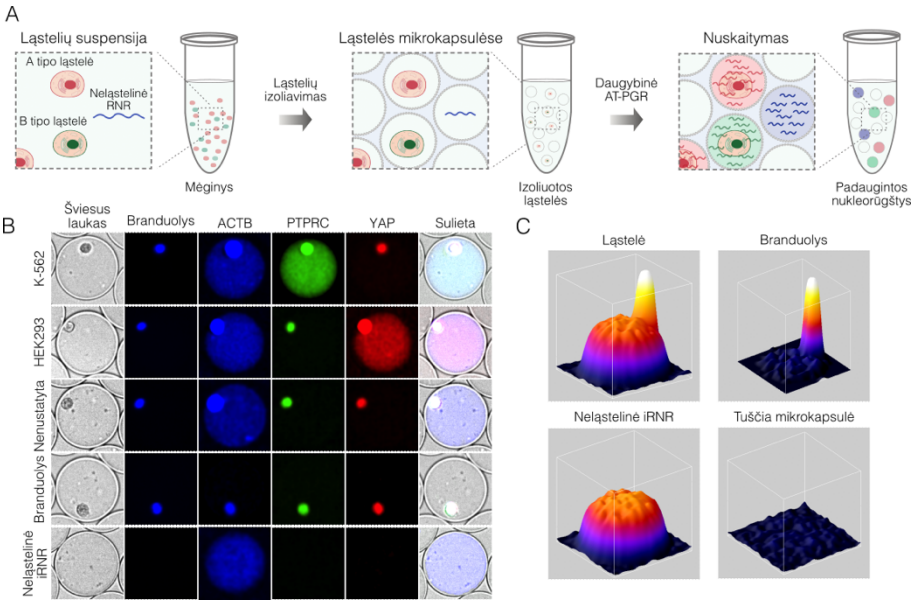

10 pav. Teisingai teigiamų ir klaidingai teigiamų įvykių nustatymas po AT-PGR. (**A**) Eksperimentinė schema, vaizduojanti mėginio, sudaryto iš ląstelių ir laisvai plaukiojančių iRNR molekulių, izoliavimą į mikrokapsules ir po to sekantį nukleorūgščių padauginimą AT-PGR. (**B**) Reprezentatyvūs mikrokapsulių mikroskopijos vaizdai po daugybinės AT-PGR, padauginant *ACTB*, *PTPRC* ir *YAP* žymenis. (**C**) Trimačiai mikrokapsulių fluorescencijos profiliai Alexa Fluor 647 (*ACTB*) kanale, atitinkantys ląstelę su PGR produktu, vien tik branduolį, padaugintą aplinkos iRNR ir tuščią mikrokapsulę. Spalvos atitinka pikselių intensyvumą.

Pasinaudojant šia analitine savybe, mėginyje su izoliuotomis K-562 ir HEK293 ląstelėmis buvo įvertintas neląstelinės iRNR kiekis naudojant tris atskaitos genus: *ACTB*, beta-2-mikroglobuliną (*B2M*) ir *TBP* (angl., *TATA - box binding protein*). Kadangi mėginio paruošimo metu neišvengiamai bent

labai maža dalis ląstelių lizuojasi ir jų iRNR patenka į ląstelių suspensiją, buvo tikimasi, kad gausiausi transkriptai ląstelėje sudarys ir didžiausią klaidingai teigiamų mikrokapsulių kiekį. Kaip ir tikėtasi, *ACTB*, būdamas gausiausias iš trijų pasirinktų transkriptų, turėjo 16 % klaidingai teigiamų mikrokapsulių, tačiau šis skaičius sumažėjo iki 0,8 % naudojant *TBP*. Remiantis literatūros duomenimis, *TBP* ekspresuojamas ~10 kopijų vienoje ląstelėje (208). Realaus laiko PGR rezultatai parodė, jog *TBP* turi ~60 kartų mažesnį raiškos lygį palyginti su *ACTB* genu.

Turint galimybę nustatyti ir kiekybiškai įvertinti teisingai/klaidingai teigiamus įvykius ir teisingai/klaidingai neigiamus įvykius, buvo galima apskaičiuoti daugybinės AT-PGR mikrokapsulėse statistines charakteristikas. Apskaičiuota, kad su HEK293 ląstelėmis *ACTB* detekcijos jautrumas buvo 98,65 %, o *YAP* – 92,57 %. Analizuojant K-562 ląsteles, *ACTB* detekcijos jautrumas buvo 98,37 %, o *PTPRC* – 71,74 %. Specifiškumas tarp skirtingų ląstelių ir žymenų siekė 97,71-99,93 %. Ląstelių tipui būdingų žymenų – *YAP* ir *PTPRC* – teigiamos prognozavimo vertės buvo atitinkamai 98,56 % ir 99,25 %. Neigiamos prognozavimo vertės taip pat buvo labai aukštos: atitinkamai 99,60 % ir 98,23 %. Tačiau verta pažymėti, kad šios vertės nėra fiksuotos ir priklauso nuo mėginio kokybės, ląstelių tipo ir fiziologinės būsenos bei žymenų pasirinkimo.

Leukemijos ląstelių atskyrimas nuo PKVL

Siekiant įvertinti sukurtos mikrokapsulių technologijos potencialą diagnostikoje, buvo atlikta pirminių žmogaus ląstelių analizė. Tuo tikslu mikrokapsulėse buvo izoliuotos atšildytos periferinio kraujo vienbranduolės ląstelės (PKVL) ir atliktas AT-PGR siekiant nustatyti dažniausiai naudojamą kraujo ląstelių žymenį *PTPRC* (taip pat žinomą kaip CD45). Atsižvelgiant į tai, kad PKVL yra teigiamos *PTPRC* žymeniui (informacija pateikta ATCC), buvo tikimasi, kad daugiau kaip 95 % mikrokapsulių su branduoliu bus stebėtas teigiamas *PTPRC* signalas. Tačiau mikroskopinė analizė parodė, kad tik 77,2 % izoliuotų ląstelių buvo teigiamos pagal *PTPRC* žymenį. Analizuojant PKVL pagal *B2M* žymenį, buvo gautas panašus detekcijos lygis (74,6 %). Šie rezultatai labai tiksliai atitiko ląstelių gyvybingumo duomenis (~77 %), kurie buvo gauti dažant ląsteles prieš izoliaciją tripano mėliu. Tai leido prieiti prie išvados, jog PKVL žymenų detekcija koreliavo su ląstelių gyvybingumu.

Patvirtinus, jog AT-PGR mikrokapsulėse yra tinkama PKVL analizei, kitame etape šios ląstelės buvo analizuotos kartu su ūminės promielocitinės leukemijos ląstelėmis (NB4). NB4 ląstelių aptikimui ir atskyrimui nuo PKVL buvo pasirinktas *PML-RARα* žymuo. Rezultatai, pateikti **11 pav.,** patvirtino,

jog NB4 ląstelės buvo detektuojamos ir jų skaičius analizuojamame mėginyje nuosekliai mažėjo dididant praskiedimą su PKVL. Šie rezultatai buvo stebėti atliekant analizę mikroskopu (**A**) bei tėkmės citometru (**B**). Tačiau buvo pastebėta, jog nustatytų NB4 ląstelių dalis buvo ~2 kartus mažesnė nei teorinės prognozės. Siekiant geriau suprasti šį neatitikimą, *PML-RARα* raiškos lygis NB4 ląstelėse buvo kiekybiškai įvertintas naudojant realaus laiko PGR. Šis eksperimentas parodė, kad *PML-RARα* raiška yra ~200 kartų mažesnė nei *PTPRC*, o tai reiškia, kad vidutiniškai vienai ląstelei tenka mažiau nei 1 *PML-RARα* transkripto kopija. Remiantis šiais rezultatais, galima daryti prielaidą, kad ne visos NB4 ląstelės tam tikru metu turi *PML-RARα* transkriptus, taip paaiškinant stebėtus rezultatus. Šiame kontekste verta paminėti, kad analizuojant K-562 ląstelėms būdingą leukemijos žymenį *BCR-ABL*, kurio raiška siekia ~40 kopijų vienoje ląstelėje (216), detekcijos jautrumas siekė 98,6 %.

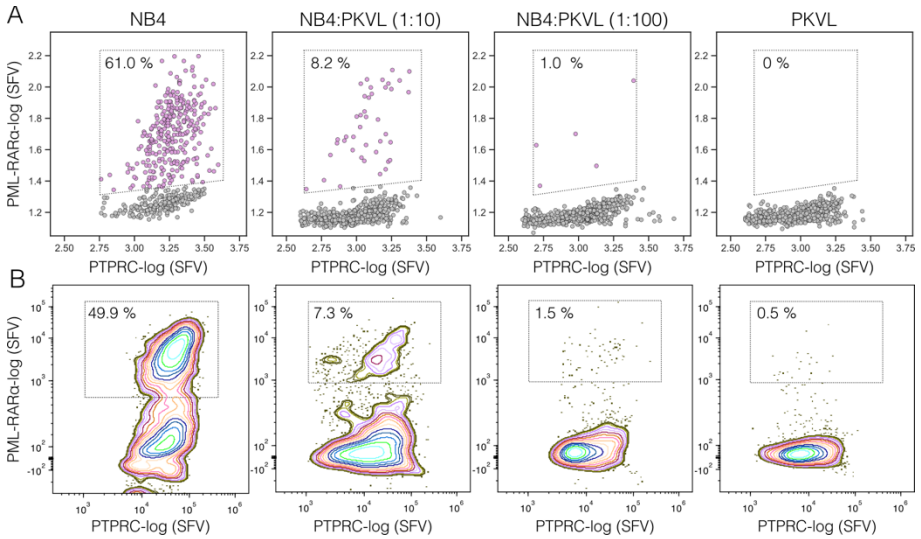

11 pav. Ūminės promielocitinės leukemijos ląstelių (NB4) ir periferinio kraujo vienbranduolių ląstelių (PKVL) RNR citometrija. (**A**) Mikroskopinės analizės ir (**B**) tėkmės citometrijos rezultatai. Pavienių ląstelių daugybinė AT-PGR buvo atlikta siekiant identifikuoti PKVL ir NB4 pagal *PTPRC* (CD45) ir *PML-RARα* žymenų raišką. PKVL nustatytos pagal *PTPRC* žymens teigiamą signalą, o NB4 ląstelės – pagal *PTPRC* ir *PML-RARα* teigiamų signalų persidengimą. Procentais pateikta *PML-RARα* teigiamų įvykių dalis nuo visų izoliuotų ląstelių, turinčių teigiamą *PTPRC* žymens signalą. Sklaidos grafikai rodo 500 (**A**) ir ~4000 (**B**) ląstelių kiekviename iš mėginių.

Transkriptominės analizės strategija

Kaip parodyta ankstesniuose skyreliuose, ŽMA mikrokapsulės užtikrina efektyvų žinduolių ląstelių izoliavimą ir iRNR paruošimą prieš fermentinių reakcijų atlikimą. Taip pat, želatininis apvalkalas užtikrina greitą ir patogų mikrokapsulių ištirpinimą ir analitės išskyrimą taikant švelnias sąlygas. Remiantis šiomis savybėmis, buvo tikimasi, kad šiame darbe sukurtos mikrokapsulės galėtų suteikti pranašumą prieš jau esamus pavienių ląstelių RNR sekoskaitos metodus, kuriuose ląstelių lizė ir iRNR barkodavimas atvirkštinės transkripcijos metu atliekamas tame pačiame reakcijos mišinyje, kas gali sudaryti neoptimalias sąlygas.

Siekiant įvertinti mikrokapsulių panaudojimą RNR sekoskaitoje, buvo įgyvendinta eksperimentinė strategija, pateikta **12 pav**. Kaip ir atliekant AT-PGR, pavienės ląstelės buvo izoliuotos mikrokapsulėse, lizuotos chaotropiniais reagentais, po kurio sekė gDNR šalinimas veikiant DNaze I (**12 pav., A**).

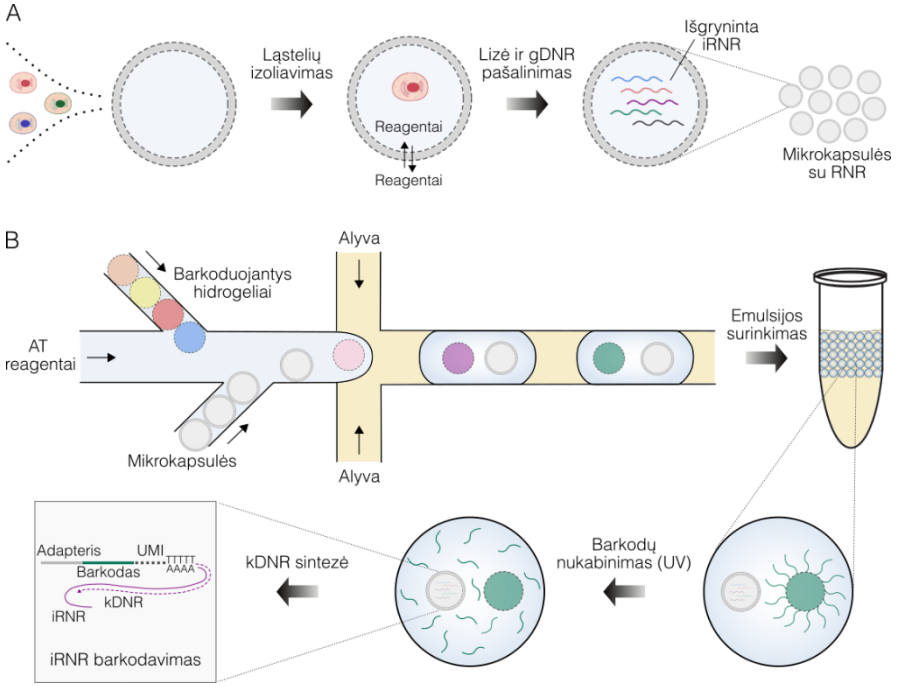

12 pav. Pavienių ląstelių iRNR sekoskaita panaudojant ŽMA mikrokapsules. (**A**) Pavienių ląstelių izoliavimas ir iRNR gryninimas. (**B**) Mikrokapsulių patalpinimas į lašelius kartu su barkoduojančiais hidrogeliais bei atvirkštinės transkripcijos reagentais. Po barkoduojančių pradmenų nukabinimo oligonukleotidai pereina per mikrokapsulės apvalkalą ir inicijuoja kDNR sintezės procesą.

Mikrokapsulės, turinčios išgrynintą iRNR, buvo barkoduojamos pasitelkiant inDrops platformą (2,86). Tuo tikslu mikrokapsulės buvo patalpintos į lašelius kartu su genetinius barkodus nešančiais hidrogeliniais rutuliukais bei atvirkštinės transkripcijos reagentais. Dėl selektyvaus apvalkalo pralaidumo tiek atvirkštinės transkripcijos reagentai, tiek barkoduojantys pradmenys patenka į mikrokapsulės vidų ir yra įtraukiamį į kDNR sintezę mikrokapsulės viduje (**12 pav.**, **B**). Po šio etapo kDNR molekulės buvo išgrynintos iš mikrokapsulių ir naudojamos bibliotekos paruošimui bei sekoskaitai (žr. medžiagas ir metodus).

Žinduolių ląstelių transkriptominė analizė

Siekiant validuoti mikrokapsulėmis paremtą viso transkriptomo analizę, pirmiesiems bandymams buvo pasirinktos kultūrinės žinduolių ląstelės. Pasirinktas ląstelių mišinys turėjo vienodą kiekį pelių NIH-3T3 ir žmogaus K- 562 ląstelių. Mikrokapsulės, turinčios pavienių ląstelių iRNR, buvo patalpintos į lašelius, kuriuose buvo atliktas iRNR genetinis barkodavimas ją verčiant į kDNR biblioteką. Šis metodas buvo pavadintas „CapDrop“. Paraleliai pavienių ląstelių barkodavimas buvo atliktas papildant atvirkštinės transkripcijos mišinį kolagenaze A, kuri tirpina želatinos apvalkalą, kas galimai galėtų pagerinti iRNR barkodavimo efektyvumą. Šis metodo variantas buvo pavadintas „CapDrop + ColA“. Transkriptomikos duomenų palyginimui taip pat buvo įtrauktas standartinis inDrops protokolas, kurio metu lašeliuose vietoje mikrokapsulių yra patalpinamos ląstelės.

Palyginamoji analizė parodė, kad pavienių ląstelių lizavimas ir RNR gryninimas prieš barkodavimą padidina nustatytų genų ir unikalių transkriptų skaičių ląstelėje apie 1,5 karto (**6 lentelė**). Šie rezultatai gali būti paaiškinami tuo, jog griežtesnės ląstelių ardymo sąlygos užtikrina geresnį iRNR prieinamumą fermentams. Taip pat, mikrokapsulių praplovimas po lizavimo gali pašalinti tam tikrus viduląstelinius slopiklius (pvz., RNazes). Verta pastebėti, jog mikrokapsulių ištirpinimas AT reakcijos metu neturėjo pastebimos įtakos iRNR molekulių barkodavimui. Tai leidžia daryti išvadą, jog AT efektyvumas lašelyje ir mikrokapsulės viduje buvo panašūs.

6 lentelė. Unikalių transkriptų ir genų skaičiaus palyginimas taikant tris iRNR barkodavimo strategijas: CapDrop, CapDrop + ColA ir inDrops. Visuose mėginiuose buvo pasiektas panašus sekoskaitos įsotinimo laipsnis (0.336-0.386).

Mėginys	Transkriptų vidurkis	Transkriptų mediana	Genų vidurkis	Genų mediana
CapDrop	12012	11659	2953	2882
CapDrop + ColA	12157	11678	3011	2920
inDrops	7637	7000	2051	1988

Antrasis CapDrop ir inDrops metodų vertinimo aspektas buvo barkodavimo specifiškumo analizė. Ląstelė, kurioje daugiau kaip 80 % visų nuskaitytų sekų atitiko žmogaus transkriptomą, buvo priskirta K-562 ląstelei, o ląstelė, kurioje daugiau kaip 80 % visų nuskaitytų sekų atitiko pelės transkriptomą, buvo priskirta NIH-3T3 ląstelei. Likę įvykiai buvo klasifikuojami kaip sumaišyti, nes juose buvo didelė dalis sekų, priklausančių abiem ląstelių linijoms. CapDrop ir inDrops parodė panašų dviejų skirtingų ląstelių barkodavimo tuo pačiu barkodu įvykių skaičių: atitinkamai 8,12 % ir 6,52 % (**13 pav., A**). Taip pat, pavienių ląstelių transkriptomo duomenų projekcija netiesinėje erdvėje (UMAP) parodė homogenišką pasiskirstymą per visas matomas populiacijas (nepriklausomai nuo taikyto metodo) patvirtinant, jog nėra ženklių skirtumų tarp lyginamų metodų (CapDrop, CapDrop + ColA ir inDrops) (**13 pav., B ir C**). Taigi, mikrokapsulių pagrindu veikianti iRNR sekoskaita yra tinkamas metodas pavienių žinduolių ląstelių transkriptominei analizei atlikti. Kitame šio darbo etape ši sistema buvo pritaikyta pavienių mikroorganizmų analizei.

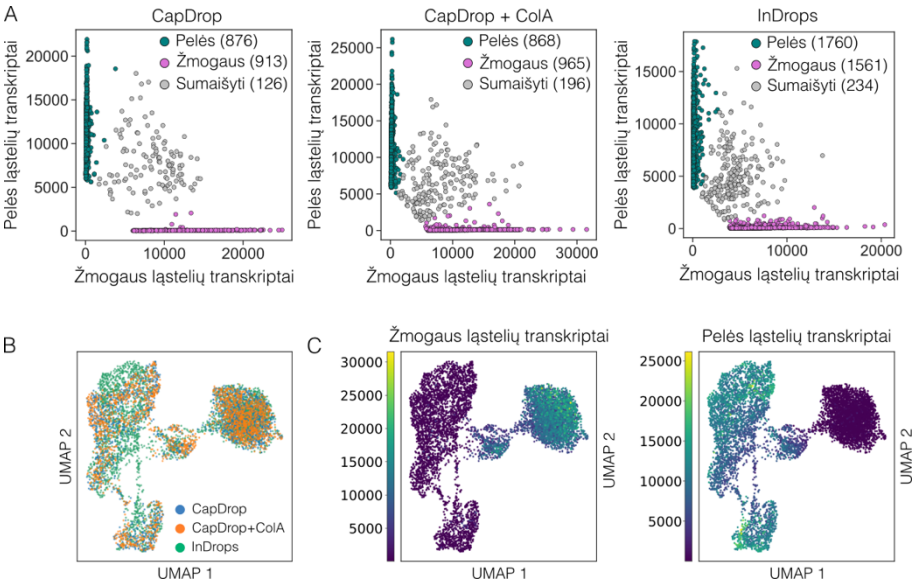

13 pav. Pavienių K-562 and NIH-3T3 ląstelių iRNR sekoskaitos rezultatų palyginimas. (**A**) Sklaidos grafikai, rodantys ląstelių priskyrimą konkrečiam tipui naudojant tris iRNR barkodavimo metodus: CapDrop, CapDrop + ColA ir inDrops. (**B**) UMAP grafikas, kuriame pavaizduoti pavienių ląstelių transkriptomų, gautų iš trijų taikytų metodikų, pasiskirstymas tarp suformuotų klasterių. (**C**) UMAP grafikai, kuriuose pavaizduotas žmogaus ir pelės transkriptomų pasiskirstymas tarp klasterių.

Bakterijų transkriptominė analizė

Palyginti su žinduolių ląstelių RNR sekoskaita, analogiški tyrimai su bakterijomis išlieka daug didesniu iššūkiu dėl mažo RNR kiekio, iRNR poliadenilinimo nebuvimo bei sudėtingo bakterijų lizavimo. Dėl šių priežasčių **12 pav.** pateikta strategija nebuvo pilnai tinkama ir reikėjo įvesti tam tikrus pakeitimus. Visų pirma, buvo atliktas dviejų etapų bakterijų lizavimas, kuomet po lizocimo inicijuotos lizės sekė veikimas chaotropiniais reagentais (žr. medžiagas ir metodus). Antra, siekiant sugauti RNR molekules per barkoduojančio pradmens poli(dT) seką, mikrokapsulės su visumine išgryninta RNR buvo perkeltos į poliadenilinimo reakcijos mišinį. Šis papildomas etapas leido pasiekti, jog visos RNR molekulės, įskaitant ir ribosominę RNR, 3'-gale būtų pažymėtos poliA uodega.

Pirminio eksperimento atlikimui, *E. coli* MG1655 ir *B. subtilis* 23857 buvo sumaišytos vienodu santykiu ir inkapsuliuotos atitinkamu skiedimu taip, kad kiekvienoje mikrokapsulėje vidutiniškai būtų ne daugiau kaip viena ląstelė. Palyginimui, *E. coli* MG1655 ir *B. subtilis* 23857 ląstelės buvo inkapsuliuotos atskirai. Izoliuotos ląstelės buvo sulizuotos, jų genominė DNR pašalinta, o RNR poliadenilinta. Mikrokapsulės su poliadenilintomis RNR molekulėmis buvo perkeltos į inDrops sistemą, kur buvo atliktas RNR barkodavimas (žr. medžiagas ir metodus). Iš kiekvieno mėginio buvo užbarkoduota ~3000 ląstelių.

Visų pirma, po sekoskaitos buvo įvertintas RNR barkodavimo specifiškumas. Analogiškai kaip ir analizuojant žinduolių ląstelių sekoskaitos duomenis, bakterinė ląstelė, kurioje daugiau kaip 80 % visų nuskaitytų sekų atitiko *E. coli* transkriptomą, buvo priskirta *E. coli* ląstelei, o ląstelė, kurioje daugiau kaip 80 % visų nuskaitytų sekų atitiko *B. subtilis* transkriptomą, buvo priskirta *B. subtilis* ląstelei. Likę įvykiai buvo klasifikuojami kaip sumaišyti. Analizės rezultatai parodė, jog 92 % barkodų buvo priskirti vienai konkrečiai bakterijų rūšiai, o likę 8 % turėjo sumaišytus bakterijų transkriptomus (**14 pav., A,** pirmasis sklaidos grafikas). Verta pastebėti, jog mėginys, kuriame *E. coli* ir *B. subtilis* buvo izoliuotos nepriklausomai ir mikrokapsulės buvo apjungtos prieš RNR barkodavimą, turėjo labai panašų kiekį sumaišytų transkriptomų (8,5 %) (**14 pav., A,** antrasis sklaidos grafikas). Šie rezultatai leidžia daryti prielaidą, jog sumaišyti transkriptomai atsirado ne dėl *E. coli* ir *B. subtilis* izoliavimo kartu vienoje mikrokapsulėje ar ląstelių tarpusavio sąveikos dar prieš įvykstant izoliacijai. Nepriklausoma *E. coli* ir *B. subtilis* analizė (**B**) parodė, kad priskyrimas atitinkamoms rūšims buvo labai specifiškas, o *B. subtilis* mėginyje pasitaikė tik keli neatitikimai: 0,2 % barkodų buvo priskirta *E. coli*, ir 0,6 % - abiem bakterijų rūšims. Remiantis šiais rezultatais, būtų galima teigti, kad daugumą sumaišytų transkriptomų

galima paaiškinti limituota barkodų įvairove (147 456) ir (arba) kelių teigiamų mikrokapsulių patekimu į vieną lašelį.

Norint įvertinti UMI kiekio pasiskirstymą, buvo pasirinktas mėginys, kuriame *E. coli* ir *B. subtilis* ląstelės buvo inkapsuliuotos vienu metu (**14 pav., A,** pirmasis sklaidos grafikas). Pasirinkus slenkstinę vertę daugiau nei 100 UMI (**C**), buvo nubraižyti visuminės RNR (**D**), rRNR (**E**) ir iRNR (**F**) kiekio pasiskirstymai. Kaip ir tikėtasi, daugiau kaip 80 % UMI sudarė rRNR sekos.

Sekoskaitos duomenys, kuriuose dominuoja rRNR, yra nepageidaujami ir rRNR turi būti bent dalinai pašalinta tam, kad būtų galima efektyviau analizuoti iRNR ir išgauti biologiškai svarbią informaciją. Dėl šios priežasties yra svarbu užtikrinti, kad kuo mažesnis rRNR kiekis dalyvautų bibliotekos paruošime ir pereitų į sekoskaitos etapą. Viename iš neseniai publikuotų darbų buvo panaudoti blokuojantys pradmenys, kurie, specifiškai prisijungdamai prie 5S, 16S ir 23S rRNR molekulių, blokuoja rRNR poliadenilinimą ir po to sekantį jų padauginimą (217). Taip pat, RNR sugavimo efektyvumui didelę įtaką daro matricos perjungimas (*angl., template-switching*) atvirkštinės transkripcijos metu. Yra žinoma, kad matricos perjungimas yra palankus RNR molekulėms, turinčioms 5'-galinę 7-metilguanilato (m7G) kepurėlę, kuri yra eukariotų, bet ne prokariotų iRNR molekulėse (218). Priešingai, prokariotų iRNR molekulės turi 5'-galinę trifosfato grupę, kuri gali būti modifikuota į m7G kepurėlę panaudojant fermentinius metodus (Vaccinia virus Capping Enzyme) (218). Dar viena galima strategija – antrosios grandinės sintezė panaudojant atsitiktinius pradmenis, pažymėtus universalia seka (219). Tokiu būdu tos iRNR molekulės, kurios buvo transkribuotos, bet matricos perjungimas nebuvo efektyvus, nebūtų pametamos ir dalyvautų kituose bibliotekos paruošimo etapuose. Taigi, yra tikimasi, jog, įtraukus rRNR pašalinimo etapą bei efektyvesnę iRNR sugavimo strategiją, bus reikšmingai pagerinta pavienių bakterijų iRNR sekoskaitos kokybė, kas yra esminis reikalavimas pereinant prie šios sistemos taikymo.

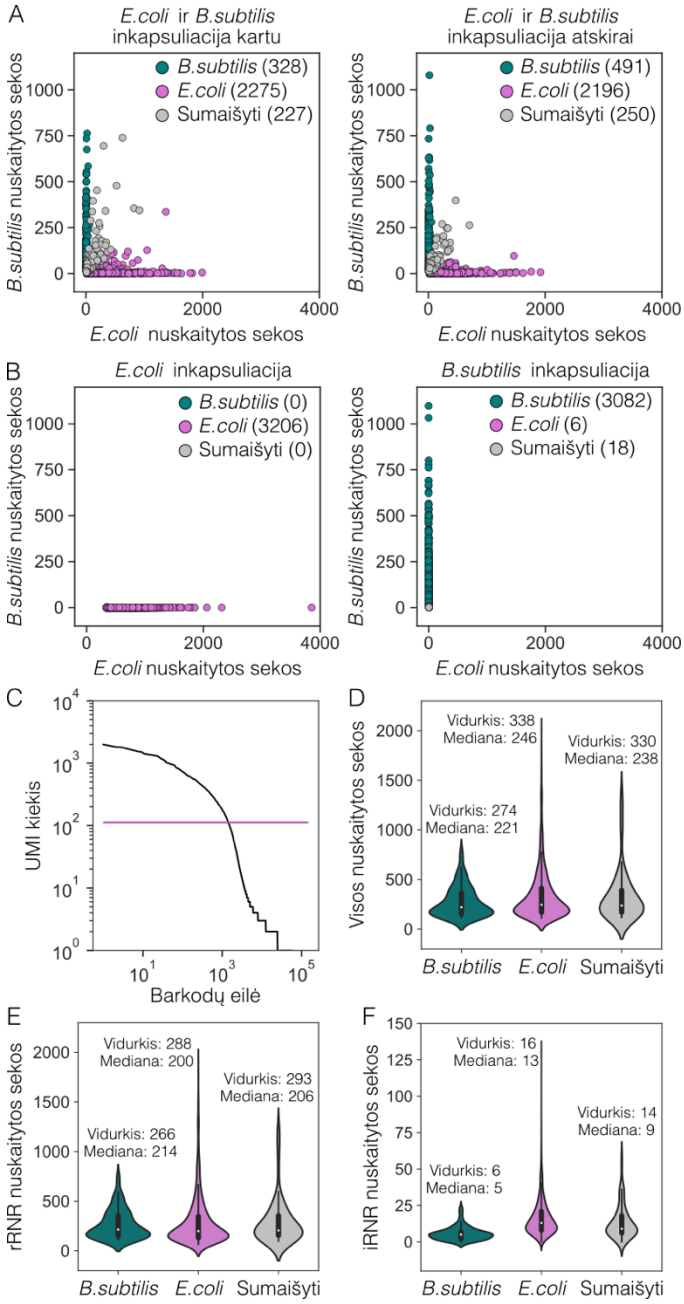

14 pav. Pavienių *E. coli* MG1655 ir *B. subtilis* 23857 ląstelių RNR sekoskaita panaudojant ŽMA mikrokapsules. Sklaidos grafikai vaizduoja bakterijų susimaišymo įvykius analizuojant bakterijų mišinį (**A**) ir kiekvieną bakterijų rūšį atskirai (**B**). (**C**) Mėginio su kartu izoliuotomis *E. coli* ir *B. subtilis* grafikas, kuris vaizduoja UMI kiekio pasiskirstymą tarp barkodų (barkodai išrikiuoti pagal UMI skaičių). Ląstelės, turinčios >100 UMI, buvo atrinktos ir toliau analizuotos vertinant visuminės RNR (**D**), rRNR (**E**) ir iRNR (**F**) pasiskirstymą tarp individualių ląstelių.

Rezultatų aptarimas

Daugiapakopės reakcijos yra itin dažnai sutinkamos įvairiuose molekulinės biologijos metoduose, kuomet reagentai yra įdedami ar pašalinami tam tikrame analizės etape. Tai ypač aktualu vykdant nukleorūgščių analizę, kuomet prieš jų padauginimą atliekamas ląstelių lizavimas ir nukleorūgščių gryninimas. Tačiau tokia analizės eiga, kuomet įtraukiami keletas atskirų etapų, yra vienas didžiausių iššūkių mikroskysčių sistemoms. Dėl šios priežasties didžioji dalis sukurtų lašelių sistemų ir aplikacijų remiasi vieno etapo reakcijomis, kuomet visi reagentai, skirti analizei atlikti, yra įtraukiami vienu metu ląstelių inkapsuliacijos pradžioje. Nors ir yra technologinių sprendimų, kaip atlikti sudėtingas daugiapakopes reakcijas lašelių formate, jie reikalauja itin specializuotų žinių ir patirties, kas apriboja jų platesnį taikymą.

Šiame darbe buvo siekiama sukurti paprastą ir praktišką sprendimą, leidžiantį atlikti didelio našumo pavienių ląstelių nukleorūgščių analizę, kuri būtų suderinama su įvairiais molekulinės biologijos protokolais. Tai buvo pasiekta sukūrus selektyviai pralaidžias mikrokapsules. Mikrokapsulių veikimas pagrįstas gan paprastu principu: pavienės ląstelės izoliuojamos į vandeninius dvifazinius lašelius, turinčius skystą vidinę dalį ir ją apgaubiantį skystą apvalkalą. Esant tam tikram stimului (šaldymui ir (arba) fotopolimerizacijai), skystas apvalkalas paverčiamas elastingu hidrogeliu. Hidrogelinis apvalkalas veikia kaip selektyviai pralaidi membrana: išlaikomos ląstelės ir didelės molekulinės masės nukleorūgštys, o fermentai ir kiti analizei reikalingi komponentai patenka difuzijos būdu į mikrokapsulės vidų ir iš jos. Tokiu būdu daugiapakopės reakcijos gali būti atliekamos perkeliant mikrokapsules iš vieno reakcijos mišinio į kitą. Biologinis suderinamumas, termostabilumas, cheminis stabilumas įvairiuose buferiniuose tirpaluose ir tirpikliuose, monodispersiškumas ir selektyvus pralaidumas – pagrindinės mikrokapsulių savybės, kurios, kaip parodyta šiame darbe, atveria naujas galimybes pavienių ląstelių tyrimuose.

Nors dar iki šio darbo pradžios ir jo metu buvo paskelbta keletas metodų mikrokapsulių paruošimui (33,39-43,189,190), tačiau tokių dalelių pritaikymas pavienių ląstelių analizei daugelyje darbų nebuvo nagrinėjamas ir pagrinde dėmesys buvo skiriamas fundamentiniams fizikiniams ir cheminiams tyrimams (42,43,189,190). Tuo tarpu, sistemos, skirtos pavienių ląstelių analizei, pasižymėjo sudėtingu ir neefektyviu mikrokapsulių formavimu, kas apribojo jų platesnį taikymą (33,40). Šiame kontekste alginato pagrindu sukurtos mikrokapsulės yra viena iš efektyviausių sistemų, nors ir apribotos taikymais ląstelių kultivavime (39).

Šiame darbe pristatomos dvi hidrogelinių mikrokapsulių sistemos, turinčios PEGDA ir ŽMA hidrogelinius apvalkalus. Abiem atvejais apvalkalai apgaubia vidinę dekstrano fazę, kurioje yra izoliuotos ląstelės ir vyksta reakcijos. Šios dvi mikrokapsulių sistemos turi daug bendrų bruožų. Visų pirma, PEGDA ir ŽMA mikrokapsulių apvalkalai užtikrina, kad izoliuotos ląstelės ir DNR molekulės (≥570 bp PEGDA ir ≥300 bp ŽMA mikrokapsulėse) būtų patikimai išlaikomos. Tuo tarpu, mažesnės molekulės (pvz., fermentai, oligonukleotidai) gali laisvai judėti per hidrogelinį apvalkalą. Taip pat, abi sistemos pasižymi geru stabilumu atliekant įvairias laboratorines procedūras, pavyzdžiui, pipetavimą, vorteksavimą, centrifugavimą, šaldymą ar kaitinimą PGR metu. Vis dėlto, dėl skirtingos apvalkalo sudėties šios dvi sistemos turi esminių skirtumų. Buvo pastebėta, jog PEGDA mikrokapsulių išorinis skersmuo ribojamas iki 40-60 μm, o didesnių tinkamai centruotų mikrokapsulių paruošimas tampa sudėtingas. Tuo tarpu, ŽMA mikrokapsulių skersmuo gali siekti 150-200 μm, išlaikant itin gerą centravimą tarp vidinės ir išorinės dalių. Kitas svarbus skirtumas yra susijęs su ląstelių išlaikymu. ŽMA mikrokapsulėse ląstelės lokalizuojasi dekstrano fazėje, o PEGDA mikrokapsulėse ląstelės pasiskirsto tarp PEGDA ir dekstrano fazių, todėl yra tinkamos tik mažesnių ląstelių analizei. Galiausiai, vienas iš svarbiausių skirtumų yra mikrokapsulių suardymas. PEGDA mikrokapsules galima ištirpinti didelės koncentracijos šarminiame tirpale ir esant aukštai temperatūrai. Tuo tarpu, ŽMA mikrokapsules galima suardyti švelniomis sąlygomis naudojant tripsiną arba kolagenazę. Atsižvelgiant į šiuos skirtumus, būtų galima teigti, jog PEGDA mikrokapsulės yra tinkamos bakterijų analizei, o ŽMA mikrokapsulės yra universalesnė sistema, tinkanti įvairių tipų ląstelėms izoliuoti ir analizuoti.

Siekiant įvertinti ir pademonstruoti mikrokapsulių privalumus įvairiuose biologiniuose tyrimuose, buvo išbandytos keturios pavienių ląstelių analizės kryptys - pavienių genomų padauginimas, daugybinė AT-PGR, RNR sekoskaita ir ląstelių kultivavimas. Pirmoje šio darbo dalyje PEGDA mikrokapsulės buvo panaudotos gramteigiamų ir gramneigiamų bakterijų izoliavimui, lizavimui ir pavienių genomų padauginimui. Analizuojant *R. rhodochrous* ir *S. mutans*, buvo pastebėta, jog efektyvus genomų padauginimas buvo pasiektas taikant dviejų etapų lizės protokolą, kuomet po lizocimo inicijuotos lizės sekė veikimas proteinaze K ir NDS. Neabejotinai, tokios griežtos lizės sąlygos yra nesuderinamos su lašelių sistemomis, kadangi šie du lizės komponentai privalo būti pilnai pašalinami prieš vykdant DNR padauginimą, tačiau reagentų pašalinimas iš lašelių yra neįmanomas. Tuo tarpu, hidrogelinės sferos, iš principo, tiktų tokiai analizei atlikti. Tačiau hidrogeliniai rutuliukai neefektyviai išlaiko izoliuotas bakterijas ir paprastai

turi mažesnę DNR išeigą po MDA reakcijos, kas apriboja jų praktinį pritaikymą. Dėl šių priežasčių PEGDA mikrokapsulės yra tinkamesnės pavienių genomų padauginimui, ypač tais atvejais, kai analizuojami sunkiai lizuojami mikroorganizmai. Naudojant PEGDA mikrokapsules, taip pat buvo pademonstruota, jog *E. coli* ląstelės mikrokapsulėse išlaiko savo fiziologinį aktyvumą ir gali būti išaugintos į izogenines mikrokolonijas tolimesnei fenotipinei analizei. Mikrokapsulėmis pagrįsta fenotipinė atranka galima, kai tikslinės molekulės arba išlieka bakterijose, arba dėl savo dydžio sulaikomos mikrokapsulės viduje, kaip buvo PHB granulių atveju (220). Kai kuriais atvejais gali prireikti išaugintų mikrokolonijų išskyrimo iš mikrokapsulių ir jų panaudojimo tolimesnei analizei (155). Tačiau gyvų ląstelių išskyrimas iš PEGDA mikrokapsulių yra neįmanomas, kadangi šių mikrokapsulių apvalkalas gali būti ištirpinamas tik veikiant didelės koncentracijos šarminiu tirpalu.

Kitame šio darbo etape buvo pristatyta alternatyvi mikrokapsulių sistema, sudaryta iš ŽMA hidrogelinio apvalkalo. Šios mikrokapsulės buvo pritaikytos žmogaus leukemijos ląstelių, embrioninių inkstų ląstelių ir periferinio kraujo vienbranduolių ląstelių (PKVL) analizei atliekant daugybinę AT-PGR, kurios metu, naudojant fluorescencine žyme žymėtus pradmenis, buvo padauginami pasirinkti ląstelės žymenys. Prieš atliekant analizę, buvo tikimasi, jog griežtos lizės sąlygos, po kurių seka gDNR pašalinimas, užtikrins didžiausią analizės efektyvumą, atsižvelgiant tiek į signalo specifiškumą, tiek į intensyvumą. Nors ir buvo gautas aiškiai detektuojamas fluorescencijos signalas, kuris specifiškas analizuojamam mėginiui, tačiau buvo pastebėta, kad mikrokapsulės su ląstelėmis ir mikrokapsulės su neląsteline iRNR turėjo labai panašų fluorescencijos signalą. Šie rezultatai aiškiai parodė, kad remiantis tik vienu padaugintu žymeniu, izoliuotų ląstelių detekcija yra netiksli. Šį analizės netikslumą galima išspręsti vienu metu padauginat du žymenis (pvz., vieną universalų ir vieną specifinį atitinkamoms ląstelėms), kuomet dviejų žymenų signalų persidengimas būtų vertinamas kaip atėjęs iš ląstelės, o ne iš laisvai plaukiojančios iRNR. Šiame darbe buvo pasiūlyta alternatyvi strategija, kuri remiasi branduolių struktūros išlaikymu taikant švelnias lizavimo sąlygas ir jų panaudojimu kaip papildomu žymeniu identifikuoti izoliuotas ląsteles jau įvykus AT-PGR. Šis paprastas ir patogus būdas leido atskirti teisingai teigiamus įvykius (mikrokapsulės su ląstelėmis) nuo klaidingai teigiamų (mikrokapsulės su padauginta neląsteline iRNR) ir tuo pačiu įvertinti kuriamo metodo statistines charakteristikas.

Mikrokapsulėse atliktos pavienių ląstelių daugybinės AT-PGR specifiškumas buvo itin aukštas (99,12 ± 0,89 %) su visais šiame darbe naudotais žymenimis ir ląstelių linijomis. Tuo tarpu, jautrumas svyravo nuo

71 iki 98 %, priklausomai nuo žymens ir ląstelių tipo. Taip pat, buvo įvertinta, jog, pasirinkus atskaitos genus, kurių raiška yra maža arba vidutino lygio (10-40 kopijų ląstelėje), klaidingai teigiamų įvykių skaičius gali būti sumažinamas iki ~0,8 %, tačiau išlaikant aukštą analizės jautrumą (97,54 %). Transkriptus, kurių raiška yra tin maža (pvz., 1 kopija ląstelėje), taip pat buvo galima aptikti atliekant AT-PGR mikrokapsulėse. Tačiau neatmetama, kad yra reikalingi papildomi optimizavimo etapai siekiant didesnio jautrumo, iš kurių vienas galėtų būti tikslinių AT pradmenų parinkimas (221).

Kitas svarbus ŽMA mikrokapsulių privalumas – galimybė išgryninti nukleorūgštis taikant įvairius lizavimo metodus, kas yra esminis etapas pereinant prie nukleorūgščių padauginimo. Taip pat, mikrokapsulių suderinamumas su šaldymu bei alkoholiais suteikia galimybę saugoti izoliuotus mėginius ilgesniam laikotarpiui. Dėl galimybės lengvai keisti mikrokapsulių turinį bet kuriame protokolo etape mikrokapsulės galėtų būti vertingos taikymuose, kur atliekami pasikartojantys etapai, pavyzdžiui, fluorescencinė *in situ* hibridizacija (222).

Šiame darbe mikrokapsulių analizė po AT-PGR buvo atlikta naudojant tiek tėkmės citometriją, tiek fluorescencinę mikroskopiją. Tais atvejais, kai laikas yra ribojantis veiksnys ir reikia išanalizuoti didelį mikrokapsulių skaičių (n >10 000), tėkmės citometrija yra tinkamesnis pasirinkimas. Kita vertus, mikroskopijos rezultatus yra lengviau interpretuoti, ypač metodo kūrimo pradžioje. Nors šiame darbe netaikyta, tikėtina, jog tėkmės citometrija, turinti vaizdinimo funkciją, galėtų būti tinkamiausias sprendimas mikrokapsulių analizei po AT-PGR ir ypač tais atvejais, kai į analizę įtraukiama ir branduolių detekcija.

Šiame darbe išvystytą pavienių ląstelių daugybinę AT-PGR mikrokapsulėse būtų galima pritaikyti įvairiems tikslams. Pavyzdžiui, nustatant genų izoformas (223), skirtingai išreikštus klinikinės svarbos žymenis (224) arba aptinkant genetines aberacijas (214,215,225,226). Taip pat, būtų galima kiekybiškai įvertinti somatinių mutacijų pasiskirstymą ir dažnumą vėžį lemiančių genų grupėje, kas būtų naudinga vėžio diagnostikai (227-229). Daugybinė persidengianti AT-PGR mikrokapsulėse taip pat galėtų būti taikoma B ir T ląstelių natyvių receptorių sekoskaitai (12,91,113,205,206,230,231).

ŽMA mikrokapsulių taikymas neapsiriboja vien tik AT-PGR. Kaip parodyta paskutinėje šio darbo dalyje, pavienių ląstelių RNR molekulės gali būti barkoduojamos ir sekvenuojamos išgaunant viso transkriptomo informaciją. Eksperimentinė strategija, naudojant mikrokapsules, skiriasi nuo šiuo metu plačiai naudojamų lašelių RNR sekoskaitos platformų (2,98), kuriose ląstelių lizės ir atvirkštinės transkripcijos etapai atliekami kartu

viename reakcijos mišinyje, iškylant rizikai turėti neoptimalias analizės sąlygas. Tai patvirtina ir šiame darbe gauti rezultatai, kuomet, naudojant mikrokapsules, buvo nustatyta maždaug 1,5 karto daugiau genų ir unikalių transkriptų. Mikrokapsulės taip pat leido atlikti pavienių bakterijų RNR sekoskaitą. Nors pirminiai sekoskaitos rezultatai parodė gan paviršutinišką transkriptomo profiliavimą, galimybė įgyvendinti bakterijų transkriptominės analizės protokolą yra reikšmingas žingsnis į priekį link naujo metodo išvystymo (232). Tikimasi, kad rRNR pašalinimas (217) ir efektyvesnis iRNR sugavimas ir padauginimas (218,219) galėtų reikšmingai pagerinti duomenų kokybę. Taip pat, ŽMA mikrokapsulės suteikia galimybę kultivuoti pavienes bakterijas ir suformuoti izogenines mikrokolonijas. Kaip parodyta ankstesniuose darbuose (29,30), izogeninių mikrokolonijų RNR sekoskaita užtikrino pakankamą RNR kiekį ir reikšmingai padidino detektuojamų unikalių transkriptų (UMI) skaičių. Taip pat, svarbu paminėti, jog mikrokapsulių su RNR barkodavimas galimas ne tik lašeliuose, tačiau ir taikant kombinatorinį indeksavimą (233,234).

Apibendrinant, būtų galima teigti, kad šioje daktaro disertacijoje pristatyta selektyviai pralaidžių mikrokapsulių koncepcija suteikia pagrindą tolimesniems pavienių ląstelių tyrimams, kurie remiasi nukleorūgščių analize bei ląstelių kultivavimu. Dėl nesudėtingo mikrokapsulių paruošimo ir patogaus jų naudojimo yra tikimasi, kad ši sistema ras pritaikymą ir tose laboratorijose, kuriose dėl techninių iššūkių mikroskysčių technologijos iki šiol nebuvo taikytos.

Išvados

1. Panaudojant vandeninę dvifazinę sistemą, sudarytą iš PEGDA ir dekstrano, buvo išvystytos selektyviai pralaidžios mikrokapsulės.
2. Nustatyta, kad PEGDA mikrokapsulės efektyviai išlaiko bakterines ląsteles bei leidžia atlikti genomų padauginimą, kultivavimą ir metabolinio aktyvumo įvertinimą.
3. Dėl žinduolių ląstelių lokalizacijos tarp išorinės ir vidinės fazių PEGDA mikrokapsulėse, šių ląstelių izoliavimas ir analizė tampa nepraktiški ir neefektyvūs.
4. Vandeninė dvifazinė sistema, sudaryta iš ŽMA ir dekstrano, gali būti naudojama kaip alternatyvi selektyviai pralaidžių mikrokapsulių kompozicija.
5. Mikrokapsulės, turinčios ŽMA apvalkalą, pasižymi efektyviu žinduolių ląstelių ir nukleorūgščių (≥300 bp) išlaikymu, stabilumu bei biologiniu

suderinamumu, todėl šios mikrokapsulės yra tinkamos nukleorūgščių analizei iš pavienių žinduolių ląstelių.

6. Pavienių ląstelių AT-PGR atlikimas ŽMA mikrokapsulėse yra tikslus ir jautrus metodas pavienių ląstelių analizei pagal tikslinius žymenis.
7. ŽMA mikrokapsulės leido sukurti naują metodą, skirtą pavienių žinduolių ląstelių ir bakterijų viso transkriptomo analizei atlikti.

TRUMPOS ŽINIOS APIE DISERTANTĘ

Vardas	Greta Leonavičienė
Adresas	Gyvybės mokslų centras, Saulėtekio al. 7, 10257, Vilnius, Lietuva
El. pašto adresas	greta.stonyte@bti.vu.lt

Išsilavinimas

2017-2021	Doktorantūros studijos, Biochemija, Vilniaus universitetas
2015-2017	Magistras, Biochemija, Vilniaus universitetas
2011-2015	Bakalauras, Biochemija, Vilniaus universitetas

Profesinė patirtis

Nuo 2018	Jaun. mokslo darbuotoja, Vilniaus universitetas, Biotechnologijos institutas
2016-2018	Biologė tyrėja, Vilniaus universitetas, Biotechnologijos institutas
2015-2016	Vizituojanti tyrėja, Harvardo medicinos mokykla, JAV
2013-2015	Asistentė, Vilniaus universitetas, Biotechnologijos institutas

Mokslinių interesų kryptys: mikroskysčių technologijos, pavienių molekulių tyrimai, pavienių ląstelių genomikos ir transkriptomikos tyrimai, 3D ląstelių kultūros.

Dalyvavimas projektuose:

SMART projektas [Nr. 01.2.2-LMT-K-718-04-0002]. „Pavienių ląstelių transkriptomikos-genomikos tyrimų paralelinės-laboratorijos įsteigimas“. 2020-2023.

Visuotinės dotacijos projektas [Nr. 09.3.3-LMT-K-712-01-0056]. „Mikroskysčių technologijos pavienių ląstelių genotipo-fenotipo tyrimams“. 2018-2021.

Lietuvos - Šveicarijos bendradarbiavimo programa „Moksliniai tyrimai ir plėtra“ [CH-3-ŠMM-01/03]. „Kompiuteryje sumodeliuotų fermentų evoliucija panaudojant mikroskysčių technologiją”. 2012-2016.

BIBLIOGRAPHY

1. Abdallah, B.Y., Horne, S.D., Stevens, J.B., Liu, G., Ying, A.Y., Vanderhyden, B., Krawetz, S.A., Gorelick, R. and Heng, H.H. (2013) Single cell heterogeneity: why unstable genomes are incompatible with average profiles. *Cell Cycle*, **12**, 3640-3649.
2. Klein, A.M., Mazutis, L., Akartuna, I., Tallapragada, N., Veres, A., Li, V., Peshkin, L., Weitz, D.A. and Kirschner, M.W. (2015) Droplet barcoding for single-cell transcriptomics applied to embryonic stem cells. *Cell*, **161**, 1187-1201.
3. Macosko, E.Z., Basu, A., Satija, R., Nemesh, J., Shekhar, K., Goldman, M., Tirosh, I., Bialas, A.R., Kamitaki, N. and Martersteck, E.M. (2015) Highly parallel genome-wide expression profiling of individual cells using nanoliter droplets. *Cell*, **161**, 1202-1214.
4. Azizi, E., Carr, A.J., Plitas, G., Cornish, A.E., Konopacki, C., Prabhakaran, S., Nainys, J., Wu, K., Kiseliovas, V. and Setty, M. (2018) Single-cell map of diverse immune phenotypes in the breast tumor microenvironment. *Cell*, **174**, 1293-1308. e1236.
5. Wagner, J., Rapsomaniki, M.A., Chevrier, S., Anzeneder, T., Langwieder, C., Dykgers, A., Rees, M., Ramaswamy, A., Muenst, S., Soysal, S.D. *et al.* (2019) A Single-Cell Atlas of the Tumor and Immune Ecosystem of Human Breast Cancer. *Cell*, **177**, 1330-1345.e1318.
6. Hummer, D., Kurth, F., Naredi-Rainer, N. and Dittrich, P.S. (2016) Single cells in confined volumes: microchambers and microdroplets. *Lab Chip*, **16**, 447-458.
7. Guo, M.T., Rotem, A., Heyman, J.A. and Weitz, D.A. (2012) Droplet microfluidics for high-throughput biological assays. *Lab on a Chip*, **12**, 2146-2155.
8. Matula, K., Rivello, F. and Huck, W.T.S. (2020) Single-Cell Analysis Using Droplet Microfluidics. *Adv Biosyst*, **4**, e1900188.
9. Ding, Y., Choo, J. and deMello, A.J. (2017) From single-molecule detection to next-generation sequencing: microfluidic droplets for high-throughput nucleic acid analysis. *Microfluid Nanofluidics*, **21**, 58.
10. Simutis, K., Stonyte, G. and Mazutis, L. (2019) Antibody discovery using microfluidic systems. *Microfluidics for Pharmaceutical Applications*.
11. Gérard, A., Woolfe, A., Mottet, G., Reichen, M., Castrillon, C., Menrath, V., Ellouze, S., Poitou, A., Doineau, R. and Briseno-Roa, L. (2020) High-throughput single-cell activity-based screening and sequencing of antibodies using droplet microfluidics. *Nature biotechnology*, **38**, 715-721.
12. Tanno, H., McDaniel, J.R., Stevens, C.A., Voss, W.N., Li, J., Durrett, R., Lee, J., Gollihar, J., Tanno, Y., Delidakis, G. *et al.* (2020) A facile

technology for the high-throughput sequencing of the paired VH:VL and TCRβ:TCRα repertoires. *Science Advances*, **6**, eaay9093.
13. Mazutis, L., Gilbert, J., Ung, W.L., Weitz, D.A., Griffiths, A.D. and Heyman, J.A. (2013) Single-cell analysis and sorting using droplet-based microfluidics. *Nature protocols*, **8**, 870-891.
14. Beneyton, T., Wijaya, I., Postros, P., Najah, M., Leblond, P., Couvent, A., Mayot, E., Griffiths, A.D. and Drevelle, A. (2016) High-throughput screening of filamentous fungi using nanoliter-range droplet-based microfluidics. *Scientific reports*, **6**, 1-10.
15. Autour, A. and Ryckelynck, M. (2017) Ultrahigh-Throughput Improvement and Discovery of Enzymes Using Droplet-Based Microfluidic Screening. *Micromachines*, **8**, 128.
16. Watterson, W.J., Tanyeri, M., Watson, A.R., Cham, C.M., Shan, Y., Chang, E.B., Eren, A.M. and Tay, S. (2020) Droplet-based high-throughput cultivation for accurate screening of antibiotic resistant gut microbes. *eLife*, **9**, e56998.
17. Stucki, A., Vallapurackal, J., Ward, T.R. and Dittrich, P.S. (2021) Droplet Microfluidics and Directed Evolution of Enzymes: An Intertwined Journey. *Angew Chem Int Ed Engl*, **60**, 24368-24387.
18. Chiu, F.W.Y. and Stavrakis, S. (2019) High-throughput droplet-based microfluidics for directed evolution of enzymes. *Electrophoresis*, **40**, 2860-2872.
19. Gegevicius, E., Goda, K. and Mazutis, L. (2021), *Droplet Microfluidics*. The Royal Society of Chemistry, pp. 89-121.
20. Ding, J., Adiconis, X., Simmons, S.K., Kowalczyk, M.S., Hession, C.C., Marjanovic, N.D., Hughes, T.K., Wadsworth, M.H., Burks, T., Nguyen, L.T. *et al.* (2020) Systematic comparison of single-cell and single-nucleus RNA-sequencing methods. *Nat Biotechnol*, **38**, 737-746.
21. Ziegenhain, C., Vieth, B., Parekh, S., Reinius, B., Guillaumet-Adkins, A., Smets, M., Leonhardt, H., Heyn, H., Hellmann, I. and Enard, W. (2017) Comparative Analysis of Single-Cell RNA Sequencing Methods. *Mol Cell*, **65**, 631-643 e634.
22. Mazutis, L., Baret, J.C. and Griffiths, A.D. (2009) A fast and efficient microfluidic system for highly selective one-to-one droplet fusion. *Lab Chip*, **9**, 2665-2672.
23. Mazutis, L., Araghi, A.F., Miller, O.J., Baret, J.-C., Frenz, L., Janoshazi, A., Taly, V., Miller, B.J., Hutchison, J.B. and Link, D. (2009) Droplet-based microfluidic systems for high-throughput single DNA molecule isothermal amplification and analysis. *Analytical chemistry*, **81**, 4813-4821.
24. Clark, I.C., Delley, C.L., Sun, C., Thakur, R., Stott, S.L., Thaploo, S., Li, Z., Quintana, F.J. and Abate, A.R. (2020) Targeted Single-Cell

RNA and DNA Sequencing With Fluorescence-Activated Droplet Merger. *Anal Chem*, **92**, 14616-14623.
25. Madrigal, J.L., Schoepp, N.G., Xu, L., Powell, C.S., Delley, C.L., Siltanen, C.A., Danao, J., Srinivasan, M., Cole, R.H. and Abate, A.R. (2022) Characterizing cell interactions at scale with made-to-order droplet ensembles (MODEs). *Proceedings of the National Academy of Sciences*, **119**, e2110867119.
26. Eastburn, D.J., Sciambi, A. and Abate, A.R. (2013) Picoinjection enables digital detection of RNA with droplet rt-PCR. *PLoS One*, **8**, e62961.
27. Gan, R., Cabezas, M.D., Pan, M., Zhang, H., Hu, G., Clark, L.G., Jewett, M.C. and Nicol, R. (2022) High-Throughput Regulatory Part Prototyping and Analysis by Cell-Free Protein Synthesis and Droplet Microfluidics. *ACS Synthetic Biology*, **11**, 2108-2120.
28. Abate, A.R. and Weitz, D.A. (2011) Faster multiple emulsification with drop splitting. *Lab Chip*, **11**, 1911-1915.
29. Bavli, D., Sun, X., Kozulin, C., Ennis, D., Motzik, A., Biran, A., Brielle, S., Alajem, A., Meshorer, E., Buxboim, A. *et al.* (2021) CloneSeq: A highly sensitive analysis platform for the characterization of 3D-cultured single-cell-derived clones. *Dev Cell*, **56**, 1804-1817 e1807.
30. Liu, L., Dalal, C.K., Heineike, B.M. and Abate, A.R. (2019) High throughput gene expression profiling of yeast colonies with microgel-culture Drop-seq. *Lab Chip*, **19**, 1838-1849.
31. Schindler, M., Siriwardena, D., Kohler, T.N., Ellermann, A.L., Slatery, E., Munger, C., Hollfelder, F. and Boroviak, T.E. (2021) Agarose microgel culture delineates lumenogenesis in naive and primed human pluripotent stem cells. *Stem Cell Reports*, **16**, 1347-1362.
32. Spencer, S.J., Tamminen, M.V., Preheim, S.P., Guo, M.T., Briggs, A.W., Brito, I.L., D, A.W., Pitkanen, L.K., Vigneault, F., Juhani Virta, M.P. *et al.* (2016) Massively parallel sequencing of single cells by epicPCR links functional genes with phylogenetic markers. *ISME J*, **10**, 427-436.
33. Tamminen, M.V. and Virta, M.P. (2015) Single gene-based distinction of individual microbial genomes from a mixed population of microbial cells. *Front Microbiol*, **6**, 195.
34. Dorobantu, L.S., Yeung, A.K., Foght, J.M. and Gray, M.R. (2004) Stabilization of oil-water emulsions by hydrophobic bacteria. *Appl Environ Microbiol*, **70**, 6333-6336.
35. Kang, Z., Yeung, A., Foght, J.M. and Gray, M.R. (2008) Hydrophobic bacteria at the hexadecane-water interface: examination of micrometre-scale interfacial properties. *Colloids Surf B Biointerfaces*, **67**, 59-66.

36. Mulas, C., Hodgson, A.C., Kohler, T.N., Agley, C.C., Humphreys, P., Kleine-Bruggeney, H., Hollfelder, F., Smith, A. and Chalut, K.J. (2020) Microfluidic platform for 3D cell culture with live imaging and clone retrieval. *Lab Chip*, **20**, 2580-2591.
37. Cai, B., Guo, F., Zhao, L., He, R., Chen, B., He, Z., Yu, X., Guo, S., Xiong, B. and Liu, W. (2014) Disk-like hydrogel bead-based immunofluorescence staining toward identification and observation of circulating tumor cells. *Microfluidics and nanofluidics*, **16**, 29-37.
38. Lan, F., Demaree, B., Ahmed, N. and Abate, A.R. (2017) Single-cell genome sequencing at ultra-high-throughput with microfluidic droplet barcoding. *Nature Biotechnology*, **35**, 640-646.
39. Bremond, N., Santanach-Carreras, E., Chu, L.-Y. and Bibette, J. (2010) Formation of liquid-core capsules having a thin hydrogel membrane: liquid pearls. *Soft Matter*, **6**, 2484-2488.
40. Sakai, S., Ito, S. and Kawakami, K. (2010) Calcium alginate microcapsules with spherical liquid cores templated by gelatin microparticles for mass production of multicellular spheroids. *Acta Biomater*, **6**, 3132-3137.
41. Kim, C., Chung, S., Kim, Y.E., Lee, K.S., Lee, S.H., Oh, K.W. and Kang, J.Y. (2011) Generation of core-shell microcapsules with three-dimensional focusing device for efficient formation of cell spheroid. *Lab on a Chip*, **11**, 246-252.
42. Yanagisawa, M., Nigorikawa, S., Sakaue, T., Fujiwara, K. and Tokita, M. (2014) Multiple patterns of polymer gels in microspheres due to the interplay among phase separation, wetting, and gelation. *Proc Natl Acad Sci U S A*, **111**, 15894-15899.
43. Mytnyk, S., Ziemecka, I., Olive, A.G.L., van der Meer, J.W.M., Totlani, K.A., Oldenhof, S., Kreutzer, M.T., van Steijn, V. and van Esch, J.H. (2017) Microcapsules with a permeable hydrogel shell and an aqueous core continuously produced in a 3D microdevice by all-aqueous microfluidics. *RSC Advances*, **7**, 11331-11337.
44. Leonaviciene, G., Leonavicius, K., Meskys, R. and Mazutis, L. (2020) Multi-step processing of single cells using semi-permeable capsules. *Lab Chip*, **20**, 4052-4062.
45. Leonaviciene, G. and Mazutis, L. (2022) RNA cytometry of single-cells using semi-permeable microcapsules. *Nucleic Acids Res*.
46. Mazutis, L., Stonyte, G., Leonavicius, K. and Zelvyte, A. (2020). Google Patents.
47. Li, X. and Wang, C.Y. (2021) From bulk, single-cell to spatial RNA sequencing. *Int J Oral Sci*, **13**, 36.
48. Thind, A.S., Monga, I., Thakur, P.K., Kumari, P., Dindhoria, K., Krzak, M., Ranson, M. and Ashford, B. (2021) Demystifying emerging bulk RNA-Seq applications: the application and utility of bioinformatic methodology. *Brief Bioinform*, **22**.

49. Chiu, C.Y. and Miller, S.A. (2019) Clinical metagenomics. *Nature Reviews Genetics*, **20**, 341-355.
50. Lloyd-Price, J., Mahurkar, A., Rahnavard, G., Crabtree, J., Orvis, J., Hall, A.B., Brady, A., Creasy, H.H., McCracken, C., Giglio, M.G. *et al.* (2017) Strains, functions and dynamics in the expanded Human Microbiome Project. *Nature*, **550**, 61-66.
51. Cao, S., Zhang, W., Ding, W., Wang, M., Fan, S., Yang, B., McMinn, A., Wang, M., Xie, B.-b., Qin, Q.-L. *et al.* (2020) Structure and function of the Arctic and Antarctic marine microbiota as revealed by metagenomics. *Microbiome*, **8**, 47.
52. Ganesh, S., Parris, D.J., DeLong, E.F. and Stewart, F.J. (2014) Metagenomic analysis of size-fractionated picoplankton in a marine oxygen minimum zone. *The ISME Journal*, **8**, 187-211.
53. Coutinho, F.H., Gregoracci, G.B., Walter, J.M., Thompson, C.C. and Thompson, F.L. (2018) Metagenomics Sheds Light on the Ecology of Marine Microbes and Their Viruses. *Trends in Microbiology*, **26**, 955-965.
54. Cha, J. and Lee, I. (2020) Single-cell network biology for resolving cellular heterogeneity in human diseases. *Exp Mol Med*, **52**, 1798-1808.
55. Hu, P., Zhang, W., Xin, H. and Deng, G. (2016) Single Cell Isolation and Analysis. *Front Cell Dev Biol*, **4**, 116.
56. Rodrigues, J., Heinrich, M.A., Teixeira, L.M. and Prakash, J. (2021) 3D in vitro model (R) evolution: unveiling tumor–stroma interactions. *Trends in cancer*, **7**, 249-264.
57. Pachiadaki, M.G., Brown, J.M., Brown, J., Bezuidt, O., Berube, P.M., Biller, S.J., Poulton, N.J., Burkart, M.D., La Clair, J.J., Chisholm, S.W. *et al.* (2019) Charting the Complexity of the Marine Microbiome through Single-Cell Genomics. *Cell*, **179**, 1623-1635 e1611.
58. Shapiro, E., Biezuner, T. and Linnarsson, S. (2013) Single-cell sequencing-based technologies will revolutionize whole-organism science. *Nat Rev Genet*, **14**, 618-630.
59. Zong, C., Lu, S., Chapman, A.R. and Xie, X.S. (2012) Genome-wide detection of single-nucleotide and copy-number variations of a single human cell. *Science*, **338**, 1622-1626.
60. Ye, M., Wilhelm, M., Gentschev, I. and Szalay, A. (2021) A Modified Limiting Dilution Method for Monoclonal Stable Cell Line Selection Using a Real-Time Fluorescence Imaging System: A Practical Workflow and Advanced Applications. *Methods Protoc*, **4**.
61. Choi, J.H., Ogunniyi, A.O., Du, M., Du, M., Kretschmann, M., Eberhardt, J. and Love, J.C. (2010) Development and optimization of a process for automated recovery of single cells identified by microengraving. *Biotechnol Prog*, **26**, 888-895.
62. Keloth, A., Anderson, O., Risbridger, D. and Paterson, L. (2018) Single Cell Isolation Using Optical Tweezers. *Micromachines*, **9**, 434.

63. Jamshidi, A., Neale, S.L., Yu, K., Pauzauskie, P.J., Schuck, P.J., Valley, J.K., Hsu, H.Y., Ohta, A.T. and Wu, M.C. (2009) NanoPen: dynamic, low-power, and light-actuated patterning of nanoparticles. *Nano Lett*, **9**, 2921-2925.
64. Blázquez-Castro, A. (2019) Optical Tweezers: Phototoxicity and Thermal Stress in Cells and Biomolecules. *Micromachines (Basel)*, **10**.
65. Wu, M.C. (2011) Optoelectronic tweezers. *Nature Photonics*, **5**, 322-324.
66. Winters, A., McFadden, K., Bergen, J., Landas, J., Berry, K.A., Gonzalez, A., Salimi-Moosavi, H., Murawsky, C.M., Tagari, P. and King, C.T. (2019) Rapid single B cell antibody discovery using nanopens and structured light. *MAbs*, **11**, 1025-1035.
67. Pedrioli, A. and Oxenius, A. (2021) Single B cell technologies for monoclonal antibody discovery. *Trends Immunol*, **42**, 1143-1158.
68. Le, K., Tan, C., Gupta, S., Guhan, T., Barkhordarian, H., Lull, J., Stevens, J. and Munro, T. (2018) A novel mammalian cell line development platform utilizing nanofluidics and optoelectro positioning technology. *Biotechnol Prog*, **34**, 1438-1446.
69. Saygin, C., Hu, E., Zhang, P., Sher, S., Lozanski, A., Doong, T.-J., Nicolet, D., Orwick, S., Labanowska, J., Skinner, J.N. *et al.* (2021) Genomic analysis of cellular hierarchy in acute myeloid leukemia using ultrasensitive LC-FACSeq. *Leukemia*, **35**, 3406-3420.
70. Stepanauskas, R., Fergusson, E.A., Brown, J., Poulton, N.J., Tupper, B., Labonte, J.M., Becraft, E.D., Brown, J.M., Pachiadaki, M.G., Povilaitis, T. *et al.* (2017) Improved genome recovery and integrated cell-size analyses of individual uncultured microbial cells and viral particles. *Nat Commun*, **8**, 84.
71. Frumkin, D., Wasserstrom, A., Itzkovitz, S., Harmelin, A., Rechavi, G. and Shapiro, E. (2008) Amplification of multiple genomic loci from single cells isolated by laser micro-dissection of tissues. *BMC Biotechnol*, **8**, 17.
72. Datta, S., Malhotra, L., Dickerson, R., Chaffee, S., Sen, C.K. and Roy, S. (2015) Laser capture microdissection: Big data from small samples. *Histol Histopathol*, **30**, 1255-1269.
73. Streets, A.M. and Huang, Y. (2014) Microfluidics for biological measurements with single-molecule resolution. *Current opinion in biotechnology*, **25**, 69-77.
74. Fung, C.W., Chan, S.N. and Wu, A.R. (2020) Microfluidic single-cell analysis-Toward integration and total on-chip analysis. *Biomicrofluidics*, **14**, 021502.
75. Caen, O., Lu, H., Nizard, P. and Taly, V. (2017) Microfluidics as a strategic player to decipher single-cell omics? *Trends in biotechnology*, **35**, 713-727.

76. Han, X., Wang, R., Zhou, Y., Fei, L., Sun, H., Lai, S., Saadatpour, A., Zhou, Z., Chen, H., Ye, F. *et al.* (2018) Mapping the Mouse Cell Atlas by Microwell-Seq. *Cell*, **173**, 1307.
77. Gierahn, T.M., Wadsworth, M.H., Hughes, T.K., Bryson, B.D., Butler, A., Satija, R., Fortune, S., Love, J.C. and Shalek, A.K. (2017) Seq-Well: portable, low-cost RNA sequencing of single cells at high throughput. *Nature Methods*, **14**, 395-398.
78. Manzoor, A.A., Romita, L. and Hwang, D.K. (2021) A review on microwell and microfluidic geometric array fabrication techniques and its potential applications in cellular studies. *The Canadian Journal of Chemical Engineering*, **99**, 61-96.
79. Gong, Y., Ogunniyi, A.O. and Love, J.C. (2010) Massively parallel detection of gene expression in single cells using subnanolitre wells. *Lab Chip*, **10**, 2334-2337.
80. Li, J., Qiu, Y., Zhang, Z., Li, C., Li, S., Zhang, W., Guo, Z., Yao, J. and Zhou, L. (2020) Heterogeneous modification of through-hole microwell chips for ultralow cross-contamination digital polymerase chain reaction. *Analyst*, **145**, 3116-3124.
81. Luo, X., Chen, J.Y., Ataei, M. and Lee, A. (2022) Microfluidic Compartmentalization Platforms for Single Cell Analysis. *Biosensors (Basel)*, **12**.
82. Hu, B., Xu, P., Ma, L., Chen, D., Wang, J., Dai, X., Huang, L. and Du, W. (2021) One cell at a time: droplet-based microbial cultivation, screening and sequencing. *Marine Life Science & Technology*, **3**, 169-188.
83. Ren, C. and Lee, A. (2021), *Droplet Microfluidics*. The Royal Society of Chemistry, pp. 1-14.
84. Zhou, W.M., Yan, Y.Y., Guo, Q.R., Ji, H., Wang, H., Xu, T.T., Makabel, B., Pilarsky, C., He, G., Yu, X.Y. *et al.* (2021) Microfluidics applications for high-throughput single cell sequencing. *J Nanobiotechnology*, **19**, 312.
85. Mazutis, L., Gilbert, J., Ung, W.L., Weitz, D.A., Griffiths, A.D. and Heyman, J.A. (2013) Single-cell analysis and sorting using droplet-based microfluidics. *Nat Protoc*, **8**, 870-891.
86. Zilionis, R., Nainys, J., Veres, A., Savova, V., Zemmour, D., Klein, A.M. and Mazutis, L. (2017) Single-cell barcoding and sequencing using droplet microfluidics. *Nature Protocols*, **12**, 44-73.
87. Baret, J.-C. (2012) Surfactants in droplet-based microfluidics. *Lab on a Chip*, **12**, 422-433.
88. Holtze, C., Rowat, A.C., Agresti, J.J., Hutchison, J.B., Angilè, F.E., Schmitz, C.H.J., Köster, S., Duan, H., Humphry, K.J., Scanga, R.A. *et al.* (2008) Biocompatible surfactants for water-in-fluorocarbon emulsions. *Lab on a Chip*, **8**, 1632-1639.
89. Galinis, R., Stonyte, G., Kiseliovas, V., Zilionis, R., Studer, S., Hilvert, D., Janulaitis, A. and Mazutis, L. (2016) DNA Nanoparticles

for Improved Protein Synthesis In Vitro. *Angew Chem Int Ed Engl*, **55**, 3120-3123.
90. Basu, A.S. (2017) Digital Assays Part I: Partitioning Statistics and Digital PCR. *SLAS Technol*, **22**, 369-386.
91. DeKosky, B.J., Ippolito, G.C., Deschner, R.P., Lavinder, J.J., Wine, Y., Rawlings, B.M., Varadarajan, N., Giesecke, C., Dorner, T., Andrews, S.F. *et al.* (2013) High-throughput sequencing of the paired human immunoglobulin heavy and light chain repertoire. *Nat Biotechnol*, **31**, 166-169.
92. Arezi, B., McCarthy, M. and Hogrefe, H. (2010) Mutant of Moloney murine leukemia virus reverse transcriptase exhibits higher resistance to common RT-qPCR inhibitors. *Anal Biochem*, **400**, 301-303.
93. Hedman, J. and Radstrom, P. (2013) Overcoming inhibition in real-time diagnostic PCR. *Methods Mol Biol*, **943**, 17-48.
94. White, A.K., VanInsberghe, M., Petriv, O.I., Hamidi, M., Sikorski, D., Marra, M.A., Piret, J., Aparicio, S. and Hansen, C.L. (2011) High-throughput microfluidic single-cell RT-qPCR. *Proc Natl Acad Sci U S A*, **108**, 13999-14004.
95. Periyannan Rajeswari, P.K., Joensson, H.N. and Andersson-Svahn, H. (2017) Droplet size influences division of mammalian cell factories in droplet microfluidic cultivation. *Electrophoresis*, **38**, 305-310.
96. Svensson, V., Vento-Tormo, R. and Teichmann, S.A. (2018) Exponential scaling of single-cell RNA-seq in the past decade. *Nat Protoc*, **13**, 599-604.
97. Rotem, A., Ram, O., Shoresh, N., Sperling, R.A., Schnall-Levin, M., Zhang, H., Basu, A., Bernstein, B.E. and Weitz, D.A. (2015) High-Throughput Single-Cell Labeling (Hi-SCL) for RNA-Seq Using Drop-Based Microfluidics. *PLOS ONE*, **10**, e0116328.
98. Zheng, G.X., Terry, J.M., Belgrader, P., Ryvkin, P., Bent, Z.W., Wilson, R., Ziraldo, S.B., Wheeler, T.D., McDermott, G.P., Zhu, J. *et al.* (2017) Massively parallel digital transcriptional profiling of single cells. *Nat Commun*, **8**, 14049.
99. Gohil, S.H., Iorgulescu, J.B., Braun, D.A., Keskin, D.B. and Livak, K.J. (2021) Applying high-dimensional single-cell technologies to the analysis of cancer immunotherapy. *Nature Reviews Clinical Oncology*, **18**, 244-256.
100. Zvirblyte, J. and Mazutis, L. (2022) Microfluidics for Cancer Biomarker Discovery, Research, and Clinical Application. *Adv Exp Med Biol*, **1379**, 499-524.
101. Jovic, D., Liang, X., Zeng, H., Lin, L., Xu, F. and Luo, Y. (2022) Single-cell RNA sequencing technologies and applications: A brief overview. *Clin Transl Med*, **12**, e694.
102. Lareau, C.A., Duarte, F.M., Chew, J.G., Kartha, V.K., Burkett, Z.D., Kohlway, A.S., Pokholok, D., Aryee, M.J., Steemers, F.J., Lebofsky,

R. *et al.* (2019) Droplet-based combinatorial indexing for massive-scale single-cell chromatin accessibility. *Nature Biotechnology*, **37**, 916-924.
103. Satpathy, A.T., Granja, J.M., Yost, K.E., Qi, Y., Meschi, F., McDermott, G.P., Olsen, B.N., Mumbach, M.R., Pierce, S.E., Corces, M.R. *et al.* (2019) Massively parallel single-cell chromatin landscapes of human immune cell development and intratumoral T cell exhaustion. *Nat Biotechnol*, **37**, 925-936.
104. Rotem, A., Ram, O., Shoresh, N., Sperling, R.A., Goren, A., Weitz, D.A. and Bernstein, B.E. (2015) Single-cell ChIP-seq reveals cell subpopulations defined by chromatin state. *Nat Biotechnol*, **33**, 1165-1172.
105. Grandi, F.C., Modi, H., Kampman, L. and Corces, M.R. (2022) Chromatin accessibility profiling by ATAC-seq. *Nat Protoc*, **17**, 1518-1552.
106. Stoeckius, M., Hafemeister, C., Stephenson, W., Houck-Loomis, B., Chattopadhyay, P.K., Swerdlow, H., Satija, R. and Smibert, P. (2017) Simultaneous epitope and transcriptome measurement in single cells. *Nat Methods*, **14**, 865-868.
107. Mimitou, E.P., Cheng, A., Montalbano, A., Hao, S., Stoeckius, M., Legut, M., Roush, T., Herrera, A., Papalexi, E., Ouyang, Z. *et al.* (2019) Multiplexed detection of proteins, transcriptomes, clonotypes and CRISPR perturbations in single cells. *Nat Methods*, **16**, 409-412.
108. Peterson, V.M., Zhang, K.X., Kumar, N., Wong, J., Li, L., Wilson, D.C., Moore, R., McClanahan, T.K., Sadekova, S. and Klappenbach, J.A. (2017) Multiplexed quantification of proteins and transcripts in single cells. *Nat Biotechnol*, **35**, 936-939.
109. Kuchina, A., Brettner, L.M., Paleologu, L., Roco, C.M., Rosenberg, A.B., Carignano, A., Kibler, R., Hirano, M., DePaolo, R.W. and Seelig, G. (2021) Microbial single-cell RNA sequencing by split-pool barcoding. *Science*, **371**.
110. Blattman, S.B., Jiang, W., Oikonomou, P. and Tavazoie, S. (2020) Prokaryotic single-cell RNA sequencing by in situ combinatorial indexing. *Nat Microbiol*, **5**, 1192-1201.
111. Baret, J.-C., Miller, O.J., Taly, V., Ryckelynck, M., El-Harrak, A., Frenz, L., Rick, C., Samuels, M.L., Hutchison, J.B. and Agresti, J.J. (2009) Fluorescence-activated droplet sorting (FADS): efficient microfluidic cell sorting based on enzymatic activity. *Lab on a Chip*, **9**, 1850-1858.
112. Eastburn, D.J., Sciambi, A. and Abate, A.R. (2013) Ultrahigh-throughput Mammalian single-cell reverse-transcriptase polymerase chain reaction in microfluidic drops. *Anal Chem*, **85**, 8016-8021.
113. Rajan, S., Kierny, M.R., Mercer, A., Wu, J., Tovchigrechko, A., Wu, H., Dall Acqua, W.F., Xiao, X. and Chowdhury, P.S. (2018)

Recombinant human B cell repertoires enable screening for rare, specific, and natively paired antibodies. *Commun Biol*, **1**, 5.
114. Ma, J., Tran, G., Wan, A.M.D., Young, E.W.K., Kumacheva, E., Iscove, N.N. and Zandstra, P.W. (2021) Microdroplet-based one-step RT-PCR for ultrahigh throughput single-cell multiplex gene expression analysis and rare cell detection. *Sci Rep*, **11**, 6777.
115. Ellefson, J.W., Gollihar, J., Shroff, R., Shivram, H., Iyer, V.R. and Ellington, A.D. (2016) Synthetic evolutionary origin of a proofreading reverse transcriptase. *Science*, **352**, 1590-1593.
116. Lee, T.Y., Choi, T.M., Shim, T.S., Frijns, R.A. and Kim, S.H. (2016) Microfluidic production of multiple emulsions and functional microcapsules. *Lab Chip*, **16**, 3415-3440.
117. Kamperman, T., Karperien, M., Le Gac, S. and Leijten, J. (2018) Single-Cell Microgels: Technology, Challenges, and Applications. *Trends Biotechnol*, **36**, 850-865.
118. Bigdeli, S., Dettloff, R.O., Frank, C.W., Davis, R.W. and Crosby, L.D. (2015) A simple method for encapsulating single cells in alginate microspheres allows for direct PCR and whole genome amplification. *PLoS One*, **10**, e0117738.
119. Lahaye, M., Yaphe, W. and Rochas, C. (1985) 13C-N.m.r.-spectral analysis of sulfated and desulfated polysaccharides of the agar type. *Carbohydrate Research*, **143**, 240-245.
120. Roach, B.L., Nover, A.B., Ateshian, G.A. and Hung, C.T. (2016) Agarose hydrogel characterization for regenerative medicine applications: Focus on engineering cartilage. *Biomaterials from Nature for Advanced Devices and Therapies; John Wiley & Sons: Hoboken, NJ, USA*, 258.
121. Xiong, J.Y., Narayanan, J., Liu, X.Y., Chong, T.K., Chen, S.B. and Chung, T.S. (2005) Topology evolution and gelation mechanism of agarose gel. *J Phys Chem B*, **109**, 5638-5643.
122. Roberts, J.J. and Martens, P.J. (2016) In Poole-Warren, L., Martens, P. and Green, R. (eds.), *Biosynthetic Polymers for Medical Applications*. Woodhead Publishing, pp. 205-239.
123. Zhu, Z., Zhang, W., Leng, X., Zhang, M., Guan, Z., Lu, J. and Yang, C.J. (2012) Highly sensitive and quantitative detection of rare pathogens through agarose droplet microfluidic emulsion PCR at the single-cell level. *Lab on a Chip*, **12**, 3907-3913.
124. Smith, B.H., Gazda, L.S., Conn, B.L., Jain, K., Asina, S., Levine, D.M., Parker, T.S., Laramore, M.A., Martis, P.C., Vinerean, H.V. *et al.* (2011) Three-dimensional culture of mouse renal carcinoma cells in agarose macrobeads selects for a subpopulation of cells with cancer stem cell or cancer progenitor properties. *Cancer Res*, **71**, 716-724.
125. Hu, C., Lu, W., Mata, A., Nishinari, K. and Fang, Y. (2021) Ions-induced gelation of alginate: Mechanisms and applications. *Int J Biol Macromol*, **177**, 578-588.

126. Caliari, S.R. and Burdick, J.A. (2016) A practical guide to hydrogels for cell culture. *Nat Methods*, **13**, 405-414.
127. Andersen, T., Auk-Emblem, P. and Dornish, M. (2015) 3D Cell Culture in Alginate Hydrogels. *Microarrays (Basel)*, **4**, 133-161.
128. Akbari, S. and Pirbodaghi, T. (2014) A droplet-based heterogeneous immunoassay for screening single cells secreting antigen-specific antibodies. *Lab Chip*, **14**, 3275-3280.
129. Shirwaiker, R., Purser, M. and Wysk, R. (2014), *Rapid Prototyping of Biomaterials*. Elsevier, pp. 176-200.
130. Rose, J.B., Pacelli, S., Haj, A.J.E., Dua, H.S., Hopkinson, A., White, L.J. and Rose, F.R.A.J. (2014) Gelatin-Based Materials in Ocular Tissue Engineering. *Materials*, **7**, 3106-3135.
131. Liguori, A., Bigi, A., Colombo, V., Focarete, M.L., Gherardi, M., Gualandi, C., Oleari, M.C. and Panzavolta, S. (2016) Atmospheric Pressure Non-Equilibrium Plasma as a Green Tool to Crosslink Gelatin Nanofibers. *Scientific Reports*, **6**, 38542.
132. Davidenko, N., Bax, D.V., Schuster, C.F., Farndale, R.W., Hamaia, S.W., Best, S.M. and Cameron, R.E. (2016) Optimisation of UV irradiation as a binding site conserving method for crosslinking collagen-based scaffolds. *J Mater Sci Mater Med*, **27**, 14.
133. Yung, C.W., Wu, L.Q., Tullman, J.A., Payne, G.F., Bentley, W.E. and Barbari, T.A. (2007) Transglutaminase crosslinked gelatin as a tissue engineering scaffold. *J Biomed Mater Res A*, **83**, 1039-1046.
134. Kirchmajer, D.M., Watson, C.A., Ranson, M. and Panhuis, M.i.h. (2013) Gelapin, a degradable genipin cross-linked gelatin hydrogel. *RSC Advances*, **3**, 1073-1081.
135. Kuijpers, A.J., Engbers, G.H.M., Krijgsveld, J., Zaat, S.A.J., Dankert, J. and Feijen, J. (2000) Cross-linking and characterisation of gelatin matrices for biomedical applications. *Journal of Biomaterials Science, Polymer Edition*, **11**, 225-243.
136. Lee, B.H., Lum, N., Seow, L.Y., Lim, P.Q. and Tan, L.P. (2016) Synthesis and Characterization of Types A and B Gelatin Methacryloyl for Bioink Applications. *Materials (Basel)*, **9**.
137. Zhu, M., Wang, Y., Ferracci, G., Zheng, J., Cho, N.-J. and Lee, B.H. (2019) Gelatin methacryloyl and its hydrogels with an exceptional degree of controllability and batch-to-batch consistency. *Scientific reports*, **9**, 1-13.
138. Fairbanks, B.D., Schwartz, M.P., Bowman, C.N. and Anseth, K.S. (2009) Photoinitiated polymerization of PEG-diacrylate with lithium phenyl-2,4,6-trimethylbenzoylphosphinate: polymerization rate and cytocompatibility. *Biomaterials*, **30**, 6702-6707.
139. Ondeck, M.G. and Engler, A.J. (2016) Mechanical Characterization of a Dynamic and Tunable Methacrylated Hyaluronic Acid Hydrogel. *J Biomech Eng*, **138**, 021003.

140. Yamanlar, S., Sant, S., Boudou, T., Picart, C. and Khademhosseini, A. (2011) Surface functionalization of hyaluronic acid hydrogels by polyelectrolyte multilayer films. *Biomaterials*, **32**, 5590-5599.
141. Burdick, J.A., Chung, C., Jia, X., Randolph, M.A. and Langer, R. (2005) Controlled degradation and mechanical behavior of photopolymerized hyaluronic acid networks. *Biomacromolecules*, **6**, 386-391.
142. Sun, J.-Y., Zhao, X., Illeperuma, W.R.K., Chaudhuri, O., Oh, K.H., Mooney, D.J., Vlassak, J.J. and Suo, Z. (2012) Highly stretchable and tough hydrogels. *Nature*, **489**, 133-136.
143. Wang, Y., Cao, T., Ko, J., Shen, Y., Zong, W., Sheng, K., Cao, W., Sun, S., Cai, L., Zhou, Y.L. *et al.* (2020) Dissolvable Polyacrylamide Beads for High-Throughput Droplet DNA Barcoding. *Adv Sci (Weinh)*, **7**, 1903463.
144. Zhang, H., Wang, L., Song, L., Niu, G., Cao, H., Wang, G., Yang, H. and Zhu, S. (2011) Controllable properties and microstructure of hydrogels based on crosslinked poly (ethylene glycol) diacrylates with different molecular weights. *Journal of Applied Polymer Science*, **121**, 531-540.
145. Browning, M.B. and Cosgriff-Hernandez, E. (2012) Development of a biostable replacement for PEGDA hydrogels. *Biomacromolecules*, **13**, 779-786.
146. Qin, H., Wang, S., Feng, K., He, Z., Virta, M.P.J., Hou, W., Dong, H. and Deng, Y. (2019) Unraveling the diversity of sedimentary sulfate-reducing prokaryotes (SRP) across Tibetan saline lakes using epicPCR. *Microbiome*, **7**, 71.
147. Roman, V.L., Merlin, C., Virta, M.P.J. and Bellanger, X. (2021) EpicPCR 2.0: Technical and Methodological Improvement of a Cutting-Edge Single-Cell Genomic Approach. *Microorganisms*, **9**.
148. Novak, R., Zeng, Y., Shuga, J., Venugopalan, G., Fletcher, D.A., Smith, M.T. and Mathies, R.A. (2011) Single-cell multiplex gene detection and sequencing with microfluidically generated agarose emulsions. *Angewandte Chemie International Edition*, **50**, 390-395.
149. Nishikawa, Y., Kogawa, M., Hosokawa, M., Wagatsuma, R., Mineta, K., Takahashi, K., Ide, K., Yura, K., Behzad, H., Gojobori, T. *et al.* (2022) Extensive single-cell genomics reveals bacterial diversity and diverse phage host ranges in the area in and around the Red Sea. *bioRxiv*, 2020.2003.2005.962001.
150. Holmes, D.L. and Stellwagen, N.C. (1991) Estimation of polyacrylamide gel pore size from Ferguson plots of linear DNA fragments. II. Comparison of gels with different crosslinker concentrations, added agarose and added linear polyacrylamide. *Electrophoresis*, **12**, 612-619.

151. Binga, E.K., Lasken, R.S. and Neufeld, J.D. (2008) Something from (almost) nothing: the impact of multiple displacement amplification on microbial ecology. *The ISME Journal*, **2**, 233-241.
152. Raghunathan, A., Ferguson Jr, H.R., Bornarth, C.J., Song, W., Driscoll, M. and Lasken, R.S. (2005) Genomic DNA amplification from a single bacterium. *Applied and environmental microbiology*, **71**, 3342-3347.
153. Lasken, R.S. (2007) Single-cell genomic sequencing using multiple displacement amplification. *Current opinion in microbiology*, **10**, 510-516.
154. Pan, X., Urban, A.E., Palejev, D., Schulz, V., Grubert, F., Hu, Y., Snyder, M. and Weissman, S.M. (2008) A procedure for highly specific, sensitive, and unbiased whole-genome amplification. *Proceedings of the National Academy of Sciences*, **105**, 15499-15504.
155. Zengler, K., Toledo, G., Rappe, M., Elkins, J., Mathur, E.J., Short, J.M. and Keller, M. (2002) Cultivating the uncultured. *Proc Natl Acad Sci U S A*, **99**, 15681-15686.
156. Zengler, K., Walcher, M., Clark, G., Haller, I., Toledo, G., Holland, T., Mathur, E.J., Woodnutt, G., Short, J.M. and Keller, M. (2005) High-throughput cultivation of microorganisms using microcapsules. *Methods Enzymol*, **397**, 124-130.
157. Berdy, B., Spoering, A.L., Ling, L.L. and Epstein, S.S. (2017) In situ cultivation of previously uncultivable microorganisms using the ichip. *Nat Protoc*, **12**, 2232-2242.
158. Chuang, J.S., Rivoire, O. and Leibler, S. (2009) Simpson's Paradox in a Synthetic Microbial System. *Science*, **323**, 272-275.
159. West, S.A., Diggle, S.P., Buckling, A., Gardner, A. and Griffin, A.S. (2007) The social lives of microbes. *Annual Review of Ecology, Evolution, and Systematics*, 53-77.
160. Toledo, G., Green, W., Gonzalez, R.A., Christoffersen, L., Podar, M., Chang, H.W., Hemscheidt, T., Trapido-Rosenthal, H., Short, J. and Bidigare, R.R. (2006) High throughput cultivation for isolation of novel marine microorganisms. *Oceanography*, **19**, 120-124.
161. Fitzsimons, M.S., Novotny, M., Lo, C.-C., Dichosa, A.E., Yee-Greenbaum, J.L., Snook, J.P., Gu, W., Chertkov, O., Davenport, K.W. and McMurry, K. (2013) Nearly finished genomes produced using gel microdroplet culturing reveal substantial intraspecies genomic diversity within the human microbiome. *Genome research*, **23**, 878-888.
162. Hereford, L.M. and Rosbash, M. (1977) Number and distribution of polyadenylated RNA sequences in yeast. *Cell*, **10**, 453-462.
163. Russell, A.D. (2003) Lethal effects of heat on bacterial physiology and structure. *Sci Prog*, **86**, 115-137.
164. Kamperman, T., Henke, S., Visser, C.W., Karperien, M. and Leijten, J. (2017) Centering Single Cells in Microgels via Delayed

Crosslinking Supports Long-Term 3D Culture by Preventing Cell Escape. *Small*, **13**, 1603711.
165. Allazetta, S. and Lutolf, M.P. (2015) Stem cell niche engineering through droplet microfluidics. *Current opinion in biotechnology*, **35**, 86-93.
166. Fornell, A., Pohlit, H., Shi, Q. and Tenje, M. (2021) Acoustic focusing of beads and cells in hydrogel droplets. *Scientific Reports*, **11**, 7479.
167. Tang, T.C., Tham, E., Liu, X., Yehl, K., Rovner, A.J., Yuk, H., de la Fuente-Nunez, C., Isaacs, F.J., Zhao, X. and Lu, T.K. (2021) Hydrogel-based biocontainment of bacteria for continuous sensing and computation. *Nat Chem Biol*, **17**, 724-731.
168. Zhang, T., Zhang, H., Zhou, W., Jiang, K., Liu, C., Wang, R., Zhou, Y., Zhang, Z., Mei, Q., Dong, W.F. *et al.* (2021) One-Step Generation and Purification of Cell-Encapsulated Hydrogel Microsphere With an Easily Assembled Microfluidic Device. *Front Bioeng Biotechnol*, **9**, 816089.
169. Alessandri, K., Sarangi, B.R., Gurchenkov, V.V., Sinha, B., Kießling, T.R., Fetler, L., Rico, F., Scheuring, S., Lamaze, C., Simon, A. *et al.* (2013) Cellular capsules as a tool for multicellular spheroid production and for investigating the mechanics of tumor progression in vitro. *Proceedings of the National Academy of Sciences*, **110**, 14843-14848.
170. Bouhlel, W., Kui, J., Bibette, J. and Bremond, N. (2022) Encapsulation of Cells in a Collagen Matrix Surrounded by an Alginate Hydrogel Shell for 3D Cell Culture. *ACS Biomater Sci Eng*, **8**, 2700-2708.
171. Domejean, H., de la Motte Saint Pierre, M., Funfak, A., Atrux-Tallau, N., Alessandri, K., Nassoy, P., Bibette, J. and Bremond, N. (2016) Controlled production of sub-millimeter liquid core hydrogel capsules for parallelized 3D cell culture. *Lab Chip*, **17**, 110-119.
172. Yue, B. (2014) Biology of the extracellular matrix: an overview. *J Glaucoma*, **23**, S20-23.
173. Lee, K.Y. and Mooney, D.J. (2012) Alginate: properties and biomedical applications. *Prog Polym Sci*, **37**, 106-126.
174. Kikuchi, A., Kawabuchi, M., Watanabe, A., Sugihara, M., Sakurai, Y. and Okano, T. (1999) Effect of Ca2+-alginate gel dissolution on release of dextran with different molecular weights. *Journal of Controlled Release*, **58**, 21-28.
175. Tang, T.-C., Tham, E., Liu, X., Yehl, K., Rovner, A.J., Yuk, H., Isaacs, F.J., Zhao, X. and Lu, T.K. (2020) Tough hydrogel-based biocontainment of engineered organisms for continuous, self-powered sensing and computation. *BioRxiv*.
176. Pereira, J.F., Freire, M.G. and Coutinho, J.A. (2020) Aqueous two-phase systems: Towards novel and more disruptive applications. *Fluid Phase Equilibria*, **505**, 112341.

177. Pereira, J.F. and Coutinho, J.A. (2020), *Liquid-phase extraction*. Elsevier, pp. 157-182.
178. Teixeira, A.G., Agarwal, R., Ko, K.R., Grant-Burt, J., Leung, B.M. and Frampton, J.P. (2018) Emerging Biotechnology Applications of Aqueous Two-Phase Systems. *Adv Healthc Mater*, **7**, e1701036.
179. Albertsson, P.A. (1970) Partition of cell particles and macromolecules in polymer two-phase systems. *Adv Protein Chem*, **24**, 309-341.
180. Iqbal, M., Tao, Y., Xie, S., Zhu, Y., Chen, D., Wang, X., Huang, L., Peng, D., Sattar, A., Shabbir, M.A. *et al.* (2016) Aqueous two-phase system (ATPS): an overview and advances in its applications. *Biol Proced Online*, **18**, 18.
181. Nam, K.-H., Chang, W.-J., Hong, H., Lim, S.-M., Kim, D.-I. and Koo, Y.-M. (2005) Continuous-Flow Fractionation of Animal Cells in Microfluidic Device Using Aqueous Two-Phase Extraction. *Biomedical Microdevices*, **7**, 189-195.
182. Meagher, R.J., Light, Y.K. and Singh, A.K. (2008) Rapid, continuous purification of proteins in a microfluidic device using genetically-engineered partition tags. *Lab on a Chip*, **8**, 527-532.
183. Vijayakumar, K., Gulati, S., deMello, A.J. and Edel, J.B. (2010) Rapid cell extraction in aqueous two-phase microdroplet systems. *Chemical Science*, **1**, 447-452.
184. Niepa, T.H., Hou, L., Jiang, H., Goulian, M., Koo, H., Stebe, K.J. and Lee, D. (2016) Microbial nanoculture as an artificial microniche. *Scientific reports*, **6**, 1-10.
185. Li, J., Lindley-Start, J., Porch, A. and Barrow, D. (2017) Continuous and scalable polymer capsule processing for inertial fusion energy target shell fabrication using droplet microfluidics. *Scientific Reports*, **7**, 6302.
186. Werner, J.r.G., Nawar, S., Solovev, A.A. and Weitz, D.A. (2018) Hydrogel microcapsules with dynamic pH-responsive properties from methacrylic anhydride. *Macromolecules*, **51**, 5798-5805.
187. Ma, S., Thiele, J., Liu, X., Bai, Y., Abell, C. and Huck, W.T. (2012) Fabrication of microgel particles with complex shape via selective polymerization of aqueous two-phase systems. *Small*, **8**, 2356-2360.
188. de Rutte, J., Dimatteo, R., Archang, M.M., van Zee, M., Koo, D., Lee, S., Sharrow, A.C., Krohl, P.J., Mellody, M., Zhu, S. *et al.* (2022) Suspendable Hydrogel Nanovials for Massively Parallel Single-Cell Functional Analysis and Sorting. *ACS Nano*.
189. Watanabe, T., Motohiro, I. and Ono, T. (2019) Microfluidic Formation of Hydrogel Microcapsules with a Single Aqueous Core by Spontaneous Cross-Linking in Aqueous Two-Phase System Droplets. *Langmuir*, **35**, 2358-2367.
190. Xu, Y., Shen, Y., Michaels, T.C., Baumann, K.N., Vigolo, D., Peter, Q., Lu, Y., Saar, K.L., Vella, D. and Zhu, H. (2021) Deformable and Robust Core–Shell Protein Microcapsules Templated by Liquid–

Liquid Phase-Separated Microdroplets. *Advanced Materials Interfaces*, **8**, 2101071.
191. Llorens-Rico, V., Simcock, J.A., Huys, G.R.B. and Raes, J. (2022) Single-cell approaches in human microbiome research. *Cell*, **185**, 2725-2738.
192. Harandi, B., Ng, S., Liddell, L.C., Gentry, D.M. and Santa Maria, S.R. (2022) Fluidic-Based Instruments for Space Biology Research in CubeSats. *Frontiers in Space Technologies*, **3**.
193. van Zee, M., de Rutte, J., Rumyan, R., Williamson, C., Burnes, T., Radakovits, R., Sonico Eugenio, A., Badih, S., Lee, S., Lee, D.-H. *et al.* (2022) High-throughput selection of cells based on accumulated growth and division using PicoShell particles. *Proceedings of the National Academy of Sciences*, **119**, e2109430119.
194. Cruise, G.M., Scharp, D.S. and Hubbell, J.A. (1998) Characterization of permeability and network structure of interfacially photopolymerized poly(ethylene glycol) diacrylate hydrogels. *Biomaterials*, **19**, 1287-1294.
195. Mazutis, L., Araghi, A.F., Miller, O.J., Baret, J.C., Frenz, L., Janoshazi, A., Taly, V., Miller, B.J., Hutchison, J.B., Link, D. *et al.* (2009) Droplet-based microfluidic systems for high-throughput single DNA molecule isothermal amplification and analysis. *Anal Chem*, **81**, 4813-4821.
196. Li, X., Bosch-Tijhof, C.J., Wei, X., de Soet, J.J., Crielaard, W., Loveren, C.V. and Deng, D.M. (2020) Efficiency of chemical versus mechanical disruption methods of DNA extraction for the identification of oral Gram-positive and Gram-negative bacteria. *J Int Med Res*, **48**, 300060520925594.
197. Meagher, R.J., Won, J.I., McCormick, L.C., Nedelcu, S., Bertrand, M.M., Bertram, J.L., Drouin, G., Barron, A.E. and Slater, G.W. (2005) End-labeled free-solution electrophoresis of DNA. *Electrophoresis*, **26**, 331-350.
198. Verlinden, R.A., Hill, D.J., Kenward, M.A., Williams, C.D. and Radecka, I. (2007) Bacterial synthesis of biodegradable polyhydroxyalkanoates. *J Appl Microbiol*, **102**, 1437-1449.
199. Chanprateep, S. (2010) Current trends in biodegradable polyhydroxyalkanoates. *J Biosci Bioeng*, **110**, 621-632.
200. Medeiros Garcia Alcantara, J., Distante, F., Storti, G., Moscatelli, D., Morbidelli, M. and Sponchioni, M. (2020) Current trends in the production of biodegradable bioplastics: The case of polyhydroxyalkanoates. *Biotechnol Adv*, **42**, 107582.
201. Spiekermann, P., Rehm, B.H.A., Kalscheuer, R., Baumeister, D. and Steinbüchel, A. (1999) A sensitive, viable-colony staining method using Nile red for direct screening of bacteria that accumulate polyhydroxyalkanoic acids and other lipid storage compounds. *Archives of Microbiology*, **171**, 73-80.

202. Hermawan, S. and Jendrossek, D. (2007) Microscopical investigation of poly(3-hydroxybutyrate) granule formation in Azotobacter vinelandii. *FEMS Microbiol Lett*, **266**, 60-64.
203. Carbonari, M., Mancaniello, D., Tedesco, T. and Fiorilli, M. (2008) Flow acetone-staining technique: a highly efficient procedure for the simultaneous analysis of DNA content, cell morphology, and immunophenotype by flow cytometry. *Cytometry A*, **73**, 168-174.
204. Wang, X., Yu, L. and Wu, A.R. (2021) The effect of methanol fixation on single-cell RNA sequencing data. *BMC Genomics*, **22**, 420.
205. DeKosky, B.J., Kojima, T., Rodin, A., Charab, W., Ippolito, G.C., Ellington, A.D. and Georgiou, G. (2015) In-depth determination and analysis of the human paired heavy- and light-chain antibody repertoire. *Nat Med*, **21**, 86-91.
206. Tanno, H., McDaniel, J.R., Stevens, C.A., Voss, W.N., Li, J., Durrett, R., Lee, J., Gollihar, J., Tanno, Y., Delidakis, G. *et al.* (2020) A facile technology for the high-throughput sequencing of the paired VH:VL and TCRbeta:TCRalpha repertoires. *Sci Adv*, **6**, eaay9093.
207. Kim, S.C., Clark, I.C., Shahi, P. and Abate, A.R. (2018) Single-Cell RT-PCR in Microfluidic Droplets with Integrated Chemical Lysis. *Anal Chem*, **90**, 1273-1279.
208. Eddington, D.T., VanInsberghe, M., Zahn, H., White, A.K., Petriv, O.I. and Hansen, C.L. (2018) Highly multiplexed single-cell quantitative PCR. *Plos One*, **13**.
209. Yao, C.J., Works, K., Romagnoli, P.A. and Austin, G.E. (2005) Effects of overexpression of HBP1 upon growth and differentiation of leukemic myeloid cells. *Leukemia*, **19**, 1958-1968.
210. Hietakangas, V., Poukkula, M., Heiskanen, K.M., Karvinen, J.T., Sistonen, L. and Eriksson, J.E. (2003) Erythroid differentiation sensitizes K562 leukemia cells to TRAIL-induced apoptosis by downregulation of c-FLIP. *Mol Cell Biol*, **23**, 1278-1291.
211. Raj, A., Peskin, C.S., Tranchina, D., Vargas, D.Y. and Tyagi, S. (2006) Stochastic mRNA synthesis in mammalian cells. *PLoS Biol*, **4**, e309.
212. Zhong, J.F., Chen, Y., Marcus, J.S., Scherer, A., Quake, S.R., Taylor, C.R. and Weiner, L.P. (2008) A microfluidic processor for gene expression profiling of single human embryonic stem cells. *Lab Chip*, **8**, 68-74.
213. Schwabe, A., Rybakova, K.N. and Bruggeman, F.J. (2012) Transcription stochasticity of complex gene regulation models. *Biophys J*, **103**, 1152-1161.
214. Gabert, J., Beillard, E., van der Velden, V.H.J., Bi, W., Grimwade, D., Pallisgaard, N., Barbany, G., Cazzaniga, G., Cayuela, J.M., Cavé, H. *et al.* (2003) Standardization and quality control studies of 'real-time' quantitative reverse transcriptase polymerase chain reaction of

fusion gene transcripts for residual disease detection in leukemia – A Europe Against Cancer Program. *Leukemia*, **17**, 2318-2357.
215. van Dongen, J.J., Macintyre, E.A., Gabert, J.A., Delabesse, E., Rossi, V., Saglio, G., Gottardi, E., Rambaldi, A., Dotti, G., Griesinger, F. *et al.* (1999) Standardized RT-PCR analysis of fusion gene transcripts from chromosome aberrations in acute leukemia for detection of minimal residual disease. Report of the BIOMED-1 Concerted Action: investigation of minimal residual disease in acute leukemia. *Leukemia*, **13**, 1901-1928.
216. Semrau, S., Crosetto, N., Bienko, M., Boni, M., Bernasconi, P., Chiarle, R. and van Oudenaarden, A. (2014) FuseFISH: Robust Detection of Transcribed Gene Fusions in Single Cells. *Cell Reports*, **6**, 18-23.
217. Wangsanuwat, C., Heom, K.A., Liu, E., O'Malley, M.A. and Dey, S.S. (2020) Efficient and cost-effective bacterial mRNA sequencing from low input samples through ribosomal RNA depletion. *BMC genomics*, **21**, 1-12.
218. Wulf, M.G., Maguire, S., Humbert, P., Dai, N., Bei, Y., Nichols, N.M., Corrêa, I.R., Jr. and Guan, S. (2019) Non-templated addition and template switching by Moloney murine leukemia virus (MMLV)-based reverse transcriptases co-occur and compete with each other. *J Biol Chem*, **294**, 18220-18231.
219. Hughes, T.K., Wadsworth, M.H., Gierahn, T.M., Do, T., Weiss, D., Andrade, P.R., Ma, F., de Andrade Silva, B.J., Shao, S., Tsoi, L.C. *et al.* (2020) Second-Strand Synthesis-Based Massively Parallel scRNA-Seq Reveals Cellular States and Molecular Features of Human Inflammatory Skin Pathologies. *Immunity*, **53**, 878-894.e877.
220. Jendrossek, D., Selchow, O. and Hoppert, M. (2007) Poly(3-hydroxybutyrate) granules at the early stages of formation are localized close to the cytoplasmic membrane in Caryophanon latum. *Appl Environ Microbiol*, **73**, 586-593.
221. Mercer, T.R., Clark, M.B., Crawford, J., Brunck, M.E., Gerhardt, D.J., Taft, R.J., Nielsen, L.K., Dinger, M.E. and Mattick, J.S. (2014) Targeted sequencing for gene discovery and quantification using RNA CaptureSeq. *Nature Protocols*, **9**, 989-1009.
222. Pichon, X., Lagha, M., Mueller, F. and Bertrand, E. (2018) A Growing Toolbox to Image Gene Expression in Single Cells: Sensitive Approaches for Demanding Challenges. *Molecular Cell*, **71**, 468-480.
223. Vandenbroucke, I.I., Vandesompele, J., Paepe, A.D. and Messiaen, L. (2001) Quantification of splice variants using real-time PCR. *Nucleic acids research*, **29**, E68-e68.
224. Weisser, M., Kern, W., Rauhut, S., Schoch, C., Hiddemann, W., Haferlach, T. and Schnittger, S. (2005) Prognostic impact of RT-

PCR-based quantification of WT1 gene expression during MRD monitoring of acute myeloid leukemia. *Leukemia*, **19**, 1416-1423.
225. Gorello, P., Cazzaniga, G., Alberti, F., Dell'Oro, M.G., Gottardi, E., Specchia, G., Roti, G., Rosati, R., Martelli, M.F., Diverio, D. *et al.* (2006) Quantitative assessment of minimal residual disease in acute myeloid leukemia carrying nucleophosmin (NPM1) gene mutations. *Leukemia*, **20**, 1103-1108.
226. Chen, X., Wang, F., Zhang, Y., Ma, X., Cao, P., Yuan, L., Wang, L., Chen, J., Zhou, X., Wu, Q. *et al.* (2021) Fusion gene map of acute leukemia revealed by transcriptome sequencing of a consecutive cohort of 1000 cases in a single center. *Blood Cancer Journal*, **11**, 112.
227. Cheng, D.T., Mitchell, T.N., Zehir, A., Shah, R.H., Benayed, R., Syed, A., Chandramohan, R., Liu, Z.Y., Won, H.H., Scott, S.N. *et al.* (2015) Memorial Sloan Kettering-Integrated Mutation Profiling of Actionable Cancer Targets (MSK-IMPACT): A Hybridization Capture-Based Next-Generation Sequencing Clinical Assay for Solid Tumor Molecular Oncology. *J Mol Diagn*, **17**, 251-264.
228. Zhao, Y., Murciano-Goroff, Y.R., Xue, J.Y., Ang, A., Lucas, J., Mai, T.T., Da Cruz Paula, A.F., Saiki, A.Y., Mohn, D., Achanta, P. *et al.* (2021) Diverse alterations associated with resistance to KRAS(G12C) inhibition. *Nature*, **599**, 679-683.
229. Martincorena, I. and Campbell, P.J. (2015) Somatic mutation in cancer and normal cells. *Science*, **349**, 1483-1489.
230. McDaniel, J.R., DeKosky, B.J., Tanno, H., Ellington, A.D. and Georgiou, G. (2016) Ultra-high-throughput sequencing of the immune receptor repertoire from millions of lymphocytes. *Nat Protoc*, **11**, 429-442.
231. Seah, Y.F.S., Hu, H. and Merten, C.A. (2018) Microfluidic single-cell technology in immunology and antibody screening. *Mol Aspects Med*, **59**, 47-61.
232. Moran, M.A., Satinsky, B., Gifford, S.M., Luo, H., Rivers, A., Chan, L.K., Meng, J., Durham, B.P., Shen, C., Varaljay, V.A. *et al.* (2013) Sizing up metatranscriptomics. *Isme j*, **7**, 237-243.
233. Vitak, S.A., Torkenczy, K.A., Rosenkrantz, J.L., Fields, A.J., Christiansen, L., Wong, M.H., Carbone, L., Steemers, F.J. and Adey, A. (2017) Sequencing thousands of single-cell genomes with combinatorial indexing. *Nat Methods*, **14**, 302-308.
234. Rosenberg, A.B., Roco, C.M., Muscat, R.A., Kuchina, A., Sample, P., Yao, Z., Graybuck, L.T., Peeler, D.J., Mukherjee, S., Chen, W. *et al.* (2018) Single-cell profiling of the developing mouse brain and spinal cord with split-pool barcoding. *Science*, **360**, 176-182.

Table S1. The Ct values of the marker genes determined by bulk RT-qPCR.

Sample	The Ct values of marker genes						
	ACTB	***B2M***	***TBP***	***PTPRC***	***YAP***	***PML-RARα***	***BCR-ABL***
K-562	16.74 ± 0.13	18.07 ± 0.03	22.80 ± 0.02	22.95 ± 0.03	No signal	Not tested	21.76 ± 0.06
HEK293	15.58 ± 0.08	18.15 ± 0.11	21.54 ± 0.11	34.01 ± 0.34	21.26 ± 0.14	Not tested	Not tested
NB-4	15.16 ± 0.19	16.27 ± 0.06	22.87 ± 0.10	21.58 ± 0.03	Not tested	29.26 ± 0.23	No signal
PBMC	20.47 ± 0.07	19.00 ± 0.05	29.62 ± 0.22	22.51 ± 0.13	Not tested	No signal	Not tested
NTC	No signal	No signal	No signal	No signal	No signal	No signal	No signal

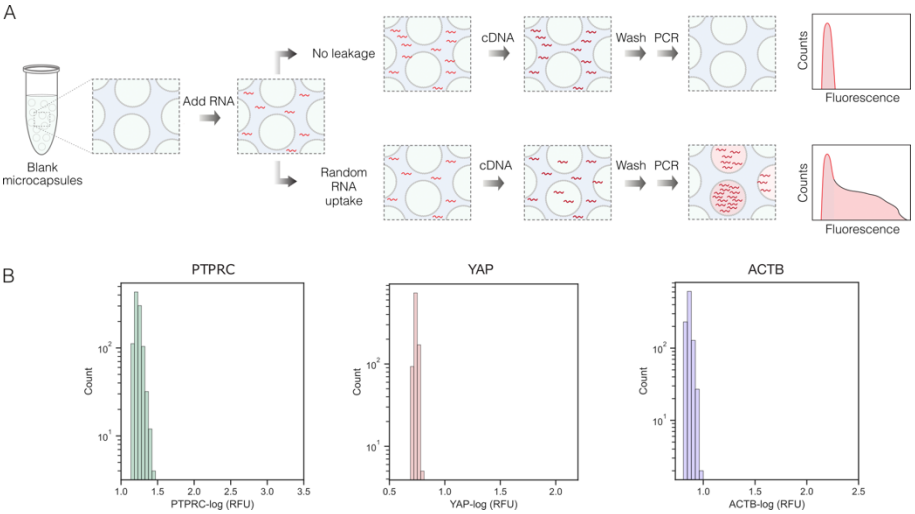

Figure S1. RNA and cDNA leakage test. (**A**) Experimental scheme. Purified total RNA (2 µg) from a mixture of HEK293:K-562 cells is added to the RT reaction mixture (V = 200 µl) supplemented with ~200.000 blank (empty) microcapsules. After cDNA synthesis, the microcapsules were washed to remove unretained RNA and cDNA molecules, and transferred to PCR reaction mixture to amplify *YAP*, *PTPRC* and *ACTB* targets. In the presence of RNA or cDNA uptake the microcapsules will show increased fluorescence, in the absence of leakage the microcapsules will remain blank (non-fluorescent). (**B**) The fluorescence histograms for *PTPRC, YAP* and *ACTB* markers were constructed by measuring the fluorescence of post-RT-PCR microcapsules (n ~1000) following the experiments scheme indicated in panel A.

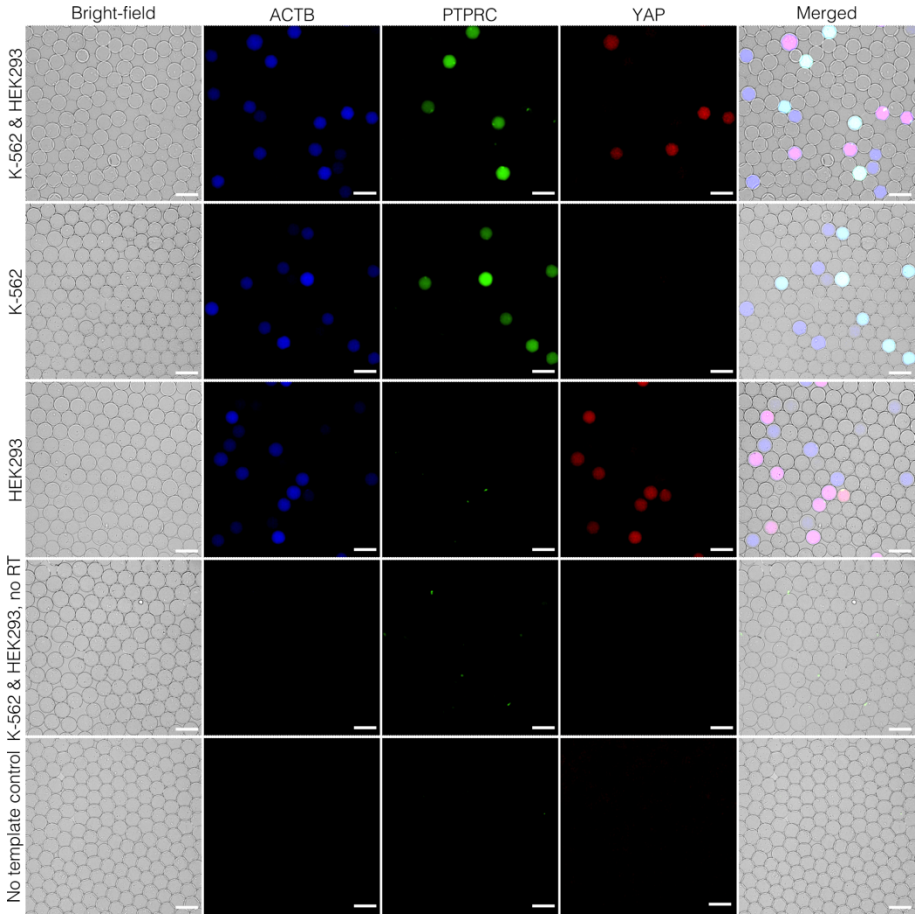

Figure S2. Microcapsule-based single-cell RT-PCR following harsh lysis and gDNA depletion. Microcapsules were subjected to multiplex RT-PCR targeting *ACTB* (blue), *PTPRC* (green), and *YAP* (red). From top to bottom microcapsules comprised: a mixture of K-562 and HEK293 cells (1st row), K-562 cells alone (2nd row), HEK293 cells alone (3rd row), no RT enzyme control (4th row), no template control (5th row) The digital images from left to right indicate: bright field, Alexa Fluor 647 fluorescence for *ACTB* marker (blue), Alexa Fluor 488 fluorescence for *PTPRC* marker (green), Alexa Fluor 555 fluorescence for *YAP* marker (red) and merged image where bright field and fluorescence photographs are superimposed. Scale bars, 100 μm.

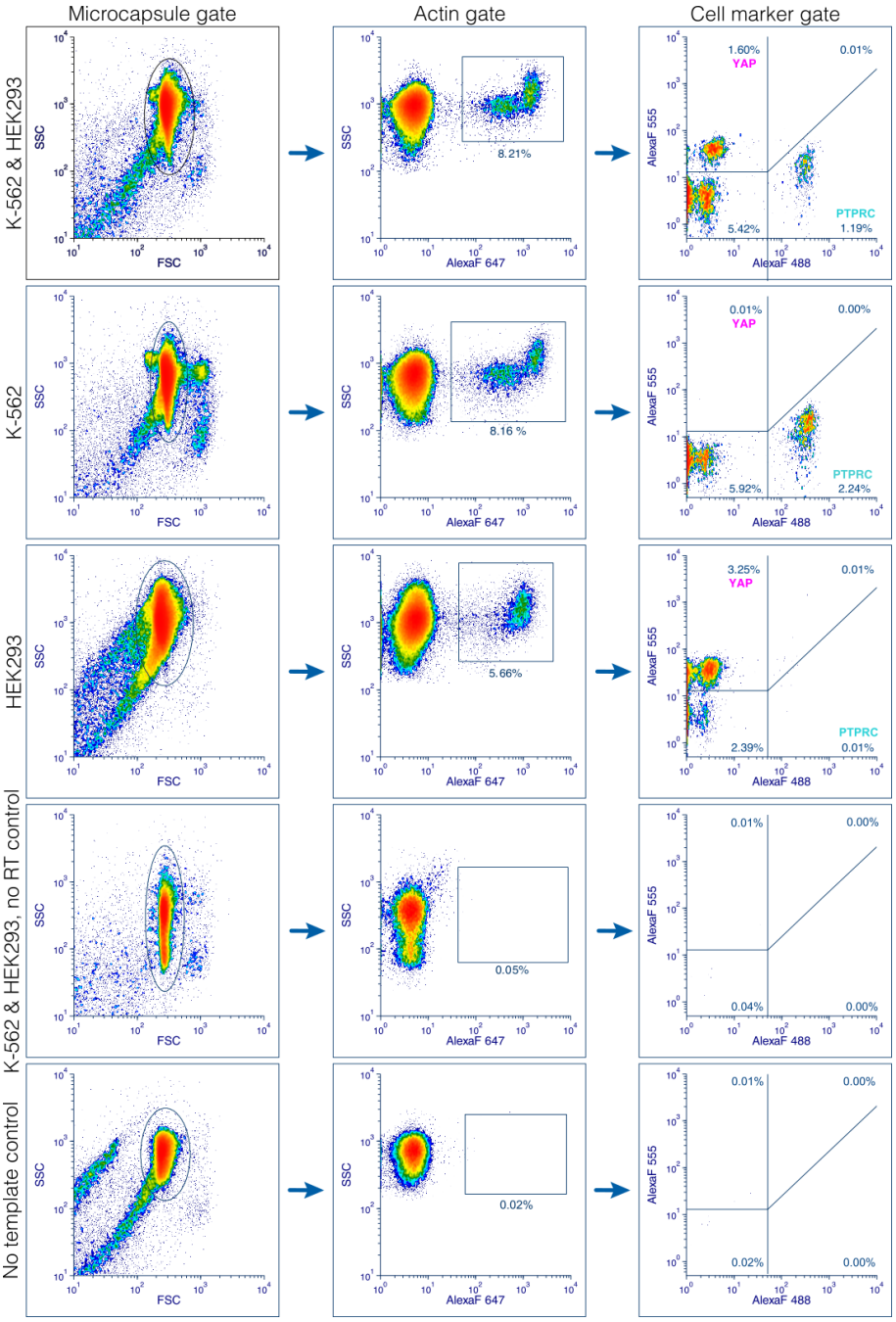

Figure S3. Flow cytometry of microcapsules following single-cell RT-PCR. The flow cytometry analysis of microcapsules prepared with a mixture of K-562 and HEK293 cells (top row), K-562 cells (2nd row), HEK293 cells (3rd row), no RT enzyme control (4th row) and no template control (5th row). The microcapsules were first gated based on forward and side scatter (Microcapsule gate), expression of *ACTB* marker (Actin gate), and then the expression of *PTPRC* and *YAP* markers was recorded (Cell marker

gate). Due to the emission overlap of Alexa Fluor 488 and Alexa Fluor 555 dyes and the imperfect compensation process, the *PTPRC*-positive population showed an increased fluorescence in the Alexa Fluor 555 channel. The percentages indicate the total events (n ~100.000).

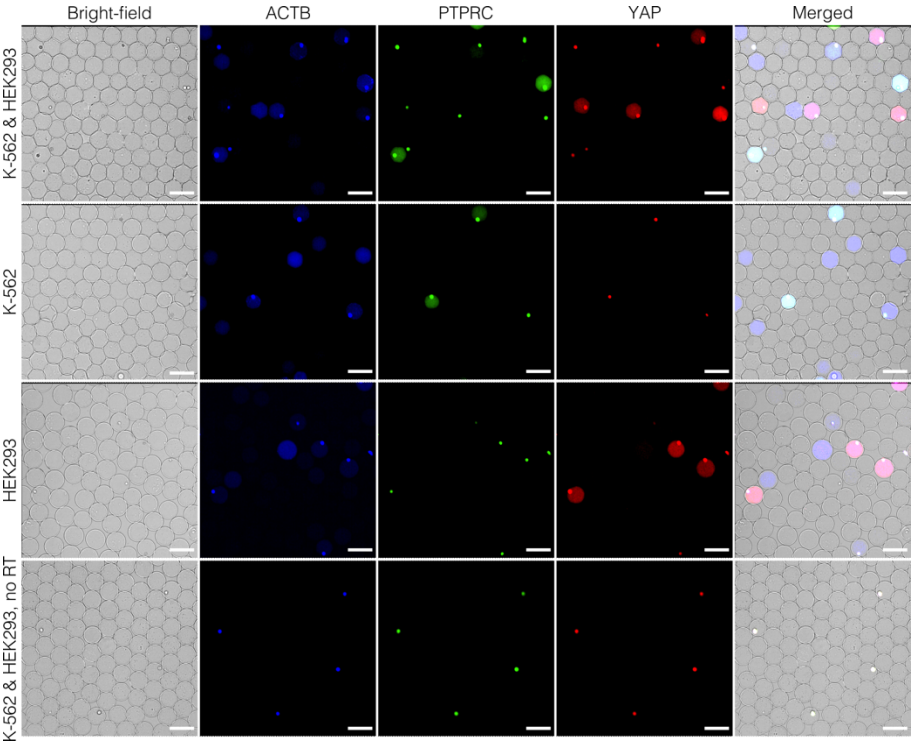

Figure S4. Microcapsule-based single-cell RT-PCR following cell preservation and mild lysis. Microcapsules were subjected to multiplex RT-PCR targeting *ACTB* (blue), *PTPRC* (green), and *YAP* (red). From top to bottom microcapsules comprised: a mixture of K-562 and HEK293 cells (1st row), K-562 cells alone (2nd row), HEK293 cells alone (3rd row), no RT enzyme control (4th row). The digital images from left to right indicate: bright field, Alexa Fluor 647 fluorescence for *ACTB* marker (blue), Alexa Fluor 488 fluorescence for *PTPRC* marker (green), Alexa Fluor 555 fluorescence for *YAP* marker (red), and merged image where bright field and fluorescence photographs are superimposed. Scale bars, 100 μm.

NOTES

Vilniaus universiteto leidykla
Saulėtekio al. 9, III rūmai, LT-10222 Vilnius
El. p. info@leidykla.vu.lt, www.leidykla.vu.lt
Tiražas 15 egz.